Guilherme Luís de Sousa Fialho Guedes

A global approach to physics beyond the Standard Model

Universidade do Minho
Escola de Ciências

UNIVERSIDAD DE GRANADA

June, 2022

Guilherme Luís de Sousa Fialho Guedes **A global approach to physics beyond the Standard Model**

UMinho | 2022

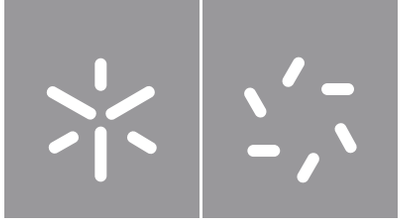

Universidade do Minho
Escola de Ciências

UNIVERSIDAD
DE GRANADA

Guilherme Luís de Sousa Fialho Guedes

A global approach to physics beyond the Standard Model

Doctoral Thesis
Programa de Doctorado en Física y Ciencias del Espacio

Work supervised by
Nuno Filipe da Silva Fernandes de Castro
José Santiago Pérez

June, 2022

Editor: Universidad de Granada. Tesis Doctorales
Autor: Guilherme Luis de Sousa Fialho Guedes
ISBN: 978-84-1117-496-1
URI https://hdl.handle.net/10481/76867

This document was created with the (pdf/Xe/Lua)LaTeX processor and the NOVAthesis template (v6.9.15).

Acknowledgements

I am extremely grateful to my supervisors, Nuno Castro and José Santiago for guiding me through this PhD. I thank Nuno for always being available to answer my questions and for sharing with me his incredible expertise. I thank him for all his advices. From José I learned the importance of being precise and doing things correctly. I thank him for always being ready to discuss with me and teaching me so much. I was very lucky to be supervised by two outstanding researchers.

I thank Miki for all the help and discussions throughout my PhD. With him I learned a lot of physics but also how to approach difficult problems. I am grateful for LIP for supporting my work and for the people there, Ana, Emanuel, Maura, Miguel and Rute. I thank Henrique who was always ready to help and Tiago who was fundamental in my learning process. I am grateful to the people at Granada for welcoming me there, either through breakfasts, football or physics discussions. I thank Adrián, Jorge, Renato, Javi Fuentes, Javi Olmedo, Álvaro and José Maria. I want to thank the awesome friends I made along the way, António, for always losing at boardgames, Supratim, for accompanying me to every coffee, Fran, for teaching me spanish memes and how to use a racket, and Pablo who besides being a truly great friend, was also an amazing collaborator with whom I hope to work again in the future.

I want to thank my friends outside of physics Nuno, Simão, Maurício, Rui and Runhas. I thank Jorge for the long friendship we have shared and for his constant support. I thank my father for always being present. I thank my mother, my sisters and my nephew for always reminding me not to forget about the important things.

Lastly I want to thank the most important person in my life, Maria. There is no doubt that without you this thesis would have been impossible. Thank you for always being there for me and for making my days much happier. When I look back, I cannot believe how lucky I was to go on strike that Halloween.

This work is supported by the projects POCI-01-0145-FEDER-007334, Proyecto de Excelencia (P18-FR-4314), CERN/FIS-PAR/0024/2019, CERN/FIS-PAR/0032/2021, by INCD through CPCA-A1-401197-2021 and by the grant SFRH/BD/144244/2019 funded by FCT.

STATEMENT OF INTEGRITY

I hereby declare having conducted this academic work with integrity. I confirm that I have not used plagiarism or any form of undue use of information or falsification of results along the process leading to its elaboration.

I further declare that I have fully acknowledged the Code of Ethical Conduct of the Universidade do Minho.

Resumo

Uma abordagem global da física para além do modelo padrão

A descoberta do bosão de Higgs representou um momento extraordinário para a Física de Partículas, uma vez que foi a verificação experimental da última peça do Modelo Padrão. No entanto, a busca por uma teoria fundamental da Natureza continua, já que o Modelo Padrão enfrenta ainda vários desafios, tanto experimentais como teóricos, motivando várias propostas de teorias para além do Modelo Padrão.

O trabalho desenvolvido na presente tese segue duas direções complementares na pesquisa por nova física: uma abordagem motivada por modelos específicos, que tem como objetivo explorar assinaturas experimentais comuns a várias classes de modelos; e uma abordagem baseada na teoria de campo efetiva, válida se a nova física for suficientemente pesada, em que podemos parametrizar os efeitos de nova física sem ter de especificar nenhum modelo.

Apesar da primeira abordagem abranger, por definição, menos modelos de nova física, é possível desenvolver estratégias para que a análise seja aplicável a várias classes de modelos. Para além disso, se a nova física incluir campos leves, esta abordagem tem necessariamente que ser seguida. No âmbito desta abordagem, considerámos modelos de Higgs composto, em que o problema da hierarquia associado ao bosão de Higgs pode ser explicado considerando que este é um bosão de Goldstone. Estas teorias compostas prevêem a presença de novos fermiões. Deste modo, desenvolvemos análises para procurar por leptões pesados em colisionadores, considerando diferentes decaimentos para os mesmos e estudando a complementaridade entre estes testes e outras observáveis associadas a matéria escura.

Na segunda abordagem, independente de modelos, extendemos os cálculos existentes no contexto da teoria efetiva do Modelo Padrão considerando operadores de dimensão 8. Estes termos são importantes do ponto de vista experimental, já que algumas observáveis recebem as principais contribuições a esta ordem, mas também porque os coeficientes destes operadores podem ser constrangidos por argumentos teóricos. Para além disso, estudámos uma extensão desta teoria efetiva incluindo um pseudo-escalar leve, motivado pelas teorias de Higgs composto. Finalmente, usámos também a teoria efetiva do Modelo Padrão para ligar resultados experimentais com nova física através da classicação sistemática de modelos que podem gerar os operadores que contribuem para o momento magnético anómolo dos muões.

Palavras-chave: Equações do Grupo de Renormalização, Fenomenologia de colisionadores, Leptões Pesados, Teoria de Campo Efetiva, Teorias para além do Modelo Padrão

Abstract

A global approach to physics beyond the Standard Model

The discovery of the Higgs boson marked an extraordinary moment in particle physics as the last piece of the Standard Model was experimentally verified. However, the quest for a fundamental theory of Nature continues as the Standard Model still faces several challenges, both from experimental evidence and from a theoretical perspective, prompting the proposal of a tremendous amount of beyond the Standard Model scenarios.

This thesis follows two complementarity directions in the search for new physics: the first one, the model-driven approach, requires the selection of a model or class of models and explores their most unique signatures; the second one, valid if new physics is heavy, is to follow the effective field theory approach and parametrize new physics effects in a model-independent way.

While the model-driven approach encompasses, by definition, less beyond the Standard Model scenarios, we can develop strategies so that the setup is applicable to a wide range of models; furthermore, if new physics predicts light degrees of freedom, then this approach must be followed. We proceed with this strategy focusing on composite Higgs models, motivated theories which explain the hierarchy problem by considering the Higgs as a pseudo-Nambu Goldstone boson. A ubiquitous prediction of the composite framework is the existence of vector-like leptons. As such, we propose dedicated analysis to search for these particles at colliders considering a generic setup for their decays and study the possible complementarity with dark matter probes.

In the model-independent approach, we extend the current calculations within the Standard Model Effective Field Theory to account for the one-loop contribution of dimension-8 terms. These terms are important not only from the experimental point of view, since certain observables receive their main contribution at this order, but also because dimension-8 Wilson coefficients are the first ones on which purely theoretical bounds can be placed. Furthermore, we consider the extension of the Standard Model Effective Field Theory with an extra light pseudo-scalar, a motivated scenario within the composite framework. Finally, we use this model-independent approach to connect experimental results with Standard Model extensions by classifying models which can generate the effective operators possibly responsible for the anomalous magnetic moment of the muon.

Keywords: Beyond the Standard Model, Collider Phenomenology, Effective Field Theory, Renormalisation Group Equations, Vector-like Leptons.

Resumen

Un enfoque global de la física más allá del modelo estándar

El descubrimiento del bosón de Higgs representó un momento extraordinario para la física de Partículas, ya que supuso la verificación experimental de la última pieza del modelo estándar. Sin embargo, la búsqueda de una teoría fundamental de la naturaleza continúa, ya que el modelo estándar todavía se enfrenta a varios retos, tanto experimentales como teóricos, lo que motiva una gran cantidad de propuestas de teorías más allá del modelo estándar.

Esta tesis persigue dos direcciones complementarias en la búsqueda de nueva física: la primera, motivada por modelos, pretende explorar las señales experimentales comunes a varias clases de los mismos; la segunda, válida si la nueva física es suficientemente pesada, consiste en utilizar las teorías de campos efectivas y parametrizar los efectos de nueva física pe manera independientemente del modelo.

Aunque el primer enfoque abarca, por definición, menos escenarios de nueva física, es posible desarrollar estrategias para que el análisis sea aplicable a un amplio rango de modelos. En el marco de este enfoque, consideramos modelos de Higgs compuestos, en los que el problema de la jerarquía asociado al bosón de Higgs puede explicarse considerando que es un pseudo-bosón de Nambu-Goldstone. Estas teorías compuestas predicen la presencia de nuevos fermiones. Por ello, desarrollamos análisis para buscar leptones pesados en los colisionadores, considerando sus diferentes desintegraciones y estudiando su posible complementariedad con otros observables asociados a la materia oscura.

En el segundo enfoque, independiente del modelo, extendemos los cálculos existentes en el contexto de la teoría efectiva del modelo estándar considerando operadores de dimensión 8. Estos términos son importantes desde un punto de vista experimental, ya que algunos observables reciben sus contribuciones dominantes a este orden, pero también porque sus coeficientes pueden ser restringidos usando argumentos teóricos. Además, estudiamos una extensión de esta teoría efectiva incluyendo un pseudoescalar ligero, motivado por las teorías de Higgs compuesto. Por último, también hemos utilizado la teoría efectiva del modelo estándar para vincular los resultados experimentales con modelos de nueva física, clasificando sistemáticamente aquellos que pueden generar los operadores que contribuyen al momento magnético anómalo del muón.

Palabras clave: Ecuaciones del grupo de renormalización, Fenomenología de colisionadores, Leptones pesados, Más allá del modelo estándar, Teorías de campos efectiva

Contents

Appendices

List of Figures

List of Tables

1 Introduction

The discovery of the Higgs boson in the Large Hadron Collider (LHC) [1, 2] was one of the most significant moments in recent history in particle physics. It was the final component of the Standard Model (SM) to be experimentally confirmed, giving rise to a consistent theory that has proven to be incredibly robust, finding agreement with experimental results in a wide array of observations.

Despite the success of the SM, it still faces theoretical and experimental challenges to which it does not provide satisfactory answers. To name a few, the SM does not possess the ingredients to account for neutrino masses nor the observed dark matter relic density; moreover the SM does not provide a dynamical explanation for the flavour hierarchy nor to the light mass of the Higgs boson. As a result, an intense effort in model-building has taken place with different theoretical ideas put forth as candidates to describe these and other unexplained phenomena and hence constitute the next step towards a more fundamental theory of Nature.

In spite of the wide motivation to study beyond the Standard Model (BSM) physics, we do not have a clear indication on what the nature of new physics should be, or, more importantly, at which scale of energy it should lie. Therefore, given the tremendous amount of theoretical ideas, the pursuit for new physics must employ a *global approach* by developing strategies which are able to probe a wide range of models.

Throughout this thesis we aim to undertake this quest for the search of BSM physics following two main directions:

1. Look for *direct* evidence for BSM physics by searching for specific signatures which are theoretically motivated. This method involves choosing a particular model or signature as a starting point which inevitably decreases the range of applicability of the analysis. To counter this, signatures which are prevalent among several classes of BSM scenarios should be chosen.

2. Look for *indirect* evidence of BSM physics by searching for deviations from the SM predictions. This can done following the effective field theory (EFT) approach, in which new physics effects are parametrized in terms of the low-energy degrees of freedom without mention of the UV dynamics. This method has the clear advantage of being model-agnostic, not requiring a commitment to any

particular theoretical or experimental motivation. However, it is only valid if there is a decoupling between the scale at which the experiment is taking place and the scale of the UV theory.

Concerning point *(1)*, the hierarchy problem (HP) is one of the main motivations to expect physics at an energy scale that could be probed by current and future experiments. The HP boils down to the idea that a light scalar is not natural, that is, its mass is not protected against quadratic contributions of heavy physics, for instance, BSM physics responsible for the generation of the observed neutrino masses. These apparently large contributions demand a large degree of fine-tuning in order to explain the observed light Higgs which, in turn, suggests the existence of some new physics lying at the TeV scale responsible for protecting the Higgs mass. Composite Higgs models (CHMs) are amongst the most explored of the hierarchy problem solutions. The core idea is that the Higgs is not an elementary scalar at small distances, being instead a composite particle. In the CHM framework, the Higgs arises as pseudo-Nambu Goldstone boson (pNGB) from a spontaneously broken symmetry which allows it to be lighter than the scale of compositeness. While the simplest versions of CHMs have been pushed by experimental null results to larger energies (such that they are no longer effective solutions to the HP), non-minimal scenarios are still viable and they provide the added benefits of being able to account for other unexplained phenomena by the SM, such as dark matter (DM), baryogenesis, B-physics anomalies, among others.

With this motivation in mind, we aim to follow approach *(1)* through the lens of CHMs. A particular signature which is ubiquitous within the composite framework (and also arises in many other models) are vector-like leptons (VLLs). While their simplest realizations have been studied at colliders, when considered as part of a complete non-minimal model, VLLs can give rise to different signatures. For example, through decays to other exotic states that can escape the target of current searches. Moreover, VLLs can be involved in the generation of a DM candidate or in explaining some flavor anomalies, which motivates the study of the complementarity between collider observables and other experimental data.

However, the lack of a clear picture on what the next step towards the construction of a more fundamental picture of Nature should be leads us to also follow the model-agnostic approach *(2)*, which we employ within the context of the Standard Model Effective Field Theory (SMEFT). The SMEFT extends the SM by including higher-dimensional operators built with the symmetries and fields of the SM. We will work towards improving the SMEFT's predictions in several directions. Firstly, by considering the non-leading order (NLO) in the SMEFT expansion, the contribution of dimension-8 operators. This is not only useful phenomenologically, as several observables receive their leading contribution at this order, but also because dimension-8 WCs are the first ones which can be subject to theoretical bounds, the so called positivity bounds, which can be used to, under some assumptions, delimit the space of EFTs that can be completed by a theory in the ultraviolet (UV). Secondly, by extending the SMEFT with extra light degrees of freedom, which is crucial to describe hierarchical BSM scenarios, that is, new physics which predicts both light and heavy new particles. Indeed non-minimal CHMs are among those scenarios where, besides heavy resonances, extra light pNGBs along with the Higgs boson are expected to arise. Finally, we will also consider the NLO (loop-level) contribution in the matching calculations of UV models to the SMEFT, which

are vital to correctly map the extensions of the SM responsible for generating specific Wilson coefficients (WCs), namely those which contribute to observables which seem to deviate from the SM prediction.

Our attempt at a global approach to physics beyond the Standard Model is organized as follows. Assuming knowledge of the main ideas behind Quantum Field Theory (QFT), chapter 2 is devoted to a brief introduction of the SM and its shortcomings. Due to the importance of collider physics in the search for BSM, we also introduce collider experiments, the relevant observables they provide and the analysis setup used. This chapter does not intend to be a review of the topics covered but simply an introduction to the relevant aspects for the remainder of the thesis. The model-driven approach is given in chapter 3, where we first present the main ideas behind CHMs and realize them within the Little Higgs scenario, motivating a signature of VLLs with exotic decays. Afterwards we present a study on collider searches for VLLs with arbitrary branching ratios (including an exotic decay) and explore the possible complementarity with DM probes. Chapter 4 is dedicated to exploring the model-independent approach following the SMEFT; we explore the dimension-8 contributions for the SMEFT, namely through the construction of a bosonic Green's basis at this order and the calculation of the renormalisation group equations (RGEs) of the dimension-8 WCs. We also extend the SMEFT with an axion-like particle and compute the RGEs of this theory. In chapter 5 we use the SMEFT to connect experiment with particular UV scenarios by considering the measurement of the anomalous magnetic moment of the muon and classifying the SM extensions which can generate the relevant operators at one-loop. Finally, we summarize and conclude in chapter 6, stressing the main results of this thesis.

Sections 3.2, 4.3, 4.4, 4.5 and 5 are based on works published during the development of this thesis [3–8].

2

A swift introduction to the Standard Model

2.1 Building blocks

The Standard Model (SM) of particle physics comprises our current knowledge of elementary particles and their interactions. The construction of the SM is based on its field content, that is, the degrees of freedom needed to describe Nature, and the symmetries the theory must respect.

The SM is governed by the set of gauge symmetries $SU(3)_C \times SU(2)_L \times U(1)_Y$. The $SU(3)_C$ symmetry – called the colour group – describes the strong force, quantum chromodynamics (QCD), with 8 corresponding gauge bosons, the gluons, G_μ^A ($A = 1...8$). The $SU(2)_L$ group corresponds to the weak interaction mediated by the 3 $W_\mu^A (A = 1...3)$ gauge bosons, whereas $U(1)_Y$ is the abelian group describing the hypercharge interaction mediated by the B_μ boson.

Matter is, on the other hand, constituted by fermions, which can be divided by whether they are charged under $SU(3)_C$ (quarks) or not (leptons). Only the left-handed (LH) projections of fermions, Ψ, are charged under $SU(2)_L$, making it therefore simpler to divide them into their chiralities, defined as $\Psi_{L,R} = P_{L,R}\Psi$, where $P_{L,R} = 1/2(1 \mp \gamma_5)$. The LH quarks and leptons transform as doublets meaning that each of them has 2 components, the up- and down-type quarks and the neutrino and charged leptons. Each of these components has a right-handed (RH) counterpart (singlet under $SU(2)_L$) except for the neutrino. There are 3 families (flavours) of each fermion which differ only in their interaction with the spin-0 particle of the theory. The up-type quark families are called the up (u), charm (c) and top (t); the down-type quark families are the down (d), strange (s) and bottom (b). The charged lepton families are the electron (e), the muon (μ) and the tau (τ) and the neutrino families are the electron-neutrino (ν_e), the muon-neutrino (ν_μ) and the tau-neutrino (ν_τ).

The spin-0 boson in the theory has a special role. Because fermion chiralities transform differently, it is not possible to construct a gauge invariant mass term for them, which is in contradiction with the observation of massive fermions. The Higgs boson plays the crucial role of generating masses for the SM particles through electroweak symmetry breaking (EWSB). The Higgs is an uncolored complex $SU(2)_L$ doublet which can be written as $\phi = (\phi_1 + i\phi_2\,, \phi_3 + i\phi_4)^T$.

	Fields	$(SU(3)_C, SU(2)_L, U(1)_Y)$
Bosons	G_μ^A	(**8**, **1**, 0)
	W_μ^A	(**1**, **3**, 0)
	B_μ	(**1**, **1**, 0)
	ϕ	(**1**, **2**, 1/2)
Fermions	$q_L = (u_L,\, d_L)^T$	(**3**, **2**, 1/6)
	$l_L = (\nu_L,\, e_L)^T$	(**1**, **2**, -1/2)
	u_R	(**3**, **1**, 2/3)
	d_R	(**3**, **1**, -1/3)
	e_R	(**1**, **1**, -1)

Table 1: The fields present in the SM and their representations under the SM gauge groups.

In table 1, the field content of the SM and how each field transforms under the gauge groups are presented. In principle, an infinite number of interactions could be written that respect the aforementioned symmetries. However, there is one last ingredient to build the SM, which is the principle of renormalisability. The SM is a renormalisable theory in the sense that it contains all the terms needed to absorb any divergence it generates. In essence, this means that it is limited to interactions of mass dimension ≤ 4. With this in mind, the Lagrangian for the SM can be written as:

$$\begin{aligned}\mathcal{L}_{\text{SM}} = &-\frac{1}{4}G^A_{\mu\nu}G^{A\,\mu\nu} - \frac{1}{4}W^a_{\mu\nu}W^{a\,\mu\nu} - \frac{1}{4}B_{\mu\nu}B^{\mu\nu} - \theta\tilde{G}^A_{\mu\nu}G^{A\,\mu\nu} \\ &+ \overline{q^\alpha_L} i\not{D} q^\alpha_L + \overline{l^\alpha_L} i\not{D} l^\alpha_L + \overline{u^\alpha_R} i\not{D} u^\alpha_R + \overline{d^\alpha_R} i\not{D} d^\alpha_R + \overline{e^\alpha_R} i\not{D} e^\alpha_R \qquad (2.1) \\ &+ \left(D_\mu\phi\right)^\dagger \left(D^\mu\phi\right) - \mu^2|\phi|^2 - \lambda|\phi|^4 - \left(y^u_{\alpha\beta}\overline{q^\alpha_L}\tilde{\phi}u^\beta_R + y^d_{\alpha\beta}\overline{q^\alpha_L}\phi d^\beta_R + y^e_{\alpha\beta}\overline{l^\alpha_L}\phi e^\beta_R + \text{h.c.}\right) \,, \qquad (2.2)\end{aligned}$$

where α and β are family (flavour) indices, $\tilde{\phi} = i\sigma_2\phi$, with σ_2 being the second Pauli matrix, and

$$G^A_{\mu\nu} = \partial_\mu G^A_\nu - \partial_\nu G^A_\mu + g_3 f^{ABC} G^B_\mu G^C_\nu \qquad (2.3)$$

$$W^a_{\mu\nu} = \partial_\mu W^a_\nu - \partial_\nu W^a_\mu + g_2 \varepsilon^{abc} W^b_\mu W^c_\nu \qquad (2.4)$$

$$B_{\mu\nu} = \partial_\mu B_\nu - \partial_\nu B_\mu \,, \qquad (2.5)$$

where f^{ABC} and ε^{abc} correspond to the structure constants of $SU(3)$ and $SU(2)$ respectively and g_3 and g_2 are the couplings strenghts of the color and weak interactions respectively.

The SM also contains the QCD θ-term, $\theta\tilde{G}^A_{\mu\nu}G^{A\,\mu\nu}$, where $\tilde{G}^A_{\mu\nu} \equiv \frac{1}{2}\epsilon^{\mu\nu\alpha\beta}G^A_{\alpha\beta}$ and $\epsilon^{\mu\nu\alpha\beta}$ is the totally antisymmetric Levi-Civita tensor. This interaction is a total derivative, however, it cannot be removed from

the Lagrangian since it is a topological term[1].

The covariant derivative, which when acting on fermions is given in its contracted form $\not{D} \equiv D_\mu \gamma^\mu$, is defined in the minus-sign convention as:

$$D_\mu = \partial_\mu - ig_1 Y B_\mu - ig_2 \frac{\sigma^I}{2} W_\mu^I - ig_3 \frac{\lambda^A}{2} G_\mu^A \,, \tag{2.6}$$

where g_1 is the coupling strength associated with $U(1)_Y$, Y is the hypercharge of the particle on which the derivate is acting upon, σ^I are the Pauli matrices and λ^A the Gell-Mann matrices.

2.2 Electroweak symmetry breaking

Knowing that λ must be positive such that the Higgs potential is bounded from below, then, for a negative μ^2, the potential develops a minimum, resulting in a non-vanishing vacuum expectation value (vev), v, for the Higgs boson. This originates the spontaneous symmetry breaking (SSB) of $SU(2)_L \times U(1)_Y \longrightarrow U(1)_{\text{em}}$ which explains why at low-energies we observe the electromagnetic interaction mediated by a massless photon.

Without loss of generality, the vev of the Higgs can be chosen to be real and aligned with its lower component such that:

$$\phi = \frac{1}{\sqrt{2}} \begin{pmatrix} 0 \\ h + v \end{pmatrix} , \tag{2.7}$$

where $v = \sqrt{-\mu^2/\lambda}$ and h is the Higgs boson. The choice in Eq. (2.7) corresponds to the unitary gauge, where by the appropriate rotations, allowed by the gauge symmetry, we remove the remaining degrees of freedom of the original Higgs doublet as they become the longitudinal components of 3 gauge bosons which, in turn, become massive [11–13]. Indeed, by taking the kinetic term of the Higgs term in Eq. (2.1) and considering now that the Higgs acquires a vev results in a mass term for W_μ^1 and W_μ^2 and mixing between the gauge bosons W_3 and B:

$$\left(D_\mu \phi\right)^\dagger \left(D^\mu \phi\right) \supset g_2^2 \frac{v^2}{8} \left[\left(W_\mu^1\right)^2 + \left(W_\mu^2\right)^2 + \left(\frac{g_1}{g_2} B_\mu - W_\mu^3\right)^2 \right] \tag{2.8}$$

where we neglected terms with h. The rotation to the mass basis results in:

$$Z_\mu \equiv c_\omega W_\mu^3 - s\omega B_\mu \tag{2.9}$$

$$A_\mu \equiv s_\omega W_\mu^3 + c_\omega B_\mu \,, \tag{2.10}$$

where $c_\omega \equiv \cos\theta_\omega$, $s_\omega \equiv \sin\theta_\omega$ and θ_ω is the Weinberg angle defined as

$$\tan\theta_\omega = \frac{g_1}{g_2} \,. \tag{2.11}$$

[1] One could think of considering terms of the same form with the other gauge bosons, but these are not physical as they can be rotated away [9, 10].

	u	c	t	d	s	b	e	μ	τ	Z	$W^{\pm}$	h
Mass (GeV)	0.002	1.27	173	0.005	0.093	4.2	0.0005	0.105	1.78	91.2	80.4	125

Table 2: Approximate mass of the SM particles. Values taken from Ref. [14], where the uncertainties associated with these quantities can also be obtained.

Applying the rotations to Eq. (2.8) results in the mass terms

$$m_{W^{\pm}} = \frac{g_2 v}{2}, \qquad m_Z = \frac{1}{c_\omega}\frac{g_2 v}{2}, \qquad m_A = 0, \tag{2.12}$$

where $W^{\pm} \equiv (W^1 \mp W^2)^2/\sqrt{2}$. We see that the gauge boson A_μ, the photon, remains massless after EWSB.

Upon considering the redefinitions of the gauge bosons, the covariant derivative becomes (up to the coupling with the gluon which remains unaltered):

$$D_\mu = \partial_\mu - ig_2\frac{\sigma^{\pm}}{\sqrt{2}}W_\mu^{\pm} - i\frac{g_2}{c_\omega}\left[\frac{\sigma^3}{2} - s_\omega^2 Q\right]Z_\mu - ig_1 c_\omega Q A_\mu, \tag{2.13}$$

where we see that $g_1 c_\omega \equiv e$ with e the electromagnetic coupling strength and the electric charge is given by $Q \equiv T_3 + Y$ where T_3 is the third component of isospin. We also redefined $\sigma^{\pm} \equiv (\sigma^1 \pm \sigma^2)/2$.

2.2.1 Fermionic Sector

Upon EWSB the fermions also gain a mass from the Yukawa sector

$$\mathcal{L}^{\text{yuk}} = -\frac{1}{\sqrt{2}}(h+v)\left(y^u_{\alpha\beta}\overline{u^\alpha_L}u^\beta_R + y^d_{\alpha\beta}\overline{d^\alpha_L}d^\beta_R + y^e_{\alpha\beta}\overline{e^\alpha_L}e^\beta_R + \text{h.c.}\right). \tag{2.14}$$

To move to the mass basis of the fermions, a unitary rotation, $U^f_{L,R}$, is applied to each chiral component of each sector $f = \{u, d, l\}$ such that it diagonalizes the Yukawa couplings:

$$U_L^{u\dagger} y^u U_R^u = \text{diag}(y_u, y_c, y_t), \tag{2.15}$$
$$U_L^{d\dagger} y^d U_R^d = \text{diag}(y_d, y_s, y_b), \tag{2.16}$$
$$U_L^{l\dagger} y^l U_R^l = \text{diag}(y_e, y_\mu, y_\tau), \tag{2.17}$$

resulting in masses of the fermions given by $m_\psi = v y^\psi/\sqrt{2}$. The masses of fermions and other particles are presented in table 2.

These rotations have no influence in the couplings with neutral gauge bosons since their effect is $U^{f\dagger}_{L,R}U^f_{L,R} = 1$. However, the couplings with the $W^{\pm}$ bosons, after taking into account the covariant derivative in Eq. (2.13) become, in the quark sector,

$$\mathcal{L}^{\text{SM}} \supset -\frac{g}{2\sqrt{2}}\overline{u}_L\gamma^\mu\left(U_L^{u\dagger}U_L^d\right)d_L W_\mu^+ + \text{h.c.}, \tag{2.18}$$

where $\left(U_L^{u\dagger}U_L^d\right) \equiv V_{\text{CKM}}$ is the Cabibbo-Kobayashi-Maskawa (CKM) matrix which is responsible for flavour-changing charged currents at tree-level in the SM. In the SM the CKM is a unitary matrix which can be parametrized by 4 physical parameters, 3 mixing angles, θ_{12}, θ_{13}, θ_{23} and a CP-violating phase, δ. Explicitly,

$$V_{\text{CKM}} = \begin{pmatrix} c_{12}c_{13} & s_{12}c_{13} & s_{13}e^{-i\delta} \\ -s_{12}c_{23} - c_{12}s_{23}s_{13}e^{i\delta} & c_{12}c_{23} - s_{12}s_{23}s_{13}e^{i\delta} & s_{23}c_{13} \\ s_{12}s_{23} - c_{12}c_{23}s_{13}e^{i\delta} & -c_{12}s_{23} - s_{12}c_{23}s_{13}e^{i\delta} & c_{23}c_{13} \end{pmatrix}, \tag{2.19}$$

where $c_{ij} = \cos\theta_{ij}$ and $s_{ij} = \sin\theta_{ij}$.

In the lepton sector the couplings with the W boson would read:

$$\mathcal{L}^{SM} \supset -\frac{g}{2\sqrt{2}}\bar{e}_L\gamma^\mu\left(U_L^{l\dagger}U_L^\nu\right)\nu_L W_\mu^+ + \text{h.c.}\,, \tag{2.20}$$

where we introduced a unitary rotation to the neutrinos U_L^ν. The leptonic counterpart of the CKM matrix is called the Pontecorvo-Maki-Nakagawa-Sakata (PMNS) matrix, where $U_{\text{PMNS}} \equiv U_L^{l\dagger}U_L^\nu$. However, since within the SM there is no Yukawa term including the neutrinos, we are free to choose $U_L^\nu = U_L^{l\dagger}$ resulting in $U_{\text{PMNS}} = 1$. Therefore, there are no flavour changing currents, either charged or neutral, in the lepton sector of the SM.

Note that even before EWSB there is freedom within the Lagrangian of Eq. (2.1) to rotate l_L and e_R such that the lepton Yukawa can always be written as a diagonal matrix. In the quark sector, since we have two Yukawa terms including q_L, there is only freedom to take either y^u or y^d diagonal.

2.3 Shortcomings of the Standard Model

As hinted before, and in the title of this thesis, despite the incredible success of the SM at describing most of the experimental data to this day, it does not provide satisfactory answers to everything that we observe, prompting the study of BSM physics. Some of the shortcomings of the SM are:

- **Gravity**

  The SM is incomplete as it does not provide a description of the gravitational interactions and therefore does not describe all the observed forces.

- **Neutrino oscillations**

  Neutrinos were observed to oscillate between their states in the flavour basis [15–22] implying that they have a mass. The SM does not include a mass term for neutrinos and as such, explaining it is among the most important directions for searches of BSM. From cosmological observations the sum of their masses is bound to be $\sum m_\nu < 0.12\,\text{eV}$ [23].

- **Dark matter**

  The anomalous rotation velocity of galaxies far from their center prompted the conjecture that there was more matter than what could be seen [24]. Other evidence for this dark matter (DM) stems from studies on gravitational lensing of clusters of galaxies [25], the observed cosmic background [23] or the observation of the bullet cluster [26] – see Refs. [27, 28] for a complete overview on the motivation for DM. However, the SM does not provide a viable DM candidate.

- **Baryon asymmetry**

  Our observations of the Universe lead to the conclusion that it is dominated by baryons instead of anti-baryons [29]. Sakharov derived 3 conditions which had to be met for baryogenesis [30] to occur: baryon number violation, C and CP-violation and departure from thermal equilibrium. The SM alone does not possess these ingredients (for instance, CP-violation present in the CKM matrix is not enough to generate the observed domination of baryons [31]) and as such, baryogenesis points to BSM scenarios.

- **Hierarchy problem**

  A scalar can receive contributions to its mass which are proportional to arbitrarily heavy scales (possibly corresponding to BSM solutions to any of the problems in this list). Therefore, to explain the observation of a light Higgs boson within the SM, a huge fine-tuning between the bare parameters of the theory and quantum corrections would be needed, deeming the theory *unnatural*. Note that if there is no BSM physics, there is no HP.

- **Strong CP-problem**

  From symmetry principles, the CP-violating interaction $\theta \tilde{G}^A_{\mu\nu} G^{\mu\nu}_A$ can be written within the strong sector of the SM. However, from measurements of the electric neutron dipole moment this term is bounded to be $|\theta| \lesssim 10^{-11}$ [32–34]. The SM does not provide any explanation for the smallness of this dimensionless coupling.

- **The flavour puzzle**

  As can be seen from table 2, the mass of fermions within the SM extends over six orders of magnitude. This has no dynamical explanation within the SM and it is simply parametrized with the degrees of freedom of the Yukawa couplings.

- **Cosmology**

  The Λ-CDM model is currently the most successful at describing the cosmological history of the Universe [23, 35]. However, some of its important aspects do not find any explanation within the SM, such as inflation and dark energy (besides the already mentioned DM candidate) [35].

- **Flavour anomalies**

  While not yet a clear indication for new physics since these observations have yet to cross the 5σ mark for discovery, recent experimental data regarding lepton flavour universality violation (LFUV) in B-meson decays seem to point to BSM. Adding to these, a recent measurement of the anomalous moment of the muon [36] seems to corroborate a deviation from the SM reported in 2006 [37]. Taken together, these two measurements result in a 4.2σ deviation from the SM prediction [38].

Some of these shortcomings are a result of direct experimental evidence, such as neutrino masses and dark matter, while others have to do with the fact that the SM does not explain its parameters dynamically, such as the flavour puzzle or the hierarchy problem. Looking at the intersection between these two approaches can be a fruitful direction since many models motivated by theoretical considerations can provide solutions to other more experimentally driven shortcomings of the SM.

Let us look in more detail at the motivations to explore BSM physics which are most relevant for this thesis.

2.3.1 The hierarchy problem

To understand why the HP only features in light elementary scalars, let us see what it means for a parameter to be naturally small.

When a parameter is the sole responsible for breaking some symmetry, which is equivalent to saying that when we take this parameter to zero a symmetry is recovered, all contributions to this quantity must be proportional to itself. This is so since we assumed there was no other coupling capable of breaking the referred symmetry. In this case, it is technically natural for the parameter to be small, following 't Hooft's criteria [39].

Within the SM, by taking fermion (gauge boson) masses to zero one recovers a chiral (gauge) symmetry. Therefore, contributions to the masses of these particles must be proportional to themselves and can consequently be considered naturally small. The Higgs boson mass, on the other hand, is not responsible for breaking any symmetry that we know of.

The Higgs mass can be written as

$$m_h = m_h^0 + \delta m_h \,, \tag{2.21}$$

where m_h is the observable Higgs mass, m_h^0 the bare parameter in the Lagrangian and δm_h the quantum corrections. If δm_h is very large, then a fine cancelation with $m_h^0 \approx -\delta m_h$ would be required. If there is no other BSM physics, the Planck scale seems like an unavoidable cut-off of the SM description which would require a fine-tuning of one part in $\sim 10^{15}$ to explain the observed Higgs mass.

We can see the dependence of the Higgs mass on a scale of new physics explicitly through a simple example. Consider extending the SM with a heavy fermion Ψ with mass M_Ψ which, besides its kinetic

term, couples to the Higgs through a Yukawa-like term as $Y_\psi \overline{\Psi} \phi \Psi$. The contribution of this heavy degree of freedom to the Higgs mass, calculated in dimensional regularization with the $\overline{\text{MS}}$ scheme, is given by:

$$\delta m_h = \frac{3Y_\psi}{16\pi^2} M_\Psi^2 \,, \tag{2.22}$$

where it becomes evident that the corrections are quadratically proportional to new physics. The same qualitative result would arise if instead of a fermion we had considered a heavy scalar for instance.

Fine-tuning does not reflect an inconsistency within the theory, but it has served us well as a guiding light in the recent past by hinting towards the existence of the ρ-meson or the charm quark for example [40]. Naturalness principles did not predict an exact value for the mass of a particle, but indicated where to expect new physical phenomena. Indeed, the HP points to new physics at the TeV scale to protect the Higgs mass. Two of the most popular solutions to the HP are supersymmetry (SUSY) and composite Higgs models (CHM); in this thesis we will focus on the latter and introduce the composite framework in section 3.1.

2.3.2 Dark Matter

To explain the DM evidences with a particle, the SM must be extended with a stable and electrically neutral candidate. Furthermore, the DM candidate needs to account for the relic abundance observed today [23]:

$$\Omega_{\text{DM}} h^2 = 0.120 \pm 0.001 \,, \tag{2.23}$$

where Ω_i corresponds to the ratio between the observed energy density of the component i and the critical density and h is the reduced Hubble parameter [14]. Let us highlight the main features of some of the most explored mechanisms to generate the correct relic density.

Consider a DM candidate, χ_1, with a mass around the EW scale which, in the early Universe, is in thermal equilibrium with the SM bath through $2 \leftrightarrow 2$ processes such as $\chi_1 \chi_1 \leftrightarrow \text{SM}\,\text{SM}$, where SM corresponds any SM particle. The evolution of the DM number density, n, is given by the Boltzmann equation:

$$\frac{dn}{dt} + 3Hn = \left(n_{\text{eq}}^2 - n^2 \right) \langle \sigma_{\text{ann}} v \rangle \,, \tag{2.24}$$

where H is the Hubble parameter, n_{eq} is the equilibrium number density which, for a non-relativistic species follows $n_{\text{eq}} \propto (m_{\chi_1} T)^{(3/2)} e^{(-m_{\chi_1}/T)}$ [41, 42], σ_{ann} is the annihilation cross-section, v is the DM velocity and $\langle \cdots \rangle$ corresponds to a thermally averaged quantity. When the right-hand side of Eq. (2.24) dominates, that is, when the interaction rate is sufficiently large, the DM number density tends to its equilibrium value. However, as the Universe expansion, second term on the left-hand side of Eq. (2.24), becomes more important, the DM becomes more dilluted and the annihilation process less efficient. Indeed, when $H \sim \langle \sigma_{\text{ann}} v \rangle \, n$, the DM decouples from the thermal bath and its comoving number density becomes constant and equal to what we observe today. Therefore, knowing the annihilation cross-section of a given DM candidate, one can solve numerically Eq. (2.24) to calculate the DM present day relic

density. This mechanism for generating the DM relic density is called *freeze-out*. For weakly interacting massive particles (WIMPs) that decouple from the thermal bath while non-relativistic, freeze-out occurs at a temperature $T_F \sim m_{\chi_1}/20$ [41–43].

Co-annihilation [44] happens when there is a particle, χ_2, with a similar mass than that of the DM candidate, χ_1, which can enhance the annihilation cross-section. The processes which are now relevant for setting the DM relic density are $\chi_1\,\chi_1 \leftrightarrow \mathrm{SM\,SM}$, $\chi_1\,\chi_2 \leftrightarrow \mathrm{SM\,SM}$ and $\chi_2\chi_2 \leftrightarrow \mathrm{SM\,SM}$.

A rough estimation of the mass splitting needed for co-annihilation to play a significant role can be obtained by assuming the same coupling strengths for the co-annihilation and standard annihilation processes. Considering that, for the two particles to be in thermal equilibrium at freeze-out, we need $m_{\chi_2} - m_{\chi_1} \sim T_F$, and, assuming $T_F \approx m_{\chi_1}/20$, the resulting mass splitting is $\Delta \equiv (m_{\chi_2} - m_{\chi_1})/m_{\chi_1} = 0.05$ [43–45].

If DM cannot reach thermal equilibrium in the early Universe, freeze-out cannot occur and another mechanism is needed. This can happen in scenarios where DM couples extremely feebly to the SM, hence why these candidates are called feebly interacting matter particles (FIMP) [41]. In such cases, the DM initial abundance is assumed to be very small, usually set by an inflationary epoch and its current day relic density can be set by a non-thermal process such as the decay of a heavier particle, which can be a SM particle $\mathrm{SM} \longrightarrow \chi_1\chi_1$ or another BSM state, $\chi_2 \longrightarrow \chi_1\mathrm{SM}$ [41]. The relic density also reaches a constant value when the particle decaying into DM is depleted from the thermal bath.

2.3.3 Flavour anomalies

Recently there have been multiple tests of LFUV which show some deviation from the SM prediction. The most significant are the measurements of the ratios

$$R_K^{(*)} = \frac{\mathrm{BR}(B \longrightarrow K^{(*)}\overline{\mu}\mu)}{\mathrm{BR}(B \longrightarrow K^{(*)}\overline{e}e)} \qquad \text{and} \qquad R_D^{(*)} = \frac{\mathrm{BR}(B \longrightarrow D^{(*)}\overline{\tau}\nu_\tau)}{\mathrm{BR}(B \longrightarrow D^{(*)}\overline{\ell}\nu_\ell)}, \tag{2.25}$$

where $\ell = e,\ \mu$. $R_K^{(*)}$ is related to a neutral $b \longrightarrow s$ transition and happens at loop-level in the SM whereas $R_D^{(*)}$ corresponds to the charged $b \longrightarrow c$ transition which in the SM takes place at tree-level. The combined measurements of R_D and R_D^* [46–54] point to a deviation from the SM prediction at 3.1σ [55]. On the other hand, the latest measurement of R_K alone deviates from the SM prediction at 3.1σ [56] and R_K^* at 2.5σ [57].

Another interesting measurement is the apparent violation of unitarity in the first row of the CKM matrix, called the Cabibbo angle anomaly (CAA). Measurements of V_{us} from the leptonic kaon decay, $K \longrightarrow \pi l \nu$, are in tension with those obtained when assuming CKM unitarity and taking V_{ud} from super-allowed β decays. These results are quite dependent on the parametrization of the β decays and the corresponding significance has been quoted as being between 3 and 5 σ [58, 59].

Finally, an anomalous magnetic moment of the muon, a_μ, has been observed in 2006 by the Brookhaven National Laboratory [37]. More recently, the Fermilab Muon g-2 Experiment has also measured this quantity [36] and seems to find agreement with the previous observation of a larger value than

the SM prediction. Combined, these results present a deviation from the SM of $4.2\,\sigma$ with

$$\Delta a_\mu = a_\mu^{\mathrm{EXP}} - a_\mu^{\mathrm{SM}} = (251 \pm 59) \times 10^{-11}, \tag{2.26}$$

where we used the SM prediction quoted in Ref. [38]. This calculation does not include the latest lattice calculation of the hadronic vacuum polarization (HVP) contribution by the Budapest-Marseille-Wuppertal collaboration [60] which seems to alleviate the tension. However, since this new result for the HVP also introduces tensions in other results such as in the $e^+e^- \longrightarrow$ hadrons cross-section [61–64], it is commonly neglected in the literature for now, until the situation becomes clearer.

2.4 Collider phenomenology

Some of the strongest constraints set on new physics come from collider experiments, which consist in colliding beams of particles and studying the kinematic distributions resulting from these collisions. The most energetic collider ever built is the Large Hadron Collider (LHC) [65] at CERN, which collides proton beams at a center of mass energy of $\sqrt{s} = 13\,\mathrm{TeV}$.

A common prediction of BSM theories is the existence of new particles which could in principle be produced (and decay) at the LHC, which would provide a clear evidence for new physics if ever observed. Collider experiments are therefore a powerful avenue to test BSM scenarios. The idea is to simulate the expected result from proton collisions given a benchmark model and compare it to the actual distribution of data. We dedicate this section to introducing the generic features of colliders and the different tools used in collider simulations aimed at searching for BSM scenarios such as the ones which we will introduce in the next chapter.

2.4.1 Features and geometry of a detector

There are 4 main detectors within the LHC:

- ATLAS [66, 67] and CMS [68, 69], multi-purpose detectors which capture particles that fly in all directions;
- LHCb [70, 71], a forward detector focusing on the study of heavy flavoured mesons;
- ALICE [72], a detector focused on heavy-ion physics.

ATLAS and CMS are the most relevant for this thesis as they are the more suitable to search for heavy new particles. While the details among the two are not the same, the general setup is similar and we will not make any distinctions when analyzing the geometry of the detectors.

These detectors are cylinder shaped, with the central axis aligned with the particle beam, the z-axis. The flight directions of particles resulting from the original collision can be parametrized through the polar angle, θ, and the azimuthal angle, ϕ; see figure 1 for an illustrative diagram of the detector.

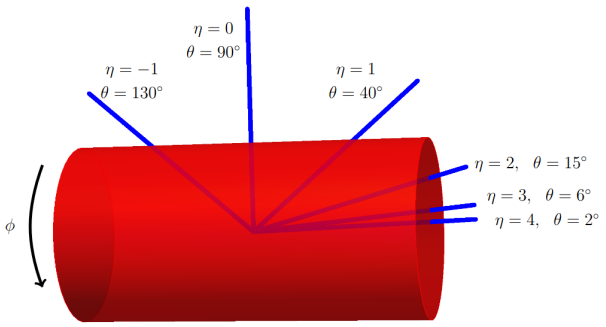

Figure 1: Scheme of a detector [73]. The detector is centered around the beam, the z-axis. The azimuthal angle, ϕ, goes around the beam and is defined as $\phi = 0$ in the x-axis. The pseudo-rapidity, η, is shown as a function of the polar angle, θ.

It is useful to define the angular distance between two tracks $\Delta R \equiv \sqrt{(\Delta\phi)^2 + (\Delta y)^2}$, where y is the rapidity defined as

$$y \equiv \frac{1}{2}\ln\frac{E + p_z}{E - p_z}\,, \tag{2.27}$$

with E and p_z denoting the components of the four momentum $p^\mu = (E, p_x, p_y, p_z)$. In the limit of massless particles, rapidity is equivalent to pseudo-rapidity, defined as $\eta \equiv -\ln\tan\frac{\theta}{2}$.

The components of the 4-momentum of particles resulting from the collision can be approximately reconstructed through the deposit of energy along the calorimeters and through the measurement of the curvature of the particle's trajectory due to effect of a strong magnetic field. This curvature also allows the distinguishing between positively and negatively charged particles.

An important observable which can be constructed from the 4-momentum of the reconstructed particles for an event (a collision) is the 2-vector missing transverse momentum

$$\overrightarrow{\not{p}_T} \equiv -\sum_i \overrightarrow{p_T}^i\,, \tag{2.28}$$

where $\overrightarrow{p_T}^i \equiv (p_x, p_y)$ is the transverse momentum of particle i and the quantity is summed over all particles in an event. The related scalar quantity missing transverse energy (MET), denoted by $\not{E}_T$, is given by:

$$\not{E}_T \equiv |\overrightarrow{\not{p}_T}|\,. \tag{2.29}$$

The relevance of this observable has to do with the fact that, since the original colliding particles are taken to be aligned with the z-axis, the transverse momentum of the initial system of particles is zero. By momentum conservation, summing all the transverse momentum of the resulting particles should also give a vanishing result. If that is not the case, then some part of the event must have gone unidentified such as a neutrino or a BSM particle which did not decay within the detector.

Particle identification is done through the layered structure of the detector: different particles transverse different layers. The innermost layer corresponds to a tracking system which identifies tracks (and their curvature) from charged particles near the collision vertex. In the next layer, the electromagnetic

calorimeter, electrons and photons deposit all of their energy. Hadrons transverse into the subsequent hadronic calorimeter, where they lose their energy. Finally, muons are detected by the outermost layer. As mentioned before, neutrinos do not interact with the detector leading to large MET signatures. Heavier particles, such as the top, tau and the massive gauge bosons decay promptly within the detector and can, in principle, be reconstructed according to the identified decay products.

Quarks and gluons are not identified at the detector level since these are only found within hadrons (the only exception is the top-quark which decays before hadronizing). Jets are objects created to capture the collection of particles arising from the same original quark or gluon through hadronization [74]. The precise definition of a jet is not unique and several algorithms have been proposed in the literature to characterize a jet. Clustering algorithms consider two distances to define a jet: d_{ij}, a distance between two hadrons i and j and d_{ib}, a distance from hadron i to the beam. If the former is the smallest, then the hadrons i and j are combined; otherwise, if d_{ib} is larger, then the object is taken from the hadron list and considered a jet [73]. Within this thesis we will use the clustering anti-k_t algorithm [75].

2.4.2 Analysis setup

When looking for new physics at colliders, from the theoretical point of view we try to predict some excess in a particular observable (the discriminating observable) when comparing with the SM prediction. This way, an experimental analysis can search for that excess which, if found, could indicate BSM physics at some confidence level.

To study how a BSM model behaves at colliders, the first step is to generate events, that is, use Monte Carlo simulators to generate the predicted results from proton-proton collisions under a theoretical scenario. At this level, these results can include photons, leptons, quarks and gluons (or any other stable BSM state that is included in the model). The properties of the particles resulting from the collision will follow the probability distribution of the underlying theory. We implement the theory under study using `FeynRules` [76] and generate a Universal Feynman Output (UFO) [77] which can then be read by `MadGraph5_aMC@NLO` [78] to simulate events following the chosen model. In general we are interested in a particular final state from the BSM scenario, so the generation of events focuses in those which result in such final state. Note that we also need to generate the SM predicted events for the same final state, that is, the *background* of our analysis.

The hadronization and showering of the generated particles in the previous step is done through `Pythia` [79] and is a model-independent computation, following mainly QCD calculations. Finally, the detector response is modelled using `Delphes` [80], which parametrizes the momentum and pseudo-rapidity thresholds for particles to be identified and considers the identification efficiencies (in terms of these kinematic observables) of a realistic detector.

The final number of events from the signal is typically many orders of magnitude smaller than the background from the SM. As such, a search strategy with selection cuts on several observables (other than the discriminant one) must be developed such that these selections reject most of the SM events

while keeping the majority of signal events. After the optimization of this strategy, a statistical analysis on the discriminant variable can be performed to bound – or quote a discovery of – the BSM physics scenario.

2.4.2.1 Statistical tools

The statistical analysis is performed according to the CL_s method [81]. This method introduces a test statistic, Q, defined as the ratio between the likelihoods associated with the signal + background hypothesis (L_{s+b}) – corresponding to new physics – and the background only hypothesis (L_b):

$$Q \equiv \frac{L_{s+b}(n)}{L_b(n)}\,, \tag{2.30}$$

where the likelihood functions are given by $L_x(n) \equiv P(n|x)$, that is, the conditional probability for the observed data, n, given a particular theory input x, which is either signal+background, or background only.

The confidence estimators on both hypotheses are given by

$$CL_{s+b} \equiv P_{s+b}(Q \leq Q_{obs})\,, \qquad CL_b \equiv P_b(Q \leq Q_{obs})\,, \tag{2.31}$$

where

$$P_x(Q \leq Q_{obs}) = \int_{-\infty}^{Q_{\rm obs}} \frac{dP_x}{dQ} dQ\,, \tag{2.32}$$

and $\frac{dP_x}{dQ}$ the probability distribution function of the test statistic for the scenario x ($s+b$ or s).

With this, if we obtain $CL_{s+b} \leq \alpha = 0.05$ for a particular model, this means that such model can be excluded at a confidence level of $CL = 1 - \alpha = 95\%$. However, when the distributions of P_b and P_{s+b} are very close, as is the case for very small signal, the CL_{s+b} method can actually exclude models which it does not have sensitivity to [81]. It is therefore common to normalize CL_{s+b} by CL_b, giving rise to the CL_s quantity:

$$CL_s \equiv \frac{CL_{s+b}}{CL_b}\,. \tag{2.33}$$

To concretize the CL_s method let us consider a simple case of a single bin experiment, based on the predictions from the SM and a BSM model. The number of events in the specific bin follows a Poissonian distribution with expected values s for the BSM scenario and b for the background SM prediction. Starting from Eq. (2.30), we can write the test statistic in its more useful form, $\ln Q$, as:

$$\begin{aligned} Q &= e^{-s}\left[1 + \frac{s}{b}\right]^n \\ \Rightarrow \ln Q &= -s + n \ln\left[1 + \frac{s}{b}\right]\,, \end{aligned} \tag{2.34}$$

where n is the number of events observed. Since n follows the same behaviour as $\ln Q$ (up to a multiplicative factor and a shift), for simplicity let us choose n as the test statistic. Consequently:

$$CL_s = \frac{P_{s+b}(n \leq n_{obs})}{P_b(n \leq n_{obs})} \tag{2.35}$$

If zero events are observed in a bin in which zero background events are expected, then any model which predicts more than 3 events could be excluded at 95% confidence level, since

$$CL_s = e^{-s} \leq 0.05 \tag{2.36}$$

$$\Rightarrow s > 2.99\,. \tag{2.37}$$

Conversely, a model which does not predict at least 3 events can never be excluded, even in the best case scenario of the analysis being background-free.

For multi-binned analysis, we will use the `OpTHyLiC` [82] tool[2] to obtain the sensitivity on new physics following the CL_s method. Given a discriminant variable and the signal and background distributions, the program outputs the signal strength modifier $\mu_{up} \equiv \sigma^{\rm up}/\sigma^{\rm th}$, where $\sigma^{\rm up}$ corresponds to the maximum cross-section allowed at a chosen confidence level and $\sigma^{\rm th}$ is the theoretical cross-section, given by `MadGraph` [78].

[2]The tool `pyhf` [83] was also used to cross-check some results.

3

Model-driven approach

The search for new physics following a model-driven approach requires, by definition, the choice of a particular model which motivates the phenomenological signature under study. CHMs are good candidates for such models as they have received considerable attention as viable explanations of the HP [84–88]. Furthermore, in their non-minimal realizations, CHMs can also provide solutions for other shortcomings of the SM, such as presenting a DM candidate. Motivated by CHMs, we choose to look for vector-like leptons (VLLs) not only because they are ubiquitous in composite scenarios (and other theoretical frameworks) but also because they have not yet been extensively studied from the experimental point of view, with most analysis making strong assumptions on their signature such as considering that they can only decay to SM particles, which is not in general the case when the VLL is considered as part of a complete model.

With this in mind we will start this chapter by introducing the idea behind CHMs in section 3.1 and building a particular realization based on the collective symmetry breaking mechanism, the Littlest Higgs model with T-parity (LHT). Within this model, VLLs are predicted to exist with decays to other exotic particles. As such, section 3.2 will be devoted to the construction of a collider search strategy to look for VLLs with arbitrary branching ratios into SM decays and an extra decay channel to another BSM particle. Note that this analysis can probe the LHT model but it is also applicable to a much wider range of scenarios. Furthermore, we will also explore the complementarity between collider probes and other observables in section 3.2.5. Section 3.2 is based in the work published in Ref. [3].

3.1 The composite Higgs idea

CHMs provide a natural solution to the hierarchy problem by considering that the Higgs boson is not an elementary light scalar, but is instead a bound state of a strongly interacting new sector. The lack of experimental evidence for such a sector so far points to a scale of compositeness above the TeV. In order for it to be lighter than this scale, the Higgs is predicted as a pseudo-Nambu Goldstone boson (pNGB) arising from a spontaneously broken continuous symmetry of this sector.

Considering the Higgs as a pNGB is quite an alluring idea since it finds a clear analogy within the SM. At low energies, the pion seems to be a light elementary scalar and would therefore suffer from a

hierarchy problem. However, at smaller distances we find out that the pion is in fact a composite particle which can be seen as a pNGB arising from the chiral symmetry breaking.

In general, from the Goldstone theorem [89], a spontaneously broken continuous symmetry $\mathcal{G} \to \mathcal{H}$, where $\mathcal{H}$ is a subgroup of $\mathcal{G}$, implies the existence of massless scalars, the Nambu-Goldstone bosons (NGBs). These NGBs parametrize the degenerate vacua of the SSB and as such, each NGB is associated with a broken generator of the coset $\mathcal{G}/\mathcal{H}$ resulting in $n = \dim(\mathcal{G}) - \dim(\mathcal{H})$ NGBs. For the Higgs boson to be explained through this mechanism, the coset $\mathcal{G}/\mathcal{H}$ must include at least 4 NGBs which must form a doublet under $SU(2)$.

If part of the original symmetry is local, the NGBs can be removed with the appropriate field redefinitions, giving mass to the gauge bosons associated with the broken generators. This process was already seen in the SM electroweak (EW) transition, in which the SSB $SU(2)_L \times U(1)_Y \to U(1)_{\text{em}}$ originated 3 NGBs which became the longitudinal degrees of freedom of the W^+, W^- and Z bosons. In general, taking $\tilde{\mathcal{G}}$ as the gauged subgroup of $\mathcal{G}$ and $\tilde{\mathcal{H}}$ as the gauged subgroup of $\mathcal{H}$, $n_g = \dim(\tilde{\mathcal{G}}) - \dim(\tilde{\mathcal{H}})$ NGBs are therefore unphysical and $n - n_g$ remain in the theory. The effective description of NGBs arising from SSB follows from employing the Callan-Coleman-Wess-Zumino formalism [90, 91].

The NGBs have an exact shift-symmetry [9, 92] which implies that another ingredient is needed to describe the SM Higgs, which has shift-breaking couplings such as a mass, a quartic coupling and Yukawa terms. Indeed, in order to explain the Higgs boson as arising from a SSB, the symmetry must be explicitly broken so that terms breaking the shift-symmetry can be generated. In this case the NGBs are actually called *pseudo-Nambu Goldstone bosons* (pNGBs) as they arise from an approximate symmetry. There are different strategies on how to explicitly break the symmetry and in this section we will go over the collective symmetry breaking mechanism, which is at the heart of Little Higgs models [93, 94].

Collective symmetry breaking was proposed as a method to explicitly break the symmetry such that the common quadratic divergences that generate a mass to the Higgs boson are actually alleviated to logarithmic divergences. This mechanism naturally accounts for a separation between the EW scale and the compositeness scale and allows for heavier fields to be responsible for generating the Higgs mass than in typical CHM scenarios. Note that when we mention quadratic or logarithmic divergences we are following the nomenclature usually used in the literature which is commonly working with the cut-off regulator scheme. Statements about these divergences are not scheme-dependent and within dimensional regularization with the $\overline{\text{MS}}$ scheme (where divergences are subtracted by appropriate counterterms), we obtain quadratic or logarithmic dependences on the masses of the heavy particles contributing to the Higgs mass, as we saw in Eq. (2.22).

3.1.1 Collective symmetry breaking

Let us introduce the mechanism of collective symmetry breaking through a toy model [92, 95]. Consider the spontaneous symmetry breaking pattern $SU(3) \times SU(3) \to SU(2) \times SU(2)$, which gives rise to 10 NGBs. The SSB is triggered by two fields, ϕ_1 and ϕ_2, which acquire a vev, each responsible for one

of the $SU(3) \longrightarrow SU(2)$ breakings. The fields can be parametrized as

$$\phi_1 = e^{\Pi_1/f} \begin{pmatrix} 0 \\ 0 \\ f \end{pmatrix}, \qquad \phi_2 = e^{\Pi_2/f} \begin{pmatrix} 0 \\ 0 \\ f \end{pmatrix}, \tag{3.1}$$

where the Goldstone matrices are given by $\Pi_{1,2} \equiv \pi^a_{1,2} T^a$ where π^a are the NGBs and T^a the broken generators of the SSB, and f is the magnitude of both vevs, which, for simplicity, we assumed to be aligned. Both Goldstone matrices will include a complex doublet under $SU(2)$, h, which we will indentify with the Higgs:

$$\Pi_i = \begin{pmatrix} \mathbf{0}_{2\times 2} & h \\ h^\dagger & 0 \end{pmatrix}, \tag{3.2}$$

where $i = 1, 2$. We neglected the remaining 6 NGBs since they will either become the longitudinal degree of freedom of massive gauge bosons or are simply not relevant for the analysis.

The symmetry is explicitly broken by gauging the diagonal subgroup of $SU(3) \times SU(3)$, $SU(3)_D$. The corresponding NGB Lagrangian is given by:

$$\mathcal{L} = |D_\mu \phi_1|^2 + |D_\mu \phi_2|^2, \tag{3.3}$$

such that the gauge interactions between two gauge bosons and two scalar fields are given by

$$\mathcal{L} \supset |g_1 X_\mu \phi_1|^2 + |g_2 X_\mu \phi_2|^2, \tag{3.4}$$

where X_μ corresponds to the $SU(3)_D$ gauge bosons. Under a generic transformation of this symmetry, $U = e^{\alpha^a T^a}$, the fields transform as [95]:

$$\phi_1 \longrightarrow e^{i\alpha_1^a T^a} \phi_1 \qquad \phi_2 \longrightarrow e^{i\alpha_2^a T^a} \phi_2 \qquad X_\mu \longrightarrow e^{-i\alpha^a T^a} X_\mu e^{i\alpha^a T^a}, \tag{3.5}$$

which leaves the Lagrangian (3.3) invariant when $\alpha_1^a = \alpha_2^a = \alpha^a$, as expected.

Let us now consider a scenario in which the second term in (3.4) does not exist, that is $g_2 = 0$. In this case, we must have $\alpha_1^a = \alpha^a$ in order to keep the Lagrangian invariant; however, ϕ_2 is free to transform with a different α_2^a. As such, the theory still possesses an $SU(3) \times SU(3)$ symmetry which has not been explicitly broken. Indeed, each of the terms in (3.3) conserves by itself $SU(3) \times SU(3)$. Only when *both* terms exist, $g_1 \neq 0$ and $g_2 \neq 0$, is the original symmetry actually explicitly broken to $SU(3)_D$, since in that case ϕ_1 and ϕ_2 must rotate with the same angle $\alpha_1^a = \alpha_2^a = \alpha^a$. The mechanism through which more than one coupling is needed in order to explicitly break a symmetry is called *collective symmetry breaking* (CSB).

Due to the CSB, any contribution to the mass of the pNGBs must therefore be proportional to both g_1 and g_2. Diagrammatically, this results in one extra propagator, which generates a logarithmically divergent contribution at one-loop. This can be seen from the diagram in figure 2. Simply from dimensional

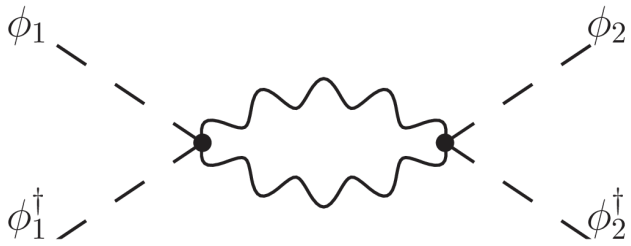

Figure 2: Diagram contributing to the pNGB mass term in collective symmetry breaking; see text for details.

analysis this can also be predicted: since any contribution must be proportional to both couplings, it must be contribution to the quartic coupling involving both fields, $|\phi_1^\dagger \phi_2|^2$, which when expanded gives $|\phi_1^\dagger \phi_2|^2 = f^4 - 2f^2 h^\dagger h + \cdots$. Any contribution to this quantity must be dimensionless and therefore, at most it can be logarithmically divergent.

The CSB method can also be applied in the fermionic sector, by embedding the SM doublet Q_L and an additional top partner, T, in a $\mathbf{3}$ of $SU(3)_D$, $\Psi = (t_L, b_L, T)$. Including also two right-handed fermions $t_{1,2}$, singlets of $SU(3)_D$, we can write the fermionic Lagrangian as

$$\mathcal{L}^{fermionic} = \lambda_1 \overline{\Psi} \phi_1 t_1 + \lambda_2 \overline{\Psi} \phi_2 t_2 + \text{h.c.}\,. \tag{3.6}$$

After expanding $\phi_{1,2}$, a combination of t_1 and t_2 will give rise to the SM right-handed top quark and another combination will correspond to the right-handed counterpart of the top partner.

Following the same reasoning as in the gauge sector, in order to explicitly break the $SU(3) \times SU(3)$ symmetry, both λ_1 and λ_2 must be non-zero. Otherwise, if λ_1 (λ_2) is zero, then ϕ_2 (ϕ_1) would be able to rotate freely, resulting in an $SU(3) \times SU(3)$ symmetry. Therefore, any contribution to the pNGBs mass must once again be proportional to both couplings which generates a contribution at most logarithmically divergent; see figure 3.

3.1.2 Littlest Higgs

The Littlest Higgs model (LHM) is amongst the most economical and realistic applications of the CSB mechanism and therefore it has been widely studied in the literature [96–98]. This model predicts that the Higgs arises as a pNGB after the SSB $SU(5) \longrightarrow SO(5)$ at the scale $f \sim 1\,\text{TeV}$ after a field in the symmetric representation of $SU(5)$ develops a vev,

$$\Sigma_0 = f \begin{pmatrix} \mathbf{0}_{2\times 2} & 0 & \mathbf{1}_{2\times 2} \\ 0 & 1 & 0 \\ \mathbf{1}_{2\times 2} & 0 & \mathbf{0}_{2\times 2} \end{pmatrix}. \tag{3.7}$$

We parametrize the resulting 14 NGBs in a similar fashion to what was done before:

$$\Sigma(x) = e^{2i\Pi/f}\Sigma_0\,, \tag{3.8}$$

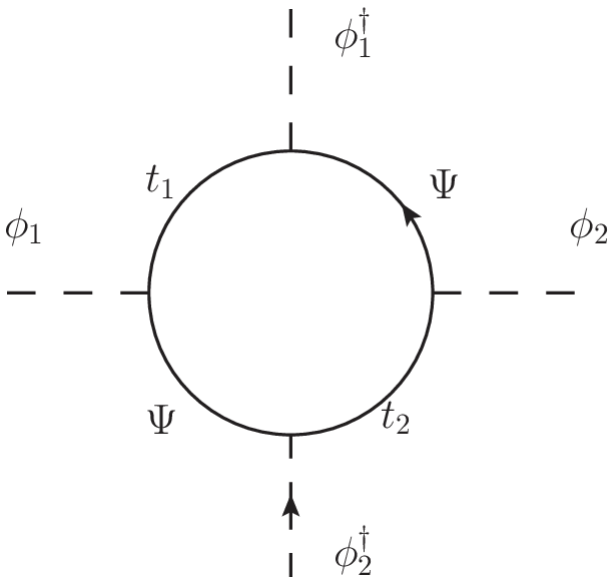

Figure 3: Diagram contributing to the pNGB mass term in the fermionic sector in collective symmetry breaking.

where $\Pi = \pi^a T^a$, π^a are the NGBs and T^a the associated broken generators of $SU(5)$.

The source of explicit symmetry breaking comes from the gauging of an $[SU(2) \times U(1)]^2$ subgroup of $SU(5)$, whose generators are given by

$$Q_1^a = \frac{1}{2}\begin{pmatrix} \sigma^a & 0 & 0 \\ 0 & 0 & 0 \\ 0 & 0 & \mathbf{0}_{2\times 2} \end{pmatrix}, \quad Y_1 = \frac{1}{10}\mathrm{diag}(3,3,-2,-2,-2)\,,$$
$$Q_2^a = \frac{1}{2}\begin{pmatrix} \mathbf{0}_{2\times 2} & 0 & 0 \\ 0 & 0 & 0 \\ 0 & 0 & -\sigma^{a*} \end{pmatrix}, \quad Y_2 = \frac{1}{10}\mathrm{diag}(2,2,2,-3,-3)\,, \tag{3.9}$$

where the subscripts 1 and 2 denote each of the gauged $SU(2) \times U(1)$.

The spontaneous breaking induced by the vev of Eq. (3.7) results in the breaking of the gauged group to a single copy of $SU(2) \times U(1)$. One combination of the $[SU(2) \times U(1)]^2$ will belong to the set of unbroken generators and its corresponding gauge bosons will be identified with the SM ones; another combination will be found within the set of broken generators and the corresponding gauge bosons will *eat* 4 of the NGBs becoming massive. The gauge bosons resulting from these combinations can be written as:

$$\begin{pmatrix} W_\mu \\ W'_\mu \end{pmatrix} = \begin{pmatrix} \cos\alpha & -\sin\alpha \\ \sin\alpha & \cos\alpha \end{pmatrix}\begin{pmatrix} W_\mu^1 \\ W_\mu^2 \end{pmatrix}, \begin{pmatrix} B_\mu \\ B'_\mu \end{pmatrix} = \begin{pmatrix} \cos\alpha' & -\sin\alpha' \\ \sin\alpha' & \cos\alpha' \end{pmatrix}\begin{pmatrix} B_\mu^1 \\ B_\mu^2 \end{pmatrix}, \tag{3.10}$$

where $\tan\alpha' = g'_2/g'_1$ and $\tan\alpha = g_2/g_1$ with g_1 and g_2 corresponding to the gauge couplings of $SU(2)_1$ and $SU(2)_2$ respectively and g'_1 and g'_2 corresponding to the gauge couplings of $U(1)_1$ and $U(1)_2$. The combinations W_μ and B_μ are the SM gauge bosons, whereas W'_μ and B'_μ are the heavy gauge bosons.

Finally, the NGBs matrix is given by:

$$\Pi = \begin{pmatrix} -\frac{\omega^0}{2} - \frac{\eta}{\sqrt{20}} & -\frac{\omega^+}{\sqrt{2}} & -i\frac{\pi^+}{\sqrt{2}} & -i\Phi^{++} & -i\frac{\Phi^+}{\sqrt{2}} \\ -\frac{\omega^-}{\sqrt{2}} & \frac{\omega^0}{2} - \frac{\eta}{\sqrt{20}} & \frac{v+h+i\pi^0}{2} & -i\frac{\Phi^+}{\sqrt{2}} & \frac{-i\Phi^0+\Phi^P}{\sqrt{2}} \\ i\frac{\pi^-}{\sqrt{2}} & \frac{v+h-i\pi^0}{2} & \sqrt{\frac{4}{5}}\eta & -i\frac{\pi^+}{\sqrt{2}} & \frac{v+h+i\pi^0}{2} \\ i\Phi^{--} & i\frac{\Phi^-}{\sqrt{2}} & i\frac{\pi^-}{\sqrt{2}} & -\frac{\omega^0}{2} - \frac{\eta}{\sqrt{20}} & -\frac{\omega^-}{\sqrt{2}} \\ i\frac{\Phi^-}{\sqrt{2}} & \frac{i\Phi^0+\Phi^P}{\sqrt{2}} & \frac{v+h-i\pi^0}{2} & -\frac{\omega^+}{\sqrt{2}} & \frac{\omega^0}{2} - \frac{\eta}{\sqrt{20}} \end{pmatrix}, \tag{3.11}$$

where $\phi = (-i\pi^+, (v + h + i\pi^0)/\sqrt{2})^T$ is the SM Higgs and Φ is an $SU(2)_L$ triplet. These pNGBs remain in the physical spectrum of the theory, whereas $\omega^\pm$, ω_0 and η become the longitudinal degrees of freedom of the heavy gauge bosons.

The presence of CSB can be seen through the way the $[SU(2) \times U(1)]^2$ generators are embedded in $SU(5)$. If we take $g_2 = g_2' = 0$ ($g_1 = g_1' = 0$), then the generators Q_1^a (Q_2^a) and Y_1 (Y_2) will commute with an $SU(3)$ group embedded in the lower right (upper left) corner of an $SU(5)$ matrix. That is, if only one of the copies of $SU(2) \times U(1)$ is gauged, then an $SU(3) \times SU(2) \times U(1)$ symmetry remains unbroken which prevents the generation of the Higgs mass. Only when all gauge couplings are taken to be non-zero is the symmetry explicitly broken to $SU(2) \times U(1)$, allowing a mass generation to the Higgs boson.

3.1.3 Littlest Higgs model with T-parity

Despite its success in explaining a light Higgs boson, the LHM introduces several problems when compared with experimental data [97–99]. In particular, the tree-level exchange of the heavy gauge bosons generates 4-fermion operators, constrained by LEP data, and also modifies the couplings of the Higgs boson to SM fermions. Furthermore, this tree-level exchange of heavy gauge bosons as well as a non-zero vev of the triplet pNGB, Φ, contribute to electroweak precision observables (EWPO). All things considered, Ref. [98] found that the scale f had to be $\geq 4\,\mathrm{TeV}$ which would still demand a significant fine-tuning to account for a light Higgs, going directly against the main motivation of these models.

In order to avoid these tree-level contributions, an additional discrete symmetry can be added to the theory, known as T-parity [100–102]. The Littlest Higgs with T-parity (LHT) is therefore endowed with a symmetry under which most of the new particles are T-odd. This T-transformation will act as an automorphism between the two copies of $SU(2) \times U(1)$ such that:

$$G_1 \overset{\mathrm{T}}{\longleftrightarrow} G_2 \,. \tag{3.12}$$

For the gauge sector to be T-even, the gauge couplings must therefore be the same $g_1 = g_2 = g$ and $g_1' = g_2' = g'$. From Eq. (3.10) this results in:

$$W^\pm = \frac{W_1 \pm W_2}{\sqrt{2}}\,, \quad B^\pm = \frac{B_1 \pm B_2}{\sqrt{2}}\,, \tag{3.13}$$

where the W^+ and B^+ are T-even and correspond to the SM gauge bosons, whereas W^- and B^- are T-odd. We relabel the latter to W_H and B_H to refer to the fact that they must be heavy in comparison with the former T-even combination. Invariance under T-parity forbids tree-level exchange of a heavy gauge boson (T-odd) by external SM particles (T-even), therefore relaxing the main constraints on the LHM. Any contribution of the heavy gauge bosons to electroweak precision observables (EWPO) can only occur at loop-level.

On the other hand, the Goldstone matrix can be taken to transform as:

$$\Pi \xrightarrow{\mathrm{T}} -\Omega\Pi\Omega \tag{3.14}$$

where $\Omega = \mathrm{diag}(-1,-1,1,-1,-1)$. This ensures that the Higgs boson is T-even, whereas the pNGB triplet, Φ, is T-odd. Consequently, the trilinear coupling $H^\dagger\Phi H$ is forbidden, preventing the triplet from acquiring a vev.

Upon EWSB, when the Higgs acquires a vev, the heavy gauge bosons in their mass basis are given by:

$$W_H^\pm = \frac{1}{\sqrt{2}}\left(W_H^1 \mp iW_H^2\right), \quad \begin{pmatrix} Z_H \\ A_H \end{pmatrix} = \begin{pmatrix} 1 & -x_H\frac{v^2}{f^2} \\ x_H\frac{v^2}{f^2} & 1 \end{pmatrix}\begin{pmatrix} W_H^3 \\ B_H \end{pmatrix}, \tag{3.15}$$

where

$$x_H = \frac{5gg'}{4\left(5g^2 - g'^2\right)}. \tag{3.16}$$

Their masses are [103, 104]:

$$M_{W_H} = M_{Z_H} = gf\left[1 - \left(\frac{v}{f}\right)^2\right], \tag{3.17}$$

$$M_{A_H} = \frac{g'}{\sqrt{5}}f\left[1 - \frac{5}{8}\left(\frac{v}{f}\right)^2\right]. \tag{3.18}$$

For the light gauge bosons, EWSB follows the same procedure as in the SM. Note that A_H is the lightest T-odd particle (LTP) introduced in the LHT [103, 105, 106] and it is therefore stable, resulting in a MET signature at colliders. This is relevant since the decay of all T-odd particles follows a chain which always ends up in the LTP, A_H, and SM particles. Furthermore, given that A_H is neutral, it is also a viable dark matter candidate. In section 3.2.5 we will study this possibility.

In order to implement T-parity in the fermionic sector we introduce two doublets ψ_1 (a doublet of $SU(2)_1$) and ψ_2 (a doublet of $SU(2)_2$) for each SM fermionic doublet. ψ_1 and ψ_2 are then embedded in incomplete $SU(5)$ multiplets

$$\Psi_1 = \begin{pmatrix} \psi_{1L} \\ 0 \\ 0 \end{pmatrix} \qquad \text{and} \qquad \Psi_2 = \begin{pmatrix} 0 \\ 0 \\ \psi_{2L} \end{pmatrix}. \tag{3.19}$$

Under T-parity, these multiplets transform as

$$\Psi_1 \xleftrightarrow{\mathrm{T}} \Omega\Sigma_0\Psi_2\,, \tag{3.20}$$

where $\Psi_1 + \Omega\Sigma_0\Psi_2$ is T-even and can therefore be recognized as a SM doublet and $\Psi_1 - \Omega\Sigma_0\Psi_2$ is T-odd and is identified with the LH component of a new particle. In order to give a mass to these heavy doublets we introduce the RH components which will also transform as a doublet under $SU(2)$ giving rise to vector-like fermions. The RH must be included in a complete multiplet, Ψ_R, which will result in the introduction of other fields. Details on the phenomenological effects of these extra fields and on the remaining pieces of the LHT Lagrangian can be found in Refs. [104, 107–109]. While important to understand the complete framework of the model, these details will not be relevant for the analysis which we aim to perform in this work.

The heavy femions acquire their mass through the Lagrangian

$$\mathcal{L}^{\mathrm{k}} = -kf\left(\overline{\Psi}_2\xi + \overline{\Psi}_1\Sigma_0\xi^\dagger\right)\Psi_R + \mathrm{h.c.}\,, \tag{3.21}$$

where $\xi = e^{i\Pi/f}$ and transforms under T-parity as $\xi \longrightarrow \Omega\xi^\dagger\Omega$. The mass of the heavy T-odd vector-like fermions is given by $m_{\psi_H} = \sqrt{2}kf$ [104, 108]. Note that k is not necessarily universal and can in principle have flavour indices [104].

Within the fermionic sector, CSB is only included for the top quark. This is done by including yet another pair of heavy fermions, T_1 and T_2, and including them in the original $\Psi_{1,2}$ of Eq. (3.19) such that

$$\Psi_1 = \begin{pmatrix} q_{1L} \\ T_1 \\ 0 \end{pmatrix} \qquad \text{and} \qquad \Psi_2 = \begin{pmatrix} 0 \\ T_2 \\ q_{2L} \end{pmatrix}. \tag{3.22}$$

The Lagrangian responsible for the mass generation of the remaning fermions is given by

$$\begin{aligned}\mathcal{L}_Y =& \frac{i\lambda_1}{2\sqrt{2}} f\epsilon^{xyz}\epsilon^{rs}\left[(\overline{\Psi_1})_x(\Sigma)_{ry}(\Sigma)_{sz} + (\overline{\Psi_2}\Sigma_0\Omega)_x(\widetilde{\Sigma})_{ry}(\widetilde{\Sigma})_{sz}\right] t_R \\ &+ \lambda_2 f\left(\overline{T_{1L}}T_{1_R} + \overline{T_{2L}}T_{2_R}\right)\mathrm{h.c.}\,,\end{aligned} \tag{3.23}$$

where $\Sigma \xrightarrow{\mathrm{T}} \widetilde{\Sigma} = \Omega\Sigma_0\Sigma^\dagger\Sigma_0\Omega$ and x, y, z and r, s sum over the indices $\{3, 4, 5\}$ and $\{1, 2\}$ respectively. The terms in Eq. (3.23) exist for all SM fermions except for the term proportional to λ_2 which is only present for the top sector to introduce CSB. If only λ_2 is non-zero the Higgs is decoupled from the top-sector; if λ_1 is the only non-zero coupling, a $SU(3)$ symmetry remains which would protect the Higgs mass.

3.2 Vector-like leptons with exotic decays

The LHT introduced several new particles, providing a rich phenomenological landscape. Amid the expected signatures, vector-like fermions (VLFs) are among the most interesting as they are prevalent in

many other CHMs realizations. For instance, in partial compositeness, the main source of explicit symmetry breaking arises from linear couplings between the SM fermions and heavy vector-like fermionic partners which are therefore crucial in generating the Higgs mass and Yukawa terms [110].

Furthermore, new heavy fermions are well motivated from a phenomenological perspective as they can function as mediators between the SM and a dark sector [111, 112]; they can help explain the anomalous magnetic moment of the muon [113, 114]; they can be related with explanations of LFUV anomalies [115–117] or of the mass generation of neutrinos [118, 119], etc.

For these reasons, the phenomenological implications of VLFs have been studied in the literature, with a particular focus on vector-like quarks (VLQs) which can be strongly produced at proton-proton colliders. On the other hand, VLLs have received much less attention due to their lower cross-section through electroweak pair production. Moreover, their mixing with the SM leptons is constrained by EWPO [120, 121], reducing the possibility of sizable single-production at colliders. This has resulted in modest limits obtained for VLLs [122–126] (when compared with VLQs), which is why we will focus on developing a strategy to probe VLLs at current and future collider experiments.

Within currently available experimental searches for VLLs, these have always been assumed to decay to SM final states through a mixing term between the VLL and a SM lepton. However, this is not always the case as, when considering the VLL as part of a fully-fledged model, other predicted BSM states can drastically change its phenomenology. As we saw in the LHT, T-parity actually forbids VLLs from decaying solely to SM particles; instead, VLLs decay to the neutral heavy gauge boson, A_H, and a SM lepton. Taking A_H as the lightest T-odd particle, the pair-production of VLLs results in a signature of MET and 2 SM leptons, similarly to what happens in slepton pair-production [127] (up to the spin of the particles involved).

More interestingly, in this section we develop a strategy which expands upon these scenarios to consider a phenomenological setup in which VLLs decay with arbitrary branching ratios (BRs) to $W\nu_\ell$, $Z\ell$, $H\ell$ and $A_H\ell$, where $\ell = e, \mu$. This general scenario has not been studied in the past from the collider point of view and is well motivated by LHT with T-parity violation [108, 128, 129] or FIMP DM models [112]. Nonetheless, given that the results can be presented as a function of arbitrary branching ratios, the original limiting scenarios such as the SM decaying VLL or the LHT VLL can be easily recovered.

Furthermore, if A_H has a lifetime larger than the age of the Universe (besides being stable at detector scales) it is a viable dark matter candidate. This is exactly the case of the LHT, in which A_H is stabilized through T-parity. As such, we will also explore this scenario, studying the complementarity between astrophysical bounds from DM experiments and collider searches.

3.2.1 Setup

The generic setup consists of a VLL singlet[1] with electric charge -1, $E_{L,R}$, and mass M_E, and a massive vector boson A_H^μ, which is taken to be stable at detector scales with mass $M_{A_H} < M_E$, so that the decay

[1] As will be noted in the section 3.2.4, results are easily applied to a doublet.

of E into A_H and a SM lepton is kinematically possible.

To show that arbitrary branching ratios can arise, an explicit realization of our model is given in Appendix A – details are, however, not relevant for the collider analysis. We will assume that E decays are given by the branching ratios $\mathrm{BR}(E \to \ell H)$, $\mathrm{BR}(E \to \nu_\ell W)$, $\mathrm{BR}(E \to \ell Z)$ and $\mathrm{BR}(E \to \ell A_H)$, where ℓ stands for either electron or muon[2]. These 4 BRs add to unity but are otherwise arbitrary; decays into SM particles are usually taken to be fixed by the quantum numbers of the VLL but mixing between heavy states can lead to different decay patterns [133].

We consider Drell-Yan pair production of E. From the possible decay channels, the easiest to detect are $E \to \ell Z$ and $E \to \ell A_H$. The decay into $\nu_\ell W$ is challenging to distinguish from the overwhelming W + jets background whereas the one into ℓH suffers from similarly overwhelming backgrounds (and a small BR of the Higgs to easy to detect final states). Thus, we will focus on the cleaner channels $\mathrm{BR}(E \to \ell Z)$ and $\mathrm{BR}(E \to \ell A_H)$; regardless we will show that our results are mostly insensitive to the two extra BRs.

There are experimental analyses sensitive to these discovery channels: searches for VLLs which decay into ℓZ [124] and slepton searches [127]. We need to recast both since they do not account for the contamination of the other decay channels in our general setup. We will also update the analysis to ℓZ to take advantage of the current higher center of mass energy.

3.2.2 Recasting existing analyses

Given that we aim to interpolate between the cases in which the VLL decays 100% of the time through the MET channel or 100% to SM final states, our starting point is to reproduce searches for these two limiting scenarios. For event simulation we follow the approach introduced in section 2.4.2. The VLL model is implemented in `FeynRules` [76] and event generation (at leading order) is performed with `MadGraph5_aMC@NLO` [78] using the `NNPDF23LO` [134] parton distribution functions. Due to the large statistics required for these analysis, we perform cuts at the level of generation. These cuts (which are always mentioned along the text) were tested to verify their minimal impact on the final yield of events after the selection cuts. Showering and hadronization are done using `Pythia8` [79], while the detector response is simulated with `Delphes 3` [80]. The default CMS detector card is used for the LHC analysis and the HL-LHC detector card for the $\sqrt{s} = 27\,\mathrm{TeV}$. The 95% C.L. limits are calculated following the CL_s [81] method using `OpTHyLic` [82].

3.2.2.1 Decays into SM particles

To explore the limiting case of a VLL decaying only to SM particles we reproduce the analysis in Ref. [135], an ATLAS analysis performed at $\sqrt{s} = 8$ TeV and an integrated luminosity of $\mathcal{L} = 20.3\ \mathrm{fb}^{-1}$, searching for a multi-lepton final state arising from a singlet VLL decaying to $Z\ell$. The production and

[2] Decays to SM final states with taus have been considered in [130–132].

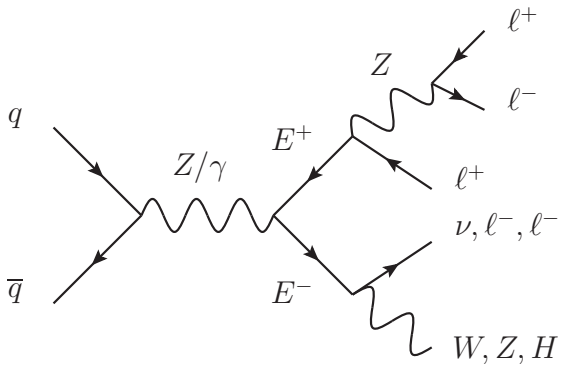

Figure 4: Drell-Yan pair production of E (VLL singlet) and the corresponding decay channels.

decay processes are shown in figure 4. The strategy which the analysis follows is to select 2 opposite sign same flavour (OSSF) leptons that reconstruct a Z boson and a third lepton with a $\Delta R < 3$ away from the reconstructed Z boson. We will call this third lepton, which respects the ΔR condition, the off-Z lepton. The description of all considered cuts and the corresponding efficiencies are presented in table 3.

The discriminant variable is chosen to be $\Delta m = m_{3\ell} - m_{\ell\ell}$, where $m_{\ell\ell}$, the mass of the reconstructed Z boson, is subtracted from $m_{3\ell}$, the invariant mass of the 3-lepton system. Moreover, signal events will be distinguished in 3 exclusive signal regions:

- 4-lepton (4ℓ) region, in case the event has at least 4 identified leptons;
- 3-lepton + jj ($3\ell + jj$) region, when precisely 3 leptons are identified together with 2 jets, j, with an invariant mass, m_{jj}, which respect $m_W - 20\ \text{GeV} < m_{jj} < 150\ \text{GeV}$, where m_W is the W boson mass;
- 3-lepton (3ℓ) only region, for events in which exactly 3 leptons are identified but which do not fit in the previous criteria.

The analysis is performed separately for a VLL coupling to first or second generation leptons which corresponds to the off-Z lepton being either an electron or a muon. The most important backgrounds to consider are ZZ, WZ and $Z\gamma$, for which the simulation accurately reproduces the shape presented by the

Selection Cuts	ZZ	WZ	$Z\gamma$
OSSF lepton pair with $\lvert m_{\ell\ell} - m_Z \rvert < 10$ GeV	0.25	0.19	0.0024
$p_T^{\ell_1} > 26$ GeV	0.25	0.19	0.0023
$\Delta R(Z, \text{off}{-}Z \text{ lepton}) < 3$	0.17	0.11	0.0008

Table 3: Cumulative efficiencies of the selection cuts when applied to the background events for the analysis done at $\sqrt{s} = 8$ TeV. Efficiencies are defined as the number of events selected over the initial number of events.

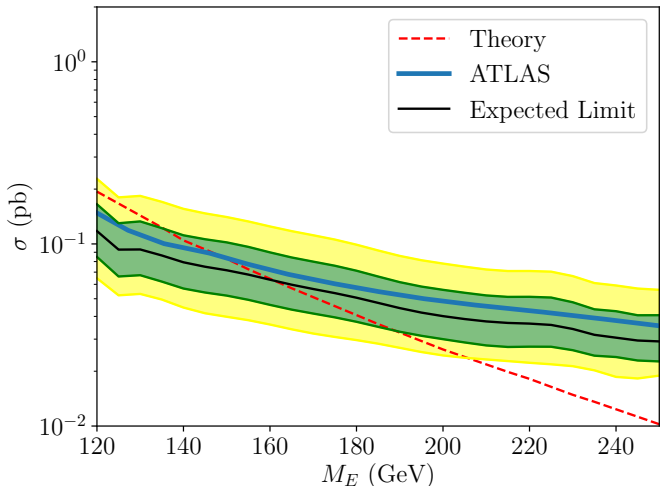

Figure 5: Comparison between the recast of the VLL search and the ATLAS collaboration results. We show the case of an electron off-Z lepton, with the 1 (green) and 2 (yellow) sigma exclusion region from our simulation and the expected limit quoted by the ATLAS analysis (solid blue line) and the theoretical pair production cross section in the dashed red line.

Selection cuts	ZZ A	ZZ B	ZZ C	WZ A	WZ B	WZ C	$Z\gamma$ ($\times 10^{-2}$) A	$Z\gamma$ ($\times 10^{-2}$) B	$Z\gamma$ ($\times 10^{-2}$) C
OSSF lepton pair with $\lvert m_{\ell\ell} - m_Z \rvert < 10$ GeV	0.25	0.25	0.25	0.18	0.18	0.18	0.48	0.48	0.48
$\Delta R(Z, \text{off}{-}Z \text{ lepton}) < 3$	0.16	0.16	0.16	0.10	0.10	0.10	0.14	0.14	0.14
$p_T^{\ell_1} > \{80,\ 100,\ 120\}$	0.054	0.029	0.0098	0.029	0.015	0.0052	0.05	0.02	0.01
$p_T^{\ell_2} > \{20,\ 40,\ 60\}$	0.054	0.025	0.0073	0.029	0.012	0.0035	0.05	0.02	0.01
$p_T^{\ell_3} > \{0,\ 0,\ 20\}$	0.054	0.025	0.0067	0.029	0.012	0.0031	0.05	0.02	<0.01
off-Z lepton = e	0.029	0.013	0.0034	0.013	0.0053	0.0014	0.03	0.01	<0.01
$m_T < 160$ GeV $(3ljj)$	0.0079	0.0043	0.0014	0.0013	0.0009	0.0004	0.01	0.01	<0.01

Table 4: Cumulative efficiencies of the selection cuts when applied to background events for the new analysis performed at $\sqrt{s} = 13$ TeV. Efficiencies are defined as the number of events selected over the initial number of events. The regions denoted by $\{A, B, C\}$ correspond to different values of the mass of the VLL, $\{M_{\rm E} < 300,\ 300 \leq M_{\rm E} < 400,\ M_{\rm E} \geq 400\}$, in GeV.

ATLAS collaboration. The simulated backgrounds are normalized to the values quoted in the experimental publication, which amounts to applying a factor between 1.4 and 3.5, which depends on the signal region and that includes the corresponding K-factor to account for the NLO cross-section considered in the original analysis. In figure 5 we show the comparison of our 1- and 2-sigma exclusion plot with the expected limit quoted by the ATLAS collaboration, together with the pair production cross-section of the VLL. This result is shown for an electron as the off-Z lepton, but the result for the muon case is very similar. The resulting limit on the VLL mass of $M_{\rm E} \gtrsim 160$ GeV represents a difference of $\sim 7\%$ when compared with the one obtained in the original analysis.

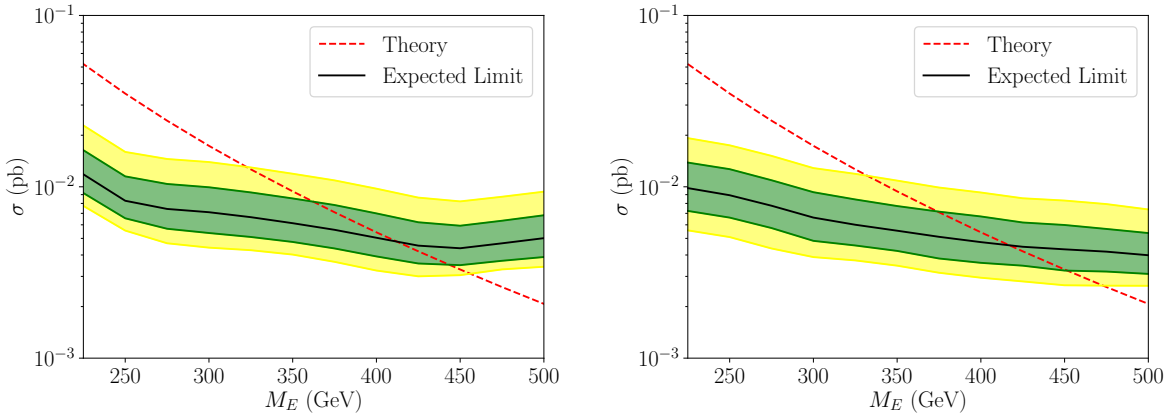

Figure 6: Limits on the mass of a VLL singlet decaying into electrons (muons) on the left (right) panel at $\sqrt{s} = 13$ TeV and an integrated luminosity of 139 fb^{-1} following the improved analysis. We present the 1 (green) and 2 (yellow) sigma exclusion regions and the theoretical pair production cross-section in the dashed red line.

To study the limits obtained with current data, at $\sqrt{s} = 13$ TeV and $\mathcal{L} = 139$ fb^{-1}, we should take advantage of the higher center of mass energy to impose more stringent cuts, particularly on the transverse momentum of the identified leptons. Because the p_T of the identified leptons in signal events increases as the VLL mass increases, we have defined 3 clusters of masses to vary the selection threshold for p_T of observed leptons. These are presented in table 4 as well as the efficiencies of all selection cuts. Following these more stringent selections, we also applied generation level cuts on the $Z\gamma$ background, simulating events in which the lepton with leading p_T respects $p_T > 62\,\text{GeV}$.

Furthermore, at these higher center of mass energies, almost the entirety of the WZ background can be removed by applying a cut on the transverse mass, m_T, of the reconstructed W boson. The effectiveness of this cut is a result of the fact that for events from $WZ \to \ell\nu\ell\ell$, the off-Z lepton is, in theory, coming from the W decay, whereas all the missing energy of the event, $\not{E}_T$, originates from the neutrino (again in theory). For events arising from the WZ background, we expect to have

$$m_T = \sqrt{2\left(\not{E}_T p_{T\ell} - \not{E}_{\mathbf{T}}.\mathbf{p}_{\mathbf{T}\ell}\right)} \leq m_W\,, \tag{3.24}$$

where $p_{T\ell}$ is the transverse momentum of the off-Z lepton. Therefore, the transverse mass calculated in this way should, in principle, be at most the mass of the W boson. To retain as many signal events as possible, this cut is only performed on the 3ℓ signal region, where most of WZ background lies. Figure 6 shows the limits obtained with this new analysis. Assuming that the expected background corresponds to observed data, one could probe a VLL with a mass up to 410 GeV (420 GeV) for the case in which the off-Z lepton is an electron (muon). Due to this similarity between the limits obtained for electron or muon off-Z lepton we will only consider the former case from now on.

Despite being developed for a singlet VLL, this analysis can be applied for an $SU(2)$ doublet, L, of hypercharge $-1/2$. In this scenario pair production of the neutral component, $p\ p \to NN$, and associated production of the neutral and charged components $p\ p \to E^{\pm}N$ are also relevant. In the limit

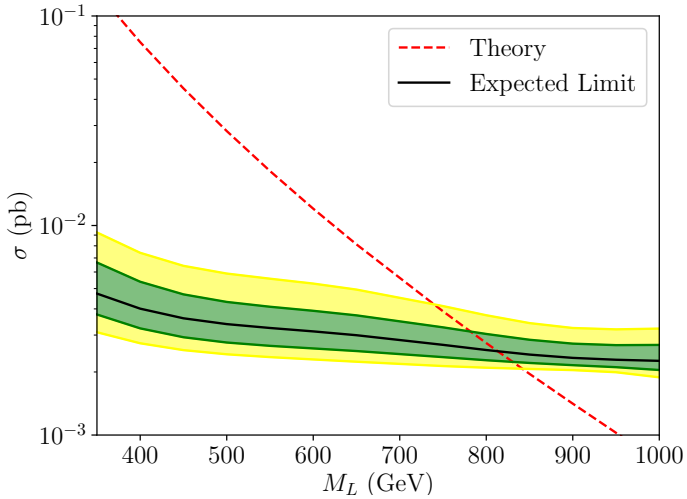

Figure 7: Limits on the mass of a VLL doublet decaying into electrons (or electron neutrinos) at $\sqrt{s} = 13$ TeV and an integrated luminosity of $139\ \mathrm{fb}^{-1}$ following our improved analysis. We present the 1 (green) and 2 (yellow) sigma exclusion regions and the theoretical pair production cross section in the dashed red line.

of large masses, and taking the neutral and charged components to have the same mass, the charged component decays with the same BR to ℓZ and ℓH, while the neutral one only decays to νW. Therefore, the relevant background remains the same and the analysis can be recast, resulting in the limits shown in figure 7. As expected by the larger cross-section, much more stringent bounds can be obtained when comparing with the singlet case, with masses up to ~ 820 GeV being excluded.

The CMS collaboration has performed an analysis searching for VLL doublets in Ref. [136] with an integrated luminosity $\mathcal{L} = 77\ \mathrm{fb}^{-1}$. The bound on $M_L \geq 790$ GeV was obtained in this analysis from the observed data, but the expected limit, which is the fair comparison to the bound we are able to compute, corresponded to $M_L^{\text{expected}} \geq 690$ GeV. Rescaling our results to the same integrated luminosity we find $M_L^{\mathcal{L}=77\ \mathrm{fb}^{-1}} \geq 730$ GeV, very close to the expected limit in the CMS search[3].

3.2.2.2 Decays with missing energy

For the case in which the VLL decays into a SM lepton and MET (originated by A_H in our case), we consider an ATLAS analysis [137] at $\sqrt{s} = 13$ TeV and an integrated luminosity of $\mathcal{L} = 36.1\ \mathrm{fb}^{-1}$ searching for pair produced sleptons. The analysis considers the sleptons decaying into a SM lepton and a neutralino, as shown in figure 8. The analysis strategy is to select events with 2 OSSF leptons (e, μ) with an invariant mass $m_{\ell\ell} > 40$ GeV. Several inclusive and exclusive signal regions are defined in which different requirements are chosen for $m_{\ell\ell}$ and the m_{T2} variable [138, 139]; m_{T2} is called the *stransverse mass* and is defined by

$$m_{T2} = \min_{\mathbf{q_T}} \left[\max(m_T(\mathbf{p_{T1}}, \mathbf{q_T}), m_T(\mathbf{p_{T2}}, \not{E}_\mathbf{T} - \mathbf{q_T}) \right], \tag{3.25}$$

[3]This analysis targeted tau decays meaning that the comparison between limits is not immediate.

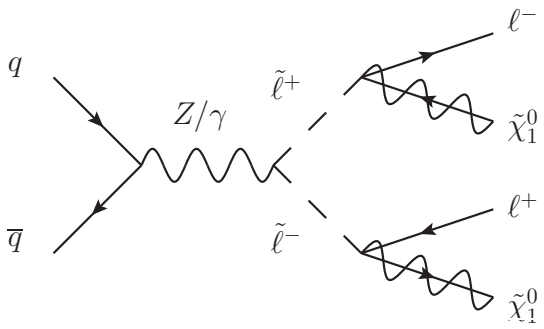

Figure 8: Pair production and subsequent decay of sleptons, where $\tilde{\ell}$ corresponds to the charged slepton and $\tilde{\chi}_1^0$ is the lightest neutralino.

Selection Cuts	ZZ	WZ	WW	$t\bar{t}$
OSSF lepton pair	0.33	0.33	0.23	0.53
$m_{\ell\ell} > 40$ GeV	0.31	0.28	0.11	0.53
$p_T^{\ell_1} > 25$ GeV	0.31	0.28	0.11	0.53
$p_T^{\ell_2} > 20$ GeV	0.28	0.26	0.095	0.51
$p_T^{b-jet} < 20$ GeV	0.24	0.24	0.093	0.13
$p_T^{jet} < 60$ GeV	0.15	0.14	0.081	0.061
$m_{T2} > 100$ GeV	0.0064	0.003	0.0002	0.0001
$m_{\ell\ell} > 110$ GeV	0.0016	0.001	0.0002	0.0001

Table 5: Cumulative efficiencies of the selection cuts when applied to the background events for the slepton search [137] done at $\sqrt{s} = 13$ TeV. Efficiencies are defined as the number of events selected over the initial number of events.

where $\mathbf{p_{T1,2}}$ denote the transverse momentum of each of the leptons and $\mathbf{q_T}$ is the vector that minimizes the maximum value of both transverse masses which are defined as

$$m_T(\mathbf{p_T}, \mathbf{q_T}) = \sqrt{2(p_T q_T - \mathbf{p_T q_T})}\,. \tag{3.26}$$

The most relevant backgrounds for this search are diboson processes (ZZ, WW and WZ) and $t\bar{t}$. To maximize the obtained statistics we require 2 leptons respecting $m_{\ell\ell} > 95$ GeV at the generator level in the final state during background simulation. The full set of selection cuts and their efficiencies are presented in table 5. We considered all signal regions of the original analysis to validate our results; however, new results are calculated considering only the signal region of $m_{\ell\ell} > 111$ GeV and $m_{T2} > 100$ GeV as we found the difference when considered all regions to not be significant.

For the validation of the analysis we implemented a slepton-neutralino model and fixed the neutralino mass to be $M_{\tilde{\chi}_1^0} = 1$ GeV. The obtained results are presented in figure 9, where we show a limit $M_{\tilde{\ell}} \geq 565$ GeV, similar to the expected limit obtained by the ATLAS collaboration, which was ~ 570 GeV.

Having validated the analysis, we can apply it to the VLL model. Unlike in the purely SM decays scenario, in this case we have an extra parameter in our analysis, the mass of the other new particle,

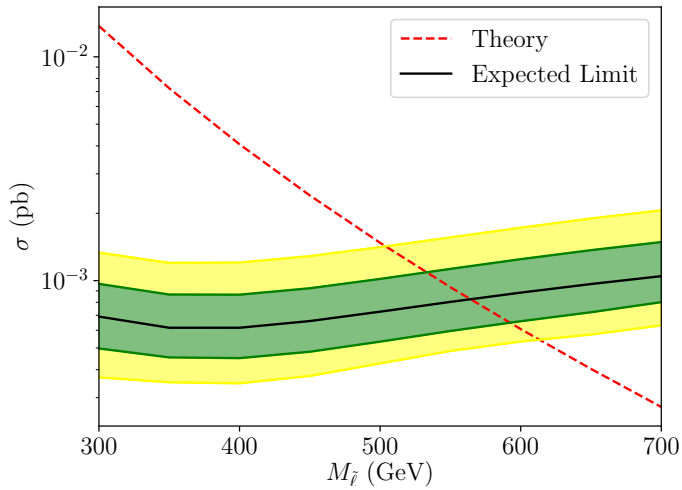

Figure 9: Obtained limit on the slepton mass, $M_{\tilde{\ell}}$, for a neutralino mass $M_{\tilde{\chi}_1^0} = 1$ GeV after recasting the analysis in [137]. We present the 1 (green) and 2 (yellow) sigma exclusion regions and the theoretical pair production cross section in the dashed red line.

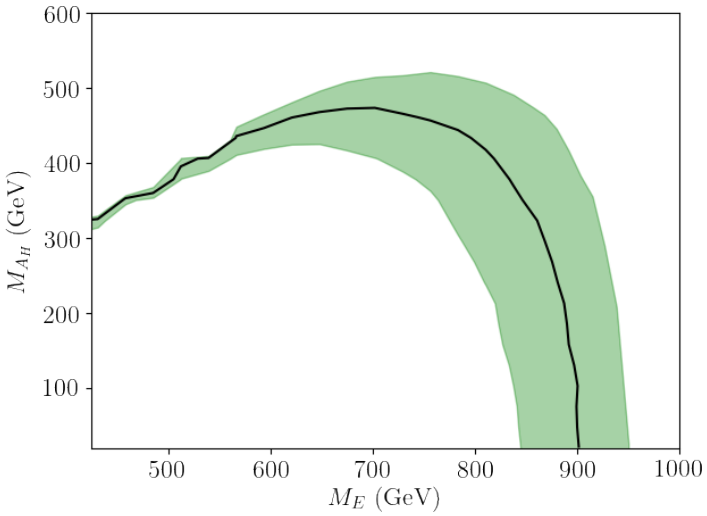

Figure 10: Limits in the $M_E - M_{A_H}$ plane from the analysis in [137]. The expected limit is given by the solid black line and green band is the 1-sigma exclusion limit.

M_{A_H}. Different models can predict different values; for instance, the LHT predicts it to be around the the EW scale, Eq. (3.18), whereas FIMP models require sub-GeV masses [112]. Therefore, for each mass point of the VLL, we vary M_{A_H} from 1 GeV up to the mass of the VLL. The obtained results are presented for $\sqrt{s} = 13$ TeV and an integrated luminosity $\mathcal{L} = 139$ fb^{-1} in figure 10. As expected, a lighter A_H results in final state leptons with larger p_T, which corresponds to points which can be better constrained. As the difference between the mass of the VLL and A_H decreases, final state leptons become softer and more difficult to identify. For $M_E \gtrsim 900$ GeV the production cross-section is too low to be constrained, regardless of M_{A_H}.

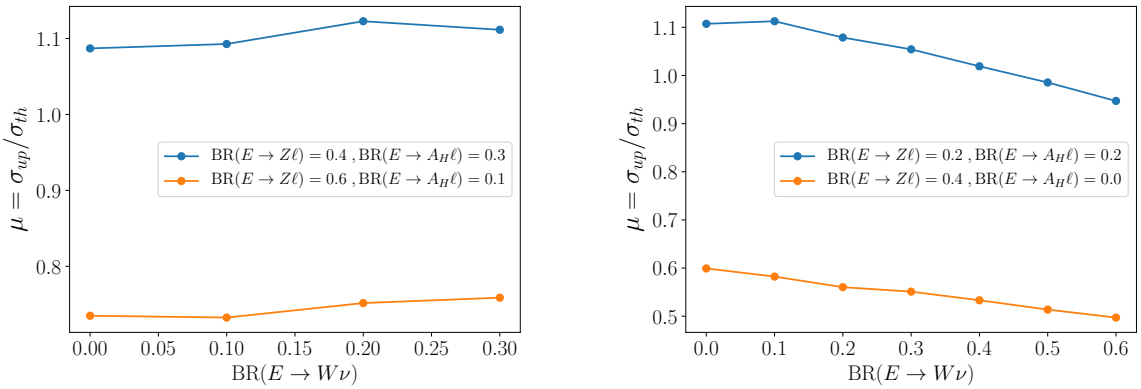

Figure 11: Dependence of the obtained signal strength, $\mu^{\text{up}} \equiv \sigma^{\text{up}}/\sigma^{\text{th}}$, on $\text{BR}(E \longrightarrow W\nu)$, varying the remaining parameters. The benchmark masses are $M_E = 500$ GeV and $M_{A_H} = 98$ GeV ($M_E = 400$ GeV and $M_{A_H} = 98$ GeV) for the left (right) panels.

3.2.3 Constraints on vector-like leptons with general decays

After verifying the accuracy of our analysis setup, we are now in a position to recast these searches for arbitrary branching fractions in the different channels. In order to avoid generating signal events for every combination of BRs, we apply a weight to each signal event according to its generator-level decay. Firstly, we generate a sample of pair-produced VLLs with $\text{BR}_g(E \longrightarrow A_H\ell) = \text{BR}_g(E \longrightarrow Z\ell) = \text{BR}_g(E \longrightarrow H\ell) = \text{BR}_g(E \longrightarrow W\nu) = 0.25$, where the g subscript describes the generated sample. To probe different BRs, each event is then weighted according to $\text{BR}_p^i/\text{BR}_g^i$, where the p subscript represents the probed BR and the i superscript corresponds to the specific decay – once again note that the particular decay of each event is determined at generator level and has nothing to do with the analysis itself at the detector level.

Depending on the particular value of the BR, either the SM decays analysis or the MET search can be more constraining. However, since these analysis target final states of ℓA_H or ℓZ, the results are presented in the $\text{BR}(E \longrightarrow A_H\ell)$ vs $\text{BR}(E \longrightarrow Z\ell)$ plane, while the other BRs are fixed to

$$\text{BR}_p(E \longrightarrow W\nu) = 2\text{BR}_p(E \longrightarrow H\ell) = \frac{2}{3}\left[1 - \text{BR}_p(E \longrightarrow A_H\ell) - \text{BR}_p(E \longrightarrow Z\ell)\right], \tag{3.27}$$

which corresponds to the large M_E limit for a singlet if $\text{BR}(E \longrightarrow A_H\ell) = 0$.

We verified that the obtained bounds are relatively insensitive to this latter choice. The dependence is mainly due to contamination between different channels into the defined signal regions. In figure 11, we represent the change in the signal strength, μ^{up}, as a function of the BR into $W\nu$, fixing the remaining parameters for two benchmark points. The signal strength changes at most by 20%, resulting in a relatively mild effect on the final limit on M_E.

The final results are presented in figure 12 for two different values of $M_{A_H} = 1$ GeV (left panel) and $M_{A_H} = 98$ GeV (right panel). Both analyses were applied for each BR point, and the most constraining result was picked. As expected, the effect of the A_H mass is more relevant when the MET signal dominates and for lighter VLL, as the smaller mass difference results in softer leptons. Even so, the differences

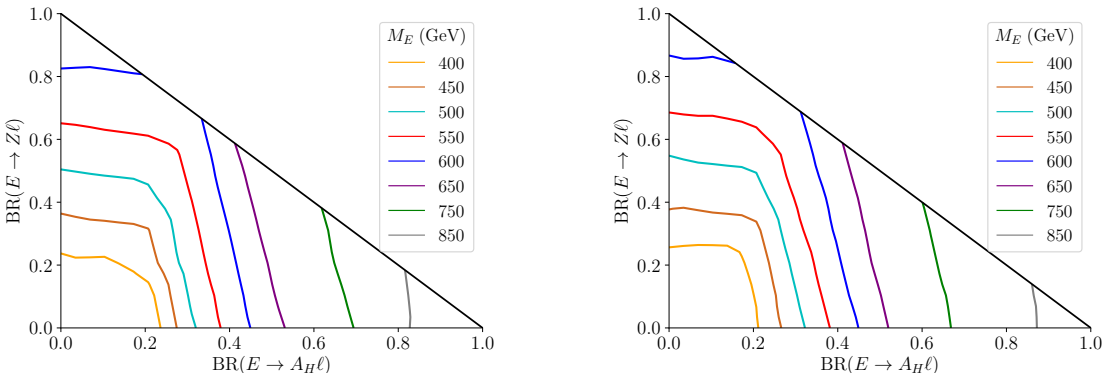

Figure 12: Bound on the VLL mass M_E as a function of $\mathrm{BR}(E \longrightarrow A_H\ell)$ and $\mathrm{BR}(E \longrightarrow Z\ell)$ considering $M_{A_H} = 1$ GeV (left panel) and $M_{A_H} = 98$ GeV (right panel). The limits are shown as contour plots for fixed M_E in which the regions above and to the right of the lines are excluded. The limits are taken by applying the analyses described in the previous section with $\sqrt{s} = 13\,\mathrm{TeV}$ and an integrated luminosity of $\mathcal{L} = 139\ \mathrm{fb}^{-1}$.

between the two different M_{A_H} points are minimal. Thus, henceforth we will report results for $M_{A_H} = 1$ GeV.

The results are presented as contours for fixed M_E, where the regions above and to the right of the contours are excluded. The bound for a VLL singlet with SM decays can be obtained by looking at the vertical axis (corresponding to $\mathrm{BR}(E \longrightarrow A_H\ell) = 0$) at the relevant (mass dependent) $\mathrm{BR}(E \longrightarrow Z\ell)$. The most constraining bounds occur when the BRs are maximized, given the sensitivity of the chosen searches to these channels. The bounds for these three relevant cases are

$$M_E \gtrsim \begin{cases} 405\ \mathrm{GeV}, & [\mathrm{VLL\ singlet}], \\ 630\ \mathrm{GeV}, & [\mathrm{BR}(E \longrightarrow \ell Z) = 1], \\ 895\ \mathrm{GeV}, & [\mathrm{BR}(E \longrightarrow \ell A_H) = 1], \end{cases} \qquad [\sqrt{s} = 13\ \mathrm{TeV}, \mathcal{L} = 139\ \mathrm{fb}^{-1}]. \tag{3.28}$$

There is a slight difference between the bound obtained here for the VLL singlet, and the one quoted in figure 6. This is a result of the fact that here the BR through the channel $Z\ell$ is fixed to 25% whereas before the BR was set by the couplings and masses of the model (the BR only tends to 25% in the large mass limit).

3.2.4 Future projections

Figure 12 presented results with current data at the LHC. In this section we explore the reach at the high-luminosity (HL-LHC) and high-energy (HE-LHC) configurations of the LHC. We will also investigate the reach of a 100 TeV hh-FCC.

At the high-luminosity phase, HL-LHC, we consider $\sqrt{s} = 13$ TeV and an integrated luminosity of $\mathcal{L} = 3\ \mathrm{ab}^{-1}$; we use the same analysis as described previously with the selection cuts detailed in table 4 and we make sure to generate enough statistics for the chosen integrated luminosity. The result is

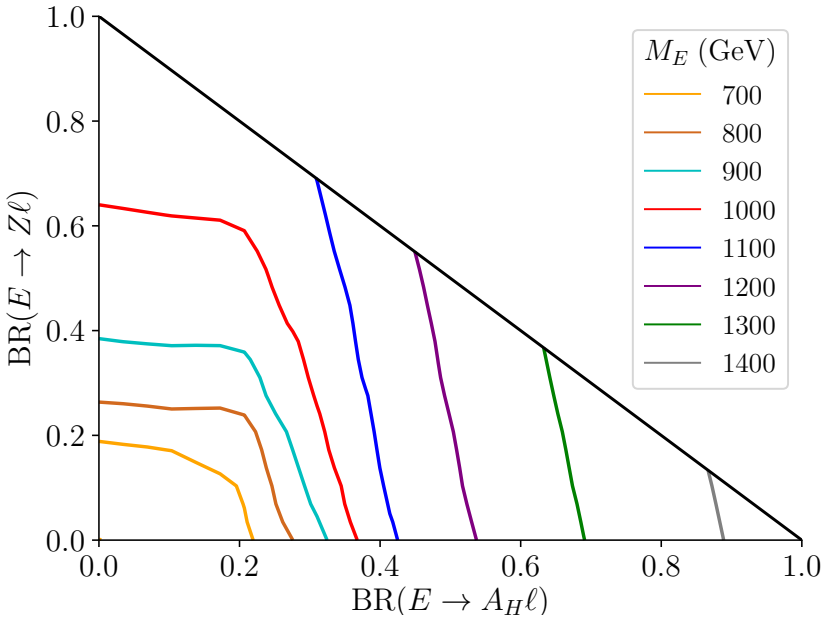

Figure 13: Projected bounds on the mass of the VLL, M_E, in the $\mathrm{BR}(E \longrightarrow A_H\ell)$ and $\mathrm{BR}(E \longrightarrow Z\ell)$ plane for the HL-LHC. Limits are shown as contour plots for fixed M_E in which the regions above and to the right of the lines are excluded.

presented, for $M_{A_H} = 1$ GeV, in figure 13, following the same conventions as before. The corresponding final reach of the HL-LHC in the three most relevant cases are

$$M_E \gtrsim \begin{cases} 785 \text{ GeV}, & [\text{VLL singlet}], \\ 1090 \text{ GeV}, & [\mathrm{BR}(E \longrightarrow \ell Z) = 1], \\ 1450 \text{ GeV}, & [\mathrm{BR}(E \longrightarrow \ell A_H) = 1], \end{cases} \qquad [\text{HL-LHC}]. \tag{3.29}$$

At the HE-LHC, for which we consider $\sqrt{s} = 27$ TeV and $\mathcal{L} = 3$ ab^{-1}, we can once more impose more stringent cuts on the different variables, in particular in the transverse momentum of the identified leptons. For the SM decays analysis, we impose a generator-level cut on all backgrounds of $p_T > 75$ GeV for the leading lepton whereas for the MET decay analysis, the cut on the leading lepton was of $p_T > 100$ GeV . We also updated the selection threshold in table 5 to $p_T^{\ell_1} > 120$ GeV. The results are shown in figure 14. The estimated bounds for the limiting cases is

$$M_E \gtrsim \begin{cases} 1295 \text{ GeV}, & [\text{VLL singlet}], \\ 1770 \text{ GeV}, & [\mathrm{BR}(E \longrightarrow \ell Z) = 1], \\ 1965 \text{ GeV}, & [\mathrm{BR}(E \longrightarrow \ell A_H) = 1], \end{cases} \qquad [\text{HE-LHC}]. \tag{3.30}$$

A detailed study of the reach at the FCC considering the full simulation of backgrounds was beyond the scope of this thesis. However, with the results already obtained, a simplified extrapolation can be performed using the `Collider Reach` tool [140]. We verify the validity of this approach by extrapolating the $\sqrt{s} = 13$ TeV and $\mathcal{L} = 139$ fb^{-1} results, given in Eq. (3.28) to the HL-LHC and to the HE-LHC and

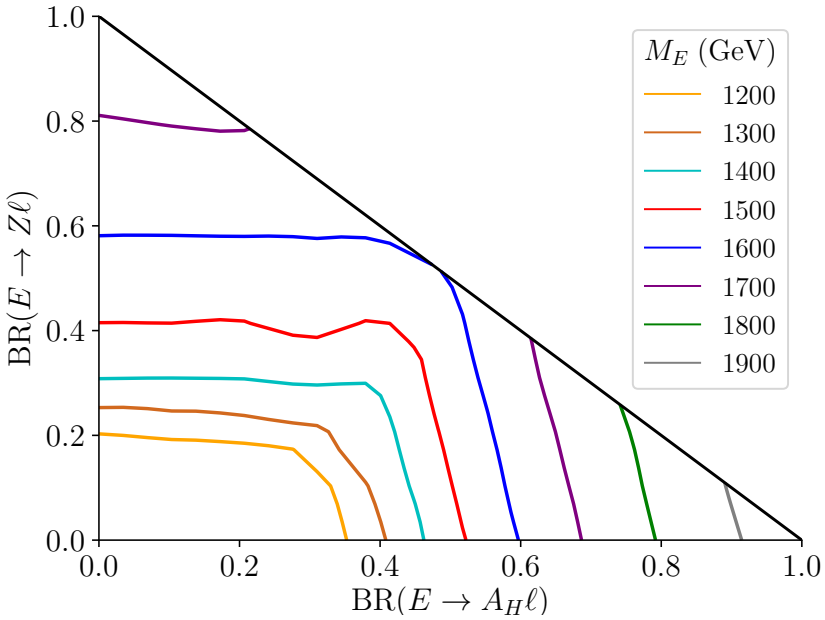

Figure 14: Projected bounds on the mass of the VLL, M_E, in the $\mathrm{BR}(E \longrightarrow A_H\ell)$ and $\mathrm{BR}(E \longrightarrow Z\ell)$ plane for the HE-LHC. Limits are shown as contour plots for fixed M_E in which the regions above and to the right of the lines are excluded.

comparing with what we obtained for these future colliders. We find that such an extrapolation agrees with our detailed simulation within $6\%(14\%)$ for the HL-LHC for the SM decays analysis (MET decay analysis) and within $6\%(35\%)$ at the HE-LHC for the SM decays analysis (MET decay analysis). The difference in regards to the analysis focusing on MET decays drops to 14 % when we extrapolate from the HL-LHC results instead.

Assuming $\sqrt{s} = 100$ TeV and $\mathcal{L} = 3$ ab^{-1} at the hh-FCC, we extrapolate the results of Eq. (3.30) and obtain the results shown in figure 15 and the following bounds:

$$M_E \gtrsim \begin{cases} 2525 \text{ GeV}, & [\text{VLL singlet}], \\ 3665 \text{ GeV}, & [\mathrm{BR}(E \longrightarrow \ell Z) = 1], \\ 3330 \text{ GeV}, & [\mathrm{BR}(E \longrightarrow \ell A_H) = 1], \end{cases} \qquad [\text{hh-FCC (extrapolation)}]. \tag{3.31}$$

The results presented so far are completely general except for the assumption of the production cross-section of a VLL singlet with hypercharge -1. For the sake of generality, we also provide in figure 16 the cross-sections used for the LHC, HE-LHC and hh-FCC searches so that one can easily translate the obtained limits to generic VLLs (for example doublets) by rescaling the pair production cross-section.

3.2.5 A dark matter candidate

The collider analysis we performed assumed only that the lifetime of A_H was large enough so that it was stable at detector scales. However, A_H can have a lifetime larger than the age of the Universe and

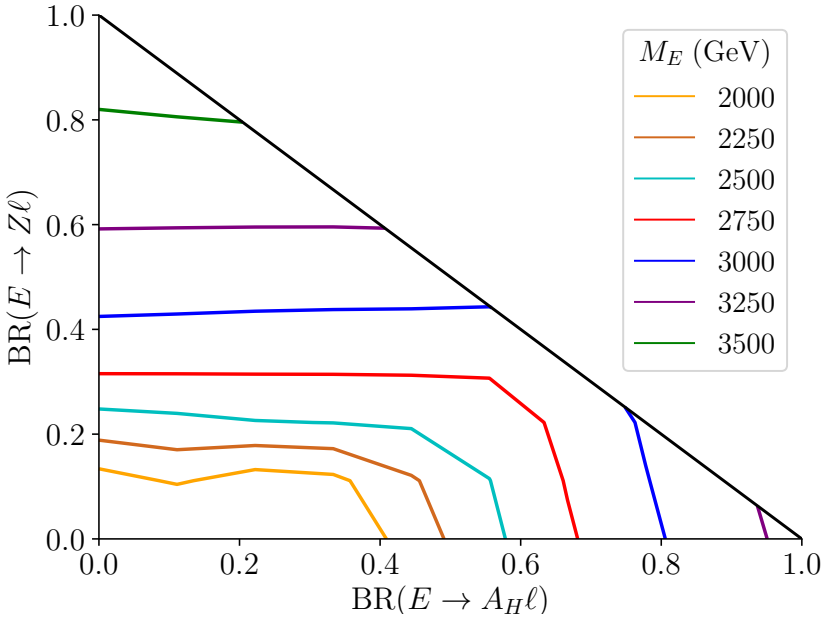

Figure 15: Projected bounds on the mass of the VLL, M_E, in the $\mathrm{BR}(E \longrightarrow A_H\ell)$ and $\mathrm{BR}(E \longrightarrow Z\ell)$ plane for the hh-FCC. Limits are obtained after extrapolating the previous results with the `Collider Reach` tool [140]. Limits are shown as contour plots for fixed M_E in which the regions above and to the right of the lines are excluded.

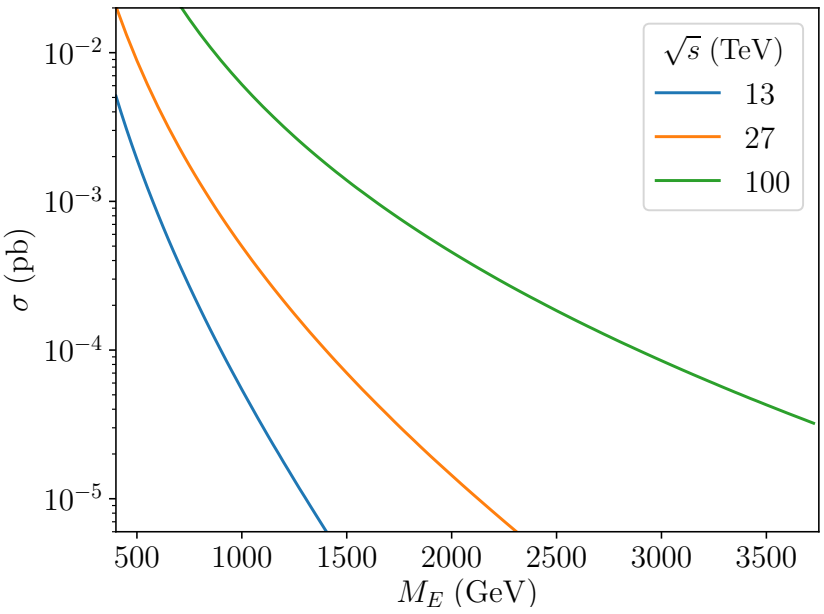

Figure 16: Cross-section of VLL singlet pair production at hadron colliders with $\sqrt{s} = 13\,, 27\,, 100\,\mathrm{TeV}$.

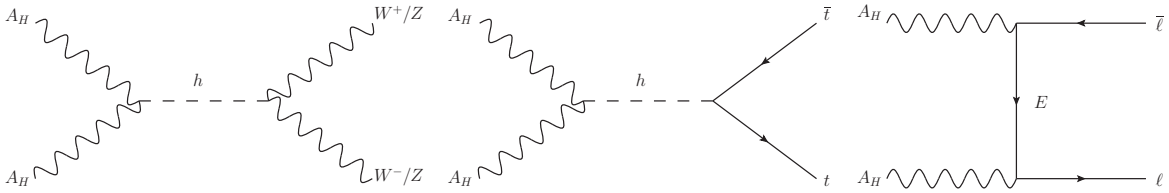

Figure 17: Relevant processes for the annihilation of DM in the freeze-out scenario.

therefore be a suitable DM candidate. In this case, DM probes such as relic density and direct detection experiments can be used to further constrain the model.

3.2.5.1 Standard freeze-out

The scenario which we find in the LHT is that of a DM candidate with a mass around the EW scale, Eq. (3.18). For a DM particle with such a mass it needs a symmetry to stabilize it (T-parity in the LHT), usually a discrete one, under which new particles are odd and the SM ones are even. In these cases the VLL decays exclusively through the MET channel explored in the previous section. The relic abundance of this DM candidate would be set through freeze-out. The relevant Lagrangian to study the freeze-out mechanism is given by:

$$\mathcal{L} = -c_{A_H h} g'^2 \left(\sqrt{2} v h A_H^\mu A_{H_\mu} + \frac{1}{2} h h A_H^\mu A_{H_\mu} \right) + q_H g' [\bar{E}_R \gamma_\mu \ell_R + \text{h.c.}] A_H^\mu + \dots , \tag{3.32}$$

where $v \approx 174$ GeV and we factorized the $U(1)_Y$ gauge coupling g' to make the connection with the LHT model more immediate. In the LHT model $c_{A_H h} = \frac{1}{8}$ and $q_H = \frac{1}{10}$ [141].

A DM model should predict a relic density equal (A_H accounts for all of DM) or smaller than (A_H is only part of DM content) the observed value of $\Omega h^2 \sim 0.12$ [142]. The processes which will dominate the DM annihilation in our model correspond to A_H annihilation to b-quarks, W^+W^- or Z bosons or top quarks (depending on the mass of the DM candidate) through an s-channel exchange of a Higgs [105]. Annihilation into leptons through the exchange of the VLL can also be relevant. The annihilation diagrams are shown in figure 17. The relic density calculation will therefore be dependent on the couplings of A_H to the Higgs and the coupling to the VLL and SM lepton introduced in Eq. (3.32). We will therefore calculate the relic density for different values of these couplings. Note also that, when the s-channel annihilation is subdominant, the mass difference between A_H and the VLL is also important.

The computations of the relic density abundance and direct detection bounds are perfomed using `MadDM` [143]. Results are shown in figure 18 for a fixed mass of the VLL of $M_E = 1$ TeV in the $M_{A_H} - c_{A_H h}$ plane for different values of q_H. The curves correspond to points in which the calculated relic abundance agrees with the observed value. The region below the curve is excluded as it corresponds to overabundant DM and the one above corresponds to an underabundant DM candidate, requiring other sources of DM. For small q_H (< 1), the s-channel annihilation through the Higgs dominates; however, as q_H increases, the VLL exchange channel becomes more relevant and a significant rise in the annihilation

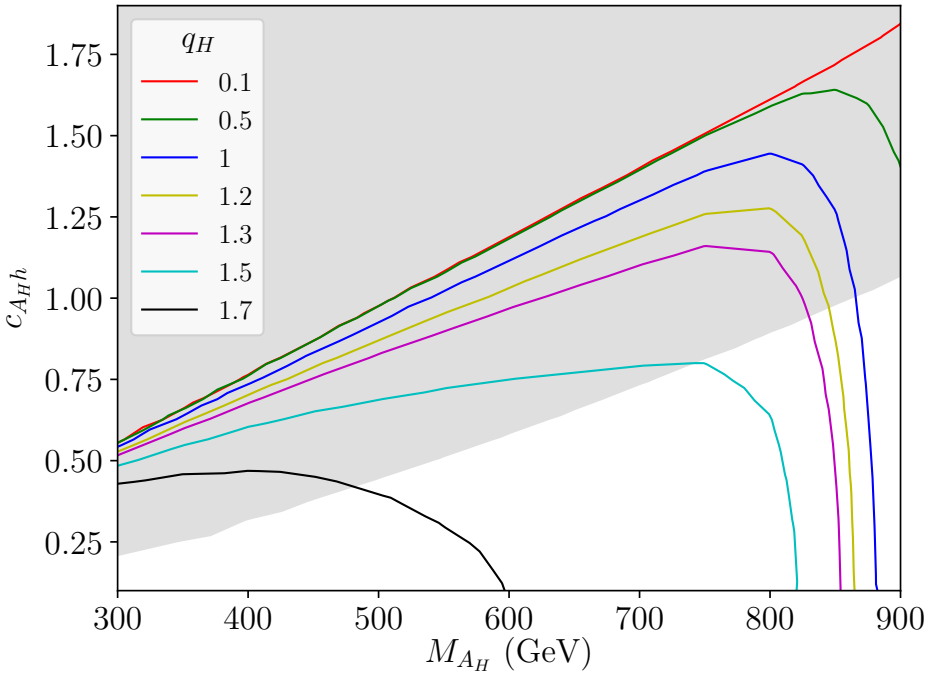

Figure 18: Contours corresponding $\Omega h^2 = 0.12$ for different values of q_H and $M_{\rm E} = 1$ TeV. The region below the curves is excluded as it results in an overabundant DM candidate. The grey region is excluded through direct detection.

cross-section occurs for a $q_H \sim 1.7$ allowing for a large part of the depicted parameter space. For large enough values of q_H, as the mass difference between the VLL and the DM candidate decreases, the VLL-mediated channel becomes dominant. The $c_{A_H h}$ coupling is also important for the direct detection as it affects the scattering cross-section with nucleons; the dominant diagram is shown in figure 19. The corresponding scattering cross-section was computed with `MadDM` and the excluded region is shown, in shaded grey, in figure 18 using the XENON1T data [144] (assuming that A_H is all the DM).

Varying q_H also affects DM-nucleon scattering cross-section. In principle q_H could be responsible for a photon-mediated 1-loop DM nucleon process. However, as noted in Ref. [145], for a real DM vector candidate, 2 DM particles and a photon can only couple through a dimension-6 operator, as the dimension-4 $A_{H_\mu} A_{H_\nu} F^{\mu\nu}$ vanishes due to the antisymmetry of $F^{\mu\nu}$. Furthermore, the resulting amplitude will be further suppressed in the non-relativistic limit. We will therefore neglect these contributions to direct detection bounds.

The coupling q_H is also responsible for generating a contribution to the the anomalous magnetic moment of both the electron and the muon (depending on which of the leptons the VLL mixes with). The latest experimental results are [36, 146]

$$\Delta a_e = a_e^{\rm Exp} - a_e^{SM} = -1.06(0.82) \times 10^{-12} \,, \tag{3.33}$$

$$\Delta a_\mu = a_\mu^{\rm Exp} - a_\mu^{SM} = 25.1(5.9) \times 10^{-10} \,, \tag{3.34}$$

where uncertainties include both the theoretical and experimental parts.

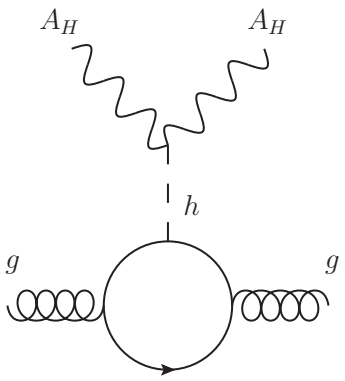

Figure 19: Relevant process for the scattering of DM with nucleons.

The new physics contribution from a VLL and a heavy vector is given by [145],

$$a_\ell = -\frac{\epsilon^2}{48\pi^2 r^2 (1-r^2)^4} q_H^2 g'^2 \left[5 - 14r^2 + 39r^4 - 38r^6 + 8r^8 + 18r^4 \ln(r^2)\right] + O(\epsilon^3) \,, \qquad (3.35)$$

where $\epsilon \equiv m_\ell / M_E$ and $r \equiv M_{A_H}/M_E$ and m_ℓ is the mass of the SM lepton for which the anomalous magnetic moment is calculated. This contribution has a fixed negative sign and it can therefore not explain the muon anomaly. Figure 20 shows the parameter space that can account for the apparent anomalous a_e and for which the contribution to a_μ is smaller than the combination of the experimental and theoretical uncertainties. For the muon case, the region above the lines is excluded.

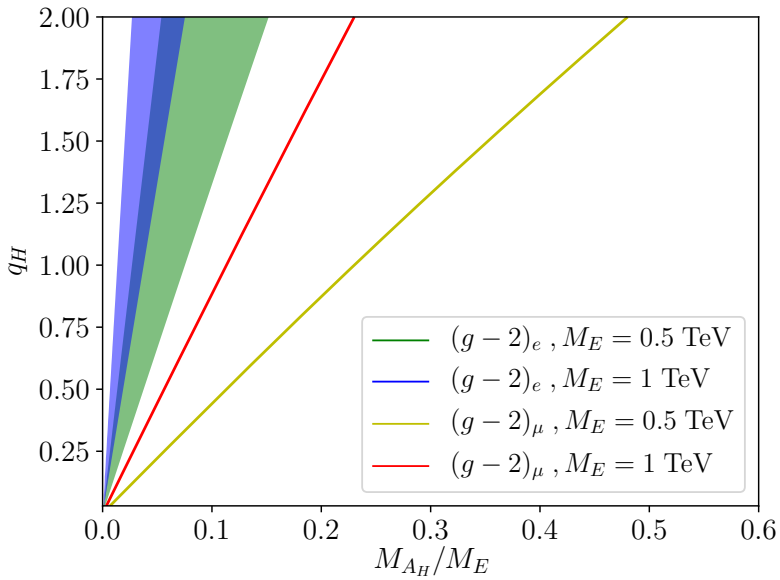

Figure 20: Region that can account for the a_e anomaly for $M_E = 500$ GeV (green) and $M_E = 1\,\text{TeV}$ (blue). The limits (2 sigma) from the contribution to a_μ are shown for $M_E = 500$ GeV (yellow solid line) and for $M_E = 1\,\text{TeV}$ (red solid line). The regions above these lines are excluded.

The relic density results shown in figure 18 reflect a tension between the production of the observed relic abundance through a Higgs portal and direct detection experiments for a WIMP. This tension can be

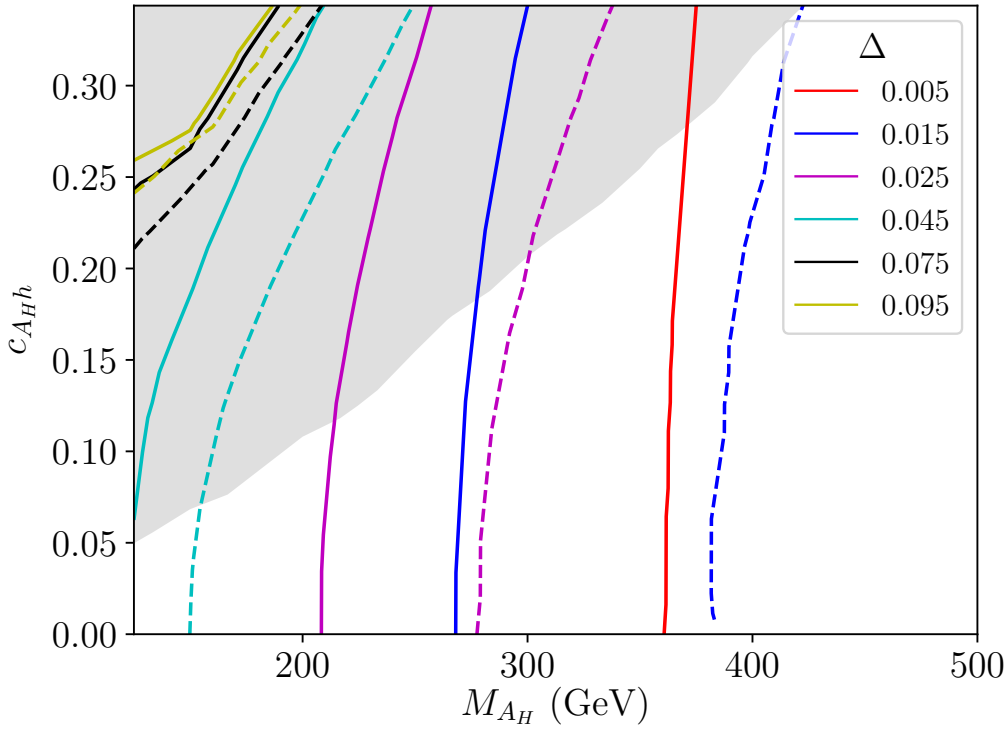

Figure 21: Contours of $\Omega h^2 = 0.12$ for different values of the mass splitting, Δ. The solid curves correspond to $q_H = 0.1$ and the dashed curves correspond to $q_H = 0.2$. The region to the right of the curve is excluded since it results in an overabundant DM candidate. The shaded grey region is excluded through direct detection.

relaxed if the VLL has a nearly degenerate (but slightly larger) mass than that of A_H. This results in the regime of co-annihilation [43] which increases the efficiency of the annihilation processes since processes such as $A_H E \longrightarrow SM\ SM$ can also contribute significantly. These processes will be more relevant as the mass difference decreases and also as the coupling q_H increases. From the estimation done in section 2.3.2, the splitting should be $\Delta \sim 0.05$, where $\Delta \equiv (M_E - M_{A_H})/M_{A_H}$, for co-annihilation to be relevant.

In figure 21 we show the results for relic density calculation considering co-annihilation. We consider two values of $q_H = 0.1$ (solid lines) and $q_H = 0.2$ (dashed lines) and plot the contours of $\Omega h^2 = 0.12$ for different mass splittings. The region to the right of the curves is excluded as it corresponds to an overabundant DM candidate. Again, direct detection bounds are shown in shaded grey. As expected, only for $\Delta \lesssim 0.05$ do we observe a significant deviation from the standard annihilation scenario.

To account also for the dependence on q_H in the co-annihilation regime we present in figure 22 the $\Omega h^2 = 0.12$ contours in the $M_{A_H} - q_H$ plane, again for different values of the mass splitting, fixing $c_{A_H h} = 1$. Direct detection exclusion is given by the shaded grey region. Before, as we increase Δ, the curves collapsed to the non co-annihilating regime. In this case, even though co-annihilation is negligible for $\Delta \gtrsim 0.05$, the annihilation process mediated by the VLL dominates and as such, the cross-section depends strongly on Δ, even outside the co-annihilation regime.

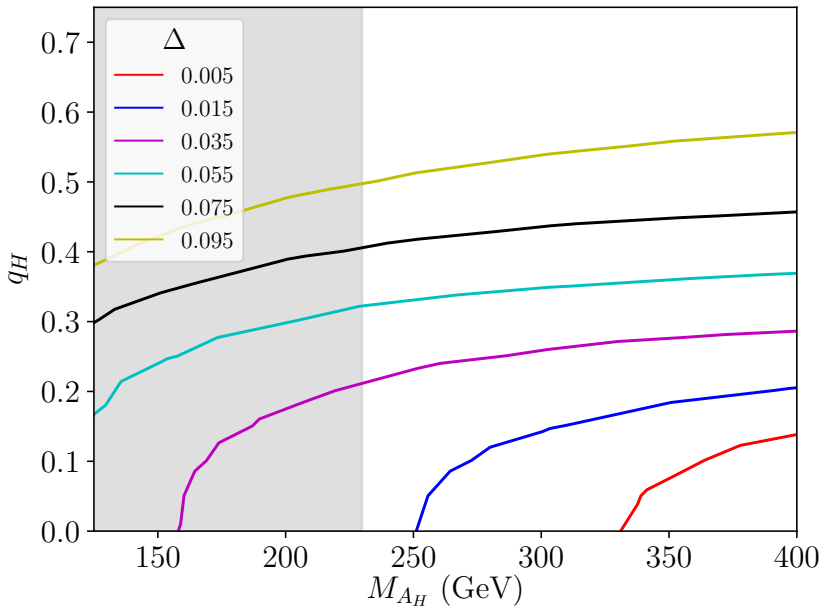

Figure 22: Contours of $\Omega h^2 = 0.12$ for different values of the mass splitting, Δ, and for a fixed value of $c_{A_H h} = 1$. The region below each curve gives an overabundant DM candidate and is therefore exclided. The shaded grey region is excluded through direct detection.

The co-annihilation scenario is complementary to the collider analysis explored previously. The small mass difference between the BSM states results in very soft, and therefore difficult to identify, leptons. More recently, analyses have focused on these compressed mass spectrums, particularly in the context of sleptons [147]. These co-annihilation results show that such an effort in the context of VLLs is also very well motivated.

3.2.5.2 Freeze-in in feebly interacting dark matter

For a very light DM candidate which couples very weakly with other particles, its abundance can be generated through the freeze-in mechanism [148]. Within our setup, the relic abundance of A_H is set through the decay of the VLL. Such a possibility has been recently investigated in [112] focusing on the DM phenomenology, therefore fixing the VLL mass to a conservative $M_E = 1$ TeV avoiding any collider constraint. Since the DM is light it can be stabilized kinematically and does not need a discrete symmetry, meaning that all decay channels for the VLL are available. Let us see if our collider results can provide any complementary information in this FIMP scenario.

This scenario can be realized by the explicit model shown in Appendix A. The relic density is given by [112]:

$$\Omega h^2 \approx 0.12 \times 10^{-9} \frac{M_E}{M_{A_H}} \left(\frac{g_H s}{5.3 \times 10^{-17}} \right)^2 , \tag{3.36}$$

where g_H and s are defined in Eqs. (A.0.4) and (A.0.7), respectively.

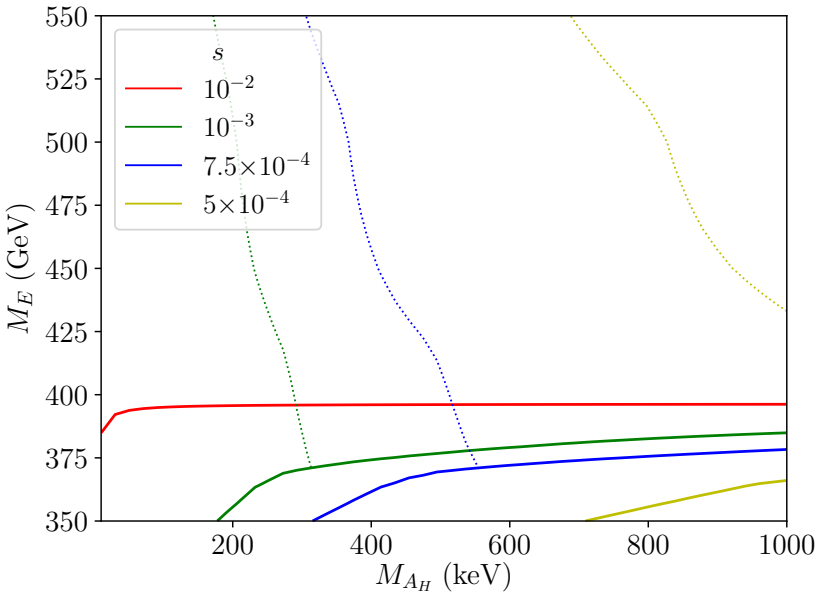

Figure 23: Contours collider limits, for the LHC with $\sqrt{s} = 13$ TeV and $\mathcal{L} = 139$ fb^{-1}, for models with a DM candidate whose relic density is set through the decay of a VLL, for different values of the mixing of the VLL and the SM lepton, s. The region below the curves is excluded by collider searches, either looking for SM decays (solid) or targeting decays through channels with missing energy (dotted). More details can be read in the text and in Appendix A.

For each mass point, requiring that A_H corresponds to all the DM, that is, Eq. (3.36) $= 0.12$, fixes $g_H \times s$. By choosing a particular value s, all BRs of the VLL are therefore fixed, allowing us to use the collider bounds obtained in the previous section.

These results are shown in figures 23 and 24 for the search at $\sqrt{s} = 13$ TeV and $\mathcal{L} = 139$ fb^{-1} and for $\mathcal{L} = 3$ ab^{-1} respectively. For each mass point, all parameters are fixed in order to explain the observed relic density, and the region below the curves can be excluded by collider searches. All lines (one for each value of s) is displayed either with a solid or dotted style, to distinguish between the cases in which the strongest constraint is a result of the analysis looking for SM decays or from the analysis searching for the MET signature. This information is important since either $E \longrightarrow Z\ell$ or $E \longrightarrow A_H\ell$ must be prompt for the collider analysis to be usable. We consider that a flight distance of 1 cm corresponds to a promptly decaying VLL.

Eq. (A.0.22) provides the minimum s so that $E \longrightarrow Z\ell$ is prompt. Note that for the chosen values of s, only a VLL that mixes with muons would decay promptly. For $E \longrightarrow A_H\ell$ the value of g_H (fixed for each mass point by requiring the correct relic density) determines the flight distance. For the parameter space probed in figures 23 and 24, no point corresponds to a prompt decay and as such, we cannot use directly the bounds obtained by the analysis focusing on the MET signature. A detailed study focusing on displaced vertices could in principle probe a significant region of the parameter space for this class of models.

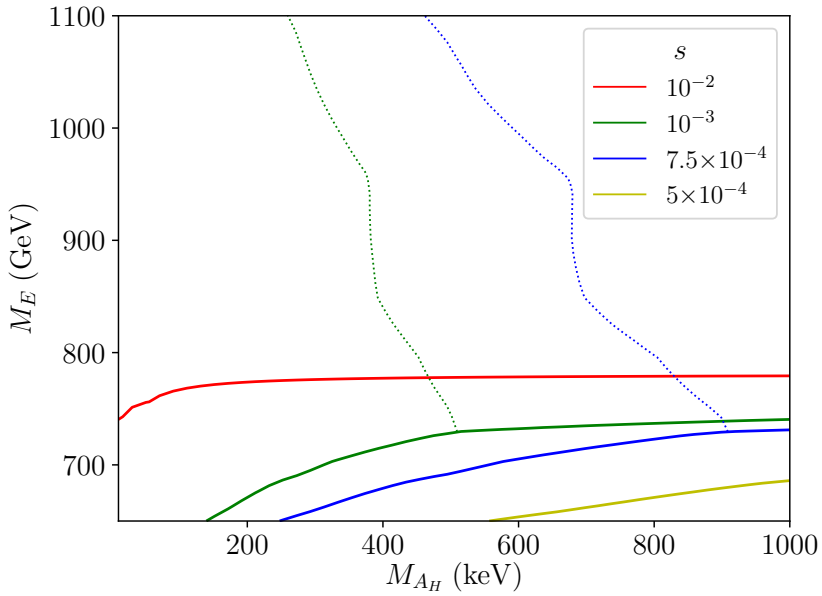

Figure 24: Contours collider limits, for the LHC with $\sqrt{s} = 13$ TeV and $\mathcal{L} = 3$ ab^{-1}, for models with a DM candidate whose relic density is set through the decay of a VLL, for different values of the mixing of the VLL and the SM lepton, s. The region below the curves is excluded by collider searches, either looking for SM decays (solid) or targeting decays through channels with missing energy (dotted). More details can be read in the text and in Appendix A.

3.2.6 Next steps

As we saw in section 3.1.3, most of the new particles predicted in the LHT were T-odd. An exception to this are the top partners, T_1 and T_2, introduced in Eq. (3.22). Similarly to what happened to the doublets introduced in Eq. (3.19), a linear combination of the top partners is going to be T-odd and the other one T-even [103]. This has important phenomenological consequences since the T-even top partner, T^+, can be singly produced at colliders.

While pair production of VLQs is more appealing due to its model-independence, as larger masses of VLQs are probed, attention has shifted towards the study of single production [149–152]. The ATLAS analysis of Ref. [153] studied the single-production of a VLQ which decayed to a SM final state with a signature of a SM top and MET. This signature was assumed to result from $T^+ \longrightarrow Z(\bar{\nu}\nu)t$. Within the LHT this signature would also arise but with a different twist. Instead of decaying directly to SM particles, T^+ can decay to its T-odd partner T^- and the lightest T-odd particle, the gauge boson A_H [103]. The T-odd partner would then decay to another A_H and a SM top [103] resulting in the signature explored in the ATLAS search Ref. [153].

Following the spirit of the VLL search proposed in the previous section, in the future we aim to recast the analysis of Ref. [153] parametrizing the decays of the VLQ so that it can be applicable to a wider range of models, including the LHT scenario.

4

Model-independent approach

4.1 A brief introduction to Effective Field Theories

The fundamental concept behind effective field theories is the idea that physics at different energy scales decouples. That is, the description of physical observables at a given energy does not entail the full knowledge of the underlying theory at much higher energies. While apparent in classical mechanics, this statement is more subtle in QFT where loop integrals involve different energy scales; however, it has been proven in the context of QFT through the Applequist-Carazzone decoupling theorem [154].

From this decoupling it follows that, making only use of degrees of freedom present at an energy scale, p, we can describe an experimental observation taking place at that energy, effectively integrating out any heavy fields – by heavy we mean that their mass is much larger than p. The information on the interactions of these heavy fields is given by the *full* theory, a theory needed to describe physics in the ultra-violet (UV). Integrating these heavy fields out results in p/Λ suppressed contributions, with Λ representing the high-energy scale (which can be understood as the mass of these heavy fields). Expanding these contributions in powers of p/Λ results in local effects captured by the low-energy theory, the *Effective Field Theory* (EFT) [9]. The EFT description is therefore only valid when $p \ll \Lambda$.

In chapter 3 we followed the approach of looking for BSM physics by considering *direct* evidence from the production of new particles at the LHC. That is, we considered that current or future experiments had enough energy to produce BSM particles on-shell. On the other hand, following the EFT approach which is only valid description at energies much lower than the mass of the BSM particle, we are actually looking for deviations on low-energy observables from the SM predictions. These deviations are suppressed by powers of the scale of new physics and as such, experimental precision must overcome this suppression to observe them.

Furthermore, regardless of how general we aimed to be, in order to proceed with a direct search for new physics we had to make bold assumptions on the nature of the BSM theory – in our case we focused on signatures from CHMs. Since the EFT description is built from the low-energy degrees of freedom, we can construct all allowed operators (respecting the symmetry considerations of the low-energy theory)

without any mention of the underlying UV theory. In this way we are searching for new physics in a *model independent* fashion; there is no need to assume a particular UV model, allowing us to probe a wide range of BSM physics.

A prime example of the use of EFTs in particle physics is the Fermi theory. Without knowledge of any particle other than leptons, Fermi's theory accurately describes the muon decay to an electron and two neutrinos by parametrizing it through the 4-fermion contact interaction

$$\mathcal{L}_F = -G_F(\overline{\psi_i}\gamma^\mu P_L\psi_j)(\overline{\psi_k}\gamma^\mu P_L\psi_l)\,, \tag{4.1.1}$$

where G_F is the Fermi constant. Nowadays, with experiments taking place at higher energy scales, we know the muon decay is actually mediated by the W-boson. Eq. (4.1.1) is the effective description of the process after integrating out this boson, and G_F is set by enforcing that the Fermi theory reproduces the SM prediction at a particular energy scale. In this effective approach, Fermi's theory parametrized the effects of a new heavier particle much before experiments could probe it directly. Hopefully, we can do the same in the near future.

4.1.1 The Standard Model Effective Field Theory

As extensively pointed out in previous sections, there are several reasons pointing towards the existence of BSM physics. The lack of evidence for physics BSM seems to point to two possibilities: either new physics is light and couples feebly with the SM or it is heavier than the energy scales current experiments have been able to probe[1]. In the latter case, a decoupling between the EW scale and the scale of new physics, Λ, is present and, as such, the SM can be considered an effective theory, the Standard Model Effective Field Theory (SMEFT) [155].

The SMEFT is constructed with the degrees of freedom of the SM and extends the SM Lagrangian with local operators which parametrize the effects of high-energy physics:

$$\mathcal{L}^{\text{SMEFT}} = \mathcal{L}^{\text{SM}} + \frac{\mathcal{L}^{(5)}}{\Lambda} + \frac{\mathcal{L}^{(6)}}{\Lambda^2} + \mathcal{O}(1/\Lambda^3) \tag{4.1.2}$$

where $\mathcal{L}^{(d)}$ are the d-dimensional components of the Lagrangian. $\mathcal{L}^{(d)}$ is composed by all Lorentz and SM gauge invariant operators at mass dimension d, $\mathcal{O}_i^{(d)}$, each multiplied by an arbitrary dimensionless coefficient $c_i^{(d)}$, denoted as Wilson coefficient (WC). In principle, the Lagrangian of Eq. (4.1.2) contains infinite terms since terms with increasing mass dimension can always be written; therefore, in order to

[1] We can also have a combination of the two scenarios, for instance, pNGBs originating from a $\sim$ TeV scale spontaneous symmetry breaking which can be naturally light. This is the case of non-minimal CHMs.

make use of this effective description, an order up to which effects will be considered needs to be chosen. Commonly the order at which the effective expansion is truncated is related with the experimental precision of the process we are interested in describing; as more precise measurements arise, more orders can be included in the expansion. Therefore, once the truncation order is fixed, the SMEFT *is* a renormalisable theory since all higher-order counter-terms are neglected.

At dimension-5 there is only one operator, the Weinberg operator [156],

$$\mathcal{L}_5 = c_{ij}^{(5)} H(\overline{L_i}^c)(L_j H) + \text{h.c.}, \tag{4.1.3}$$

which is a lepton number violating (LNV) interaction. This operator could be responsible for generating a Majorana mass to neutrinos, with a high-energy scale $\Lambda \sim 10^{14}\,\text{GeV}$ for $c^{(5)} \sim \mathcal{O}(1)$ in order to comply with the bounds on neutrino masses.

The leading contribution from non-LNV new physics arises at dimension-6. Contributions at this order have been widely studied in the literature [155]. The minimal set of operators to describe physics at this order, comprised by 59 operators (neglecting flavour), is given in the well-known Warsaw basis [157], presented in tables 6 and 7. This is not a unique basis, different sets of operators could have been chosen [158–160]; however, the Warsaw basis has been by far the most used in the literature and the one we will use throughout this thesis.

Knowing the SMEFT Lagrangian at order $\mathcal{O}(1/\Lambda^2)$, its contributions to observables at this order can be calculated. In this way low-energy experiments can provide bounds on the WCs of the operators of the chosen basis, without any mention of the particular dynamics of UV physics. This approach which is focused solely in the EFT is called the *bottom-up* approach.

Despite the model independence which characterizes the EFT approach, at some point it might be pertinent to trade this description by a specific model. This is particularly relevant in case a set of WCs is preferred to be non-zero by experimental data; the next question to answer would be about the nature of the UV physics responsible for generating those WCs. We can trade the generality of the EFT description by a particular UV model by requiring that the EFT reproduces the results of that particular UV theory at low-energies (within the range of validity of the EFT), effectively writing the WC in terms of the parameters of the UV theory. This is achieved through *matching*, which we will go into more detail in section 4.1.2. In essence this allows the translation of bounds obtained on WCs onto the parameter space of the parameters of a more complete theory. The study of the connection between the EFT description and particular SM extensions is called the *top-down* approach. Results for the matching at tree-level onto the SMEFT (for generic UV extensions of the SM) are given in [161].

Class	Operators		Operators	
$(\bar{\psi}_L\psi_L)\,(\bar{\psi}_R\psi_R)$	$(\bar{l}_L\gamma_\mu l_L)\,(\bar{e}_R\gamma^\mu e_R)$	O_{le}	$(\bar{q}_L\gamma_\mu q_L)\,(\bar{e}_R\gamma^\mu e_R)$	O_{qe}
	$(\bar{l}_L\gamma_\mu l_L)\,(\bar{u}_R\gamma^\mu u_R)$	O_{lu}	$(\bar{l}_L\gamma_\mu l_L)\,(\bar{d}_R\gamma^\mu d_R)$	O_{ld}
	$(\bar{q}_L\gamma_\mu q_L)\,(\bar{u}_R\gamma^\mu u_R)$	$O^{(1)}_{qu}$	$(\bar{q}_L\gamma_\mu T_A q_L)\,(\bar{u}_R\gamma^\mu T_A u_R)$	$O^{(8)}_{qu}$
	$(\bar{q}_L\gamma_\mu q_L)\,(\bar{d}_R\gamma^\mu d_R)$	$O^{(1)}_{qd}$	$(\bar{q}_L\gamma_\mu T_A q_L)\,(\bar{d}_R\gamma^\mu T_A d_R)$	$O^{(8)}_{qd}$
$(\bar{\psi}_L\psi_L)\,(\bar{\psi}_L\psi_L)$	$(\bar{l}_L\gamma_\mu l_L)\,(\bar{l}_L\gamma^\mu l_L)$	O_{ll}		
	$(\bar{q}_L\gamma_\mu q_L)\,(\bar{q}_L\gamma^\mu q_L)$	$O^{(1)}_{qq}$	$(\bar{q}_L\gamma_\mu\sigma_a q_L)\,(\bar{q}_L\gamma^\mu\sigma_a q_L)$	$O^{(3)}_{qq}$
	$(\bar{l}_L\gamma_\mu l_L)\,(\bar{q}_L\gamma^\mu q_L)$	$O^{(1)}_{lq}$	$(\bar{l}_L\gamma_\mu\sigma_a l_L)\,(\bar{q}_L\gamma^\mu\sigma_a q_L)$	$O^{(3)}_{lq}$
$(\bar{\psi}_R\psi_R)\,(\bar{\psi}_R\psi_R)$	$(\bar{e}_R\gamma_\mu e_R)\,(\bar{e}_R\gamma^\mu e_R)$	O_{ee}		
	$(\bar{u}_R\gamma_\mu u_R)\,(\bar{u}_R\gamma^\mu u_R)$	O_{uu}	$(\bar{d}_R\gamma_\mu d_R)\,(\bar{d}_R\gamma^\mu d_R)$	O_{dd}
	$(\bar{u}_R\gamma_\mu u_R)\,(\bar{d}_R\gamma^\mu d_R)$	$O^{(1)}_{ud}$	$(\bar{u}_R\gamma_\mu T_A u_R)\,(\bar{d}_R\gamma^\mu T_A d_R)$	$O^{(8)}_{ud}$
	$(\bar{e}_R\gamma_\mu e_R)\,(\bar{u}_R\gamma^\mu u_R)$	O_{eu}	$(\bar{e}_R\gamma_\mu e_R)\,(\bar{d}_R\gamma^\mu d_R)$	O_{ed}
$(\bar{\psi}_L\psi_R)\,(\bar{\psi}_R\psi_L)$	$(\bar{l}_L e_R)\,(\bar{d}_R q_L)$	O_{ledq}		
$(\bar{\psi}_L\psi_R)\,(\bar{\psi}_L\psi_R)$	$(\bar{q}_L u_R)\,i\sigma_2\,(\bar{q}_L d_R)^{\mathrm{T}}$	$O^{(1)}_{quqd}$	$(\bar{q}_L T_A u_R)\,i\sigma_2\,(\bar{q}_L T_A d_R)^{\mathrm{T}}$	$O^{(8)}_{quqd}$
	$(\bar{l}_L e_R)\,i\sigma_2\,(\bar{q}_L u_R)^{\mathrm{T}}$	$O^{(1)}_{lequ}$	$(\bar{l}_L\sigma_{\mu\nu} e_R)\,i\sigma_2\,(\bar{q}_L\sigma^{\mu\nu} u_R)^{\mathrm{T}}$	$O^{(3)}_{lequ}$
Baryon number violating			$\epsilon_{ABC}\,(\bar{d}_R^{c\,A} u_R^B)\,(\bar{q}_L^{c\,C} i\sigma_2 l_L)$	O_{duq}
			$\epsilon_{ABC}\,(\bar{q}_L^{c\,A} i\sigma_2 q_L^B)\,(\bar{u}_R^{c\,C} e_R)$	O_{qqu}
			$\epsilon_{ABC}\,(\bar{d}_R^{c\,A} u_R^B)\,(\bar{u}_R^{c\,C} e_R)$	O_{duu}
		$\epsilon_{ABC}(i\sigma_2)_{\alpha\delta}(i\sigma_2)_{\beta\gamma}\left(\bar{q}_L^{c\,A\alpha} q_L^{B\beta}\right)\left(\bar{q}_L^{c\,C\gamma} l_L^{\delta}\right)$		O_{qqq}

Table 6: Four-fermion operators of the Warsaw basis. We follow the notation of Ref. [161] and adapt the tables therein. Flavour indices are absent.

Class	Operators		Operators	
X^3	$\varepsilon_{abc} W_\mu^{a\,\nu} W_\nu^{b\,\rho} W_\rho^{c\,\mu}$	$\mathcal{O}_W$	$\varepsilon_{abc} \tilde{W}_\mu^{a\,\nu} W_\nu^{b\,\rho} W_\rho^{c\,\mu}$	$\mathcal{O}_{\tilde{W}}$
	$f_{ABC} G_\mu^{A\,\nu} G_\nu^{B\,\rho} G_\rho^{C\,\mu}$	$\mathcal{O}_G$	$f_{ABC} \tilde{G}_\mu^{A\,\nu} G_\nu^{B\,\rho} G_\rho^{C\,\mu}$	$\mathcal{O}_{\tilde{G}}$
ϕ^6	$\left(\phi^\dagger \phi\right)^3$	$\mathcal{O}_\phi$		
$\phi^4 D^2$	$\left(\phi^\dagger \phi\right) \Box \left(\phi^\dagger \phi\right)$	$\mathcal{O}_{\phi\Box}$	$\left(\phi^\dagger D_\mu \phi\right) \left(\left(D^\mu \phi\right)^\dagger \phi\right)$	$\mathcal{O}_{\phi D}$
$X^2 \phi^2$	$\phi^\dagger \phi B_{\mu\nu} B^{\mu\nu}$	$\mathcal{O}_{\phi B}$	$\phi^\dagger \phi \tilde{B}_{\mu\nu} B^{\mu\nu}$	$\mathcal{O}_{\phi\tilde{B}}$
	$\phi^\dagger \phi W_{\mu\nu}^a W^{a\,\mu\nu}$	$\mathcal{O}_{\phi W}$	$\phi^\dagger \phi \tilde{W}_{\mu\nu}^a W^{a\,\mu\nu}$	$\mathcal{O}_{\phi\tilde{W}}$
	$\phi^\dagger \sigma_a \phi W_{\mu\nu}^a B^{\mu\nu}$	$\mathcal{O}_{\phi WB}$	$\phi^\dagger \sigma_a \phi \tilde{W}_{\mu\nu}^a B^{\mu\nu}$	$\mathcal{O}_{\phi\tilde{W}B}$
	$\phi^\dagger \phi G_{\mu\nu}^A G^{A\,\mu\nu}$	$\mathcal{O}_{\phi G}$	$\phi^\dagger \phi \tilde{G}_{\mu\nu}^A G^{A\,\mu\nu}$	$\mathcal{O}_{\phi\tilde{G}}$
$\psi^2 \phi^3$	$\left(\phi^\dagger \phi\right) \left(\bar{l}_L \phi e_R\right)$	$\mathcal{O}_{e\phi}$		
	$\left(\phi^\dagger \phi\right) \left(\bar{q}_L \phi d_R\right)$	$\mathcal{O}_{d\phi}$	$\left(\phi^\dagger \phi\right) \left(\bar{q}_L \tilde{\phi} u_R\right)$	$\mathcal{O}_{u\phi}$
$\psi^2 X \phi$	$\left(\bar{l}_L \sigma^{\mu\nu} e_R\right) \phi B_{\mu\nu}$	$\mathcal{O}_{eB}$	$\left(\bar{l}_L \sigma^{\mu\nu} e_R\right) \sigma^a \phi W_{\mu\nu}^a$	$\mathcal{O}_{eW}$
	$\left(\bar{q}_L \sigma^{\mu\nu} u_R\right) \tilde{\phi} B_{\mu\nu}$	$\mathcal{O}_{uB}$	$\left(\bar{q}_L \sigma^{\mu\nu} u_R\right) \sigma^a \tilde{\phi} W_{\mu\nu}^a$	$\mathcal{O}_{uW}$
	$\left(\bar{q}_L \sigma^{\mu\nu} d_R\right) \phi B_{\mu\nu}$	$\mathcal{O}_{dB}$	$\left(\bar{q}_L \sigma^{\mu\nu} d_R\right) \sigma^a \phi W_{\mu\nu}^a$	$\mathcal{O}_{dW}$
	$\left(\bar{q}_L \sigma^{\mu\nu} T_A u_R\right) \tilde{\phi} G_{\mu\nu}^A$	$\mathcal{O}_{uG}$	$\left(\bar{q}_L \sigma^{\mu\nu} T_A d_R\right) \phi G_{\mu\nu}^A$	$\mathcal{O}_{dG}$
$\psi^2 \phi^2 D$	$\left(\phi^\dagger i \overleftrightarrow{D}_\mu \phi\right) \left(\bar{l}_L \gamma^\mu l_L\right)$	$\mathcal{O}_{\phi l}^{(1)}$	$\left(\phi^\dagger i \overleftrightarrow{D}_\mu^a \phi\right) \left(\bar{l}_L \gamma^\mu \sigma_a l_L\right)$	$\mathcal{O}_{\phi l}^{(3)}$
	$\left(\phi^\dagger i \overleftrightarrow{D}_\mu \phi\right) \left(\bar{e}_R \gamma^\mu e_R\right)$	$\mathcal{O}_{\phi e}$		
	$\left(\phi^\dagger i \overleftrightarrow{D}_\mu \phi\right) \left(\bar{q}_L \gamma^\mu q_L\right)$	$\mathcal{O}_{\phi q}^{(1)}$	$\left(\phi^\dagger i \overleftrightarrow{D}_\mu^a \phi\right) \left(\bar{q}_L \gamma^\mu \sigma_a q_L\right)$	$\mathcal{O}_{\phi q}^{(3)}$
	$\left(\phi^\dagger i \overleftrightarrow{D}_\mu \phi\right) \left(\bar{u}_R \gamma^\mu u_R\right)$	$\mathcal{O}_{\phi u}$	$\left(\phi^\dagger i \overleftrightarrow{D}_\mu \phi\right) \left(\bar{d}_R \gamma^\mu d_R\right)$	$\mathcal{O}_{\phi d}$
	$\left(\tilde{\phi}^\dagger i D_\mu \phi\right) \left(\bar{u}_R \gamma^\mu d_R\right)$	$\mathcal{O}_{\phi ud}$		

Table 7: Bosonic and 2-fermion operators of the Warsaw basis. We follow the notation of Ref. [161] and adapt the tables therein. Flavour indices are absent.

Due to the different energy scales at play in the EFT description, the knowledge of how the WCs evolve with energy is fundamental; this evolution follows the renormalisation group equations (RGE), whose calculation we will go over in section 4.1.4. Indeed, a significant amount of work has been done in the computation of the RGEs of the SMEFT, in particular at dimension-6 [162–167].

The full power of the EFT approach can be seen when we combine these approaches: *(1)* The bottom-up approach allows us to set experimental constraints on the WCs in a model-independent way; *(2)* Using the RGEs, the value of the bounded WCs at the experimental scale can be calculated at any other energy, namely at the matching scale; *(3)* Knowing the matching conditions of a particular UV theory to the SMEFT, the bounds on the WCs can be traded by constraints on the parameter space of our favorite model.

An advantage of this setup is that each step can be worked on separately, and the loss of generality, that is, the commitment to a particular UV model only occurs in step *(3)*.

In this thesis, works which tackle each of these 3 steps are presented with the aim of extending the current knowledge of the SMEFT. Before delving into the details of these works, let us present some of the theoretical framework needed to do those calculations within the SMEFT.

4.1.2 UV matching

Trading the arbitrary WCs of the EFT by the parameters in a particular full theory is done by requiring that the EFT reproduces the results of the UV theory at some energy scale. We mentioned an example of this procedure in the Fermi theory in which, in order to set the value for G_F, the muon decay calculated at a determinate energy scale through the EFT 4-fermion interaction and through the W-boson exchange in the full theory had to match.

In general, this matching can be achieved at the level of the Green's functions, by requiring that the Green's functions with light external particles are the same in both theories. This amounts to equating the light field dependent part of the generating functionals of both theories:

$$Z[J_\phi, J_\Phi = 0] = Z_{eff}[J_\phi]\,, \tag{4.1.4}$$

where J_ϕ (J_Φ) is the source term for light (heavy) fields. Respecting this condition corresponds to calculating the one-light-particle irreducible (1LPI) diagrams in the full theory for a particular process, and matching them to the EFT 1PI diagrams of the same process, effectively setting the WCs matching conditions at a particular energy scale. This is called *off-shell matching*.

The condition above can be further relaxed; since we are interested in observables and not exactly in Green's functions, the EFT can instead be required to reproduce the same S-matrix elements as the

full theory in its regime of validity. For this calculation, we now need to compute all connected and amputated diagrams for a given process for both theories and equate the results to obtain the WCs matching conditions at a given energy scale. In this process, the external light-particles are on-shell and therefore this is called *on-shell matching*.

From the LSZ formula, it can be seen that S-matrix elements are invariant under non-singular field redefinitions [9, 168, 169]. As such, one can greatly reduce the number of operators in the EFT Lagrangian needed to reproduce the full theory by applying appropriate field redefinitions. The operators which can be removed by the use of field redefinitions are called *redundant*, whereas the remaining ones compose the physical basis of effective operators. We will go over the removal of these redundant operators in more detail in the section 4.1.3.

Since the end goal of any EFT calculation is to calculate observables, any obtained result can be translated into the physical basis through field redefinitions. Given its minimality it is actually preferable to work with a physical basis and that is why most results at dimension-6 are quoted in term of the WCs of the physical Warsaw basis.

At first sight it might therefore seem counter intuitive to perform off-shell matching if results from on-shell matching are directly obtained in terms of the minimal set of WCs. However, from the computational point of view, on-shell matching demands the calculation of more diagrams, whose number scales much faster as we go to higher dimensions with more external legs when comparing with the 1LPI calculations of off-shell matching. On the other hand, the main argument against off-shell matching is that it requires the knowledge of a larger set of operators – and how they are reduced to the minimal physical basis – which are not trivial to construct; however, this work only has to be done once for a given EFT.

For these reasons, unless stated otherwise, in this thesis all EFT calculations will be done off-shell and only at the end will we trade the redundant operators for those in the physical basis.

4.1.3 Constructing a minimal basis

When building the basis of EFT operators with which we perform calculations, we want to work with the most minimal set of operators possible, that is, the smallest set of parameters which are independent among themselves. There is no physical issue with working with an over-redundant set of operators, however this just adds undesirable complexity to the computations.

When performing off-shell calculations, operators are related by algebraic or group-theory identities

and also through integration by parts (IBP)[2]. The minimal set of operators that can be built with the low-energy degrees of freedom which are not related through IBP or other identities is called the *Green's basis*.

As mentioned in the previous section, if we are interested in calculating observables, Green's basis operators can be further reduced through appropriate field redefinitions. The remaining more minimal set of operators composes the physical, or on-shell, basis.

Let us illustrate this with a simple example of an EFT of a real light scalar, ϕ:

$$\mathcal{L} = \frac{1}{2}\partial_\mu\phi\partial^\mu\phi - \frac{m^2}{2}\phi^2 - \lambda\phi^4 + \frac{c_1^{(6)}}{\Lambda^2}\phi^6 + \frac{c_2^{(6)}}{\Lambda^2}\phi^3\partial^2\phi + O(1/\Lambda^4)\,, \tag{4.1.5}$$

where, for simplicity, we imposed a $\mathbb{Z}_2$ symmetry, so that only even powers of ϕ exist, and we only considered 2 effective operators.

Knowing that observables are invariant under field redefinitions, we can apply the redefinition $\phi \longrightarrow \phi + \frac{k}{\Lambda^2}\phi^3$, such that

$$\mathcal{L} \longrightarrow \mathcal{L} + \frac{k}{\Lambda^2}\phi^3\left(-\partial^2 - m^2 - 4\lambda\phi^2\right)\phi + O(1/\Lambda^4)\,. \tag{4.1.6}$$

By taking $k = c_2^{(6)}$ we can remove the operator $\phi^3\partial^2\phi$ of Eq. (4.1.5), which is therefore a redundant operator. The Lagrangian would now be given by:

$$\mathcal{L} = \frac{1}{2}\partial_\mu\phi\partial^\mu\phi - \frac{m^2}{2}\phi^2 - \left(\lambda - \frac{c_2^{(6)}}{\Lambda^2}m^2\right)\phi^4 + \left(\frac{c_1^{(6)}}{\Lambda^2} - 4\lambda\frac{c_2^{(6)}}{\Lambda^2}\right)\phi^6 + O(1/\Lambda^4)\,, \tag{4.1.7}$$

where it can be seen that, besides removing the redundant operator, contributions to the other non-redundant operators are also generated.

Note that the quantity within the parenthesis in Eq. (4.1.6) is actually the EOM of ϕ, obtained with the dimension-4 operators of Eq.(4.1.5); indeed, performing a field redefinition such as

$$\phi \longrightarrow \phi + kF(\phi)\,, \tag{4.1.8}$$

where $F(\phi)$ is a function of fields and derivatives, is equivalent to adding a term to the Lagrangian proportional to the EOMs, or analogously, to applying the EOMs on redundant operators. This statement is only true up to higher-order effects [170], that is, up to $O(1/\Lambda^4)$ in the example above.

[2]This is due to the vanishing of total derivatives when we integrate over space-time taking the limit of fields going to zero at infinity (only valid up to topological effects).

Indeed, in Eq. (4.1.6) we only showed explicitly the effects of the field redefinition when applied to the dimension-4 terms; when applied instead to the dimension-6 operators it generates contributions linear in k but of $O(1/\Lambda^4)$. These effects would not be captured by simply using the EOM of dimension-4 terms but instead the EOMs of the dimension-6 Lagrangian would need to be taken into account. However, even when using the higher-order EOMs, we would not capture the quadratic terms on k, which once again, since k is suppressed by $1/\Lambda^2$ in order to remove an effective operator, would only show up at $O(1/\Lambda^4)$.

Let us make more explicit the origin of these k^2 terms by considering the mass term of Eq. (4.1.5) after applying the field redefinition of Eq. (4.1.8) where, once more, $F(\phi) = \phi^3$:

$$\frac{m^2}{2}\phi^2 \to \frac{m^2}{2}\phi^2 + m^2\frac{k}{\Lambda^2}\phi^4 + \frac{m^2}{2}\frac{k^2}{\Lambda^4}\phi^6\,, \tag{4.1.9}$$

where we wrote k as k/Λ^2 to make the mass dimension clearer. The last term cannot be reproduced by the use of EOMs, either at dimension-4 or at dimension-6. The only way to get a contribution proportional to m^2/Λ^4 would be to apply the EOMs to a redundant dimension-8 operator, such as $\phi^5\partial^2\phi$; however, this term would be proportional to the WC of the redundant dimension-8 operator, whereas k is fixed to remove a dimension-6 term ($k = c_2^{(6)}$ above); therefore applying EOMs would not reproduce the result of (4.1.9)[3]. This fact that EOMs and field-redefinitions are only equivalent at leading order has been recently studied in [170].

However, in the case of one-loop computations – as is the case of a RGE calculation –, in which the redundant WCs are suppressed by a loop factor, quadratic effects on k are formally a two-loop effect. If we are limiting our computation accuracy to one-loop then we can safely use EOMs to remove operators. This is not the case for the calculation of the matching conditions of a UV extension onto the SMEFT which involves also tree-level contributions. There are no clear reasons why quadratic terms in k could be neglected which invalidates the use of EOMs in favour of using the sometimes cumbersome field redefinitions.

4.1.4 Renormalisation Group Equations

As has been pointed out throughout this chapter, EFTs deal with several energy scales, namely, the scale at which the EFT is matched to an underlying UV completion and the energy scale at which experiments to probe WCs take place. Therefore, for a coherent analysis, it is paramount to take into account how the couplings of the SMEFT theory evolve with energy. This knowledge is important when we want to combine

[3] Note that in order to remove the term $c^{(8)}/\Lambda^4\phi^5\partial^2\phi$ from the Lagragian, a different field redefinition like Eq. (4.1.8) would be needed, where k would be of order $1/\Lambda^4$.

experimental measurements at relatively different scales, for instance, bounds associated with B-meson decays with probes of EWPO, or when we want to translate the bounds obtained in a global fit to limits on the couplings of specific models at their matching scale. The evolution of the theory couplings with energy is encoded in the RGEs; let us look at how to calculate them.

We perform calculations in the dimensional regularization scheme, where the dimensions of the theory are analitically continued to $d = 4 - 2\epsilon$ and divergencies appear as $1/\epsilon$-proportional terms from loop diagrams. Within the $\overline{\text{MS}}$ scheme, these divergences are subtracted by introducing counterterms with the appropriate coefficient (and loop-suppression factor) in order to cancel the generated divergency, producing finite results. These counterterms can be seen as arising by a rescaling of the fields and couplings on the original Lagrangian, the *bare* Lagrangian.

Let us show this more explicitly with a simple example of a theory of a massless real scalar, ϕ, with an assumed $\mathbb{Z}_2$-symmetry where we rescale $\phi^0 \to \sqrt{Z_\phi}\phi$ and the quartic coupling $\lambda^0 \to \lambda\mu^{2\epsilon}Z_\lambda$:

$$\begin{aligned}\mathcal{L} &= (\partial_\mu\phi^0)(\partial_\mu\phi^0) + \lambda^0(\phi^0)^4 \\ &= (\partial_\mu\phi)(\partial_\mu\phi) + \mu^{2\epsilon}\lambda\phi^4 + (Z_\phi - 1)(\partial_\mu\phi)(\partial_\mu\phi) + \mu^{2\epsilon}\lambda(Z_\lambda Z_\phi - 1)\phi^4\,,\end{aligned} \tag{4.1.10}$$

where the superscript 0 corresponds to bare quantities. We introduce the scale μ in order to have $[\mathcal{L}] = 4 - 2\epsilon$ while keeping λ dimensionless. The Z_ϕ term – called the wave function renormalisation (WFR) – is going to be fixed by requiring that it cancels the terms proportional to the pole $1/\epsilon$ in the $\phi \to \phi$ process, whereas Z_λ is fixed by cancelling the divergences in the $\phi\phi \to \phi\phi$ process.

Let us now see how this works in an EFT scenario. Consider a generic Lagrangian at a certain fixed scale constructed with operators of arbitrary mass dimensions, $\mathcal{L} = \sum_i c_i O_i$. This Lagrangian generates divergences at 1-loop which can be absorbed by the appropriate counterterms such that:

$$\mathcal{L}_{div} = \frac{\alpha_j}{16\pi^2}O_j\,, \tag{4.1.11}$$

where α_j is a function of all couplings in the theory, not only the WC corresponding to O_j. Note that the operators present in the divergent Lagrangian can in fact contain operators which were not part of the original Lagrangian. In principle, in order to capture all possible generated divergences, a basis (either physical or off-shell depending on how we are performing calculations) is needed.

This divergent Lagrangian can be canceled by the rescaling of the bare couplings such that:

$$c_i^{(0)}O_i^{(0)} = \mu^{n_j}Z_j c_j Z_j^F O_j\,, \tag{4.1.12}$$

where once again n_j is chosen so that the coupling keeps its mass dimension in $4-2\epsilon$ space-time dimensions, Z_j is defined as

$$Z_j = 1 + \frac{k_j}{\epsilon}\,, \tag{4.1.13}$$

and Z^F corresponds to the WFR of the fields which constitute the operator $\mathcal{O}_j$, that is, the divergent contribution to the kinetic terms of those fields, as we saw in Eq. (4.1.10). Therefore, the Z^F factors can be removed by canonically normalizing the kinetic terms. In the following, we will consider that such a canonical normalization is performed and therefore Z_F no longer appears explicitly.

In order to cancel the generated divergences we have $k_j c_j = -\alpha_j/(16\pi^2)$, where it becomes clear that, as α_j, k_j can receive contributions from all couplings in the theory.

The RGE of a coefficient c_j follows from the condition that the bare coupling does not depend on the introduced renormalisation scale, that is,

$$\begin{aligned} \mu\frac{d}{d\mu}c_j^0 \equiv \dot{c}_j^0 &= 0 \\ 0 &= \mu^{n_j\epsilon}\left[n_j\epsilon Z_j c_j + \dot{Z}_j c_j + Z_j \dot{c}_j\right]\,. \end{aligned} \tag{4.1.14}$$

In general one can calculate n_j as

$$n_j = N_X^j + N_S^j + N_\psi^j - 2\,, \tag{4.1.15}$$

where N_X^j, N_S^j and N_ψ^j correspond to the number of field strengths, scalars and fermions that constitute $\mathcal{O}_j$ respectively.

We can rewrite Eq. (4.1.14) as:

$$\dot{c}_j = -n_j\epsilon c_j - \dot{k}_j\frac{c_j}{\epsilon}\,, \tag{4.1.16}$$

where the first term corresponds to a tree-level contribution (which is why n_j is commonly called the tree-level anomalous dimension) and the second term is a one-loop contribution. The latter term can be expanded as:

$$-\dot{k}_j\frac{c_j}{\epsilon} = -\frac{\partial k_j}{\partial c_l}\frac{\dot{c}_l}{e}c_j = \frac{\partial k_j}{\partial c_l}n_l c_l c_j\,, \tag{4.1.17}$$

where in the last equality we took $\dot{c}_l = -n_l\epsilon c_l + \cdots$ neglecting the second term in Eq. (4.1.16) because it would result in a two-loop effect here.

Finally we can write a master formula for the calculation of the RGEs:

$$\frac{d}{d\mu}c_j = c_j\sum_l \frac{\partial k_j}{\partial c_l}n_l c_l\,, \tag{4.1.18}$$

where c_l sums over all couplings in the theory.

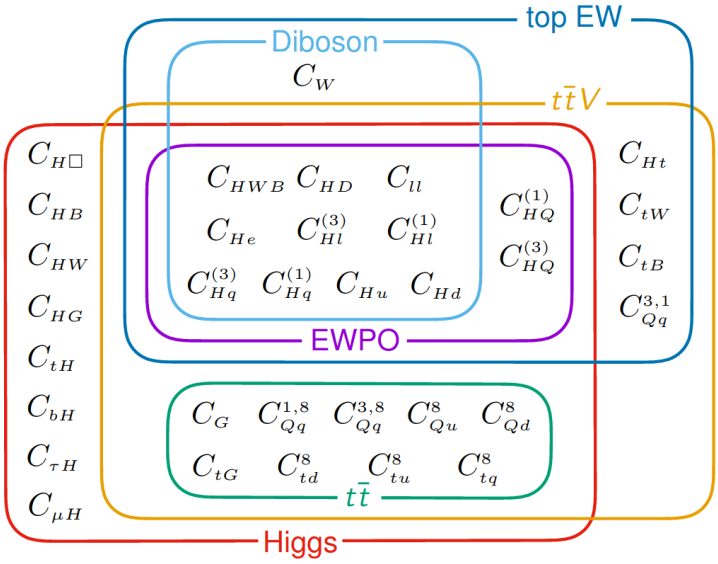

Figure 25: A scheme of the WCs constrained by different classes of observables. Taken from [171].

4.1.5 Experimental constraints

While the EFT parametrization allows the study of a wide range of new physics models, this comes with the added price of introducing a large number of free parameters to our theory.

This has become less of an issue in recent years due to the immense number of observables that have been measured by the experimental community. Indeed, recent studies have considered more than 341 observations to constrain the SMEFT [171].

This process of fitting the SMEFT WCs with different experimental data is called a *global fit*. The WCs are fitted to the values which minimize the difference between the SMEFT prediction and the experimental measurement across a range of observations. By taking different observables at the same time, these analyses not only constrain the allowed parameter space of the SMEFT but can also take into account important correlations between WCs.

The minimization function can be written as a χ^2 function, defined as

$$\chi^2(\theta) = [\vec{O}_{\text{exp}} - \vec{O}_{\text{th}}(\theta)]^T V^{-1} [\vec{O}_{\text{exp}} - \vec{O}_{\text{th}}(\theta)]\,, \tag{4.1.19}$$

where θ are the free parameters of the theory – the WCs –, $\vec{O}_{\text{exp}}$ are the observations, $\vec{O}_{\text{th}}(\theta)$ are the corresponding theory predictions for a set of the WCs and V is the covariance matrix, defined as $V_{ij} = \sigma_i \rho_{ij} \sigma_j$ where σ are the experimental errors and ρ the correlation matrix. Clearly, in order to proceed with the minimization of Eq. (4.1.19) one needs to know the contribution of the free parameters,

the WCs, to the considered observable. Predictions from the SMEFT at dimension-6 have been included in several available tools [172–176].

A recent global fit has been performed in Ref. [171]. In this work the authors considered experimental data from top physics, EWPO, Higgs physics and diboson processes, allowing them to constrain the operators in figure 25.

Following the *top-down* approach, particular models can also be probed by trading the WCs by the particular matching conditions of the corresponding UV extension and considering the degrees of freedom – the θ in Eq. (4.1.19) which will minimize the χ^2 function – to be the model's couplings and masses instead of generic WCs. This will in general result in more stringent bounds since the correlations between WCs are enforced from the matching conditions [171, 177].

4.1.6 Theoretical constraints

In the previous section we explored setting experimental bounds on WCs. However, assuming only the analytical properties of scattering amplitudes and unitarity of the underlying theory, we can further constrain the parameter space of the EFT theoretically by enforcing its consistency with these principles. These constraints are commonly denoted *positivity bounds* since they imply positivity conditions on certain combinations of WCs [178–188].

Let us consider the forward limit of a $2 \longrightarrow 2$ scattering process of scalars, such that the amplitude is only a function of s, i.e., $\mathcal{A}(s, t = 0)$. The derivation of the positivity bounds is based on the fact that, when written in terms of complex momenta, these scattering amplitudes are analytic, except for the single poles and branch cuts along the real axis of s [179]. Let us define the integral

$$\mathcal{I} = \frac{1}{2\pi i} \oint_C \frac{\mathcal{A}(s)}{s^3} ds \,, \tag{4.1.20}$$

where C denotes a circular contour around the origin. From Cauchy's theorem, this contour integral is given by the residue of $\frac{\mathcal{A}(s)}{s^3}$ at $s = 0$, which will allow us to isolate the s^2-proportional term of the amplitude, i.e. the second derivative of the amplitude with respect to s when evaluated at the origin.

Due to the analytic properties of $\mathcal{A}(s)$, we can deform the circle C to infinity wherever it does not intersect discontinuities, resulting in the contour C' shown in figure 26. The Froissart bound [189] states that the scattering amplitude evolves at most as $\mathcal{A}(s) \propto s \log^2 s$; as such, the integrand in Eq. (4.1.20) vanishes in the circular part of the contour C' as $s \longrightarrow \infty$. We are then left only with the discontinuities

near the real axis. The integral can then be solved as

$$\mathcal{I} = \frac{1}{\pi i}\int_{s_d}^{+\infty} \lim_{\epsilon\to 0}\left(\mathcal{A}(s+i\epsilon) - \mathcal{A}(s-i\epsilon)\right) \tag{4.1.21}$$

$$= \frac{1}{\pi i}\int_{s_d}^{+\infty} i2Im(\mathcal{A}(s))\,, \tag{4.1.22}$$

where s_d corresponds to the beginning of the branch cut. We assumed a cross symmetric amplitude, invariant under $s \longrightarrow -s$ which allows us to only consider the integral in the positive branch cut. In the second equality we used the Schwarz reflection principle, $\mathcal{A}(s^*) = [\mathcal{A}(s)]^*$ [179]. Unitarity leads us to the optical theorem which relates the imaginary part of an amplitude with the cross-section, such that:

$$\mathcal{I} = \frac{2}{\pi}\int_{s_d}^{+\infty} \frac{\sigma(s)}{s^2} ds\,, \tag{4.1.23}$$

which is always a positive quantity. Therefore, we finally conclude that

$$\left.\frac{d^2\mathcal{A}(s)}{ds}\right|_{s=0} \geq 0\,. \tag{4.1.24}$$

From this result, we can calculate a scattering amplitude in the SMEFT and infer positivity conditions on WCs. Note that a $2 \longrightarrow 2$ amplitude is dimensionless ($[\mathcal{A}] = 4 - n = 0$, where n is the number of external particles); therefore, the s^2-proportional term in the amplitude must be suppressed by Λ^4, that is, the condition of Eq. (4.1.24) is only relevant for dimension-8 operators.

As an example, calculating at tree-level the scattering amplitudes $\phi_1\phi_2 \longrightarrow \phi_1\phi_2$, $\phi_1\phi_3 \longrightarrow \phi_1\phi_3$ and $\phi_1\phi_1 \longrightarrow \phi_1\phi_1$, where ϕ_i are the components of the Higgs doublet, $\phi = (\phi_1 + i\phi_2, \phi_3 + i\phi_4)^T$, the following positivity constraints on dimension-8 4-Higgses WCs can be obtained [179]:

$$\begin{aligned} c_{\phi^4}^{(2)} &\geq 0\,,\\ c_{\phi^4}^{(1)} + c_{\phi^4}^{(2)} &\geq 0\,,\\ c_{\phi^4}^{(1)} + c_{\phi^4}^{(2)} + c_{\phi^4}^{(3)} &\geq 0\,, \end{aligned} \tag{4.1.25}$$

where the WCs correspond to the dimension-8 operators defined in table 19.

Further bounds can be derived from Eq. (4.1.24) by considering different processes [181, 190]; we will explore some of those and the stability of Eq. (4.1.25) under one-loop effects in section 4.4.3.

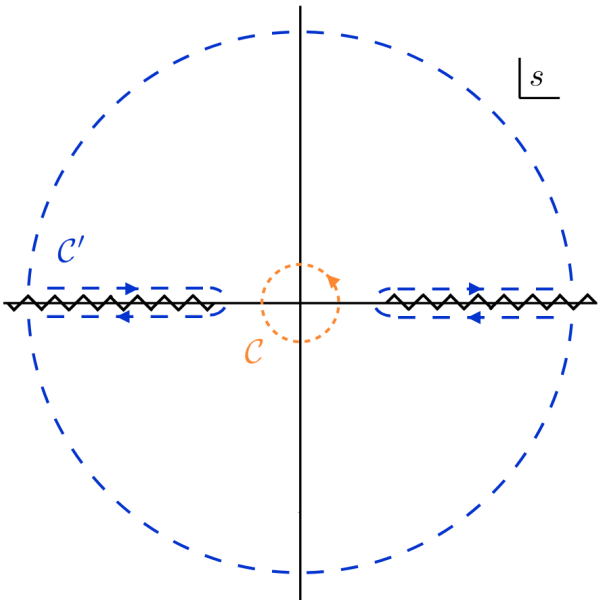

Figure 26: Analytical structure of the forward $2 \longrightarrow 2$ scattering amplitude in the s complex plane, where the discontinuities (zigzag lines) can include branch cuts and poles. Taken from [179].

4.2 SMEFT at dimension-8

One direction in which to extend the SMEFT approach is to consider further orders in the $1/\Lambda$ expansion. Most of the SMEFT studies done so far focus only on dimension-6 operators, that is up to $1/\Lambda^2$ order; neglecting LNV operators, the next relevant contributions arise by dimension-8 terms.

While these contributions are expected to be less important due to the extra $1/\Lambda^2$ suppression, there are several phenomenological reasons which motivate their study:

- Some observables can receive their leading contribution at dimension-8 either because dimension-6 operators do not contribute or the relevant dimension-6 may not be generated at tree-level by weakly-coupled UV theories. Examples of the former case are light-by-light scattering [191], which has been observed recently by ATLAS [192], pure anomalous quartic gauge couplings [193–197] – changes to the quartic gauge couplings which do not affect triple gauge couplings – or neutral triple gauge couplings [198–200];

- The precision of several measurements is so large which, for a fixed Λ, allows the probing of dimension-8 contributions [201–204].

From the theoretical point of view there are also interesting factors which only come into play at this order:

- Neglecting odd-dimensional operators, order $1/\Lambda^4$ is the first one in which co-leading contributions arise: two insertions of dimension-6 operators or one dimension-8. *A priori* there are no reasons to expect one to dominate over the other;
- Classes of dimension-8 WCs are subject to positivity bounds which limit the parameter space of the SMEFT and can be used as priors on global fits, or give us windows to probe the building blocks of the underlying QFT, that is, unitarity and analyticity [178].

Following these motivations, more recently, the interest within the SMEFT community has shifted towards considering these dimension-8 contributions [205–208]. These efforts culminated in the construction of the full dimension-8 on-shell basis [191, 209], which we present in Appendix B[4]. However, as previously argued for, working off-shell offers many advantages; in particular, the amount of diagrams needed to compute at dimension-8 (with up to 8 external legs) in an on-shell approach would be very large.

Therefore, in order to begin our work towards extending the SMEFT at dimension-8, we will start by the construction of a Green's basis at this order which will allow us to compute quantities off-shell. Due to the inherent challenge of this task – the Green's basis at dimension-8 is comprised of 1649 operators on top of the 993 of the physical basis [191, 209] — we will focus for now on the bosonic sector.

4.3 A Green's basis for the bosonic SMEFT at dimension 8

Knowledge of the set of independent operators which form the Green's basis is fundamental to perform off-shell calculations in the SMEFT. Automatic tools that can count the number of operators which form this basis exist, `Basisgen` [211] and `Sym2Int` [212]. In spite of this, the explicit construction of those operators and their reduction to a defined physical basis is a task which is yet to be automatized – Ref. [213] has been the latest development in this direction. Besides algebraic and group theory identities relations, one must check whether the operators are independent under IBP, Fierz identities and Bianchi identities, which read

$$D_\mu F^{\nu\rho} + D_\nu F^{\rho\mu} + D_\rho F^{\mu\nu} = 0\,, \tag{4.3.1}$$

[4]We only present the classes of operators which will be relevant throughout this thesis, namely all bosonic operators and the 2-fermion operators which can be generated at tree-level by weakly coupled UV theories [210]. We follow the notation of Ref. [191] and adapt the tables therein. The purpose of this appendix is to keep the thesis as self-contained as possible.

where F is a field-strenght tensor.

While it might seem straightforward to check whether two operators are related under these identities, it becomes quite cumbersome at dimension-8 when the operators are composed of several fields and derivatives.

Therefore, in order to simplify the task at hand, we work in momentum space, where independent operators contribute to 1PI tree-level amplitudes through independent kinematic invariants. In momentum space, IBP is equivalent to enforcing momentum conservation, whereas other identities manifest automatically through relations between different Feynman rules. This section is based on the work published in Ref. [4].

4.3.1 Off-shell independence in momentum space

As hinted above, we will study operator independence by studying their contribution to a 1PI amplitude for a given process. Let us take $\{O_i\}_{i=1\ldots N}$ as N operators whose independence we are trying to ascertain, and study their contribution to the amplitude $\mathcal{A}(a \to b)$. One can write the contribution of each operator, O_i, to the process in terms of *independent* kinematics invariants $\{\kappa_\alpha\}$. At tree level:

$$\mathcal{A}(a \to b) = c_i \sum_\alpha f^i_\alpha(g)\kappa_\alpha \,, \tag{4.3.2}$$

where f is a matrix which represents the contribution of an operator O^i, as a function of the SM gauge couplings, g, to the kinematic invariant κ_α.

For two operators to be independent, that is, to describe different off-shell physics, then there must exist at least one process for which the corresponding $f^i_\alpha = (f^i_{\alpha_1}, f^i_{\alpha_2}, \ldots)$ and $f^j_\alpha = (f^j_{\alpha_1}, f^j_{\alpha_2}, \ldots)$ are non-collinear vectors (since κ are independent). More generally, this means that if there is at least one amplitude in which the associate matrix M with elements $(M)_{ij} = f^i_j$ has rank N, then the operators $\{O_i\}_{i=1\ldots N}$ are independent.

Let us exemplify this by considering the following dimension-8 hermitian six-Higgs operators:

$$O_1 = (\phi^\dagger\phi)D_\mu(\phi^\dagger\phi)D^\mu(\phi^\dagger\phi)\,, \tag{4.3.3}$$

$$O_2 = (\phi^\dagger\phi)^2(D^2\phi^\dagger\phi + \phi^\dagger D^2\phi)\,, \tag{4.3.4}$$

$$O_3 = (\phi^\dagger\phi)^2 D_\mu\phi^\dagger D^\mu\phi\,. \tag{4.3.5}$$

The 1PI amplitude for $\varphi^0(p_1) \to \varphi^0(p_2)\varphi^+(p_3)\varphi^-(p_4)\varphi^+(p_5)\varphi^-(p_6)$ reads:

$$\mathcal{A} = 2i\,c_1(2\kappa_{13} + 2\kappa_{14} + 2\kappa_{15} + 2\kappa_{16} - 2\kappa_{23} - 2\kappa_{24} - 2\kappa_{25} - 2\kappa_{26}$$

$$
\begin{aligned}
&\quad - \kappa_{34} - 2\kappa_{35} - \kappa_{36} - \kappa_{45} - 2\kappa_{46} - \kappa_{56}) \\
&- 4i\, c_2(\kappa_{11} + \kappa_{22} + \kappa_{33} + \kappa_{44} + \kappa_{55} + \kappa_{66}) \\
&+ 2i\, c_3(2\kappa_{12} - \kappa_{34} - \kappa_{36} - \kappa_{45} - \kappa_{56})\,, \qquad (4.3.6)
\end{aligned}
$$

where $\kappa_{ij} = p_i \cdot p_j$.

At first sight one might think the matrix M associated with this process has rank 3. Indeed, taking for simplicity the sub-matrix $\hat{M}$ associated to the invariants κ_{11}, κ_{12}, κ_{13}

$$
\hat{M} = \begin{bmatrix} 0 & 0 & 4i \\ -4i & 0 & 0 \\ 0 & 4i & 0 \end{bmatrix} \Longrightarrow 3 \geq \mathrm{Rank}(M) \geq \mathrm{Rank}(\hat{M}) = 3\,. \qquad (4.3.7)
$$

However, the kinematic invariants with which we wrote our amplitude are not independent. By momentum conservation $p_1 = p_2 + p_3 + p_4 + p_5 + p_6$, and therefore κ_{i1} can always be reduced to other kinematic invariants. Taking this into account, we arrive at:

$$
\begin{aligned}
\mathcal{A} &= 2i\, c_1(2\kappa_{33} + 3\kappa_{43} + 2\kappa_{44} + 2\kappa_{53} + 3\kappa_{54} + 2\kappa_{55} + 3\kappa_{63} + 2\kappa_{64} + 3\kappa_{65} + 2\kappa_{66}) \\
&\quad - 8i\, c_2(\kappa_{22} + \kappa_{32} + \kappa_{33} + \kappa_{42} + \kappa_{43} + \kappa_{44} + \kappa_{52} + \kappa_{53} + \kappa_{54} + \kappa_{55} + \kappa_{62} + \kappa_{63} \\
&\qquad + \kappa_{64} + \kappa_{65} + \kappa_{66}) \\
&\quad + 2i\, c_3(2\kappa_{22} + 2\kappa_{32} + 2\kappa_{42} - \kappa_{43} + 2\kappa_{52} - \kappa_{54} + 2\kappa_{62} - \kappa_{63} - \kappa_{65})\,. \qquad (4.3.8)
\end{aligned}
$$

The corresponding matrix now only has rank 2. This can be seen from the fact that the first and third lines in the equation above add to minus half the second one. In other words, $O_2 = -2(O_1 + O_3)$. At the Lagrangian level, this could be seen through IBP:

$$
\begin{aligned}
D_\mu\Big[(\phi^\dagger\phi)^2 D^\mu(\phi^\dagger\phi)\Big] &= 2(\phi^\dagger\phi) D_\mu(\phi^\dagger\phi) D^\mu(\phi^\dagger\phi) \\
&\quad + (\phi^\dagger\phi)^2(D^2\phi^\dagger\phi + \phi^\dagger D^2\phi) \\
&\quad + 2(\phi^\dagger\phi)^2 D_\mu\phi^\dagger D^\mu\phi\,. \qquad (4.3.9)
\end{aligned}
$$

Let us also explore a slightly more elaborated case. Let us consider the following three operators composed of two Higgses and two $B_{\mu\nu}$:

$$
O_1 = D_\mu(\phi^\dagger\phi) D^\nu B^{\mu\rho} B_{\nu\rho}\,, \qquad (4.3.10)
$$

$$
O_2 = (D^2\phi^\dagger\phi + \phi^\dagger D^2\phi) B^{\nu\rho} B_{\nu\rho}\,, \qquad (4.3.11)
$$

$$\mathcal{O}_3 = D_\mu \phi^\dagger D^\mu \phi B^{\nu\rho} B_{\nu\rho} \,. \tag{4.3.12}$$

The amplitude for the process $\varphi^0(p_1) \longrightarrow \varphi^0(p_2) B(p_3) B(p_4)$ is given by:

$$\begin{aligned}
\mathcal{A} = & -ic_1(\kappa_{3334} + 2\kappa_{3434} + \kappa_{3444} - \kappa'_{4333} - 2\kappa'_{4334} - \kappa'_{4344}) \\
& + 4ic_2(2\kappa_{2234} + 2\kappa_{2334} + 2\kappa_{2434} + \kappa_{3334} + 2\kappa_{3434} + \kappa_{3444} - 2\kappa'_{4322} - 2\kappa'_{4323} \\
& \quad - 2\kappa'_{4324} - \kappa'_{4333} - 2\kappa - 2\kappa'_{4334} - \kappa_{4344}) \\
& - 4ic_3(\kappa_{2234} + \kappa_{2334} + \kappa_{2434} - \kappa'_{4322} - \kappa_{4323} - \kappa_{4324}) \,;
\end{aligned} \tag{4.3.13}$$

where we removed p_1 using momentum conservation, and the kinematic invariants are: $\kappa_{ijkl} = (\varepsilon_3 \cdot \varepsilon_4)(p_i \cdot p_j)(p_k \cdot p_l)$ and $\kappa'_{ijkl} = (\varepsilon_3 \cdot p_i)(\varepsilon_4 \cdot p_j)(p_k \cdot p_l)$, where ε represents a polarization vector. The rank of the corresponding matrix is 2, so one of the operators is a linear combination of the other two. From inspection of the equation above, one arrives at $\mathcal{O}_1 = -\frac{1}{4}\mathcal{O}_2 - \frac{1}{2}\mathcal{O}_3$. This result can again be obtained at the Lagrangian level through the following relations:

$$\begin{aligned}
\mathcal{O}_1 &= -D_\mu(\phi^\dagger\phi) D^\mu B^{\rho\nu} B_{\nu\rho} - D_\mu(\phi^\dagger\phi) D^\rho B^{\nu\mu} B_{\nu\rho} \\
&= -D_\mu(\phi^\dagger\phi) D^\mu B^{\rho\nu} B_{\nu\rho} - D_\mu(\phi^\dagger\phi) D^\nu B^{\mu\rho} B_{\nu\rho} \\
&= -D_\mu(\phi^\dagger\phi) D^\mu B^{\rho\nu} B_{\nu\rho} - \mathcal{O}_1 \\
\Rightarrow \mathcal{O}_1 &= -\frac{1}{2} D_\mu(\phi^\dagger\phi) D^\mu B^{\rho\nu} B_{\nu\rho} \\
&= \frac{1}{2} D^2(\phi^\dagger\phi) B^{\rho\nu} B^{\nu\rho} - \frac{1}{2} D_\mu(\phi^\dagger\phi) B^{\rho\nu} D^\mu B_{\nu\rho} \\
&= \frac{1}{2} D^2(\phi^\dagger\phi) B^{\rho\nu} B_{\nu\rho} - \mathcal{O}_1 \\
\Rightarrow \mathcal{O}_1 &= \frac{1}{4} D^2(\phi^\dagger\phi) B^{\rho\nu} B_{\nu\rho} \\
&= -\frac{1}{4}(D^2\phi^\dagger\phi + \phi^\dagger D^2\phi) B^{\nu\rho} B_{\nu\rho} - \frac{1}{4}(2 D_\mu\phi^\dagger D^\mu\phi) B^{\nu\rho} B_{\nu\rho} \\
&= -\frac{1}{4}\mathcal{O}_2 - \frac{1}{2}\mathcal{O}_3 \,.
\end{aligned} \tag{4.3.14}$$

In the first equality we used the Bianchi identity whereas in the second we simply renamed the indices as $\nu \leftrightarrow \rho$ in the last operator; in the fifth equality we have integrated by parts the derivative acting on $B^{\rho\nu}$ while in the penultimate equality we have simply expanded the derivative. In all steps, we have also taken into account that B is anti-symmetric: $B^{\nu\rho} = -B^{\rho\nu}$.

These example calculations might look straightforward to address from the Lagrangian (position space) perspective. However, as hinted in the second example, things can get more involved when several

operators are involved. More importantly, the examples above demonstrate that, at the Lagrangian level, relations between *dependent* operators can be derived; however, proving whether operators are indeed independent at the Lagrangian level, entails proving that they are not related by whatever combination of operations you can perform. The power of tackling this issue in momentum space is that through this approach, calculating the rank of the corresponding matrix is enough to prove independence of operators.

One last issue to be taken care of when constructing the kinematic invariants has to do with the fact that we are working in 4-dimensions. This applies only to operators which involve dual field strength tensors, as the fully anti-symmetric Levi-Civita symbol $\epsilon^{\mu\nu\rho\lambda}$ is a 4-dimensional object which respects the Schouten identity:

$$g_{\mu\nu}\epsilon_{\alpha\beta\gamma\delta} + g_{\mu\alpha}\epsilon_{\beta\gamma\delta\nu} + g_{\mu\beta}\epsilon_{\gamma\delta\nu\alpha} + g_{\mu\gamma}\epsilon_{\delta\nu\alpha\beta} + g_{\mu\delta}\epsilon_{\nu\alpha\beta\gamma} = 0\,. \tag{4.3.15}$$

This can be translated into the following relations involving an arbitrary tensor T and field strength tensors, X and F:

$$T_{[\mu\nu]}X^{\mu}_{\ \rho}\widetilde{F}^{\nu\rho} = T_{[\mu\nu]}\widetilde{X}^{\mu}_{\ \rho}F^{\nu\rho}\,, \tag{4.3.16}$$

$$T_{\{\mu\nu\}}X^{\mu}_{\ \rho}\widetilde{F}^{\nu\rho} = -T_{\{\mu\nu\}}\widetilde{X}^{\mu}_{\ \rho}F^{\nu\rho} + \frac{1}{2}T^{\mu}_{\mu}\widetilde{X}^{\nu\rho}F_{\nu\rho}\,, \tag{4.3.17}$$

$$T_{\mu\nu}X^{\mu\rho}\widetilde{X}^{\nu}_{\ \rho} = \frac{1}{4}T^{\mu}_{\mu}X^{\nu\rho}\widetilde{X}_{\nu\rho}\,, \tag{4.3.18}$$

where $[\mu\nu]$ and $\{\mu\nu\}$ denote, anti-symmetrisation and symmetrisation, respectively. The relations hold in $D = 4$ space-time dimensions, and as such, we need to impose this in momentum space. This is done by requiring that momenta and polarization vectors involved are indeed four-vectors, that is, there can at most be 4 independent Lorentz vectors, with the others being simply a linear combination of those 4. We require this by writing, for instance:

$$p_4 = a_1\varepsilon_3 + a_2\varepsilon_4 + a_3p_2 + a_4p_3\,, \tag{4.3.19}$$

where $a_1\,, a_2\,, a_3$ and a_4 are arbitrary coefficients.

Let us see an example of using this condition, by considering the following operators:

$$O_1 = i(D_\mu\phi^\dagger\sigma^I D_\nu\phi - D_\nu\phi^\dagger\sigma^I D_\mu\phi)B^{\mu}_{\ \rho}\widetilde{W}^{I\nu\rho}\,, \tag{4.3.20}$$

$$O_2 = i(D_\mu\phi^\dagger\sigma^I D_\nu\phi - D_\nu\phi^\dagger\sigma^I D_\mu\phi)\widetilde{B}^{\mu}_{\ \rho}W^{I\nu\rho}\,, \tag{4.3.21}$$

which are related through Eq. (4.3.16).

Let us calculate the amplitude associated with the process $\varphi^0(p_1) \longrightarrow \varphi^0(p_2)W^3(p_3)B(p_4)$:

$$\mathcal{A} = c_1(-\kappa_{323443} - \kappa_{323444} + \kappa_{343424} + \kappa_{342334} + \kappa_{342344})$$

$$+ c_2(-\kappa_{423433} - \kappa_{423434} - \kappa_{343423} + \kappa_{342433} + \kappa_{342434})\,; \tag{4.3.22}$$

where $\kappa_{ijklmn} = \epsilon_{\mu\nu\rho\lambda}\varepsilon_i^\mu p_j^\nu p_k^\rho p_l^\lambda(\varepsilon_m \cdot p_n)$ and $\kappa'_{ijklmn} = \epsilon_{\mu\nu\rho\lambda}\varepsilon_i^\mu \varepsilon_j^\nu p_k^\rho p_l^\lambda(p_m \cdot p_n)$ and we have already applied momentum conservation in order to remove p_1. By considering that the rank of the associated matrix is 2 one would think that these operators are independent.

However, imposing $D = 4$ through Eq. (4.3.19) results in

$$\begin{aligned}\mathcal{A} = (c_1 + c_2)\Big[&a_3\kappa_{342323} + a_3(1+a_4)\kappa_{342323} + a_4(1+a_4)\kappa_{342333} \\ &+ a_1a_3\kappa_{342332} + a_1(1+2a_4)\kappa_{342333} + a_2a_4\kappa_{342343} + a_1^2\kappa_{342333}\Big]\,.\end{aligned} \tag{4.3.23}$$

Clearly, both operators describe the same off-shell physics and are therefore not independent. The difference between the two vanishes in $D = 4$ and is therefore an *evanescent* term. Knowing now how to prove operator independence, the strategy for finding the minimal set of operators in the Green's basis is to build all operators which can contribute to a particular process whose rank is the same as the number of off-shell operators provided by `Sym2Int` and `Basisgen` and eliminating operators whose removal does not affect the rank of the system.

4.3.2 Explicit form of the operators

We are expanding upon the on-shell basis showed in Appendix B [191], and as such, we will only include here the redundant operators. There are 2 *redundant* operators in the class ϕ^6D^2, 10 in ϕ^4D^4, 1 in ϕ^2D^6, 4 in $X\phi^4D^2$, 44 in $X^2\phi^2D^2$, 6 in $X\phi^2D^4$, 16 in X^3D^2 and 3 in the class X^2D^4.

4.3.2.1 Operators in the class ϕ^6D^2

$$\mathcal{O}^{(3)}_{\phi^6} = (\phi^\dagger\phi)^2(\phi^\dagger D^2\phi + \text{h.c.})\,, \tag{4.3.24}$$

$$\mathcal{O}^{(4)}_{\phi^6} = (\phi^\dagger\phi)^2 D_\mu(\phi^\dagger \mathrm{i}\overleftrightarrow{D}^\mu\phi)\,. \tag{4.3.25}$$

4.3.2.2 Operators in the class ϕ^4D^4

$$\mathcal{O}^{(4)}_{\phi^4} = D_\mu\phi^\dagger D^\mu\phi(\phi^\dagger D^2\phi + \text{h.c.})\,, \tag{4.3.26}$$

$$\mathcal{O}^{(5)}_{\phi^4} = D_\mu\phi^\dagger D^\mu\phi(\phi^\dagger \mathrm{i}D^2\phi + \text{h.c.})\,, \tag{4.3.27}$$

$$\mathcal{O}^{(6)}_{\phi^4} = (D_\mu\phi^\dagger\phi)(D^2\phi^\dagger D_\mu\phi) + \text{h.c.}\,, \tag{4.3.28}$$

$$O_{\phi^4}^{(7)} = (D_\mu\phi^\dagger\phi)(D^2\phi^\dagger \mathrm{i}D_\mu\phi) + \text{h.c.}\,, \tag{4.3.29}$$

$$O_{\phi^4}^{(8)} = (D^2\phi^\dagger\phi)(D^2\phi^\dagger\phi) + \text{h.c.}\,, \tag{4.3.30}$$

$$O_{\phi^4}^{(9)} = (D^2\phi^\dagger\phi)(\mathrm{i}D^2\phi^\dagger\phi) + \text{h.c.}\,, \tag{4.3.31}$$

$$O_{\phi^4}^{(10)} = (D^2\phi^\dagger D^2\phi)(\phi^\dagger\phi)\,, \tag{4.3.32}$$

$$O_{\phi^4}^{(11)} = (\phi^\dagger D^2\phi)(D^2\phi^\dagger\phi)\,, \tag{4.3.33}$$

$$O_{\phi^4}^{(12)} = (D_\mu\phi^\dagger\phi)(D^\mu\phi^\dagger D^2\phi) + \text{h.c.}\,, \tag{4.3.34}$$

$$O_{\phi^4}^{(13)} = (D_\mu\phi^\dagger\phi)(D^\mu\phi^\dagger \mathrm{i}D^2\phi) + \text{h.c.}\,. \tag{4.3.35}$$

4.3.2.3 Operators in the class $X\phi^4D^2$

$$O_{W\phi^4D^2}^{(5)} = (\phi^\dagger\phi)D_\nu W^{I\mu\nu}(D_\mu\phi^\dagger\sigma^I\phi + \text{h.c.})\,, \tag{4.3.36}$$

$$O_{W\phi^4D^2}^{(6)} = (\phi^\dagger\phi)D_\nu W^{I\mu\nu}(D_\mu\phi^\dagger \mathrm{i}\sigma^I\phi + \text{h.c.})\,, \tag{4.3.37}$$

$$O_{W\phi^4D^2}^{(7)} = \epsilon^{IJK}(D_\mu\phi^\dagger\sigma^I\phi)(\phi^\dagger\sigma^J D_\nu\phi)W^{K\mu\nu}\,, \tag{4.3.38}$$

$$O_{B\phi^4D^2}^{(3)} = (\phi^\dagger\phi)D_\nu B^{\mu\nu}(D_\mu\phi^\dagger \mathrm{i}\phi + \text{h.c.})\,. \tag{4.3.39}$$

4.3.2.4 Operators in the class ϕ^2D^6

$$O_{\phi^2} = D^2\phi^\dagger D_\mu D_\nu D^\mu D^\nu\phi\,. \tag{4.3.40}$$

4.3.2.5 Operators in the class $X\phi^2D^4$

$X = B$

$$O_{B\phi^2D^4}^{(1)} = i(D_\nu\phi^\dagger D^2\phi - D^2\phi^\dagger D_\nu\phi)D_\mu B^{\mu\nu}\,, \tag{4.3.41}$$

$$O_{B\phi^2D^4}^{(2)} = (D_\nu\phi^\dagger D^2\phi + D^2\phi^\dagger D_\nu\phi)D_\mu B^{\mu\nu}\,, \tag{4.3.42}$$

$$O_{B\phi^2D^4}^{(3)} = i(D_\rho D_\nu\phi^\dagger D^\rho\phi - D^\rho\phi^\dagger D_\rho D_\nu\phi)D_\mu B^{\mu\nu}\,. \tag{4.3.43}$$

$X = W$

$$O_{W\phi^2D^4}^{(1)} = i(D_\nu\phi^\dagger\sigma^I D^2\phi - D^2\phi^\dagger\sigma^I D_\nu\phi)D_\mu W^{I\mu\nu}\,, \tag{4.3.44}$$

$$O_{W\phi^2D^4}^{(2)} = (D_\nu\phi^\dagger\sigma^I D^2\phi + D^2\phi^\dagger\sigma^I D_\nu\phi)D_\mu W^{I\mu\nu}\,, \tag{4.3.45}$$

$$O_{B\phi^2D^4}^{(3)} = i(D_\rho D_\nu\phi^\dagger\sigma^I D^\rho\phi - D^\rho\phi^\dagger\sigma^I D_\rho D_\nu\phi)D_\mu W^{I\mu\nu}\,. \tag{4.3.46}$$

4.3.2.6 Operators in the class $X^2\phi^2D^2$

$X^2 = B^2$

$$\mathcal{O}^{(4)}_{B^2\phi^2D^2} = (D_\mu\phi^\dagger\phi + \phi^\dagger D_\mu\phi)D_\nu B^{\mu\rho}B^\nu{}_\rho\,, \tag{4.3.47}$$

$$\mathcal{O}^{(5)}_{B^2\phi^2D^2} = i(\phi^\dagger D_\mu D_\nu\phi - D_\mu D_\nu\phi^\dagger\phi)B^{\mu\rho}B^\nu{}_\rho\,, \tag{4.3.48}$$

$$\mathcal{O}^{(6)}_{B^2\phi^2D^2} = \phi^\dagger\phi D_\mu D_\nu B^{\mu\rho}B^\nu{}_\rho\,, \tag{4.3.49}$$

$$\mathcal{O}^{(7)}_{B^2\phi^2D^2} = i(\phi^\dagger D_\nu\phi - D_\nu\phi^\dagger\phi)D_\mu B^{\mu\rho}B^\nu{}_\rho\,, \tag{4.3.50}$$

$$\mathcal{O}^{(8)}_{B^2\phi^2D^2} = (\phi^\dagger D_\nu\phi + D_\nu\phi^\dagger\phi)D_\mu B^{\mu\rho}B^\nu{}_\rho\,, \tag{4.3.51}$$

$$\mathcal{O}^{(9)}_{B^2\phi^2D^2} = (\phi^\dagger D^2\phi + D^2\phi^\dagger\phi)B^{\nu\rho}\widetilde{B}_{\nu\rho}\,, \tag{4.3.52}$$

$$\mathcal{O}^{(10)}_{B^2\phi^2D^2} = i(\phi^\dagger D^2\phi - D^2\phi^\dagger\phi)B^{\nu\rho}\widetilde{B}_{\nu\rho} \tag{4.3.53}$$

$$\mathcal{O}^{(11)}_{B^2\phi^2D^2} = (\phi^\dagger D_\nu\phi + D_\nu\phi^\dagger\phi)D_\mu B^{\mu\rho}\widetilde{B}^\nu{}_\rho \tag{4.3.54}$$

$$\mathcal{O}^{(12)}_{B^2\phi^2D^2} = i(\phi^\dagger D_\nu\phi - D_\nu\phi^\dagger\phi)D_\mu B^{\mu\rho}\widetilde{B}^\nu{}_\rho\,. \tag{4.3.55}$$

$X^2 = W^2$

$$\mathcal{O}^{(7)}_{W^2\phi^2D^2} = i\epsilon^{IJK}(\phi^\dagger\sigma^I D^\nu\phi - D^\nu\phi^\dagger\sigma^I\phi)D_\mu W^{J\mu\rho}\widetilde{W}^K_{\nu\rho}\,, \tag{4.3.56}$$

$$\mathcal{O}^{(8)}_{W^2\phi^2D^2} = \epsilon^{IJK}\phi^\dagger\sigma^I\phi D_\nu D_\mu W^{J\mu\rho}\widetilde{W}^{K\nu}{}_\rho\,, \tag{4.3.57}$$

$$\mathcal{O}^{(9)}_{W^2\phi^2D^2} = i(\phi^\dagger D_\nu\phi - D_\nu\phi^\dagger\phi)D_\mu W^{I\mu\rho}\widetilde{W}^{I\nu}{}_\rho\,, \tag{4.3.58}$$

$$\mathcal{O}^{(10)}_{W^2\phi^2D^2} = (\phi^\dagger D_\nu\phi + D_\nu\phi^\dagger\phi)D_\mu W^{I\mu\rho}\widetilde{W}^{I\nu}{}_\rho\,, \tag{4.3.59}$$

$$\mathcal{O}^{(11)}_{W^2\phi^2D^2} = (\phi^\dagger D_\nu\phi + D_\nu\phi^\dagger\phi)D_\mu W^{I\mu\rho}W^{I\nu}{}_\rho\,, \tag{4.3.60}$$

$$\mathcal{O}^{(12)}_{W^2\phi^2D^2} = i(\phi^\dagger D_\nu\phi - D_\nu\phi^\dagger\phi)D_\mu W^{I\mu\rho}W^{I\nu}{}_\rho\,, \tag{4.3.61}$$

$$\mathcal{O}^{(13)}_{W^2\phi^2D^2} = \phi^\dagger\phi D_\mu W^{I\mu\rho}D_\nu W^{I\nu}{}_\rho\,, \tag{4.3.62}$$

$$\mathcal{O}^{(14)}_{W^2\phi^2D^2} = (D_\mu\phi^\dagger\phi + \phi^\dagger D_\mu\phi)W^{I\nu\rho}D^\mu W^I_{\nu\rho}\,, \tag{4.3.63}$$

$$\mathcal{O}^{(15)}_{W^2\phi^2D^2} = i(D_\mu\phi^\dagger\phi - \phi^\dagger D_\mu\phi)W^{I\nu\rho}D^\mu W^I_{\nu\rho}\,, \tag{4.3.64}$$

$$\mathcal{O}^{(16)}_{W^2\phi^2D^2} = (D_\mu\phi^\dagger\phi + \phi^\dagger D_\mu\phi)D^\mu W^{I\nu\rho}\widetilde{W}^I_{\nu\rho}\,, \tag{4.3.65}$$

$$\mathcal{O}^{(17)}_{W^2\phi^2D^2} = i(D_\mu\phi^\dagger\phi - \phi^\dagger D_\mu\phi)D^\mu W^{I\nu\rho}\widetilde{W}^I_{\nu\rho}\,, \tag{4.3.66}$$

$$\mathcal{O}^{(18)}_{W^2\phi^2D^2} = \epsilon^{IJK}(\phi^\dagger\sigma^I D^\nu\phi + D^\nu\phi^\dagger\sigma^I\phi)D_\mu W^{J\mu\rho}W^K_{\nu\rho}\,, \tag{4.3.67}$$

$$\mathcal{O}^{(19)}_{W^2\phi^2D^2} = i\epsilon^{IJK}(\phi^\dagger\sigma^I D^\nu\phi - D^\nu\phi^\dagger\sigma^I\phi)D_\mu W^{J\mu\rho}W^K_{\nu\rho}\,. \tag{4.3.68}$$

$X^2 = WB$

$$\mathcal{O}^{(7)}_{WB\phi^2D^2} = i(\phi^\dagger\sigma^I D^\mu\phi - D^\mu\phi^\dagger\sigma^I\phi)D_\mu B^{\nu\rho}W^I_{\nu\rho}\,, \tag{4.3.69}$$

$$\mathcal{O}^{(8)}_{WB\phi^2D^2} = (\phi^\dagger\sigma^I D^\nu\phi + D^\nu\phi^\dagger\sigma^I\phi)D_\mu B^{\mu\rho}W^I_{\nu\rho}\,, \tag{4.3.70}$$

$$\mathcal{O}^{(9)}_{WB\phi^2D^2} = i(\phi^\dagger\sigma^I D^\nu\phi - D^\nu\phi^\dagger\sigma^I\phi)D_\mu B^{\mu\rho}W^I_{\nu\rho}\,, \tag{4.3.71}$$

$$\mathcal{O}^{(10)}_{WB\phi^2D^2} = (\phi^\dagger\sigma^I\phi)D^\mu B_{\mu\rho}D_\nu W^{I\nu\rho}\,, \tag{4.3.72}$$

$$\mathcal{O}^{(11)}_{WB\phi^2D^2} = (D_\nu\phi^\dagger\sigma^I\phi + \phi^\dagger\sigma^I D_\nu\phi)B_{\mu\rho}D^\mu W^{I\nu\rho}\,, \tag{4.3.73}$$

$$\mathcal{O}^{(12)}_{WB\phi^2D^2} = i(D_\nu\phi^\dagger\sigma^I\phi - \phi^\dagger\sigma^I D_\nu\phi)B_{\mu\rho}D^\mu W^{I\nu\rho}\,, \tag{4.3.74}$$

$$\mathcal{O}^{(13)}_{WB\phi^2D^2} = (\phi^\dagger\sigma^I\phi)B_{\mu\rho}D_\nu D^\mu W^{I\nu\rho}\,, \tag{4.3.75}$$

$$\mathcal{O}^{(14)}_{WB\phi^2D^2} = i(D_\nu\phi^\dagger\sigma^I\phi - \phi^\dagger\sigma^I D_\nu\phi)D^\mu B_{\mu\rho}\widetilde{W}^{I\nu\rho}\,, \tag{4.3.76}$$

$$\mathcal{O}^{(15)}_{WB\phi^2D^2} = i(\phi^\dagger\sigma^I D_\mu\phi - D_\mu\phi^\dagger\sigma^I\phi)D^\mu B_{\nu\rho}\widetilde{W}^{I\nu\rho}\,, \tag{4.3.77}$$

$$\mathcal{O}^{(16)}_{WB\phi^2D^2} = (\phi^\dagger\sigma^I\phi)(D^2B^{\nu\rho})\widetilde{W}^I_{\nu\rho}\,, \tag{4.3.78}$$

$$\mathcal{O}^{(17)}_{WB\phi^2D^2} = (\phi^\dagger\sigma^I\phi)(D^\rho D_\mu W^{I\mu\nu})\widetilde{B}_{\nu\rho}\,, \tag{4.3.79}$$

$$\mathcal{O}^{(18)}_{WB\phi^2D^2} = i(D^\nu\phi^\dagger\sigma^I\phi - \phi^\dagger\sigma^I D^\nu\phi)\widetilde{B}^{\mu\rho}D_\mu W^I_{\nu\rho}\,, \tag{4.3.80}$$

$$\mathcal{O}^{(19)}_{WB\phi^2D^2} = (D^\nu\phi^\dagger\sigma^I\phi + \phi^\dagger\sigma^I D^\nu\phi)\widetilde{B}^{\mu\rho}D_\mu W^I_{\nu\rho}\,. \tag{4.3.81}$$

$X^2 = G^2$

$$\mathcal{O}^{(4)}_{G^2\phi^2D^2} = (D_\mu\phi^\dagger\phi + \phi^\dagger D_\mu\phi)D_\nu G^{A\mu\rho}G^{A\nu}_{\ \ \rho}\,, \tag{4.3.82}$$

$$\mathcal{O}^{(5)}_{G^2\phi^2D^2} = i(\phi^\dagger D_\mu D_\nu\phi - D_\mu D_\nu\phi^\dagger\phi)G^{A\mu\rho}G^{A\nu}_{\ \ \rho}\,, \tag{4.3.83}$$

$$\mathcal{O}^{(6)}_{G^2\phi^2D^2} = \phi^\dagger\phi D_\mu D_\nu G^{A\mu\rho}G^{A\nu}_{\ \ \rho}\,, \tag{4.3.84}$$

$$\mathcal{O}^{(7)}_{G^2\phi^2D^2} = i(\phi^\dagger D_\nu\phi - D_\nu\phi^\dagger\phi)D_\mu G^{A\mu\rho}G^{A\nu}_{\ \ \rho}\,, \tag{4.3.85}$$

$$\mathcal{O}^{(8)}_{G^2\phi^2D^2} = (\phi^\dagger D_\nu\phi + D_\nu\phi^\dagger\phi)D_\mu G^{A\mu\rho}G^{A\nu}_{\ \ \rho}\,, \tag{4.3.86}$$

$$\mathcal{O}^{(9)}_{G^2\phi^2D^2} = (\phi^\dagger D^2\phi + D^2\phi^\dagger\phi)G^{A\nu\rho}\widetilde{G}^{A\nu}_{\ \ \rho}\,, \tag{4.3.87}$$

$$\mathcal{O}^{(10)}_{G^2\phi^2D^2} = i(\phi^\dagger D^2\phi - D^2\phi^\dagger\phi)G^{A\nu\rho}\widetilde{G}^A_{\nu\rho} \tag{4.3.88}$$

$$\mathcal{O}^{(11)}_{G^2\phi^2D^2} = (\phi^\dagger D_\nu\phi + D_\nu\phi^\dagger\phi)D_\mu G^{A\mu\rho}\widetilde{G}^{A\nu}_{\ \ \rho} \tag{4.3.89}$$

$$\mathcal{O}^{(12)}_{G^2\phi^2D^2} = i(\phi^\dagger D_\nu\phi - D_\nu\phi^\dagger\phi)D_\mu G^{A\mu\rho}\widetilde{G}^{A\nu}_{\ \ \rho}\,. \tag{4.3.90}$$

4.3.2.7 Operators in the class X^3D^2

$X^3 = W^2B$

$$\mathcal{O}^{(1)}_{W^2BD^2} = B_{\mu\nu}D_\rho W^{I\mu\nu}D_\sigma W^{I\rho\sigma}\,, \tag{4.3.91}$$
$$\mathcal{O}^{(2)}_{W^2BD^2} = B_{\mu\nu}(D^2W^{I\mu\rho})W^{I\nu}{}_\rho\,, \tag{4.3.92}$$
$$\mathcal{O}^{(3)}_{W^2BD^2} = \widetilde{B}_{\mu\nu}D_\rho W^{I\mu\nu}D_\sigma W^{I\rho\sigma}\,, \tag{4.3.93}$$
$$\mathcal{O}^{(4)}_{W^2BD^2} = \widetilde{B}_{\mu\nu}(D^2W^{I\mu\rho})W^{I\nu}{}_\rho\,. \tag{4.3.94}$$

$X^3 = G^2B$

$$\mathcal{O}^{(1)}_{G^2BD^2} = B_{\mu\nu}D_\rho G^{A\mu\nu}D_\sigma G^{A\rho\sigma}\,, \tag{4.3.95}$$
$$\mathcal{O}^{(2)}_{G^2BD^2} = B_{\mu\nu}(D^2G^{A\mu\rho})G^{A\nu}{}_\rho\,, \tag{4.3.96}$$
$$\mathcal{O}^{(3)}_{G^2BD^2} = \widetilde{B}_{\mu\nu}D_\rho G^{A\mu\nu}D_\sigma G^{A\rho\sigma}\,, \tag{4.3.97}$$
$$\mathcal{O}^{(4)}_{G^2BD^2} = \widetilde{B}_{\mu\nu}(D^2G^{A\mu\rho})G^{A\nu}{}_\rho\,. \tag{4.3.98}$$

$X^3 = W^3$

$$\mathcal{O}^{(1)}_{W^3D^2} = \epsilon^{IJK}W^I_{\mu\nu}D_\rho W^{J\mu\nu}D_\sigma W^{K\rho\sigma}\,, \tag{4.3.99}$$
$$\mathcal{O}^{(2)}_{W^3D^2} = \epsilon^{IJK}W^I_{\mu\nu}D_\rho W^{J\rho\mu}D_\sigma W^{K\sigma\nu}\,, \tag{4.3.100}$$
$$\mathcal{O}^{(3)}_{W^3D^2} = \epsilon^{IJK}\widetilde{W}^I_{\mu\nu}D_\rho W^{J\mu\nu}D_\sigma W^{K\rho\sigma}\,, \tag{4.3.101}$$
$$\mathcal{O}^{(4)}_{W^3D^2} = \epsilon^{IJK}\widetilde{W}^I_{\mu\nu}D_\rho W^{J\rho\mu}D_\sigma W^{K\sigma\nu}\,. \tag{4.3.102}$$

$X^3 = G^3$

$$\mathcal{O}^{(1)}_{G^3D^2} = f^{ABC}G^A_{\mu\nu}D_\rho G^{B\mu\nu}D_\sigma G^{C\rho\sigma}\,, \tag{4.3.103}$$
$$\mathcal{O}^{(2)}_{G^3D^2} = f^{ABC}G^A_{\mu\nu}D_\rho G^{B\rho\mu}D_\sigma G^{C\sigma\nu}\,, \tag{4.3.104}$$
$$\mathcal{O}^{(3)}_{G^3D^2} = f^{ABC}\widetilde{G}^A_{\mu\nu}D_\rho G^{B\mu\nu}D_\sigma G^{C\rho\sigma}\,, \tag{4.3.105}$$
$$\mathcal{O}^{(4)}_{G^3D^2} = f^{ABC}\widetilde{G}^A_{\mu\nu}D_\rho G^{B\rho\mu}D_\sigma G^{C\sigma\nu}\,, \tag{4.3.106}$$

4.3.2.8 Operators in the class X^2D^4

$X = B$

$$\mathcal{O}_{B^2D^4} = (D_\sigma D_\mu B^{\mu\nu})(D^\sigma D^\rho B_{\rho\nu})\,. \tag{4.3.107}$$

$X = W$

$$\mathcal{O}_{W^2D^4} = (D_\sigma D_\mu W^{I\mu\nu})(D^\sigma D^\rho W^I_{\rho\nu})\,. \tag{4.3.108}$$

$X = G$

$$\mathcal{O}_{G^2D^4} = (D_\sigma D_\mu G^{A\mu\nu})(D^\sigma D^\rho G^A_{\rho\nu})\,. \tag{4.3.109}$$

4.3.3 On-shell relations

For the RGEs calculations we will perform in the next sections, we can remove the redundant operators by using the SM EOM. Neglecting fermions, the SM EOMs read:

$$D^2\phi^i = -2\lambda(\phi^\dagger\phi)\phi^i\,, \tag{4.3.110}$$

$$\partial^\nu B_{\mu\nu} = \frac{g_1}{2}(\phi^\dagger i D_\mu\phi - D_\mu\phi^\dagger i\phi)\,, \tag{4.3.111}$$

$$D^\nu W^I_{\mu\nu} = \frac{g_2}{2}(\phi^\dagger i D_\mu\sigma^I\phi - \phi^\dagger i\sigma^I D_\mu\phi)\,, \tag{4.3.112}$$

where we neglected here the contribution proportional to μ in the Higgs EOM. The shift on the WCs of on-shell operators from the removal of the redundant ones is given by:

$$\begin{aligned}
c_{\phi^8} \to\ & c_{\phi^8} - \frac{1}{2}c_{B^2D^4}g_1^2g_2^2\lambda + \frac{1}{2}c^{(8)}_{B^2\phi^2D^2}g_1^2\lambda + 2c^{(1)}_{B\phi^2D^4}g_1\lambda^2 + \frac{1}{4}c^{(3)}_{B\phi^2D^4}g_1g_2^2\lambda \\
& - 2c^{(3)}_{B\phi^2D^4}g_1\lambda^2 + c^{(3)}_{B\phi^4D^2}g_1\lambda + 4c^{(10)}_{\phi^4}\lambda^2 + 4c^{(11)}_{\phi^4}\lambda^2 - 4c^{(12)}_{\phi^4}\lambda^2 + 8c^{(8)}_{\phi^4}\lambda^2 \\
& - c_{W^2D^4}g_1^2g_2^2\lambda - \frac{1}{2}c_{W^2D^4}g_2^4\lambda + \frac{1}{2}c^{(11)}_{W^2\phi^2D^2}g_2^2\lambda - \frac{1}{2}c^{(13)}_{W^2\phi^2D^2}g_2^2\lambda - c^{(19)}_{W^2\phi^2D^2}g_2^2\lambda \\
& - c^{(1)}_{W^3D^2}g_2^3\lambda + \frac{1}{2}c^{(2)}_{W^3D^2}g_2^3\lambda - \frac{1}{2}c^{(10)}_{WB\phi^2D^2}g_1g_2\lambda + \frac{c^{(11)}_{WB\phi^2D^2}g_1g_2\lambda}{4} + c^{(13)}_{WB\phi^2D^2}g_1g_2\lambda \\
& + 2c^{(1)}_{W\phi^2D^4}g_2\lambda^2 + \frac{1}{2}c^{(3)}_{W\phi^2D^4}g_1^2g_2\lambda - 2c^{(3)}_{W\phi^2D^4}g_2\lambda^2 + c^{(6)}_{W\phi^4D^2}g_2\lambda + \frac{c^{(7)}_{W\phi^4D^2}g_2\lambda}{2} \\
& - 4c^{(3)}_{\phi^6}\lambda - c_{\phi^2}\left(g_1^2\lambda^2 + g_2^2\lambda^2 + 32\lambda^3\right)\,,
\end{aligned} \tag{4.3.113}$$

$$\begin{aligned}
c^{(1)}_{\phi^6} \to\ & c^{(1)}_{\phi^6} + c_{B^2D^4}g_1^2g_2^2 - \frac{3c^{(8)}_{B^2\phi^2D^2}g_1^2}{4} - 3c^{(1)}_{B\phi^2D^4}g_1\lambda - \frac{1}{2}c^{(3)}_{B\phi^2D^4}g_1g_2^2 + 3c^{(3)}_{B\phi^2D^4}g_1\lambda \\
& - \frac{3c^{(3)}_{B\phi^4D^2}g_1}{2} + \frac{3}{2}c_{\phi^2}g_1^2\lambda + \frac{5}{2}c_{\phi^2}g_2^2\lambda + 8c_{\phi^2}\lambda^2 + 4c^{(12)}_{\phi^4}\lambda - 4c^{(4)}_{\phi^4}\lambda - 2c^{(6)}_{\phi^4}\lambda \\
& + \frac{3}{2}c_{W^2D^4}g_1^2g_2^2 + \frac{5c_{W^2D^4}g_2^4}{4} - \frac{5c^{(11)}_{W^2\phi^2D^2}g_2^2}{4} + \frac{5c^{(13)}_{W^2\phi^2D^2}g_2^2}{4} + \frac{5c^{(19)}_{W^2\phi^2D^2}g_2^2}{2}
\end{aligned}$$

$$+\frac{5c^{(1)}_{W^3D^2}g_2^3}{2}-\frac{5c^{(2)}_{W^3D^2}g_2^3}{4}+\frac{3c^{(10)}_{WB\phi^2D^2}g_1g_2}{4}-\frac{c^{(11)}_{WB\phi^2D^2}g_1g_2}{4}-\frac{3c^{(13)}_{WB\phi^2D^2}g_1g_2}{2}$$
$$+\frac{c^{(8)}_{WB\phi^2D^2}g_1g_2}{4}-5c^{(1)}_{W\phi^2D^4}g_2\lambda-\frac{3}{4}c^{(3)}_{W\phi^2D^4}g_1^2g_2+5c^{(3)}_{W\phi^2D^4}g_2\lambda-\frac{5c^{(6)}_{W\phi^4D^2}g_2}{2}$$
$$-c^{(7)}_{W\phi^4D^2}g_2\,, \tag{4.3.114}$$

$$c^{(2)}_{\phi^6}\to c^{(2)}_{\phi^6}+\frac{1}{4}c_{B^2D^4}g_1^2g_2^2-\frac{c^{(8)}_{B^2\phi^2D^2}g_1^2}{2}-2c^{(1)}_{B\phi^2D^4}g_1\lambda-\frac{1}{8}c^{(3)}_{B\phi^2D^4}g_1g_2^2+2c^{(3)}_{B\phi^2D^4}g_1\lambda$$
$$-c^{(3)}_{B\phi^4D^2}g_1+c_{\phi^2}g_1^2\lambda+2c^{(12)}_{\phi^4}\lambda-2c^{(6)}_{\phi^4}\lambda+c_{W^2D^4}g_1^2g_2^2+\frac{c^{(10)}_{WB\phi^2D^2}g_1g_2}{2}$$
$$-\frac{c^{(8)}_{WB\phi^2D^2}g_1g_2}{4}-\frac{3c^{(11)}_{WB\phi^2D^2}g_1g_2}{8}-c^{(13)}_{WB\phi^2D^2}g_1g_2-\frac{1}{2}c^{(3)}_{W\phi^2D^4}g_1^2g_2$$
$$-\frac{c^{(7)}_{W\phi^4D^2}g_2}{4}\,, \tag{4.3.115}$$

$$c^{(1)}_{\phi^4}\to c^{(1)}_{\phi^4}+c_{B^2D^4}g_1^2-c^{(3)}_{B\phi^2D^4}g_1-c_{W^2D^4}g_2^2+c^{(3)}_{W\phi^2D^4}g_2\,, \tag{4.3.116}$$

$$c^{(2)}_{\phi^4}\to c^{(2)}_{\phi^4}-c_{B^2D^4}g_1^2+c^{(3)}_{B\phi^2D^4}g_1-c_{W^2D^4}g_2^2+c^{(3)}_{W\phi^2D^4}g_2\,, \tag{4.3.117}$$

$$c^{(3)}_{\phi^4}\to c^{(3)}_{\phi^4}+2c_{W^2D^4}g_2^2-2c^{(3)}_{W\phi^2D^4}g_2\,, \tag{4.3.118}$$

$$c^{(1)}_{G^3\phi^2}\to c^{(1)}_{G^3\phi^2}+g_3c^{(6)}_{G^2\phi^2D^2}\,, \tag{4.3.119}$$

$$c^{(1)}_{W^3\phi^2}\to c^{(1)}_{W^3\phi^2}-\frac{c^{(1)}_{W^3D^2}g_2^2}{2}\,, \tag{4.3.120}$$

$$c^{(2)}_{W^3\phi^2}\to c^{(2)}_{W^3\phi^2}-\frac{c^{(3)}_{W^3D^2}g_2^2}{2}\,, \tag{4.3.121}$$

$$c^{(1)}_{W^2B\phi^2}\to c^{(1)}_{W^2B\phi^2}-\frac{c^{(1)}_{W^3D^2}g_1g_2}{2}+\frac{c^{(11)}_{WB\phi^2D^2}g_2}{2}+c^{(13)}_{WB\phi^2D^2}g_2\,, \tag{4.3.122}$$

$$c^{(2)}_{W^2B\phi^2}\to c^{(2)}_{W^2B\phi^2}+\frac{c^{(3)}_{W^3D^2}g_1g_2}{4}+\frac{c^{(19)}_{WB\phi^2D^2}g_2}{2}\,, \tag{4.3.123}$$

$$c^{(1)}_{G^2\phi^4}\to c^{(1)}_{G^2\phi^4}+\lambda c^{(4)}_{G^2\phi^2D^2}\,, \tag{4.3.124}$$

$$c^{(2)}_{G^2\phi^4}\to c^{(2)}_{G^2\phi^4}-4\lambda c^{(9)}_{G^2\phi^2D^2}\,, \tag{4.3.125}$$

$$c^{(1)}_{W^2\phi^4}\to c^{(1)}_{W^2\phi^4}-\frac{1}{8}c_{B^2D^4}g_1^2g_2^2+\frac{1}{16}c^{(3)}_{B\phi^2D^4}g_1g_2^2-\frac{c_{W^2D^4}g_2^4}{8}+\frac{c^{(11)}_{W^2\phi^2D^2}g_2^2}{4}$$
$$+2c^{(14)}_{W^2\phi^2D^2}\lambda-\frac{c^{(19)}_{W^2\phi^2D^2}g_2^2}{2}-\frac{c^{(1)}_{W^3D^2}g_2^3}{2}+\frac{c^{(2)}_{W^3D^2}g_2^3}{4}-\frac{c^{(11)}_{WB\phi^2D^2}g_1g_2}{16}$$

$$- \frac{c^{(8)}_{WB\phi^2D^2} g_1 g_2}{8} + \frac{c^{(7)}_{W\phi^4D^2} g_2}{8} - \frac{1}{2} c_{\phi^2} g_2^2 \lambda \,, \tag{4.3.126}$$

$$c^{(2)}_{W^2\phi^4} \to c^{(2)}_{W^2\phi^4} + \frac{c^{(10)}_{W^2\phi^2D^2} g_2^2}{4} + 2c^{(16)}_{W^2\phi^2D^2}\lambda - \frac{c^{(7)}_{W^2\phi^2D^2} g_2^2}{2} + \frac{c^{(3)}_{W^3D^2} g_2^3}{2} + \frac{c^{(4)}_{W^3D^2} g_2^3}{4} + \frac{c^{(16)}_{WB\phi^2D^2} g_1 g_2}{4} + \frac{c^{(19)}_{WB\phi^2D^2} g_1 g_2}{16} \,, \tag{4.3.127}$$

$$c^{(3)}_{W^2\phi^4} \to c^{(3)}_{W^2\phi^4} + \frac{1}{16} c^{(3)}_{B\phi^2D^4} g_1 g_2^2 + \frac{c^{(7)}_{W\phi^4D^2} g_2}{8} + \frac{c^{(8)}_{WB\phi^2D^2} g_1 g_2}{8} + \frac{c^{(11)}_{WB\phi^2D^2} g_1 g_2}{16} \,, \tag{4.3.128}$$

$$c^{(4)}_{W^2\phi^4} \to c^{(4)}_{W^2\phi^4} - \frac{c^{(16)}_{WB\phi^2D^2} g_1 g_2}{4} - \frac{c^{(19)}_{WB\phi^2D^2} g_1 g_2}{16} \,, \tag{4.3.129}$$

$$c^{(1)}_{WB\phi^4} \to c^{(1)}_{WB\phi^4} - \frac{c^{(6)}_{B^2\phi^2D^2} g_1 g_2}{4} + \frac{c^{(8)}_{B^2\phi^2D^2} g_1 g_2}{4} + \frac{1}{8} c^{(3)}_{B\phi^2D^4} g_1^2 g_2 - \frac{1}{2} c_{W^2D^4} g_1 g_2^3 + \frac{c^{(11)}_{W^2\phi^2D^2} g_1 g_2}{4} - \frac{c^{(19)}_{W^2\phi^2D^2} g_1 g_2}{2} - \frac{1}{2} c^{(1)}_{W^3D^2} g_1 g_2^2 + \frac{1}{4} c^{(2)}_{W^3D^2} g_1 g_2^2 + \frac{c^{(11)}_{WB\phi^2D^2} g_2^2}{8} + c^{(11)}_{WB\phi^2D^2}\lambda + \frac{c^{(13)}_{WB\phi^2D^2} g_2^2}{4} + \frac{1}{4} c^{(3)}_{W\phi^2D^4} g_1 g_2^2 + \frac{c^{(7)}_{W\phi^4D^2} g_1}{4} - c_{\phi^2} g_1 g_2 \lambda \,, \tag{4.3.130}$$

$$c^{(2)}_{WB\phi^4} \to c^{(2)}_{WB\phi^4} + \frac{c^{(11)}_{B^2\phi^2D^2} g_1 g_2}{4} + \frac{c^{(10)}_{W^2\phi^2D^2} g_1 g_2}{4} - \frac{c^{(7)}_{W^2\phi^2D^2} g_1 g_2}{2} + \frac{1}{2} c^{(3)}_{W^3D^2} g_1 g_2^2 + \frac{1}{4} c^{(4)}_{W^3D^2} g_1 g_2^2 - \frac{c^{(19)}_{WB\phi^2D^2} g_2^2}{4} + c^{(19)}_{WB\phi^2D^2}\lambda - \frac{c^{(17)}_{WB\phi^2D^2} g_2^2}{4} \,, \tag{4.3.131}$$

$$c^{(1)}_{B^2\phi^4} \to c^{(1)}_{B^2\phi^4} + \frac{c_{B^2D^4} g_1^4}{8} + c^{(4)}_{B^2\phi^2D^2}\lambda - \frac{c^{(6)}_{B^2\phi^2D^2} g_1^2}{4} + \frac{c^{(8)}_{B^2\phi^2D^2} g_1^2}{4} - \frac{3}{8} c_{W^2D^4} g_1^2 g_2^2 + \frac{c^{(11)}_{WB\phi^2D^2} g_1 g_2}{8} + \frac{c^{(13)}_{WB\phi^2D^2} g_1 g_2}{4} + \frac{1}{4} c^{(3)}_{W\phi^2D^4} g_1^2 g_2 - \frac{1}{2} c_{\phi^2} g_1^2 \lambda \,, \tag{4.3.132}$$

$$c^{(2)}_{B^2\phi^4} \to c^{(2)}_{B^2\phi^4} + \frac{c^{(11)}_{B^2\phi^2D^2} g_1^2}{4} - 4c^{(9)}_{B^2\phi^2D^2}\lambda - \frac{c^{(19)}_{WB\phi^2D^2} g_1 g_2}{4} - \frac{c^{(17)}_{WB\phi^2D^2} g_1 g_2}{4} \,, \tag{4.3.133}$$

$$c^{(2)}_{G^2\phi^2D^2} \to c^{(2)}_{G^2\phi^2D^2} - \frac{1}{2} c^{(4)}_{G^2\phi^2D^2} \,, \tag{4.3.134}$$

$$c^{(2)}_{W^2\phi^2D^2} \to c^{(2)}_{W^2\phi^2D^2} - c^{(14)}_{W^2\phi^2D^2} \,, \tag{4.3.135}$$

$$c^{(3)}_{W^2\phi^2D^2} \to c^{(3)}_{W^2\phi^2D^2} - c^{(16)}_{W^2\phi^2D^2} \,, \tag{4.3.136}$$

$$c^{(4)}_{W^2\phi^2D^2} \to c^{(4)}_{W^2\phi^2D^2} - 2c^{(1)}_{W^3D^2} g_2 \,, \tag{4.3.137}$$

$$c^{(6)}_{W^2\phi^2D^2} \to c^{(6)}_{W^2\phi^2D^2} - c^{(3)}_{W^3D^2}g_2\,, \tag{4.3.138}$$

$$c^{(1)}_{WB\phi^2D^2} \to c^{(1)}_{WB\phi^2D^2} - \frac{c^{(11)}_{WB\phi^2D^2}}{2}\,, \tag{4.3.139}$$

$$c^{(2)}_{WB\phi^2D^2} \to c^{(2)}_{WB\phi^2D^2} - \frac{c^{(19)}_{WB\phi^2D^2}}{2}\,, \tag{4.3.140}$$

$$c^{(3)}_{WB\phi^2D^2} \to c^{(3)}_{WB\phi^2D^2} - c^{(1)}_{W^2BD^2}g_2 + c^{(2)}_{W^2BD^2}g_2 + c^{(12)}_{WB\phi^2D^2} + 2c^{(7)}_{WB\phi^2D^2}\,, \tag{4.3.141}$$

$$c^{(5)}_{WB\phi^2D^2} \to c^{(5)}_{WB\phi^2D^2} - c^{(3)}_{W^2BD^2}g_2 + \frac{3c^{(4)}_{W^2BD^2}g_2}{2} + 2c^{(15)}_{WB\phi^2D^2} + c^{(18)}_{WB\phi^2D^2}\,, \tag{4.3.142}$$

$$c^{(2)}_{B^2\phi^2D^2} \to c^{(2)}_{B^2\phi^2D^2} - \frac{c^{(4)}_{B^2\phi^2D^2}}{2}\,, \tag{4.3.143}$$

$$\begin{aligned} c^{(1)}_{W\phi^4D^2} \to\ & c^{(1)}_{W\phi^4D^2} - c_{B^2D^4}g_1^2g_2 + \frac{c^{(3)}_{B\phi^2D^4}g_1g_2}{2} - c_{W^2D^4}g_2^3 + c^{(11)}_{W^2\phi^2D^2}g_2 - 4c^{(19)}_{W^2\phi^2D^2}g_2 \\ & - 4c^{(1)}_{W^3D^2}g_2^2 + 2c^{(2)}_{W^3D^2}g_2^2 - \frac{c^{(11)}_{WB\phi^2D^2}g_1}{2} - c^{(8)}_{WB\phi^2D^2}g_1 - \frac{c^{(3)}_{W\phi^2D^4}g_2^2}{2} \\ & + 2c^{(7)}_{W\phi^4D^2}\,, \end{aligned} \tag{4.3.144}$$

$$\begin{aligned} c^{(2)}_{W\phi^4D^2} \to\ & c^{(2)}_{W\phi^4D^2} + c^{(10)}_{W^2\phi^2D^2}g_2 - 4c^{(7)}_{W^2\phi^2D^2}g_2 + 4c^{(3)}_{W^3D^2}g_2^2 + 2c^{(4)}_{W^3D^2}g_2^2 + 2c^{(16)}_{WB\phi^2D^2}g_1 \\ & + \frac{c^{(19)}_{WB\phi^2D^2}g_1}{2}\,, \end{aligned} \tag{4.3.145}$$

$$\begin{aligned} c^{(3)}_{W\phi^4D^2} \to\ & c^{(3)}_{W\phi^4D^2} + \frac{c^{(1)}_{W^2BD^2}g_1g_2}{2} + c^{(12)}_{W^2\phi^2D^2}g_2 + c^{(18)}_{W^2\phi^2D^2}g_2 - \frac{c^{(12)}_{WB\phi^2D^2}g_1}{2} - c^{(7)}_{WB\phi^2D^2}g_1 \\ & - c^{(9)}_{WB\phi^2D^2}g_1\,, \end{aligned} \tag{4.3.146}$$

$$\begin{aligned} c^{(4)}_{W\phi^4D^2} \to\ & c^{(4)}_{W\phi^4D^2} + \frac{c^{(3)}_{W^2BD^2}g_1g_2}{2} + \frac{c^{(4)}_{W^2BD^2}g_1g_2}{4} - c^{(8)}_{W^2\phi^2D^2}g_2 + c^{(9)}_{W^2\phi^2D^2}g_2 + c^{(14)}_{WB\phi^2D^2}g_1 \\ & - c^{(15)}_{WB\phi^2D^2}g_1 - \frac{c^{(18)}_{WB\phi^2D^2}g_1}{2}\,, \end{aligned} \tag{4.3.147}$$

$$\begin{aligned} c^{(1)}_{B\phi^4D^2} \to\ & c^{(1)}_{B\phi^4D^2} + c_{B^2D^4}g_1^3 - c^{(6)}_{B^2\phi^2D^2}g_1 + c^{(8)}_{B^2\phi^2D^2}g_1 - \frac{c^{(3)}_{B\phi^2D^4}g_1^2}{2} - 3c_{W^2D^4}g_1g_2^2 \\ & + \frac{3c^{(11)}_{WB\phi^2D^2}g_2}{2} + 3c^{(13)}_{WB\phi^2D^2}g_2 + \frac{3c^{(3)}_{W\phi^2D^4}g_1g_2}{2}\,, \end{aligned} \tag{4.3.148}$$

$$c^{(2)}_{B\phi^4D^2} \to c^{(2)}_{B\phi^4D^2} + c^{(11)}_{B^2\phi^2D^2}g_1 - 3c^{(19)}_{WB\phi^2D^2}g_2 - 3c^{(17)}_{WB\phi^2D^2}g_2\,. \tag{4.3.149}$$

4.3.4 Some applications

4.3.4.1 Automated one-loop matching

Recently, automated tools to calculate one-loop matching conditions of generic UV extensions onto the SMEFT have been developed [214–217]. Of those, `matchmakereft` [217] performs off-shell matching and as such, it requires knowledge of a Green's basis of the SMEFT. The program already provides a Green's basis at dimension-6, but if the user wants to perform calculations at dimension-8, an off-shell basis at this order must be provided as well as the reduction to the on-shell basis.

Let us perform the one-loop matching of a heavy singlet scalar, $\mathcal{S} \sim (1,1,0)$, where the numbers within parentheses represent the $SU(3)_c$, $SU(2)_L$ quantum numbers and the hypercharge, respectively. Let us also impose a $\mathbb{Z}_2$ symmetry $\mathcal{S} \to -\mathcal{S}$. The full theory Lagrangian is given by:

$$\mathcal{L}_{\text{NP}} = \frac{1}{2}(D_\mu \mathcal{S})(D^\mu \mathcal{S}) - \frac{1}{2}m_{\mathcal{S}}^2 \mathcal{S}^2 - \lambda_{\mathcal{S}\phi}\mathcal{S}^2\phi^\dagger\phi - \lambda_{\mathcal{S}}\mathcal{S}^4 \,. \tag{4.3.150}$$

Due to the required $\mathbb{Z}_2$ symmetry, effective operators do not arise at tree-level. Thus, by implementing this Lagrangian, together with the Green's basis of dimension-8 operators and the reduction to the on-shell basis in `matchmakereft` [217], one can automatically calculate the following one-loop matching conditions.

$$\frac{c_{\phi^6}^{(1)}}{\Lambda^4} = \frac{1}{1920\, m_{\mathcal{S}}^4\, \pi^2}\lambda_{\mathcal{S}\phi}^2\left(5\lambda_{\mathcal{S}\phi} - 8\lambda\right) \,, \tag{4.3.151}$$

$$\frac{c_{\phi^4}^{(3)}}{\Lambda^4} = \frac{1}{960\, m_{\mathcal{S}}^4\, \pi^2}\lambda_{\mathcal{S}\phi}^2 \,, \tag{4.3.152}$$

where we have taken the limit $g_2 \to 0$ for simplicity.

Let us also present a more complex example in which we extend the SM with a quadruplet scalar, Θ $(1,4,1/2)$. The relevant full theory Lagrangian is given by:

$$\mathcal{L}_{\text{NP}} = D_\mu\Theta^\dagger D^\mu\Theta - m_\Theta^2\Theta^\dagger\Theta - \lambda_\Theta(\phi^\dagger\sigma^I\phi)C_{I\beta}^{\alpha}\tilde{\phi}^\beta\epsilon_{\alpha\gamma}\Theta^\gamma + \text{h.c.} \,, \tag{4.3.153}$$

where $C_{I\beta}^{\alpha}$ is the Clebsh-Gordan needed to form a $SU(2)_L$ singlet from a quadruplet, a doublet and a triplet. Ignoring for simplicity contributions proportional to g_2, we obtain:

$$\frac{c_{B^4}^{(1)}}{\Lambda^4} = \frac{7g_1^4}{92160\, m_\Theta^4\, \pi^2} \,, \tag{4.3.154}$$

$$\frac{c_{B^4}^{(2)}}{\Lambda^4} = \frac{g_1^4}{92160\, m_\Theta^4\, \pi^2} \,, \tag{4.3.155}$$

$$\frac{c_{\phi^6}^{(1)}}{\Lambda^4} = \frac{|\lambda_\Theta|^2}{3\,m_\Theta^2} + \frac{-6440\,g_1^2\,|\lambda_\Theta|^2 + 103040\,|\lambda_\Theta|^2\lambda}{80640\,m_\Theta^4\,\pi^2}\,, \tag{4.3.156}$$

$$\frac{c_{\phi^6}^{(2)}}{\Lambda^4} = -\frac{|\lambda_\Theta|^2}{2\,m_\Theta^2} + \frac{+3640\,g_1^2|\lambda_\Theta|^2\, - 655200\,|\lambda_\Theta|^2\,\lambda}{483840\,m_\Theta^4\,\pi^2}\,, \tag{4.3.157}$$

$$\frac{c_{\phi^4}^{(1)}}{\Lambda^4} = \frac{4480\,|\lambda_\Theta|^2 - 3g_1^4}{40320\,m_\Theta^4\,\pi^2}\,, \tag{4.3.158}$$

$$\frac{c_{\phi^4}^{(2)}}{\Lambda^4} = \frac{3g_1^4 + 1120\,|\lambda_\Theta|^2}{40320\,m_\Theta^4\,\pi^2}\,, \tag{4.3.159}$$

$$\frac{c_{\phi^4}^{(3)}}{\Lambda^4} = -\frac{|\lambda_\Theta|^2}{18\,m_\Theta^4\,\pi^2}\,, \tag{4.3.160}$$

$$\frac{c_{B^2\phi^4}^{(1)}}{\Lambda^4} = \frac{1960\,g_1^2|\lambda_\Theta|^2 - 3g_1^6}{322560\,m_\Theta^4\,\pi^2}\,, \tag{4.3.161}$$

$$\frac{c_{B\phi^4D^2}^{(1)}}{\Lambda^4} = -\frac{g_1^5}{13440\,m_\Theta^4\,\pi^2}\,. \tag{4.3.162}$$

We find agreement with the tree-level contribution to $c_{\phi^6}^{(1)}$ and $c_{\phi^6}^{(2)}$ in Ref. [191] and with the contribution to $c_{B^4}^{(1)}$ and $c_{B^4}^{(2)}$ previously computed in Refs. [179, 218].

4.3.4.2 Reduction to a physical basis

Another approach to matching is to use functional methods which integrate over the heavy dynamical fields in the path integral [219–221]. One of the main advantages of this approach is that it does not require the construction of an EFT basis. However, the drawback of this is that the matching result is given in terms of redundant operators, whose reduction to a physical basis is not *a priori* known.

While automated tools to perform this matching at one-loop exist [214–216], the problem of obtaining the matching result in a redundant set of operators can even be observed in simple models at tree-level. Let us focus on an extension of the SM with a heavy vector triplet $\mathcal{W} \sim (1,3,0)$, with the relevant Lagrangian given by:

$$\mathcal{L}_{\text{NP}} = \frac{1}{2}\left[D_\mu\mathcal{W}_\nu^\dagger D^\nu\mathcal{W}^\mu - D_\mu\mathcal{W}_\nu^\dagger D^\mu\mathcal{W}^\nu + m_\mathcal{W}^2\mathcal{W}_\mu^\dagger\mathcal{W}^\mu + (g_\mathcal{W}^\phi\mathcal{W}^\mu\phi^{I\dagger}\sigma^I iD_\mu\phi + \text{h.c.})\right]. \tag{4.3.163}$$

The results for the tree-level matching of this theory (up to order $1/m_{\mathcal{W}}^4$) with `MatchingTools` [222] are given by:

$$\begin{aligned}
\mathcal{L}_{\text{EFT}}^{(8)} = \frac{(g_{\mathcal{W}}^{\phi})^2}{m_{\mathcal{W}}^4}\Big[&2(D_\mu\phi^\dagger D_\nu\phi)(D^\mu\phi^\dagger D^\nu\phi) + 4(D_\nu\phi^\dagger D^\nu D^\mu\phi)(D_\mu\phi^\dagger\phi) - 2(D_\mu\phi^\dagger D_\nu\phi)(\phi^\dagger D^\mu D^\nu\phi)\\
&- 4(D_\mu\phi^\dagger\phi)(D^\mu D_\nu\phi^\dagger D^\nu\phi) + 2(D_\mu\phi^\dagger D_\nu\phi)(D^\mu D^\nu\phi^\dagger\phi) - 4(D_\mu\phi^\dagger D^\mu\phi)(D_\nu\phi^\dagger D^\nu\phi)\\
&+ 2(D_\mu\phi^\dagger D_\nu\phi)(D^\nu\phi^\dagger D^\mu\phi) + \frac{1}{2}(\phi^\dagger D_\mu D_\nu\phi)(\phi^\dagger D^\mu D^\nu\phi) - 2(D_\nu D_\rho\phi^\dagger D^\nu D^\rho\phi)(\phi^\dagger\phi)\\
&+ (D_\mu D_\nu\phi^\dagger\phi)(\phi^\dagger D^\mu D^\nu\phi) - 4(\phi^\dagger D_\rho\phi)(D_\nu\phi^\dagger D^\rho D^\nu\phi) + 2(\phi^\dagger D_\nu D_\mu\phi)(D^\mu\phi^\dagger D^\nu\phi)\\
&+ \frac{1}{2}(D_\mu D_\nu\phi^\dagger\phi)(D^\mu D^\nu\phi^\dagger\phi) + 4(D_\rho D_\nu\phi^\dagger D^\rho\phi)(D^\nu\phi^\dagger\phi) - 2(D_\nu D_\mu\phi^\dagger\phi)(D^\mu\phi^\dagger D^\nu\phi)\\
&- \frac{1}{2}(\phi^\dagger D_\nu D_\mu\phi)(\phi^\dagger D^\mu D^\nu\phi) + 2(D_\rho D_\nu\phi^\dagger D^\nu D^\rho\phi)(\phi^\dagger\phi) - (D^\nu D^\mu\phi^\dagger\phi)(\phi^\dagger D_\mu D_\nu\phi)\\
&- \frac{1}{2}(D_\nu D_\mu\phi^\dagger\phi)(D^\mu D^\nu\phi^\dagger\phi)\Big].
\end{aligned}$$

We reproduce exactly the result given by the automatic calculation, even when operators are related by renaming of the indices. Automating the reduction of such a result to a physical basis could be easily done following our approach by exporting $\mathcal{L}_{\text{EFT}}^{(8)}$ to `FeynArts` [223], calculating the needed 1PI tree-level off-shell amplitudes and projecting the results onto our basis, which can then be reduced to the physical basis through the relations presented in section 4.3.3. The much simpler result in the physical basis is given by:

$$\begin{aligned}
\mathcal{L}_{\text{EFT}}^{(8)} = \frac{(g_{\mathcal{W}}^{\phi})^2}{m_{\mathcal{W}}^4}\Big[&2O_{\phi^4}^{(1)} + 2O_{\phi^4}^{(2)} - 4O_{\phi^4}^{(3)} - \frac{1}{4}g_2^2 O_{W^2\phi^4}^{(1)} + \frac{1}{2}g_1g_2 O_{WB\phi^4}^{(1)}\\
&+ \frac{3}{4}g_1^2 O_{B^2\phi^4}^{(1)} - 2g_2 O_{W\phi^4D^2}^{(1)} + 6g_1 O_{B\phi^4D^2}^{(1)} + 2g_1 O_{B\phi^4D^2}^{(3)}\Big].
\end{aligned} \tag{4.3.164}$$

Note that results from phenomenological studies of the SMEFT, such as global fits, are presented in the most minimal basis, a physical basis. As such, if one wants to interpret these bottom-up studies as bounds (or preferred regions) for the parameters of a particular model, the matching calculations must be given in a physical basis and therefore, knowledge of a Green's basis and its reduction to the physical one can be useful even for functional methods.

4.4 The renormalisation group equations of the bosonic SMEFT at dimension-8

The importance of knowing a theory's RGEs has already been stressed in section 4.1.4; let us furthermore argue why they are important to be considered even at dimension-8:

- Even before explicitly calculating the RGEs, it is known that several classes of dimension-8 interactions which are one-loop generated by weakly-coupled UV completions can be renormalised by tree-level generated dimension-8 terms [210][5]. This running might therefore be the leading contribution for certain observables where loop-induced dimension-8 operators are the first SMEFT correction;

- Neglecting odd-dimensional operators, dimension-8 is the lowest dimension at which there are co-leading contributions to the RGEs: an insertion of a dimension-8 operator or 2 insertions of dimension-6 terms. Non-renormalisation theorems have been derived for contributions of the first kind [210], but in order to get any information on the second contribution, the RGEs have to be explicitly calculated;

- Dimension-8 WCs can be subject to positivity bounds [179–181, 183, 184, 224, 225]. Studying whether these relations hold when considering the one-loop running effects is also one of the aims of studying the dimension-8 RGEs.

Following from these arguments, in this section we present the RGEs of the bosonic sector of the dimension-8 SMEFT.

For the calculation of the divergences with which we will calculate the RGEs we use the background field method and work in the Feynman gauge in dimensional regularisation with space-time dimension $\mathrm{d} = 4 - 2\epsilon$. The one-loop divergences are computed using dedicated routines that rely on `FeynRules` [76], `FeynArts` [226] and `FormCalc` [227]. We have used `matchmakereft` [217] to cross-check most of the calculations.

The co-leading contributions to the dimension-8 RGEs from a single insertion of a dimension-8 term or 2 dimension-6 interactions are given by:

$$16\pi^2\mu\frac{dc_i^{(8)}}{d\mu} = \gamma'_{ijk}c_j^{(6)}c_k^{(6)} + \gamma_{ij}c_j^{(8)}\,. \tag{4.4.1}$$

[5] This only happened in one case at dimension-6 for the loop-level induced operators of the class $X\psi^2\phi$ [210].

We will study both contributions separately; in section 4.4.1 we will show the computation of the first term in the right-hand side of Eq. (4.4.1), the structure of the resulting RGEs and some phenomenological implications of those results. This section is based on the work published in Ref. [5]. In section 4.4.2, a similar analysis will be conducted for the second term of Eq. (4.4.1) and it is based on the work presented in Ref. [6]. Due to their large nature, we provide these RGEs in a mathematica notebook in https://github.com/SMEFT-Dimension8-RGEs instead of in writing in order to ease their use for further calculations. Regardless, we will consider parts of the RGEs when relevant for the discussion.

4.4.1 Insertion of pairs of dimension-6 terms

Let us start by considering the contribution to the dimension-8 RGEs from two insertions of dimension-6 interactions, the first term in the right-hand side of Eq. (4.4.1). As we are only focused on the renormalisation of the bosonic sector, we do not need to consider dimension-6 four-fermion operators since, at one-loop, a process without fermions in the external legs is impossible to be generated from a four-fermion vertex. Even considering generating redundant fermionic operators, these would never be reduced to only bosonic operators as can be seen from the fermionic EOMs [228]. The opposite is not true since a bosonic redundant operator can be turned into a fermionic operator under the use of the gauge bosons and Higgs EOMs.

We will also limit ourselves to insertions of operators which can be generated at tree-level by weakly-coupled UV completions of the SM; one-loop generated operators would formally result in a two-loops contribution. With this in mind, the relevant dimension-6 Lagrangian can be written as

$$\begin{aligned}\mathcal{L}_{\text{UV}} = \mathcal{L}_{\text{SM}} + \frac{1}{\Lambda^2}\Big\{ & c_\phi (\phi^\dagger\phi)^3 + c_{\phi\Box}(\phi^\dagger\phi)\Box(\phi^\dagger\phi) + c_{\phi D}(\phi^\dagger D^\mu\phi)^*(\phi^\dagger D_\mu\phi) \\ & + c^{(1)}_{\phi\psi_L}(\phi^\dagger i\overleftrightarrow{D}_\mu\phi)(\overline{\psi_L}\gamma^\mu\psi_L) + c^{(3)}_{\phi\psi_L}(\phi^\dagger i\overleftrightarrow{D}^I_\mu\phi)(\overline{\psi_L}\gamma^\mu\sigma^I\psi_L) + c_{\phi\psi_R}(\phi^\dagger i\overleftrightarrow{D}_\mu\phi)(\overline{\psi_R}\gamma^\mu\psi_R) \\ & + \left[c_{\phi ud}(\widetilde{\phi} iD_\mu\phi)(\overline{u_R}\gamma^\mu d_R) + c_{\psi_R\phi}(\phi^\dagger\phi)\overline{\psi_L}\widetilde{\phi}\psi_R + \text{h.c.}\right]\Big\}, \end{aligned} \tag{4.4.2}$$

with $\psi_R = u_R, d_R, e_R$ and $\psi_L = q_L, l_L$. Since we are restricting to the bosonic sector of the SMEFT, only dimension-eight operators with Higgs bosons will be renormalised (at one-loop) from the constructed Lagrangian.

The bosonic one-loop divergent Lagrangian, involving Higgs bosons, can be written as:

$$16\pi^2\epsilon\,\mathcal{L}_{\text{DIV}} = \tilde{K}_\phi(D_\mu\phi)^\dagger(D^\mu\phi) + \tilde{\mu}^2|\phi|^2 - \tilde{\lambda}|\phi|^4 + \tilde{c}^{(6)}_i\frac{O^{(6)}_i}{\Lambda^2} + \tilde{c}^{(8)}_j\frac{O^{(8)}_j}{\Lambda^4}, \tag{4.4.3}$$

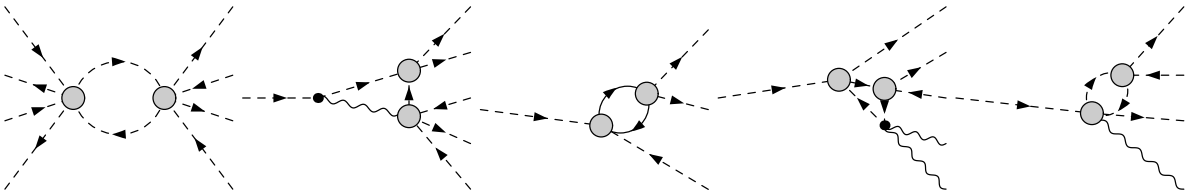

Figure 27: Illustrative diagrams responsible for renormalising the classes of operators ϕ^8 (first), $\phi^6 D^2$ (second), $\phi^4 D^2$ (third), $X^2\phi^4$ (fourth) and $X\phi^4 D^2$ (fifth) through 2 insertions of dimension-6 terms, which are denoted by the grey vertices.

where i and j run over operators in the Green's basis of dimension-6 and dimension-8, respectively. For the former we will consider the Warsaw basis and extend it with the redundant operators in table 8, whereas for the latter we will use the dimension-8 Green's basis constructed in section 4.3. In figure 27 we show an example of the diagrams which will be responsible for renormalising the dimension-8 WCs.

The removal of the contributions to redundant operators will follow from applying the dimension-6 SMEFT EOMs [228]:

$$D^2\phi^i = -\mu^2\phi^i - 2\lambda(\phi^\dagger\phi)\phi^i + \frac{1}{\Lambda^2}\Big\{3c_\phi(\phi^\dagger\phi)^2\phi^i + 2c_{\phi\Box}\phi^i\Box(\phi^\dagger\phi) - c_{\phi D}\left[(D^\mu\phi)^i\left(\phi^\dagger\overleftrightarrow{D}_\mu\phi\right) + \phi^i\partial^\mu\left(\phi^\dagger D_\mu\phi\right)\right]\Big\} + \cdots, \tag{4.4.4}$$

$$\partial^\nu B_{\mu\nu} = \frac{g_1}{2}\phi^\dagger i\overleftrightarrow{D}_\mu\phi + \frac{c_{\phi D}}{\Lambda^2}\frac{g_1}{2}\left(\phi^\dagger\phi\right)\left(\phi^\dagger i\overleftrightarrow{D}_\mu\phi\right) + \cdots, \tag{4.4.5}$$

$$D^\nu W^I_{\mu\nu} = \frac{g_2}{2}\phi^\dagger i\overleftrightarrow{D}^I_\mu\phi + \frac{c_{\phi D}}{\Lambda^2}g_2\left(\phi^\dagger\sigma^I\phi\right)\left(\phi^\dagger i\overleftrightarrow{D}_\mu\phi\right) + \cdots, \tag{4.4.6}$$

where the ellipses represent the neglected contributions from fermionic operators. Besides the dimensionful term μ^2 which can reduce divergent contributions for dimension-8 (6) redundant operators into dimension-6 (4) terms, these EOMs also have $1/\Lambda^2$ terms which can turn dimension-6 redundant contributions into dimension-8 when projected onto the physical basis.

Because of these effects, in order to perform a full study of the contribution for the renormalisation of bosonic operators at $\mathcal{O}(1/\Lambda^4)$, we need to not only compute divergences at this order, but also the contributions to redundant dimension-6 terms at $\mathcal{O}(1/\Lambda^2)$. Furthermore, we also need the $\mathcal{O}(1/\Lambda^2)$ for the kinetic term of the Higgs which, under canonical normalisation, can also result in higher dimensional contributions.

Applying the EOMs on the redundant dimension-6 and dimension-8 operators results in the following

	Operator	Notation	Operator	Notation
$\boldsymbol{\phi^2 D^4}$	$(D_\mu D^\mu \phi^\dagger)(D_\nu D^\nu \phi)$	$O_{D\phi}$		
$\boldsymbol{\phi^4 D^2}$	$(\phi^\dagger \phi)(D_\mu \phi)^\dagger (D^\mu \phi)$	$O'_{\phi D}$	$(\phi^\dagger \phi) D^\mu (\phi^\dagger \mathrm{i} \overleftrightarrow{D}_\mu \phi)$	$O''_{\phi D}$
$\boldsymbol{X\phi^2 D^2}$	$D_\nu W^{I\mu\nu} (\phi^\dagger \mathrm{i} \overleftrightarrow{D}^I_\mu \phi)$	$O_{WD\phi}$	$\partial_\nu B^{\mu\nu} (\phi^\dagger \mathrm{i} \overleftrightarrow{D}_\mu \phi)$	$O_{BD\phi}$

Table 8: Redundant dimension-6 operators relevant for our calculations, following the notation of Ref. [229].

shift for the physical dimension-4 and dimension-6 WCs:

$$\lambda \to \lambda - \frac{\mu^2}{\Lambda^2} c'_{\phi D} - \frac{\mu^4}{\Lambda^4}\left[-2\left(c^{(4)}_{\phi^4} - c^{(8)}_{\phi^4}\right) + c^{(10)}_{\phi^4} + c^{(11)}_{\phi^4}\right], \tag{4.4.7}$$

$$\begin{aligned} c_\phi \to\ & c_\phi + 2\lambda c'_{\phi D} + \frac{\mu^2}{2\Lambda^4}\Big[3(c_{\phi D} + 2c_{\phi\Box})c_\phi - \left(c_{\phi D} - 8c_{\phi\Box}\right)\left(c'_{\phi D} + 2g_2 c_{WD\phi}\right) \\ & - 2g_2 c_{\phi D} c_{WD\phi} - g_1 c_{\phi D} c_{BD\phi} - 4c^{(3)}_{\phi^6} + 4\lambda\left\{-2c^{(4)}_{\phi^4} + 4c^{(8)}_{\phi^4} + 2c^{(10)}_{\phi^4} + 2c^{(11)}_{\phi^4} - c^{(12)}_{\phi^4}\right\} \\ & + g_2 c^{(6)}_{W\phi^4 D^2} + \frac{g_2}{2} c^{(7)}_{W\phi^4 D^2} + g_1 c^{(3)}_{B\phi^4 D^2}\Big], \end{aligned} \tag{4.4.8}$$

$$c_{\phi D} \to c_{\phi D} + 2\frac{\mu^2}{\Lambda^4}\left[\frac{1}{2}(c_{\phi D} + 2c_{\phi\Box})c_{\phi D} - c^{(6)}_{\phi^4} + c^{(12)}_{\phi^4}\right], \tag{4.4.9}$$

$$c_{\phi\Box} \to c_{\phi\Box} + \frac{1}{2} c'_{\phi D} + \frac{\mu^2}{\Lambda^4}\left[(c_{\phi D} + 2c_{\phi\Box})c_{\phi\Box} - c^{(4)}_{\phi^4} + c^{(12)}_{\phi^4}\right], \tag{4.4.10}$$

where we canonically normalised the Higgs kinetic term.

4.4.1.1 The renormalisation group equations

In this section we provide an overview of the structure of the RGEs of the dimension-8 WCs. Since these contributions arise from the insertion of 2 dimension-6 terms, this structure is easily seen in a symmetric matrix for each dimension-8 WC, $c^{(8)}_i$, with the collumns and rows being the relevant dimension-6 WCs. For each entry in the matrix, we denote with a $\times$ a non-zero contribution, with a 0 a trivial zero, that is, a case in which all contributions in the Green's basis vanish (for example if there are no possible diagrams), and with a $\emptyset$ a non-trivial zero, for the cases in which the contribution is non-zero in the Green's basis but cancels once we reduce all redundant operators to the physical basis.

The matrices for each dimension-8 WC are:

$\gamma'_{\mathbf{c}^8_\phi}$	c_ϕ	$c_{\phi D}$	$c_{\phi\Box}$	$c^{(1)}_{\phi\psi_L}$	$c^{(3)}_{\phi\psi_L}$	$c_{\phi\psi_R}$	$c_{\phi ud}$	$c_{\psi_R\phi}$
c_ϕ	×	×	×	0	×	0	×	×
$c_{\phi D}$		×	×	×	×	×	×	×
$c_{\phi\Box}$			×	0	×	0	×	×
$c^{(1)}_{\phi\psi_L}$				×	×	×	0	×
$c^{(3)}_{\phi\psi_L}$					×	×	0	×
$c_{\phi\psi_R}$						×	0	×
$c_{\phi ud}$							×	0
$c_{\psi_R\phi}$								×

$\gamma'_{\mathbf{c}^{(1)}_{\phi^4}}$	c_ϕ	$c_{\phi D}$	$c_{\phi\Box}$	$c^{(1)}_{\phi\psi_L}$	$c^{(3)}_{\phi\psi_L}$	$c_{\phi\psi_R}$	$c_{\phi ud}$	$c_{\psi_R\phi}$
c_ϕ	0	0	0	0	0	0	0	0
$c_{\phi D}$		×	×	0	0	0	0	0
$c_{\phi\Box}$			×	0	0	0	0	0
$c^{(1)}_{\phi\psi_L}$				×	0	0	0	0
$c^{(3)}_{\phi\psi_L}$					×	0	0	0
$c_{\phi\psi_R}$						×	0	0
$c_{\phi ud}$							×	0
$c_{\psi_R\phi}$								0

(4.4.11)

$\gamma'_{\mathbf{c}^{(2)}_{\phi^4}}$	c_ϕ	$c_{\phi D}$	$c_{\phi\Box}$	$c^{(1)}_{\phi\psi_L}$	$c^{(3)}_{\phi\psi_L}$	$c_{\phi\psi_R}$	$c_{\phi ud}$	$c_{\psi_R\phi}$
c_ϕ	0	0	0	0	0	0	0	0
$c_{\phi D}$		×	×	0	0	0	0	0
$c_{\phi\Box}$			×	0	0	0	0	0
$c^{(1)}_{\phi\psi_L}$				×	0	0	0	0
$c^{(3)}_{\phi\psi_L}$					×	0	0	0
$c_{\phi\psi_R}$						×	0	0
$c_{\phi ud}$							0	0
$c_{\psi_R\phi}$								0

$\gamma'_{\mathbf{c}^{(3)}_{\phi^4}}$	c_ϕ	$c_{\phi D}$	$c_{\phi\Box}$	$c^{(1)}_{\phi\psi_L}$	$c^{(3)}_{\phi\psi_L}$	$c_{\phi\psi_R}$	$c_{\phi ud}$	$c_{\psi_R\phi}$
c_ϕ	0	0	0	0	0	0	0	0
$c_{\phi D}$		×	×	0	0	0	0	0
$c_{\phi\Box}$			×	0	0	0	0	0
$c^{(1)}_{\phi\psi_L}$				0	0	0	0	0
$c^{(3)}_{\phi\psi_L}$					×	0	0	0
$c_{\phi\psi_R}$						0	0	0
$c_{\phi ud}$							×	0
$c_{\psi_R\phi}$								0

(4.4.12)

$\gamma'_{\mathbf{c}^{(1)}_{\phi^6}}$	c_ϕ	$c_{\phi D}$	$c_{\phi\Box}$	$c^{(1)}_{\phi\psi_L}$	$c^{(3)}_{\phi\psi_L}$	$c_{\phi\psi_R}$	$c_{\phi ud}$	$c_{\psi_R\phi}$
c_ϕ	0	×	×	0	0	0	0	0
$c_{\phi D}$		×	×	×	×	×	×	×
$c_{\phi\Box}$			×	0	×	0	×	×
$c^{(1)}_{\phi\psi_L}$				×	×	×	0	×
$c^{(3)}_{\phi\psi_L}$					×	×	×	×
$c_{\phi\psi_R}$						×	0	×
$c_{\phi ud}$							×	×
$c_{\psi_R\phi}$								×

$\gamma'_{\mathbf{c}^{(2)}_{\phi^6}}$	c_ϕ	$c_{\phi D}$	$c_{\phi\Box}$	$c^{(1)}_{\phi\psi_L}$	$c^{(3)}_{\phi\psi_L}$	$c_{\phi\psi_R}$	$c_{\phi ud}$	$c_{\psi_R\phi}$
c_ϕ	0	×	0	0	0	0	0	0
$c_{\phi D}$		×	×	×	×	×	×	×
$c_{\phi\Box}$			×	0	0	0	0	0
$c^{(1)}_{\phi\psi_L}$				×	×	×	0	×
$c^{(3)}_{\phi\psi_L}$					×	×	×	0
$c_{\phi\psi_R}$						×	0	×
$c_{\phi ud}$							×	×
$c_{\psi_R\phi}$								×

(4.4.13)

$\gamma'_{c^{(1)}_{W^2\phi^4}}$	c_ϕ	$c_{\phi D}$	$c_{\phi\Box}$	$c^{(1)}_{\phi\psi_L}$	$c^{(3)}_{\phi\psi_L}$	$c_{\phi\psi_R}$	$c_{\phi ud}$	$c_{\psi_R\phi}$
c_ϕ	0	0	0	0	0	0	0	0
$c_{\phi D}$		×	∅	0	0	0	0	0
$c_{\phi\Box}$			0	0	0	0	0	0
$c^{(1)}_{\phi\psi_L}$				×	0	0	0	0
$c^{(3)}_{\phi\psi_L}$					×	0	0	0
$c_{\phi\psi_R}$						×	0	0
$c_{\phi ud}$							×	0
$c_{\psi_R\phi}$								0

$\gamma'_{c^{(3)}_{W^2\phi^4}}$	c_ϕ	$c_{\phi D}$	$c_{\phi\Box}$	$c^{(1)}_{\phi\psi_L}$	$c^{(3)}_{\phi\psi_L}$	$c_{\phi\psi_R}$	$c_{\phi ud}$	$c_{\psi_R\phi}$
c_ϕ	0	0	0	0	0	0	0	0
$c_{\phi D}$		∅	∅	0	0	0	0	0
$c_{\phi\Box}$			0	0	0	0	0	0
$c^{(1)}_{\phi\psi_L}$				∅	0	0	0	0
$c^{(3)}_{\phi\psi_L}$					0	0	0	0
$c_{\phi\psi_R}$						∅	0	0
$c_{\phi ud}$							∅	0
$c_{\psi_R\phi}$								0

(4.4.14)

$\gamma'_{c^{(1)}_{WB\phi^4}}$	c_ϕ	$c_{\phi D}$	$c_{\phi\Box}$	$c^{(1)}_{\phi\psi_L}$	$c^{(3)}_{\phi\psi_L}$	$c_{\phi\psi_R}$	$c_{\phi ud}$	$c_{\psi_R\phi}$
c_ϕ	0	0	0	0	0	0	0	0
$c_{\phi D}$		∅	∅	0	0	0	0	0
$c_{\phi\Box}$			0	0	0	0	0	0
$c^{(1)}_{\phi\psi_L}$				∅	0	0	0	0
$c^{(3)}_{\phi\psi_L}$					0	0	0	0
$c_{\phi\psi_R}$						∅	0	0
$c_{\phi ud}$							∅	0
$c_{\psi_R\phi}$								0

$\gamma'_{c^{(1)}_{B^2\phi^4}}$	c_ϕ	$c_{\phi D}$	$c_{\phi\Box}$	$c^{(1)}_{\phi\psi_L}$	$c^{(3)}_{\phi\psi_L}$	$c_{\phi\psi_R}$	$c_{\phi ud}$	$c_{\psi_R\phi}$
c_ϕ	0	0	0	0	0	0	0	0
$c_{\phi D}$		×	0	0	0	0	0	0
$c_{\phi\Box}$			0	0	0	0	0	0
$c^{(1)}_{\phi\psi_L}$				×	0	0	0	0
$c^{(3)}_{\phi\psi_L}$					×	0	0	0
$c_{\phi\psi_R}$						×	0	0
$c_{\phi ud}$							×	0
$c_{\psi_R\phi}$								0

(4.4.15)

$\gamma'_{c^{(1)}_{W\phi^4D^2}}$	c_ϕ	$c_{\phi D}$	$c_{\phi\Box}$	$c^{(1)}_{\phi\psi_L}$	$c^{(3)}_{\phi\psi_L}$	$c_{\phi\psi_R}$	$c_{\phi ud}$	$c_{\psi_R\phi}$
c_ϕ	0	0	0	0	0	0	0	0
$c_{\phi D}$		×	∅	0	0	0	0	0
$c_{\phi\Box}$			0	0	0	0	0	0
$c^{(1)}_{\phi\psi_L}$				×	0	0	0	0
$c^{(3)}_{\phi\psi_L}$					×	0	0	0
$c_{\phi\psi_R}$						×	0	0
$c_{\phi ud}$							×	0
$c_{\psi_R\phi}$								0

$\gamma'_{c^{(1)}_{B\phi^4D^2}}$	c_ϕ	$c_{\phi D}$	$c_{\phi\Box}$	$c^{(1)}_{\phi\psi_L}$	$c^{(3)}_{\phi\psi_L}$	$c_{\phi\psi_R}$	$c_{\phi ud}$	$c_{\psi_R\phi}$
c_ϕ	0	0	0	0	0	0	0	0
$c_{\phi D}$		×	0	0	0	0	0	0
$c_{\phi\Box}$			0	0	0	0	0	0
$c^{(1)}_{\phi\psi_L}$				×	0	0	0	0
$c^{(3)}_{\phi\psi_L}$					×	0	0	0
$c_{\phi\psi_R}$						×	0	0
$c_{\phi ud}$							×	0
$c_{\psi_R\phi}$								0

(4.4.16)

For all other γ' matrices their entries correspond to trivial zeros.

In table 9 we show another way to examinate the RGEs structure by representing for each pair of dimension-6 terms the class of dimension-8 WCs which are renormalised by them.

	c_ϕ	$c_{\phi D}$	$c_{\phi\Box}$	$c^{(1)}_{\phi\psi_L}$	$c^{(3)}_{\phi\psi_L}$	$c_{\phi\psi_R}$	$c_{\phi ud}$	$c_{\psi_R\phi}$
c_ϕ	ϕ^8	$\phi^8, \phi^{6(1)}, \phi^{6(2)}$	$\phi^8, \phi^{6(1)}$		ϕ^8		ϕ^8	ϕ^8
$c_{\phi D}$		$\phi^8, \phi^{6(1)}, \phi^{6(2)}$ $\phi^{4(1)}, \phi^{4(2)}, \phi^{4(3)}$ $V^2\phi^{4(1)}, V\phi^4 D^{2(1)}$	$\phi^8, \phi^{6(1)}, \phi^{6(2)}$ $\phi^{4(1)}, \phi^{4(2)}, \phi^{4(3)}$	$\phi^8, \phi^{6(1)}, \phi^{6(2)}$	$\phi^8, \phi^{6(1)}, \phi^{6(2)}$	$\phi^8, \phi^{6(1)}, \phi^{6(2)}$	$\phi^8, \phi^{6(1)}, \phi^{6(2)}$	$\phi^8, \phi^{6(1)}, \phi^{6(2)}$
$c_{\phi\Box}$			$\phi^8, \phi^{6(1)}, \phi^{6(2)}$ $\phi^{4(1)}, \phi^{4(2)}, \phi^{4(3)}$		$\phi^8, \phi^{6(1)}$		$\phi^8, \phi^{6(1)}$	$\phi^8, \phi^{6(1)}$
$c^{(1)}_{\phi\psi_L}$				$\phi^8, \phi^{6(1)}, \phi^{6(2)}$ $\phi^{4(1)}, \phi^{4(2)}$ $V^2\phi^{4(1)}, V\phi^4 D^{2(1)}$	$\phi^8, \phi^{6(1)}, \phi^{6(2)}$	$\phi^8, \phi^{6(1)}, \phi^{6(2)}$		$\phi^8, \phi^{6(1)}, \phi^{6(2)}$
$c^{(3)}_{\phi\psi_L}$					$\phi^8, \phi^{6(1)}, \phi^{6(2)}$ $\phi^{4(1)}, \phi^{4(2)}, \phi^{4(3)}$ $V^2\phi^{4(1)}, V\phi^4 D^{2(1)}$	$\phi^8, \phi^{6(1)}, \phi^{6(2)}$	$\phi^{6(1)}, \phi^{6(2)}$	$\phi^8, \phi^{6(1)}$
$c_{\phi\psi_R}$						$\phi^8, \phi^{6(1)}, \phi^{6(2)}$ $\phi^{4(1)}, \phi^{4(2)}$ $V^2\phi^{4(1)}, V\phi^4 D^{2(1)}$		$\phi^8, \phi^{6(1)}, \phi^{6(2)}$
$c_{\phi ud}$							$\phi^8, \phi^{6(1)}, \phi^{6(2)}$ $\phi^{4(1)}, \phi^{4(3)}$ $V^2\phi^{\iota 4(1)}, V\phi^4 D^{2(1)}$	$\phi^{6(1)}, \phi^{6(2)}$
$c_{\psi_R\phi}$								$\phi^8, \phi^{6(1)}, \phi^{6(2)}$

Table 9: Dimension-8 operators which are renormalised by the dimension-6 terms in the corresponding column and row. V corresponds to either W or B.

4.4.1.2 Phenomenological implications

Let us discuss some of the implications of the results presented without the intention of being as comprehensive as possible:

- Dimension-8 operators which had non-zero contributions to their RGEs can be tree-level generated by weakly-coupled UV theories [210]. This is also true for dimension-6 bosonic operators which results that, in the bosonic sector of the SMEFT, dimension-6 tree-level generated operators do not mix into loop-level induced interactions to order $1/\Lambda^4$. This was already known at order $1/\Lambda^2$ [230]. However, this result could have been deduced beforehand; dimension-8 operators which can only arise at loop level involve two Higgs fields, which one can not achieve with two insertions of the tree-level dimension-6 operators considered.

- Several non-trivial zeros can be seen in the γ' matrices. Particularly, the RGEs associated with the operators $c^{(3)}_{W^2\phi^4}$ and $c^{(1)}_{WB\phi^4}$ are zero despite that not being the case off-shell. Such results maybe better understood following the helicity-amplitude formalism [231, 232].

- The Peskin-Takeuchi parameters [233] S and U do not receive contributions through renormalisation at order v^4/Λ^4 (by tree-level generated dimension-6 operators). The contributions to these parameters in the SMEFT are [191, 206]:

$$\frac{1}{16\pi}S = \frac{v^2}{\Lambda^2}\left[c_{\phi WB} + c^{(1)}_{WB\phi^4}\frac{v^4}{\Lambda^4}\right], \quad \frac{1}{16\pi}U = \frac{v^4}{\Lambda^4}c^{(3)}_{W^2\phi^4}\,. \tag{4.4.17}$$

  From the results pointed out in the previous point, $c^{(1)}_{WB\phi^4}$ and $c^{(3)}_{W^2\phi^4}$ do not renormalise on-shell. Together with the known non-renormalisation of $c_{\phi WB}$ [167], means that these parameters are not generated by tree-level induced dimension-6 operators.

- In the context of the Peskin-Takeuchi parameters, the T parameter, defined by [191]

$$\alpha T = -\frac{1}{2}\frac{v^2}{\Lambda^2}\left[c_{\phi D} + c^{(2)}_{\phi^6}\frac{v^2}{\Lambda^2}\right], \tag{4.4.18}$$

  with $\alpha \sim 1/137$ the fine-structure constant, receives the leading contribution from the operator $\mathcal{O}_{\phi ud}$ at order v^4/Λ^4 ($c_{\phi D}$ is not renormalised by one insertion of $\mathcal{O}_{\phi ud}$ [166]). From the bounds

on T from Ref. [234], and assuming that only the flavour structure $c_{\phi tb}$ is non-vanishing, we conclude $c_{\phi tb} \leq 5.9$ for $\Lambda = 1$ TeV. This bound obtained through running is at the level of the one quoted in Ref. [235], $c_{\phi tb} \leq 5.3$.

- Some of the numerical coefficients in the RGEs are significantly larger than the naive estimate of $\mathcal{O}(1)$. To see how large their effect can be, let us see the importance of one-loop v^4/Λ^4 effects for the EW phase transition (EWPT) occurring from modifications of the Higgs potential [236–241]. Assuming c_ϕ as the only non-zero WC in the UV (and neglecting gauge and Yukawa couplings), the Higgs potential is given by running c_ϕ – defined at a high-energy scale, Λ – to the EW scale. At the EW scale we have:

$$V \sim -\mu^2|\phi|^2 + \lambda|\phi|^4 + \frac{c_\phi}{\Lambda^2}\left(1 - \frac{108}{16\pi^2}\lambda \log\frac{\Lambda}{v}\right)|\phi|^6 + \frac{126}{16\pi^2\Lambda^4}\log\frac{\Lambda}{v}c_\phi^2\,|\phi|^8\,, \tag{4.4.19}$$

  where we take the renormalisable couplings as scale-invariant for simplicity.

  EW baryogenesis requires a first and strong order EWPT [242], which can occur if $500\ \text{GeV} \lesssim \Lambda/\sqrt{c_{\text{eff}}} \lesssim 750\ \text{GeV}$ [241, 243], where $c_{\text{eff}} = c_\phi + 3/2\, v^2/\Lambda^2 c_{\phi^8}$. Taking $\Lambda = 1$ TeV, a first order strong phase transition occurs for:

$$1.7\,\text{TeV}^{-2} \lesssim c_\phi \lesssim 3.7\,\text{TeV}^{-2} \tag{4.4.20}$$

  without the c_{ϕ^8} contribution. Considering it we obtain:

$$1.5\,\text{TeV}^{-2} \lesssim c_\phi \lesssim 2.6\,\text{TeV}^{-2}\,. \tag{4.4.21}$$

  This $30\,\%$ change in the upper limit shows the potential value of including dimension-8 running in phenomenological studies.

4.4.2 Insertions of a dimension-8 term

To complete the work done in the previous section, let us now focus on the contribution to the renormalisation of the SMEFT at dimension-8 by insertions of other dimension-8 operators, the second term in the right-hand side of Eq. (4.4.1). Note that for this component, non-renormalisation theorems [210] are already known which we will cross-check by explicit calculation.

Ref. [244] had already calculated some partial results, namely contributions up to quadratic order in gauge or Yukawa couplings or linear order in λ, following on-shell methods – in Appendix C we show

how one can compare the results in our basis to theirs. However, considering higher orders in the SM couplings results in mixing between certain classes of operators; moreover, in particular for the strong coupling or the top Yukawa, there are no reasons to neglect higher orders in these couplings.

As was the case before, we will consider in the UV only operators which can be generated at tree-level by weakly coupled extensions of the SM [210], with at most 2 fermions, which corresponds to the classes ϕ^8, $\phi^6 D^2$, $\phi^4 D^4$, $X\phi^4 D^2$, $X^2\phi^4$, $\psi^2 X\phi^3$, $\psi^2\phi^2 D^3$, $\psi^2\phi^5$, $\psi^2\phi^4 D$, $\psi^2 X\phi^2 D$, $\psi^2\phi^3 D^2$.

We need to calculate the divergent contributions at order $1/\Lambda^4$ to be absorbed by the dimension-8 Green's basis (introduced in section 4.3), the contributions proportional to μ^2/Λ^4 which contribute to the Green's basis at dimension-6 (the Warsaw basis extended with the operators of table 8) and μ^4/Λ^4 which will contribute to renormalisable couplings.

Note that, unlike what happened when there were dimension-6 operators in the UV Lagrangian, in this case using the SM EOMs to remove the redundant operators will suffice as all divergences must already be suppressed by 4 powers of Λ. The shift in the WCs of dimension-8 (dimension-6 and below) by removing redundant operators is given in section 4.3.3 (section 4.4.1).

We will also need the WFR factors, that is, the divergent contributions to the kinetic terms, given by:

$$\begin{aligned} Z_\phi &= 1 + \frac{1}{32\pi^2\epsilon}\left[g_1^2 + 3g_2^2 - 2\gamma_\phi^{(Y)}\right], \\ Z_B &= 1 - \frac{41g_1^2}{96\pi^2\epsilon}, \\ Z_W &= 1 + \frac{19g_2^2}{96\pi^2\epsilon}, \\ Z_G &= 1 + \frac{14g_3^2}{32\pi^2\epsilon}, \end{aligned} \tag{4.4.22}$$

where these Z-factors have been defined in section 4.1.4 and where we have defined

$$\gamma_\phi^{(Y)} \equiv \mathrm{Tr}\left[y^{e\,\dagger}y^e + 3y^{u\,\dagger}y^u + 3y^{d\,\dagger}y^d\right], \tag{4.4.23}$$

In the next section we will comment on the structure of the obtained RGEs. Note that the full results, including the contribution from the insertion of 2 dimension-6 terms, can be found in https://github.com/SMEFT-Dimension8-RGEs.

	ϕ^4D^4	$B\phi^4D^2$	$W\phi^4D^2$	$B^2\phi^4$	$W^2\phi^4$	$WB\phi^4$	$G^2\phi^4$	ϕ^6D^2	ϕ^8
$B^2\phi^2D^2$	g_1^2	0	0	0	0	0	0	0	0
$W^2\phi^2D^2$	g_2^2	0	0	0	0	0	0	0	0
$WB\phi^2D^2$	g_1g_2	0	0	0	0	0	0	0	0
$G^2\phi^2D^2$	0	0	0	0	0	0	0	0	0
$W^3\phi^2$	0	0	0	0	0	0	0	0	0
$W^2B\phi^2$	0	0	0	0	0	0	0	0	0
$G^3\phi^2$	0	0	0	0	0	0	0	0	0
ϕ^4D^4	g_2^2	0	0	0	0	0	0	0	0
$B\phi^4D^2$	$g_1g_2^2$	λ	0	0	0	0	0	0	0
$W\phi^4D^2$	g_2^3	0	g_2^2	0	0	0	0	0	0
$B^2\phi^4$	$g_1^2g_2^2$	$g_1\lambda$	$g_1^2g_2$	λ	0	g_1g_2	0	0	0
$W^2\phi^4$	g_2^4	$g_1g_2^2$	g_2^3	0	λ	g_1g_2	0	0	0
$WB\phi^4$	$g_1g_2^3$	$g_2\lambda$	$g_1\lambda$	g_1g_2	g_1g_2	λ	0	0	0
$G^2\phi^4$	0	0	0	0	0	0	g_3^2	0	0
ϕ^6D^2	g_2^4	$g_1\lambda$	$g_2\lambda$	0	0	0	0	λ	0
ϕ^8	λ^3	$g_1\lambda^2$	$g_2\lambda^2$	$g_1^2\lambda$	$g_2^2\lambda$	$g_1g_2\lambda$	0	λ^2	λ

Table 10: Structure of RGEs of the bosonic dimension-8 terms triggered by other bosonic dimension-8 terms. The entries correspond the order in SM couplings of the leading contribution. Entries in blue are terms that deviate significantly from naive dimensional analysis. The WC in gray are loop-level generated in weakly-coupled UV completions of the SMEFT.

4.4.2.1 Structure of the anomalous dimension matrix

The structure of the anomalous dimension matrix is depicted in tables 10 and 11 for insertions of bosonic or fermionic operators respectively. Operators composed solely of gauge bosons are not renormalised because insertions of the tree-level generated operators will result, at one-loop, in diagrams with external Higgses. This happens because only two particles from these operators can be taken to be internal at one-loop: for the fermionic operators these must be the 2 fermions while for the bosonic ones these are all composed by at least four Higgses.

From looking at tables 10 and 11, it can be seen that terms which are responsible for mixing among

	$\psi^2B\phi^3$	$\psi^2W\phi^3$	$\psi^2G\phi^3$	$\psi^2\phi^2D^3$	$\psi^2\phi^5$	$\psi^2\phi^4D$	$\psi^2B\phi^2D$	$\psi^2W\phi^2D$	$\psi^2G\phi^2D$	$\psi^2\phi^3D^2$
$B^2\phi^2D^2$	0	0	0	g_1^2	0	0	0	0	0	0
$W^2\phi^2D^2$	0	0	0	g_2^2	0	0	0	0	0	0
$WB\phi^2D^2$	0	0	0	g_1g_2	0	0	0	0	0	0
$G^2\phi^2D^2$	0	0	0	g_3^2	0	0	0	0	0	0
$W^3\phi^2$	0	0	0	0	0	0	0	0	0	0
$W^2B\phi^2$	0	0	0	0	0	0	0	0	0	0
$G^3\phi^2$	0	0	0	0	0	0	0	0	0	0
ϕ^4D^4	0	0	0	$\lvert y^t\rvert^2$	0	0	0	0	0	0
$B\phi^4D^2$	0	0	0	$g_1\lvert y^t\rvert^2$	0	0	$\lvert y^t\rvert^2$	0	0	g_1y^t
$W\phi^4D^2$	0	0	0	$g_2\lvert y^t\rvert^2$	0	0	0	$\lvert y^t\rvert^2$	0	g_2y^t
$B^2\phi^4$	g_1y^t	0	0	$g_1^2\lvert y^t\rvert^2$	0	0	$g_1\lvert y^t\rvert^2$	0	0	$g_1^2y^t$
$W^2\phi^4$	0	g_2y^t	0	$g_2^2\lvert y^t\rvert^2$	0	g_2^2	0	$g_2\lvert y^t\rvert^2$	0	$g_2^2y^t$
$WB\phi^4$	g_2y^t	g_1y^t	0	$g_1g_2\lvert y^t\rvert^2$	0	g_1g_2	$g_2\lvert y^t\rvert^2$	$g_1\lvert y^t\rvert^2$	0	$g_1g_2y^t$
$G^2\phi^4$	0	0	g_3y^t	0	0	0	0	0	0	0
ϕ^6D^2	0	0	0	$g_2^2\lvert y^t\rvert^2$	0	$\lvert y^t\rvert^2$	$g_1\lvert y^t\rvert^2$	$g_2\lvert y^t\rvert^2$	0	$y^t\lvert y^t\rvert^2$
ϕ^8	0	0	0	$\lambda\lvert y^t\rvert^4$	$y^t\lvert y^t\rvert^2$	$\lambda\lvert y^t\rvert^2$	$g_1\lambda\lvert y^t\rvert^2$	$g_2\lambda\lvert y^t\rvert^2$	0	$\lambda y^t\lvert y^t\rvert^2$

Table 11: Structure of RGEs of the bosonic dimension-8 terms triggered by fermionic dimension-8 terms. The entries correspond the order in SM couplings of the leading contribution. Entries in blue are terms that deviate significantly from naive dimensional analysis. The WC in gray are loop-level generated in weakly-coupled UV completions of the SMEFT.

most classes only arises with higher order in gauge couplings or λ than what was calculated in Ref. [244]. There are several terms which deviate significantly from the naive estimate of $\gamma_{ij} \sim 1$. We highlight in blue those that respect $\gamma_{ij} \gtrsim 10$.

A result that arises at dimension-8, which had been hinted at before, is that operators which only arise at loop-level in weakly-coupled UV completions of the SM, are renormalised by tree-level generated operators. An example of this is the renormalisation of the class $X^2\phi^2D^2$ by the class ϕ^4D^4.

Almost all zeros in tables 10 and 11 were expected from the results of Ref. [210]. Unlike what happened with the insertion of pairs of dimension-6 operators, in this case only the RGE of the WC $\mathcal{O}^{(1)}_{W^2B\phi^2}$ corresponds to a non-trivial zero, that is, a cancellation when reducing to the physical basis. Off-shell we have:

$$c^{(1)}_{W^2B\phi^2} = \frac{g_2}{192\pi^2\epsilon} c^{(1)}_{B\phi^4D^2}\,, \tag{4.4.24}$$

$$c^{(11)}_{WB\phi^2D^2} = 0\,, \tag{4.4.25}$$

	ϕ^4D^4	$B\phi^4D^2$	$W\phi^4D^2$	$B^2\phi^4$	$W^2\phi^4$	$WB\phi^4$	$G^2\phi^4$	ϕ^6D^2	ϕ^8
ϕ^2	μ^6	0	0	0	0	0	0	0	0
ϕ^4	$\lambda\mu^4$	$g_1\mu^4$	$g_2\mu^4$	0	0	0	0	μ^4	0
$B^2\phi^2$	$g_1^2\mu^2$	$g_1\mu^2$	0	μ^2	0	0	0	0	0
$W^2\phi^2$	$g_2^2\mu^2$	0	$g_2\mu^2$	0	μ^2	0	0	0	0
$WB\phi^2$	$g_1g_2\mu^2$	$g_2\mu^2$	$g_1\mu^2$	0	0	μ^2	0	0	0
$G^2\phi^2$	0	0	0	0	0	0	μ^2	0	0
ϕ^4D^2	$\lambda\mu^2$	$g_1\mu^2$	$g_2\mu^2$	0	0	0	0	μ^2	0
ϕ^6	$\lambda^2\mu^2$	$\lambda g_1\mu^2$	$\lambda g_2\mu^2$	$g_1^2\mu^2$	$g_2^2\mu^2$	$g_1g_2\mu^2$	0	$\lambda\mu^2$	μ^2

Table 12: Structure of RGEs of the bosonic dimension-6, dimension-4 and dimension-2 terms triggered by bosonic dimension-8 terms. The entries correspond the order in SM couplings of the leading contribution. Entries in blue are terms that deviate significantly from naive dimensional analysis. The WC in gray are loop-level generated in weakly-coupled UV completions of the SMEFT.

$$c^{(13)}_{WB\phi^2D^2} = -\frac{g_2}{192\pi^2\epsilon}c^{(1)}_{B\phi^4D^2}\,. \tag{4.4.26}$$

However, the WC $c^{(1)}_{W^2B\phi^2}$ is shifted on-shell to

$$c^{(1)}_{W^2B\phi^2} \to c^{(1)}_{W^2B\phi^2} + \frac{g_2}{2}c^{(11)}_{WB\phi^2D^2} + g_2c^{(13)}_{WB\phi^2D^2}\,, \tag{4.4.27}$$

thus taking $c^{(1)}_{W^2B\phi^2}$ to zero on-shell.

In tables 12 and 13 we show the same results as in tables 10 and 11 but this time for the renormalisation of the bosonic SM Lagrangian terms and dimension-6 operators. Once again, loop-generated dimension-6 operators can be renormalised by dimension-8 tree-level generated terms.

4.4.3 A discussion on positivity bounds

In this section we aim to discuss the effect of the RGEs of dimension-8 WCs, on the translation of the positivity condition on the second derivative of the amplitude with respect to s, Eq. (4.1.24), to bounds on the WCs of the SMEFT, for example, Eq. (4.1.25).

Following the strategy employed in Ref. [245], let us make explicit the fact that WCs can be generated at different orders in the loop expansion by writing them as $c = c^{\text{tree}} + c^{\text{loop}}/(16\pi^2) + \cdots$, where c

	$\psi^2B\phi^3$	$\psi^2W\phi^3$	$\psi^2G\phi^3$	$\psi^2\phi^2D^3$	$\psi^2\phi^5$	$\psi^2\phi^4D$	$\psi^2B\phi^2D$	$\psi^2W\phi^2D$	$\psi^2G\phi^2D$	$\psi^2\phi^3D^2$
ϕ^2	0	0	0	0	0	0	0	0	0	0
ϕ^4	0	0	0	$\mu^4\lvert y^t\rvert^2$	0	0	0	0	0	$\mu^4 y^t$
$B^2\phi^2$	0	0	0	0	0	0	0	0	0	0
$W^2\phi^2$	0	0	0	0	0	0	0	0	0	0
$WB\phi^2$	0	0	0	0	0	0	0	0	0	0
$G^2\phi^2$	0	0	0	0	0	0	0	0	0	0
ϕ^4D^2	0	0	0	$\mu^2\lvert y^t\rvert^2$	0	0	0	0	0	$\mu^2 y^t$
ϕ^6	0	0	0	$\lambda\mu^2\lvert y^t\rvert^2$	$\mu^2 y^t$	$\mu^2\lvert y^t\rvert^2$	$\mu^2\lvert y^t\rvert^2$	$\mu^2\lvert y^t\rvert^2$	0	$\mu^2 y^t\lvert y^t\rvert^2$

Table 13: Structure of RGEs of the bosonic dimension-6, dimension-4 and dimension-2 terms triggered by fermionic dimension-8 terms. The entries correspond the order in SM couplings of the leading contribution. Entries in blue are terms that deviate significantly from naive dimensional analysis. The WC in gray are loop-level generated in weakly-coupled UV completions of the SMEFT.

corresponds to any coupling in the theory. A forward $2 \to 2$ cross-symmetric scattering amplitude of Higgs doublet components reads, schematically:

$$\begin{aligned}\mathcal{A}(s) \sim \lambda^{\text{tree}} &+ \left[\frac{\lambda^{\text{loop}}}{16\pi^2} + \frac{(\lambda^{\text{tree}})^2}{16\pi^2}\log\left(\frac{\Lambda^2}{s}\right)\right] \\ &+ \left[c_{\phi^4}^{(i)\text{tree}} + \frac{c_{\phi^4}^{(i)\text{loop}}}{16\pi^2} - \mu\frac{dc_{\phi^4}^{(i)}}{d\mu}\log\left(\frac{\Lambda^2}{s}\right)\right]\frac{s^2}{\Lambda^4}\,,\end{aligned} \tag{4.4.28}$$

where we ignored the particular numerical coefficients which accompany each term and, following Ref. [245], neglected contributions with gauge couplings in order to simplify the analysis[6]. The combination of coefficients $c_{\phi^4}^{(i)}$ which participate in the amplitude depends on the particular components of the Higgs doublet which are being scattered.

$$\begin{aligned}\phi_1\phi_2 \to \phi_1\phi_2 \;:&\quad c_{\phi^4}^{(i)} = c_{\phi^4}^{(2)}\,,\\ \phi_1\phi_3 \to \phi_1\phi_3 \;:&\quad c_{\phi^4}^{(i)} = c_{\phi^4}^{(1)} + c_{\phi^4}^{(2)}\,,\\ \phi_1\phi_1 \to \phi_1\phi_1 \;:&\quad c_{\phi^4}^{(i)} = c_{\phi^4}^{(1)} + c_{\phi^4}^{(2)} + c_{\phi^4}^{(3)}\,.\end{aligned} \tag{4.4.29}$$

The last term in Eq. (4.4.28) corresponds to the running of the relevant dimension-8 operators and can be written as in Eq. (4.4.1), with contributions from 2 insertions of dimension-6 operators and 1 dimension-8 term.

[6] All conclusions can also be extrapolated for non-zero gauge couplings [245].

To use the argument presented in section 4.1.6, we need to give a small mass, m, to the Higgs, to avoid the branch cut from the logarithm to extend to $s = 0$, which would not generate the needed analytic structure [178, 245]. We can then study the limit of vanishing m after expanding the logarithm $\log[\Lambda^2/(s+m^2)]$.

Let us look at Eq. (4.4.28) in the case[7] of $\lambda^{\text{tree}} = 0$and $c_{\phi^4}^{(i)\text{tree}} = 0$; the leading contribution is given by [245]:

$$\mathcal{A}(s) \sim -\gamma'_{ij} c_{(6)}^{(i)} c_{(6)}^{(j)} \log\left[\frac{\Lambda^2}{m^2}\right] \frac{s^2}{\Lambda^4} + \cdots , \tag{4.4.30}$$

where the $\cdots$ correspond to to higher order terms in s/m^2 from the expansion of the logarithm, γ'_{ij}, is the anomalous dimension matrix corresponding to the insertion of 2 dimension-6 terms – as defined in Eq. (4.4.1) – and $c_{(6)}^{(i)}$ correspond to the dimension-6 WCs which renormalise the relevant dimension-8 WCs. Respecting the positivity constraint on the scattering amplitude, Eq. (4.1.24), we can arrive at two conclusions:

1. If the combination of $c_{\phi^4}^{(i)}$ coeffcients contributing to the $2 \longrightarrow 2$ scattering are only generated at loop-level, given that the amplitude is then dominated by the RGE effects, $c_{\phi^4}^{(i)}$ do not have to respect the conditions of Eqs. (4.1.25).

2. The RGEs of the $c_{\phi^4}^{(i)}$ driven by two insertions of dimension-6 terms must always respect

$$\gamma'_{ij} c_{(6)}^{(i)} c_{(6)}^{(j)} < 0 \,. \tag{4.4.31}$$

   In Appendix D we show an example of a UV completion in which arbitrary dimension-6 coefficients can be generated compatible with $c_{\phi^4}^{(i)\text{tree}} = 0$, meaning that the result of Eq. (4.4.31) holds, irrespective of the values of $c_{(6)}^{(i)}$.

Point 1. was verified in Ref. [245] where they show that a neutral scalar singlet or a scalar triplet do not generate $c_{\phi^4}^{(2)}$ at tree-level, and at one-loop $c_{\phi^4}^{(2)} < 0$ going against Eqs. (4.1.25). Furthermore they also verify that in case no 4-Higgs operator is generated at tree-level (dimension-6 and dimension-8) but only at loop-level – as is the case of heavy scalar quadruplets with hyprecharge $Y = 1/2$ or $Y = 3/2$ – then Eqs. 4.1.25 are respected at one-loop.

Point 2. can be seen from the explicit results of the full RGEs. Let us rewrite here the RGEs of the 4-Higgs dimension-8 operators driven by 2 insertions of dimension-6 as:

[7] Note that this is can always be achieved by tuning of the renormalisable Lagrangian.

$$16\pi^2\beta^{(1)}_{\phi^4} = \frac{8}{3}\Bigg[-2(c_{\phi\Box})^2 - \frac{11}{8}(c_{\phi D})^2 + 4c^{(1)}_{\phi\Box}c_{\phi_D} \\ \underline{+3c^2_{\phi d}}\ \underline{\underline{+c^2_{\phi e}}}\ \underline{\underline{\underline{+2(c^{(1)}_{\phi l})^2}}} - 2(c^{(3)}_{\phi l})^2 \underline{\underline{\underline{+6(c^{(1)}_{\phi q})^2}}} - 6(c^{(3)}_{\phi q})^2 + \underline{\underline{\underline{3c^2_{\phi u}}}} - 3c^2_{\phi ud}\Bigg], \tag{4.4.32}$$

$$16\pi^2\beta^{(2)}_{\phi^4} = \frac{8}{3}\Bigg[-2(c_{\phi\Box})^2 - 2c_{\phi\Box}c_{\phi_D} - \frac{5}{8}(c_{\phi D})^2 \\ \underline{-3c^2_{\phi d}}\ \underline{\underline{-c^2_{\phi e}}}\ \underline{\underline{\underline{-2(c^{(1)}_{\phi l})^2}}} - 2(c^{(3)}_{\phi l})^2 \underline{\underline{\underline{-6(c^{(1)}_{\phi q})^2}}} - 6(c^{(3)}_{\phi q})^2 \underline{\underline{\underline{-3c^2_{\phi u}}}}\Bigg], \tag{4.4.33}$$

$$16\pi^2\beta^{(3)}_{\phi^4} = \frac{8}{3}\Bigg[-5(c_{\phi\Box})^2 + \frac{7}{8}(c_{\phi_D})^2 - 2c_{\phi\Box}c_{\phi_D} + 4(c^{(3)}_{\phi l})^2 + 12(c^{(3)}_{\phi q})^2 + 3c^2_{\phi ud}\Bigg], \tag{4.4.34}$$

where the fermionic WCs squared should be read as the trace in flavour space, that is, $c^2 \equiv \mathrm{Tr}[c^\dagger c]$. The RGE of $c^{(2)}_{\phi^4}$ is always negative; for $c^{(1)}_{\phi^4} + c^{(2)}_{\phi^4}$, the definite negative sign arises from the cancelation of the terms underlined (note that terms cancel according to the number of lines underneath them). For the combination $c^{(1)}_{\phi^4} + c^{(2)}_{\phi^4} + c^{(3)}_{\phi^4}$ the fermionic terms with positive sign in Eq. (4.4.34) are canceled by the remaining (not underlined) fermionic terms in Eqs. (4.4.32) and (4.4.33). Indeed we see that our results agree with point 2., that is, the RGEs of 4-Higgs operators triggered by dimension-6 terms respect Eq. (4.4.31).

Let us now consider the contribution from the RGE triggered by an insertion of a dimension-8 operator. In this case, as confirmed in Ref. [245], since there are lower-dimensional operators which can contribute at the same coupling order to the amplitude as the dimension-8 operator (and dominate the amplitude) the RGE from the dimension-8 operator does not have a fixed sign. Let us show this with a simple example taking $c^{(2)\mathrm{tree}}_{\phi^4} = 0$ and considering its renormalisation by the other $c^{(i)}_{\phi^4}$ and λ. Neglecting dimension-6 contributions, which we already know fulfill Eq. (4.4.31), the part of the amplitude of the scattering process $\phi_1\phi_2 \to \phi_1\phi_2$ proportional to s^2 reads:

$$\mathcal{A}(s) \sim \left[\frac{(\lambda^{\mathrm{tree}})^2}{16\pi^2}\frac{\Lambda^4}{m^4} - \gamma_i\lambda^{\mathrm{tree}}c^{(i)\mathrm{tree}}_{H^4D^4}\log\left(\frac{\Lambda^2}{m^2}\right)\right]\frac{s^2}{\Lambda^4}, \tag{4.4.35}$$

where γ_i corresponds to anomalous dimension matrix from the renormalisation of $c^{(2)}_{\phi^4}$ through an insertion of a dimension-8 term. Even if the term λ in the renormalisable Lagrangian is zero, the diagram responsible for generating $c^{(i)}_{\phi^4}$ can in principle also generate a contribution to λ^{tree}. The two terms will

scale as $c_{\phi^4}^{(i)} \sim \kappa^2/M^2$, and $\lambda^{\text{tree}} \sim \kappa^2/M^2$, where κ is the coupling between 2 Higgs and whatever heavy field was integrated out to generate these relevant operators and M is the mass of said heavy field. Therefore, first term in Eq. (4.4.35) scales as $\sim \kappa^4/M^4$, while the second one as $\sim \kappa^4/M^8$ (the extra mass suppresion comes from the Λ^4 of the effective operator which we are identifying with the mass of the heavy particle). The amplitude is therefore dominated by the first term in this case. As such, nothing can be said in general regarding the sign of $\gamma_i c_{(8)}^{(i)\text{tree}}$.

Indeed, by looking at the contribution to the RGEs of $c_{\phi^4}^{(i)\text{tree}}$ from tree-level generated dimension-8 terms, both in our full results and in Ref. [245], we concluded that there is no definite sign for the RGEs of the 4-Higgs operators from insertions of other dimension-8 terms.

Positivity bounds have also been derived for the dimension-8 operators $X^2\phi^2D^2$. These were obtained in Ref. [181] through amplitudes $V_1V_2 \longrightarrow V_1V_2$, with $V_i = W^\pm, Z, \gamma$, in the broken phase of the SM. They can also be derived from the amplitude $\phi V \longrightarrow \phi V$ in the unbroken phase. For this amplitude, contrary to what happened for the 4-Higgs scattering amplitude, no lower-dimensional operator can dominate the amplitude in general, since the contributions from different dimension terms will always scale differently. Furthermore the RGEs of $X^2\phi^2D^2$ WCs do not receive contributions from 2 insertions of dimension-6 operators. Given also that the WCs of the $X^2\phi^2D^2$ operators are not generated at tree-level by weakly-coupled UV theories, the s^2-proportional part of the amplitude $\phi V \longrightarrow \phi V$ can in general be dominated by the renormalisation of $X^2\phi^2D^2$ triggered by other dimension-8 terms, which should therefore have a definite sign.

The relevant operators considered in Ref. [181] are in a different basis defined as $O_{M,i}$, for $i = 1, ..., 5, 7$. The translation of their WCs to the ones in our basis is given by:

$$f_{M,0} = -\frac{2}{g_2^2}c^{(2)}_{W^2\phi^2D^2}\,, f_{M,1} = \frac{2}{g_2^2}(c^{(1)}_{W^2\phi^2D^2} + c^{(4)}_{W^2\phi^2D^2})\,, f_{M,2} = -\frac{4}{g_1^2}c^{(2)}_{B^2\phi^2D^2}\,,$$
$$f_{M,3} = \frac{4}{g_1^2}c^{(1)}_{B^2\phi^2D^2}\,, f_{M,4} = -\frac{4}{g_1g_2}c^{(1)}_{WB\phi^2D^2}\,, f_{M,5} = -\frac{8}{g_1g_2}c^{(4)}_{WB\phi^2D^2}\,, f_{M,7} = \frac{4}{g_2^2}c^{(4)}_{W^2\phi^2D^2}\,. \tag{4.4.36}$$

The positivity bounds obtained by Ref [181], when translated to our basis, read:

$$g_1^2c^{(1)}_{B^2\phi^2D^2} + g_2^2c^{(1)}_{W^2\phi^2D^2} + 2g_1g_2c^{(4)}_{WB\phi^2D^2} \leq 0\,, \tag{4.4.37}$$
$$g_1^2c^{(1)}_{B^2\phi^2D^2} + g_2^2c^{(1)}_{W^2\phi^2D^2} - 2g_1g_2c^{(4)}_{WB\phi^2D^2} \leq 0\,, \tag{4.4.38}$$
$$c^{(1)}_{W^2\phi^2D^2} \leq 0\,, \tag{4.4.39}$$
$$g_1^2c^{(1)}_{W^2\phi^2D^2} + 2g_1g_2c^{(4)}_{WB\phi^2D^2} + g_2^2c^{(1)}_{B^2\phi^2D^2} \leq 0\,, \tag{4.4.40}$$
$$g_1^2c^{(1)}_{W^2\phi^2D^2} - 2g_1g_2c^{(4)}_{WB\phi^2D^2} + g_2^2c^{(1)}_{B^2\phi^2D^2} \leq 0\,. \tag{4.4.41}$$

Given that these operators are not generated at tree-level, their value at energies much lower than the matching scale is dominated by the running triggered by single insertions of (tree-level) dimension-8 operators. Considering the RGEs of the $X^2\phi^2D^2$ WCs, at leading-log, results in

$$2c^{(1)}_{\phi^4} + 3c^{(2)}_{\phi^4} + c^{(3)}_{\phi^4} \geq 0\,, \tag{4.4.42}$$

$$c^{(1)}_{\phi^4} + 2c^{(2)}_{\phi^4} + c^{(3)}_{\phi^4} \geq 0\,, \tag{4.4.43}$$

$$c^{(1)}_{\phi^4} + c^{(2)}_{\phi^4} \geq 0\,, \tag{4.4.44}$$

$$\left[c^{(1)}_{\psi_R^2\phi^2D^3} + c^{(2)}_{\psi_R^2\phi^2D^3}\right]_{\alpha_1,\alpha_1} \leq 0\,, \tag{4.4.45}$$

$$\left[c^{(1)}_{\psi_L^2\phi^2D^3} + c^{(2)}_{\psi_L^2\phi^2D^3} + c^{(3)}_{\psi_L^2\phi^2D^3} + c^{(4)}_{\psi_L^2\phi^2D^3}\right]_{\alpha_1,\alpha_1} \leq 0\,, \tag{4.4.46}$$

$$\left[c^{(1)}_{\psi_L^2\phi^2D^3} + c^{(2)}_{\psi_L^2\phi^2D^3} - c^{(3)}_{\psi_L^2\phi^2D^3} - c^{(4)}_{\psi_L^2\phi^2D^3}\right]_{\alpha_1,\alpha_1} \leq 0\,; \tag{4.4.47}$$

for $\psi_L = l, q$ and $\psi_R = e, u, d$. The WCs are defined at a high-energy (matching) scale. The first three inequalities are simply linear combinations of the already presented positivity bounds in Eqs. (4.1.25) and as such always hold true since all WCs in the equations above must be generated at tree-level. The last three inequalities are equivalent to those obtained in Ref. [190] which have been obtained by applying the positivity constrain to the amplitude $\phi\psi \longrightarrow \phi\psi$; see Ref. [246] for the positivity of amplitudes involving particles with spin. As such, we showed that for $X^2\phi^2D^2$ the positivity relations quoted in Eqs. (4.4.37 – 4.4.41) are always respected through one-loop running.

4.5 Running in the ALPs

An important assumption that has been present in our SMEFT analysis so far is that at low energies there are no extra degrees of freedom besides the SM ones. However, it is possible that light particles exist that have, for some reason, avoided direct detection so far. Singlets of the SM gauge groups which couple feebly to the SM are good candidates of such particles since they cannot be EW produced and are therefore very difficult to search for at colliders. In this section we will study the SMEFT+ALP, an extension of the SMEFT with a light pseudo-scalar, s, which is commonly called an axion-like particle (ALP).

The clearest motivation to study ALPs comes from axions (hence the name ALP) which aim to solve the strong CP problem [247–249]. CHMs also predict several light scalars (CP-odd or even) which arise from the spontaneous breaking of the underlying global symmetry which can generate not only the Higgs, but other pNGBs which are naturally light [250]. ALPs have also been studied as DM candidates [251, 252] or as part of several flavour theories [253, 254].

In the literature, ALPs are generically taken to be endowed with a shift-symmetry, $s \longrightarrow s + a$, with a being an arbitrary constant, broken only by its mass term. However, this shift-symmetry arises as a consequence of the periodicity condition required to solve the strong CP-problem [255]; other motivations for light pseudo-scalars, such as CHMs, do not require such a symmetry. Therefore, and for the sake of generality, we will not enforce shift-symmetry in our theory; we will comment on this choice in section 4.5.1.

Given their ubiquitous theoretical motivation, the experimental effort in searching for ALPs has been far-reaching, spanning a wide range of energy scales. In figure 28 we can see that bounds are obtained from different experiments; heavier ALPs are mostly constrained by collider searches [256, 257], with a center of mass energy of $\sqrt{s} = 13\,\mathrm{TeV}$, whereas lighter ones are constrained by astrophysical probes, with, for instance, the observation of anomalous red giant cooling providing bounds at an energy scale of around the keV [258]. In order to correctly interpret these bounds, knowledge of how the couplings in the ALP theory vary with the energy scale (and how the couplings mix among themselves) is therefore essential. In this section we will compute the RGEs of couplings in the SMEFT+ALP at dimension-5 assuming only CP conservation, and study some of the phenomenological implications of considering these contributions. This section is based on the work published in Ref. [7].

4.5.1 Building the basis

The renormalisable Lagrangian of an extension of the SM with an ALP is given by:

$$\mathcal{L}^{D\leq 4} = \mathcal{L}_{SM} + \frac{1}{2}\left(\partial_\mu s\right)\left(\partial^\mu s\right) - \frac{1}{2}m^2 s^2 - \frac{\kappa_s}{3!}s^3 - \frac{\lambda_s}{4!}s^4 - \kappa_{s\phi}\, s|\phi|^2 - \frac{\lambda_{s\phi}}{2}s^2|\phi|^2\,, \tag{4.5.1}$$

with real coefficients.

Due to its singlet nature, the most interesting phenomenology of ALPs – its couplings to fermions and gauge bosons – arises through dimension-5 operators, which, unlike in the SMEFT, are not LNV. We will therefore perform our analysis up to $O(1/\Lambda)$. We construct the Green's basis at this order which is shown in table 14.

We defined the operators in their hermitian form such that the WCs associated with operators with flavour indices are followed by 3×3 real matrices, whereas the other WCs are real numbers. The operators represented with an $\mathcal{R}$ are the redundant ones and can be reduced to the physical basis by EOMs; since the renormalisable Lagrangian is no longer just the SM one, these EOMs are now given by:

$$\partial^2 s = -m^2 s - \frac{\kappa_s}{2}s^2 - \frac{\lambda_s s^3}{3!} - \kappa_{s\phi}|\phi|^2 - \lambda_{s\phi}\, s|\phi|^2\,, \tag{4.5.2}$$

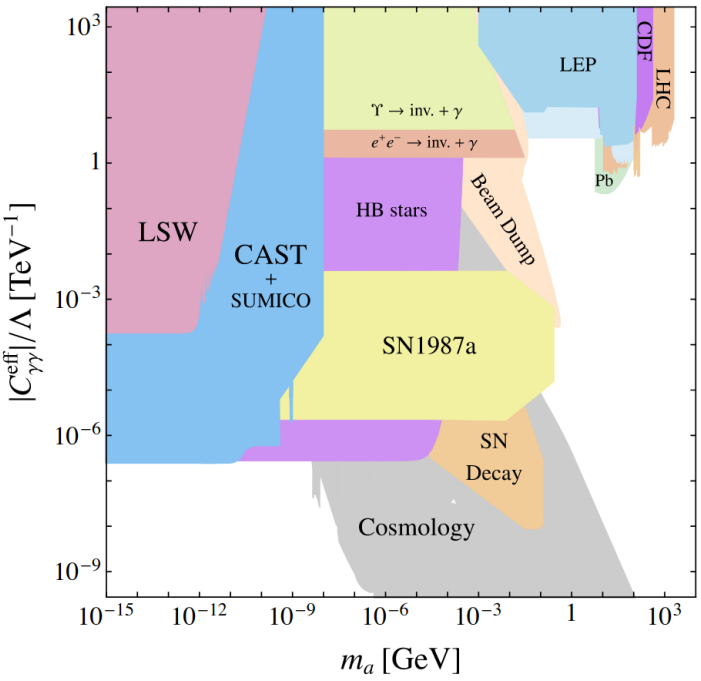

Figure 28: Illustration of the probes of the coupling between an ALP and photons as a function of the mass of the ALP. Taken from [259].

$$D^2\phi_k = -\mu^2\phi_k - 2\lambda|\phi|^2\phi_k - \kappa_{s\phi}s\phi_k - \frac{\lambda_{s\phi}}{2}s^2\phi_k - y^u_{\alpha\beta}\overline{q^\alpha_{Lj}}\epsilon_{jk}u^\beta_R - y^{d\,*}_{\alpha\beta}\overline{d^\beta_R}q^\alpha_{Lk} - y^{e\,*}_{\alpha\beta}\overline{e^\beta_R}l^\alpha_{Lk}\,, \tag{4.5.3}$$

$$i\not{D}q^\alpha_{Lk} = y^d_{\alpha\beta}\phi_k d^\beta_R + y^u_{\alpha\beta}\widetilde{\phi}_k u^\beta_R\,, \qquad i\not{D}l^\alpha_{Lk} = y^e_{\alpha\beta}\phi_k e^\beta_R\,, \tag{4.5.4}$$

$$i\not{D}u^\alpha_R = y^{u\,*}_{\beta\alpha}\widetilde{\phi}^\dagger_k q^\beta_{Lk}\,, \qquad i\not{D}d^\alpha_R = y^{d\,*}_{\beta\alpha}\phi^\dagger_k q^\beta_{Lk}\,, \qquad i\not{D}e^\alpha_R = y^{e\,*}_{\beta\alpha}\phi^\dagger_k l^\beta_{Lk}\,. \tag{4.5.5}$$

The resulting shift in the physical (CP-even) WCs read:

$$a_{su\phi} \longrightarrow a_{su\phi} - r_{s\phi\Box}y^u - r_{sq}y^u + y^u r'^{\rm T}_{su}\,, \tag{4.5.6}$$

$$a_{sd\phi} \longrightarrow a_{sd\phi} + r_{s\phi\Box}y^d - r_{sq}y^d + y^d r^{\rm T}_{sd}\,, \tag{4.5.7}$$

$$a_{se\phi} \longrightarrow a_{se\phi} + r_{s\phi\Box}y^e - r_{sl}y^e + y^e r^{\rm T}_{se}\,. \tag{4.5.8}$$

A comment regarding the choice of basis is in order [260]. In the literature it is common to find a derivative basis to describe the SMEFT+ALP which is given by:

$$\mathcal{L}_{\rm derivative} = \sum_\Psi (\partial_\mu s)\,\overline{\Psi}C_\Psi\gamma^\mu\Psi + C_B g_1^2 s B_{\mu\nu}\widetilde{B}^{\mu\nu} + C_W g_2^2 s W^a_{\mu\nu}\widetilde{W}^{\mu\nu}_a + C_G g_3^2 s G^A_{\mu\nu}\widetilde{G}^{\mu\nu}_A\,, \tag{4.5.9}$$

This choice stems from the shift-symmetry motivation for the ALP that we mentioned before; due to its derivative nature, this basis explicitly respects this symmetry.

Scalar	Yukawa	Derivative	Gauge
	$O_{su\phi}^{\alpha\beta} = \mathrm{i}s(\overline{q_L^\alpha}\widetilde{\phi}u_R^\beta - \overline{u_R^\beta}\widetilde{\phi}^\dagger q_L^\alpha)$	$\mathcal{R}_{s\phi\Box} = \mathrm{i}s(\phi^\dagger D^2\phi - (D^2\phi)^\dagger\phi)$	$O_{s\widetilde{G}} = sG_{\mu\nu}^A\widetilde{G}_A^{\mu\nu}$
	$O_{sd\phi}^{\alpha\beta} = \mathrm{i}s(\overline{q_L^\alpha}\phi d_R^\beta - \overline{d_R^\beta}\phi^\dagger q_L^\alpha)$	$\mathcal{R}_{sq}^{\alpha\beta} = s(\overline{q_L^\alpha}\not{D}q_L^\beta + \overline{q_L^\beta}\overleftarrow{\not{D}}q_L^\alpha)$	$O_{s\widetilde{W}} = sW_{\mu\nu}^a\widetilde{W}_a^{\mu\nu}$
	$O_{se\phi}^{\alpha\beta} = \mathrm{i}s(\overline{l_L^\alpha}\phi e_R^\beta - \overline{e_R^\beta}\phi^\dagger l_L^\alpha)$	$\mathcal{R}_{sl}^{\alpha\beta} = s(\overline{l_L^\alpha}\not{D}l_L^\beta + \overline{l_L^\beta}\overleftarrow{\not{D}}l_L^\alpha)$	$O_{s\widetilde{B}} = sB_{\mu\nu}\widetilde{B}^{\mu\nu}$
		$\mathcal{R}_{su}^{\alpha\beta} = s(\overline{u_R^\alpha}\not{D}u_R^\beta + \overline{u_R^\beta}\overleftarrow{\not{D}}u_R^\alpha)$	
		$\mathcal{R}_{sd}^{\alpha\beta} = s(\overline{d_R^\alpha}\not{D}d_R^\beta + \overline{d_R^\beta}\overleftarrow{\not{D}}d_R^\alpha)$	
		$\mathcal{R}_{se}^{\alpha\beta} = s(\overline{e_R^\alpha}\not{D}e_R^\beta + \overline{e_R^\beta}\overleftarrow{\not{D}}e_R^\alpha)$	
$O_{s^5} = s^5$	$O_{\widetilde{su\phi}}^{\alpha\beta} = s(\overline{q_L^\alpha}\widetilde{\phi}u_R^\beta + \overline{u_R^\beta}\widetilde{\phi}^\dagger q_L^\alpha)$	$\mathcal{R}_{s\Box} = s^2\partial_\mu\partial^\mu s$	$O_{sG} = sG_{\mu\nu}^A G_A^{\mu\nu}$
$O_{s^3} = s^3\lvert\phi\rvert^2$	$O_{\widetilde{sd\phi}}^{\alpha\beta} = s(\overline{q_L^\alpha}\phi d_R^\beta + \overline{d_R^\beta}\phi^\dagger q_L^\alpha)$	$\mathcal{R}_{\phi s\Box} = \lvert\phi\rvert^2\partial^2 s$	$O_{sW} = sW_{\mu\nu}^a W_a^{\mu\nu}$
$O_s = s\lvert\phi\rvert^4$	$O_{\widetilde{se\phi}}^{\alpha\beta} = s(\overline{l_L^\alpha}\phi e_R^\beta + \overline{e_R^\beta}\phi^\dagger l_L^\alpha)$	$\mathcal{R}_{\widetilde{s\phi\Box}} = s(\phi^\dagger D^2\phi + (D^2\phi)^\dagger\phi)$	$O_{sB} = sB_{\mu\nu}B^{\mu\nu}$
		$\mathcal{R}_{\widetilde{sq}}^{\alpha\beta} = s(\overline{q_L^\alpha}\mathrm{i}\not{D}q_L^\beta - \overline{q_L^\beta}\mathrm{i}\overleftarrow{\not{D}}q_L^\alpha)$	
		$\mathcal{R}_{\widetilde{sl}}^{\alpha\beta} = s(\overline{l_L^\alpha}\mathrm{i}\not{D}l_L^\beta - \overline{l_L^\beta}\mathrm{i}\overleftarrow{\not{D}}l_L^\alpha)$	
		$\mathcal{R}_{\widetilde{su}}^{\alpha\beta} = s(\overline{u_R^\alpha}\mathrm{i}\not{D}u_R^\beta - \overline{u_R^\beta}\mathrm{i}\overleftarrow{\not{D}}u_R^\alpha)$	
		$\mathcal{R}_{\widetilde{sd}}^{\alpha\beta} = s(\overline{d_R^\alpha}\mathrm{i}\not{D}d_R^\beta - \overline{d_R^\beta}\mathrm{i}\overleftarrow{\not{D}}d_R^\alpha)$	
		$\mathcal{R}_{\widetilde{se}}^{\alpha\beta} = s(\overline{e_R^\alpha}\mathrm{i}\not{D}e_R^\beta - \overline{e_R^\beta}\mathrm{i}\overleftarrow{\not{D}}e_R^\alpha)$	

Table 14: Green's basis of SMEFT+ALP at dimension-5. All operators are hermitian (operators with flavour indices are hermitian for each fixed value of α and β, $(O_{\alpha\beta})^\dagger = O_{\alpha\beta}$). Operators in the top panel are CP-conserving, whereas those in the bottom are CP-violating.

In order to simplify the analysis, let us look at the leptonic sector to compare both bases. The basis introduced in table 14, which we will refer to as Yukawa-like, has 18 free parameters to describe the leptonic sector from the operators $O_{se\phi}$ and $O_{\widetilde{se\phi}}$. The derivative basis is also composed by 18 parameters from the WCs C_ℓ and C_e. However, the Yukawa-like basis describes both shift-symmetric and shift-breaking physics; as such, using the same number of parameters it seems to describe a wider range of physical models. However, at first sight it might seem counter-intuitive that the Yukawa-like operators can also describe shift-invariant physics. To see this, let us consider the following Lagrangian:

$$\mathcal{L} = -\overline{l_L}(y^l - \mathrm{i}s\alpha_e)\phi e_R + \mathrm{h.c.}\,, \tag{4.5.10}$$

where α_e is an arbitrary matrix in flavour space of order $1/\Lambda$. Shifting $s \longrightarrow s + \sigma$ induces the following

change:

$$\mathcal{L} \to \mathcal{L} - \left[\overline{l_L}(-\mathrm{i}\sigma\alpha_e)\phi e_R + \text{h.c.}\right] . \tag{4.5.11}$$

We can now perform arbitrary chiral rotations which, to the order we are considering, read

$$l_L \to (1 + A_L)l_L, \qquad e_R \to (1 + A_R)e_R\,, \tag{4.5.12}$$

where $A_{L,R}$ are anti-hermitian matrices of order σ/Λ, resulting in

$$\mathcal{L} \to \mathcal{L} - \left[\overline{l_L}(y^e A_{e_R} - A_{l_L} y^l - \mathrm{i}\sigma\alpha_e)\phi e_R + \text{h.c.}\right] . \tag{4.5.13}$$

A sufficient condition such that α_e respects shift-symmetry is that

$$\alpha_e^{\text{shift}-\text{inv}} = H_{l_L} y^l + y^l H_{e_R}\,, \tag{4.5.14}$$

with H_{l_L,e_R} being arbitrary hermitian matrices, corresponding to $\pm\mathrm{i}A_{l_L,e_R}/\sigma$ in Eq. (4.5.13), respectively. Relating α_e and the WCs in the Yukawa-like basis

$$a_{se\phi} = \text{Re}\alpha_e, \qquad a_{\widetilde{se\phi}} = -\text{Im}\alpha_e\,, \tag{4.5.15}$$

(and expanding the same conclusions to the quark sector) we get the following constrains on the form of the WCs so that they describe shift-invariant physics:

$$a_{su\phi}^{\text{shift}-\text{inv}} = \text{Re}(H_{q_L} y^u + y^u H_{u_R})\,, \tag{4.5.16}$$

$$a_{\widetilde{su\phi}}^{\text{shift}-\text{inv}} = -\text{Im}(H_{q_L} y^u + y^u H_{u_R})\,, \tag{4.5.17}$$

$$a_{sd\phi}^{\text{shift}-\text{inv}} = \text{Re}(H_{q_L} y^d + y^d H_{d_R})\,, \tag{4.5.18}$$

$$a_{\widetilde{sd\phi}}^{\text{shift}-\text{inv}} = -\text{Im}(H_{q_L} y^d + y^d H_{d_R})\,, \tag{4.5.19}$$

$$a_{se\phi}^{\text{shift}-\text{inv}} = \text{Re}(H_{l_L} y^e + y^e H_{e_R})\,, \tag{4.5.20}$$

$$a_{\widetilde{se\phi}}^{\text{shift}-\text{inv}} = -\text{Im}(H_{l_L} y^e + y^e H_{e_R})\,, \tag{4.5.21}$$

where once again H_{q_L,l_L,u_R,d_R,e_R} are arbitrary hermitian matrices.

Knowing these conditions, we can repeat the comparison with the derivative basis considering how both of them describe the same shift-invariant physics. Once again, considering the leptonic sector and taking the further simplification of the ALP coupling only to 1 family, the derivative basis is composed of 2 free parameters, one from C_ℓ and one from C_e. However, in this assumed limit, the Yukawa-like basis has only one free parameter, $a_{se\phi}$ (note that from the conditions derived in Eq. (4.5.21) the CP-odd

component is zero in the 1 family case). As hinted before, this implies that there is some redundancy in the derivative basis.

In general, we derive the following on-shell relation:

$$\partial_\mu s\overline{l_L} C_l \gamma^\mu l_L = \partial_\mu s\overline{e_R} H \gamma^\mu e_R + s\overline{e_R}(\mathrm{i}A)\mathrm{i}\overleftrightarrow{\not{D}} e_R\,, \tag{4.5.22}$$

where $\overleftrightarrow{D_\mu} \equiv D_\mu - \overleftarrow{D_\mu}$ and H and A are hermitian and anti-hermitian matrices, respectively, given by

$$A = \frac{1}{2}\left[(y^e)^{-1} C_l y^e - y^{e\dagger} C_l (y^e)^{-1\dagger}\right], \tag{4.5.23}$$

$$H = -\frac{1}{2}\left[(y^e)^{-1} C_l y^e + y^{e\dagger} C_l (y^e)^{-1\dagger}\right]. \tag{4.5.24}$$

If A vanishes, the operator corresponding to the LH and RH fermions are equivalent. A sufficient condition for this is that the Yukawa commutes with C_l, which can happen in the example explored before when the ALP couples only to a single lepton family.

4.5.2 Renormalisation of the SMEFT+ALP

Following the same procedure as in the previous sections, we calculate the RGEs of the SMEFT+ALP. Besides the WFRs presented in Eqs. (4.4.22) we also need the fermionic ones given by:

$$Z_{q_L} = 1 - \frac{1}{96\pi^2\epsilon}\left[\frac{1}{6}g_1^2 + \frac{9}{2}g_2^2 + 8g_3^2 + 3y^u y^{u\,\dagger} + 3y^d y^{d\,\dagger}\right], \tag{4.5.25}$$

$$Z_{l_L} = 1 - \frac{1}{64\pi^2\epsilon}\left[g_1^2 + 3g_2^2 + 2y^e y^{e\,\dagger}\right], \tag{4.5.26}$$

$$Z_{u_R} = 1 - \frac{1}{48\pi^2\epsilon}\left[\frac{4}{3}g_1^2 + 4g_3^2 + 3y^{u\,\dagger} y^u\right], \tag{4.5.27}$$

$$Z_{d_R} = 1 - \frac{1}{48\pi^2\epsilon}\left[\frac{1}{3}g_1^2 + 4g_3^2 + 3y^{d\,\dagger} y^d\right], \tag{4.5.28}$$

$$Z_{e_R} = 1 - \frac{1}{16\pi^2\epsilon}\left[g_1^2 + y^{e\,\dagger} y^e\right]. \tag{4.5.29}$$

Defining the beta function of an arbitrary coupling a_n as

$$\beta_{a_n} = 16\pi^2\mu\frac{da_n}{d\mu} = \gamma_{nm} a_m\,, \tag{4.5.30}$$

where γ_{nm} is the anomalous dimension matrix, the resulting beta functions for the SMEFT+ALP theory are given by:

$$\begin{aligned}\beta_{a_{su\phi}} = 2\Bigg[&\left(\lambda_{s\phi} - \frac{17g_1^2}{24} - \frac{9g_2^2}{8} - 4g_3^2 + \frac{1}{2}\gamma_\phi^{(Y)}\right)a_{su\phi} \\ &- \frac{3}{4}y^d y^{d\dagger}a_{su\phi} + \frac{5}{4}y^u y^{u\dagger}a_{su\phi} + a_{su\phi}y^{u\dagger}y^u + y^d a_{sd\phi}^{\mathrm{T}}y^u - \frac{1}{2}a_{sd\phi}y^{d\dagger}y^u \\ &- \left(\frac{17g_1^2}{6}a_{s\widetilde{B}} + \frac{9g_2^2}{2}a_{s\widetilde{W}} + 16g_3^2 a_{s\widetilde{G}} + \mathrm{Tr}\left[y^e a_{se\phi}^{\mathrm{T}} + 3y^d a_{sd\phi}^{\mathrm{T}} - 3a_{su\phi}y^{u\dagger})\right]\right)y^u\Bigg], \end{aligned} \tag{4.5.31}$$

$$\begin{aligned}\beta_{a_{sd\phi}} = 2\Bigg[&\left(\lambda_{s\phi} - \frac{5g_1^2}{24} - \frac{9g_2^2}{8} - 4g_3^2 + \frac{1}{2}\gamma_\phi^{(Y)}\right)a_{sd\phi} \\ &- \frac{3}{4}y^u y^{u\dagger}a_{sd\phi} + \frac{5}{4}y^d y^{d\dagger}a_{sd\phi} + a_{sd\phi}y^{d\dagger}y^d + y^u a_{su\phi}^{\mathrm{T}}y^d - \frac{1}{2}a_{su\phi}y^{u\dagger}y^d \\ &- \left(\frac{5g_1^2}{6}a_{s\widetilde{B}} + \frac{9g_2^2}{2}a_{s\widetilde{W}} + 16g_3^2 a_{s\widetilde{G}} - \mathrm{Tr}\left[y^e a_{se\phi}^{\mathrm{T}} + 3y^d a_{sd\phi}^{\mathrm{T}} - 3a_{su\phi}y^{u\dagger})\right]\right)y^d\Bigg], \end{aligned} \tag{4.5.32}$$

$$\begin{aligned}\beta_{a_{se\phi}} = 2\Bigg[&a_{se\phi}\left(\lambda_{s\phi} - \frac{15g_1^2}{8} - \frac{9g_2^2}{8} + \frac{1}{2}\gamma_\phi^{(Y)}\right) + \frac{5}{4}y^e y^{e\dagger}a_{se\phi} + a_{se\phi}y^{e\dagger}y^e \\ &- \left(\frac{15g_1^2}{2}a_{s\widetilde{B}} + \frac{9g_2^2}{2}a_{s\widetilde{W}} - \mathrm{Tr}\left[y^e a_{se\phi}^{\mathrm{T}} + 3y^d a_{sd\phi}^{\mathrm{T}} - 3a_{su\phi}y^{u\dagger})\right]\right)y^e\Bigg], \end{aligned} \tag{4.5.33}$$

$$\beta_{a_{s\widetilde{B}}} = \frac{41}{3}g_1^2 a_{s\widetilde{B}}, \tag{4.5.34}$$

$$\beta_{a_{s\widetilde{W}}} = -\frac{19}{3}g_2^2 a_{s\widetilde{W}}, \tag{4.5.35}$$

$$\beta_{a_{s\widetilde{G}}} = -14g_3^2 a_{s\widetilde{G}}. \tag{4.5.36}$$

A more illustrative picture of the operator mixing can be obtained by taking the limit of diagonal flavour cuplings $a_{\alpha\beta} = \delta_{\alpha\beta}a_\alpha$ (and neglecting off-diagonal Yukawa couplings as well). Writing γ_{nm}, where n runs over $\mathcal{O}_{su\phi}^\alpha$, $\mathcal{O}_{sd\phi}^\alpha$, $\mathcal{O}_{se\phi}^\alpha$, $\mathcal{O}_{s\widetilde{G}}$, $\mathcal{O}_{s\widetilde{W}}$ and $\mathcal{O}_{s\widetilde{B}}$, and m over the same operators but with flavour index ρ, we

can express the anomalous dimensions in the following form:

$$\gamma = \begin{pmatrix} \gamma_{11} + 6y_u^\alpha y_u^\rho & y_d^\alpha y_u^\alpha - 6y_u^\alpha y_d^\rho & -2y_u^\alpha y_e^\rho & -32g_3^2 y_u^\alpha & -9g_2^2 y_u^\alpha & -\frac{17}{3}g_1^2 y_u^\alpha \\ y_u^\alpha y_d^\alpha - 6y_d^\alpha y_u^\rho & \gamma_{22} + 6y_d^\alpha y_d^\rho & 2y_d^\alpha y_e^\rho & -32g_3^2 y_d^\alpha & -9g_2^2 y_d^\alpha & -\frac{5}{3}g_1^2 y_d^\alpha \\ -6y_e^\alpha y_u^\rho & 6y_e^\alpha y_d^\rho & \gamma_{33} + 2y_e^\alpha y_e^\rho & 0 & -9g_2^2 y_e^\alpha & -15g_1^2 y_e^\alpha \\ 0 & 0 & 0 & -14g_3^2 & 0 & 0 \\ 0 & 0 & 0 & 0 & -\frac{19}{3}g_2^2 & 0 \\ 0 & 0 & 0 & 0 & 0 & \frac{41}{3}g_1^2 \end{pmatrix}, \tag{4.5.37}$$

where a $\delta_{\alpha\rho}$ should be understood in every entry in which the ρ-index does not explicitly appear, and we have defined

$$\gamma_{11} = 2\lambda_{s\phi} - \frac{3}{2}\left(y_d^\alpha\right)^2 + \frac{9}{2}\left(y_u^\alpha\right)^2 - \frac{17}{12}g_1^2 - \frac{9}{4}g_2^2 - 8g_3^2 + \gamma_\phi^{(Y)}, \tag{4.5.38}$$

$$\gamma_{22} = 2\lambda_{s\phi} - \frac{3}{2}\left(y_u^\alpha\right)^2 + \frac{9}{2}\left(y_d^\alpha\right)^2 - \frac{5}{12}g_1^2 - \frac{9}{4}g_2^2 - 8g_3^2 + \gamma_\phi^{(Y)}, \tag{4.5.39}$$

$$\gamma_{33} = 2\lambda_{s\phi} + \frac{9}{2}\left(y_e^\alpha\right)^2 - \frac{15}{4}g_1^2 - \frac{9}{4}g_2^2 + \gamma_\phi^{(Y)}. \tag{4.5.40}$$

Note that, despite having considered flavour diagonal couplings, due to the contribution from $r_{s\phi\Box}$, there is inter-generational mixing. The choice of diagonal Wilson coefficients is radiatively stable (up to the small non-diagonal terms in the SM Yukawa couplings).

The running of the renormalisable couplings was obtained with the tool `Pyr@te` [261], and is given by:

$$\beta_{g_1} = \frac{41}{6}g_1^3, \tag{4.5.41}$$

$$\beta_{g_2} = -\frac{19}{6}g_2^3, \tag{4.5.42}$$

$$\beta_{g_3} = -7g_3^3, \tag{4.5.43}$$

$$\beta_{m^2} = 4\lambda_{s\phi}\mu^2 + \lambda_s m^2, \tag{4.5.44}$$

$$\beta_{\mu^2} = \lambda_{s\phi} m^2 + \left[2\mathrm{Tr}(y^e y^{e\dagger}) + 6\mathrm{Tr}(y^u y^{u\dagger}) + 6\mathrm{Tr}(y^d y^{d\dagger}) - \frac{3}{2}g_1^2 - \frac{9}{2}g_2^2 - 12\lambda\right]\mu^2, \tag{4.5.45}$$

$$\beta_{\lambda_s} = 3\lambda_s^2 + 12\lambda_{s\phi}^2, \tag{4.5.46}$$

$$\beta_{\lambda_{s\phi}} = \left[\lambda_s + 4\lambda_{s\phi} + 2\text{Tr}(y^e y^{e\dagger}) + 6\text{Tr}(y^u y^{u\dagger}) + 6\text{Tr}(y^d y^{d\dagger}) + 12\lambda - \frac{3}{2}g_1^2 - \frac{9}{2}g_2^2\right]\lambda_{s\phi}\,, \tag{4.5.47}$$

$$\begin{aligned}\beta_\lambda = {}& \frac{1}{2}\lambda_{s\phi}^2 - 6\text{Tr}(y^u y^{u\dagger} y^u y^{u\dagger}) - 6\text{Tr}(y^d y^{d\dagger} y^d y^{d\dagger}) - 2\text{Tr}(y^e y^{e\dagger} y^e y^{e\dagger}) + \frac{3}{8}g_1^4 + \frac{9}{8}g_2^4 + \frac{3}{4}g_1^2 g_2^2 \\ & + \left[24\lambda - 3g_1^2 - 9g_2^2 + 4\text{Tr}(y^e y^{e\dagger}) + 12\text{Tr}(y^u y^{u\dagger}) + 12\text{Tr}(y^d y^{d\dagger})\right]\lambda\,,\end{aligned} \tag{4.5.48}$$

$$\beta_{y^u} = \left\{\frac{3}{2}y^u y^{u\dagger} - \frac{3}{2}y^d y^{d\dagger} + 3\left[\text{Tr}(y^u y^{u\dagger}) + \text{Tr}(y^d y^{d\dagger})\right] + \text{Tr}(y^e y^{e\dagger}) - \frac{17}{12}g_1^2 - \frac{9}{4}g_2^2 - 8g_3^2\right\}y^u\,, \tag{4.5.49}$$

$$\beta_{y^d} = \left\{\frac{3}{2}y^d y^{d\dagger} - \frac{3}{2}y^u y^{u\dagger} + 3\left[\text{Tr}(y^u y^{u\dagger}) + \text{Tr}(y^d y^{d\dagger})\right] + \text{Tr}(y^e y^{e\dagger}) - \frac{5}{12}g_1^2 - \frac{9}{4}g_2^2 - 8g_3^2\right\}y^d\,, \tag{4.5.50}$$

$$\beta_{y^e} = \left\{\frac{3}{2}y^e y^{e\dagger} + 3\left[\text{Tr}(y^u y^{u\dagger}) + \text{Tr}(y^d y^{d\dagger})\right] + \text{Tr}(y^e y^{e\dagger}) - \frac{15}{4}g_1^2 - \frac{9}{4}g_2^2\right\}y^e\,. \tag{4.5.51}$$

Given the wide usage of the derivative basis, we use the results of the previous sections to translate the obtained RGEs to that basis. In the limit of vanishing complex phases for the Yukawa couplings we arrive at:

$$\begin{aligned}\beta_{C_u} = {}& y^{u\,\dagger} y^u C_u + 2C_u y^{u\,\dagger} y^u + 2\lambda_{s\phi} C_u + (y^u)^{-1} y^d C_d y^{d\,\dagger} y^u \\ & + \frac{17}{3}g_1^4 C_B + 9g_2^4 C_W + 32 C_G g_3^4 C_G - 2\gamma'\,,\end{aligned} \tag{4.5.52}$$

$$\begin{aligned}\beta_{C_d} = {}& y^{d\,\dagger} y^d C_d + 2C_d y^{d\,\dagger} y^d + 2\lambda_{s\phi} C_d + (y^d)^{-1} y^u C_u y^{u\,\dagger} y^d \\ & + \frac{5}{3}g_1^4 C_B + 9g_2^4 C_W + 32 g_3^4 C_G + 2\gamma'\,,\end{aligned} \tag{4.5.53}$$

$$\beta_{C_e} = y^{e\,\dagger} y^e C_e + 2C_e y^{e\,\dagger} y^e + 2\lambda_{s\phi} C_e + 15 g_1^4 C_B + 9 g_2^4 C_W + 2\gamma'\,, \tag{4.5.54}$$

with

$$\gamma' \equiv \text{Tr}\left[y^e C_e y^{e\,\dagger} + 3 y^d C_d y^{d\,\dagger} - 3 y^u C_u y^{u\,\dagger}\right]\,. \tag{4.5.55}$$

4.5.3 Renormalisation of the LEFT+ALP

Below the EW scale, we can describe the ALP phenomenology by a low-energy theory, which we call the ALP LEFT, in which the high-energy scale is now the vev of the Higgs and we integrated out the now massive top quark, the Higgs, the Z and the W bosons. Assuming still CP conservation, the corresponding on-shell ALP LEFT Lagrangian, to dimension five, can be written as:

$$\mathcal{L}_{\text{LEFT}} = \frac{1}{2}(\partial_\mu s)(\partial^\mu s) - \frac{1}{2}\tilde{m}^2 s^2 - \frac{\tilde{\lambda}_s}{4!}s^4 - \frac{1}{4}A_{\mu\nu}A^{\mu\nu} - \frac{1}{4}G^A_{\mu\nu}G^{A\,\mu\nu}$$

$$
\begin{aligned}
&+ \sum_{\psi=u,d,e} \left\{ \overline{\psi^\alpha} \mathrm{i} \not{D} \psi^\alpha - \left[(\tilde{m}_\psi)_{\alpha\beta} \overline{\psi_L^\alpha} \psi_R^\beta - s\, \mathrm{i} (\tilde{c}_\psi)_{\alpha\beta} \overline{\psi_L^\alpha} \psi_R^\beta + \text{h.c.} \right] \right\} \\
&+ \tilde{a}_{s\widetilde{G}} s\, G^A_{\mu\nu} \widetilde{G}^{A\,\mu\nu} + \tilde{a}_{s\widetilde{A}} s A_{\mu\nu} \widetilde{A}^{\mu\nu} \\
&+ \sum_{\psi=u,d,e} \left\{ (\tilde{a}_{\psi A})_{\alpha\beta} \overline{\psi_L^\alpha} \sigma^{\mu\nu} \psi_R^\beta A_{\mu\nu} + (\tilde{a}_{\psi G})_{\alpha\beta} \overline{\psi_L^\alpha} \sigma^{\mu\nu} T_A \Psi_R^\beta G^A_{\mu\nu} + s^2 (\tilde{a}_\psi)_{\alpha\beta} \overline{\psi_L^\alpha} \psi_R^\beta + \text{h.c.} \right\},
\end{aligned}
\tag{4.5.56}
$$

where α, β are flavour indices that run over the three families for d and e and over the lighter two families for the case of u. The assumed CP invariance forces all coefficients to be real (matrices in case flavour is involved). Contrary to what we saw before, there are now effective operators of the same dimension with and without the ALP.

The following redundant operators should also be considered:

$$
\mathcal{L}_R = \sum_{\psi=u,d,e} \left[\left(\tilde{r}_{\psi\Box}\right)_{\alpha\beta} \overline{\psi_L^\alpha} D^2 \psi_R^\beta + \mathrm{i} \left(\tilde{r}_{s\psi_L}\right)_{\alpha\beta} s \overline{\psi_L^\alpha} \mathrm{i} \not{D} \psi_L^\beta + \mathrm{i} \left(\tilde{r}_{s\psi_R}\right)_{\alpha\beta} s \overline{\psi_R^\alpha} \mathrm{i} \not{D} \psi_R^\beta + \text{h.c.} \right], \tag{4.5.57}
$$

where, due to CP invariance, we have real WCs. The purely SMEFT redundant operator can be removed by making use of the relation

$$
D^2 = \not{D}^2 + \frac{\sigma_{\mu\nu}}{2} \left(\tilde{e} Q A^{\mu\nu} + \tilde{g}_3 G_A^{\mu\nu} T_A \right), \tag{4.5.58}
$$

and the fermion EOM

$$
\mathrm{i} \not{D} \psi_\alpha = m_{\alpha\beta} \psi_R^\beta + m^\dagger_{\alpha\beta} \psi_L^\beta - \mathrm{i} \left(\tilde{c}_\psi\right)_{\alpha\beta} s \psi_R^\beta + \mathrm{i} (\tilde{c}^\dagger_\psi)_{\alpha\beta} s \psi_L^\beta . \tag{4.5.59}
$$

To fix the parameters of the ALP LEFT at the scale $\mu = v$, one has to choose which physics lies above the EW scale. While all results in this section hold for general models above the EW scale, if we consider that the SMEFT+ALP (the theory studied in section 4.5.2) is valid above the EW scale, then the matching conditions at tree-level are given by:

$$
\tilde{e} = g_2 s_w = g_1 c_w \,, \qquad \tilde{m}^2 = m^2 + \frac{\lambda_{s\phi}}{2} v^2 \,, \tag{4.5.60}
$$

$$
\tilde{g}_3 = g_3 \,, \qquad \tilde{\lambda}_s = \lambda_s - 3 \frac{v^2}{m_h^2} \lambda_{s\phi}^2 \,, \tag{4.5.61}
$$

$$
(\tilde{m}_u)_{\alpha\beta} = \frac{v}{\sqrt{2}} (y^u)_{\alpha\beta} \,, \qquad (\tilde{c}_u)_{\alpha\beta} = \frac{v}{\sqrt{2}} (a_{su\phi})_{\alpha\beta} \,, \tag{4.5.62}
$$

$$(\tilde{m}_d)_{\alpha\beta} = \frac{v}{\sqrt{2}}(y^d)_{\alpha\beta}\,, \qquad (\tilde{c}_d)_{\alpha\beta} = \frac{v}{\sqrt{2}}(a_{sd\phi})_{\alpha\beta}\,, \tag{4.5.63}$$

$$(\tilde{m}_e)_{\alpha\beta} = \frac{v}{\sqrt{2}}(y^e)_{\alpha\beta}\,, \qquad (\tilde{c}_e)_{\alpha\beta} = \frac{v}{\sqrt{2}}(a_{se\phi})_{\alpha\beta}\,, \tag{4.5.64}$$

$$\tilde{a}_{s\widetilde{G}} = a_{s\widetilde{G}}\,, \qquad \tilde{a}_{s\widetilde{A}} = a_{s\widetilde{W}}s_w^2 + a_{s\widetilde{B}}c_w^2\,; \tag{4.5.65}$$

where, as before, α and β are flavour indices that run over the three families for d and e and over the first two for u. All the other Wilson coefficients vanish at the order we are computing.

As the energy scale approaches the mass of the fermions in the theory, we can integrate them out. The effective Lagrangian is of the same form as in Eq. (4.5.56) except that the flavour indices now run only over the remaining fermions and the WCs have to be matched at each mass threshold.

The WFRs needed to calculate the RGEs in ALP LEFT are given by:

$$Z_{e_L} = 1 - \frac{\alpha}{4\pi\epsilon} - \frac{1}{32\pi^2\epsilon}\left(\tilde{c}_e\tilde{c}_e^\dagger\right) - \frac{3\tilde{e}}{16\pi^2\epsilon}\left(m_e\tilde{a}_{eA}^\dagger + \tilde{a}_{eA}m_e^\dagger\right)\,, \tag{4.5.66}$$

$$Z_{e_R} = 1 - \frac{\alpha}{4\pi\epsilon} - \frac{1}{32\pi^2\epsilon}\left(\tilde{c}_e^\dagger\tilde{c}_e\right) - \frac{3\tilde{e}}{16\pi^2\epsilon}\left(\tilde{a}_{eA}^\dagger m_e + m_e^\dagger\tilde{a}_{eA}\right)\,, \tag{4.5.67}$$

$$\begin{aligned} Z_{d_L} = 1 &- \frac{1}{3\pi\epsilon}\left[\frac{1}{12}\alpha + \alpha_s\right] - \frac{1}{32\pi^2\epsilon}\left(\tilde{c}_d\tilde{c}_d^\dagger\right) \\ &- \frac{\tilde{e}}{16\pi^2\epsilon}\left(m_d\tilde{a}_{dA}^\dagger + \tilde{a}_{dA}m_d^\dagger\right) + \frac{\tilde{g}_3}{4\pi^2\epsilon}\left(m_d\tilde{a}_{dG}^\dagger + \tilde{a}_{dG}m_d^\dagger\right)\,, \end{aligned} \tag{4.5.68}$$

$$\begin{aligned} Z_{d_R} = 1 &- \frac{1}{3\pi\epsilon}\left[\frac{1}{12}\alpha + \alpha_s\right] - \frac{1}{32\pi^2\epsilon}\left(\tilde{c}_d^\dagger\tilde{c}_d\right) \\ &- \frac{\tilde{e}}{16\pi^2\epsilon}\left(\tilde{a}_{dA}^\dagger m_d + m_d^\dagger\tilde{a}_{dA}\right) + \frac{\tilde{g}_3}{4\pi^2\epsilon}\left(\tilde{a}_{dG}^\dagger m_d + m_d^\dagger\tilde{a}_{dG}\right)\,, \end{aligned} \tag{4.5.69}$$

$$\begin{aligned} Z_{u_L} = 1 &- \frac{1}{3\pi\epsilon}\left[\frac{1}{3}\alpha + \alpha_s\right] - \frac{1}{32\pi^2\epsilon}\left(\tilde{c}_u\tilde{c}_u^\dagger\right) \\ &+ \frac{2\tilde{e}}{16\pi^2\epsilon}\left(m_u\tilde{a}_{uA}^\dagger + \tilde{a}_{uA}m_u^\dagger\right) + \frac{\tilde{g}_3}{4\pi^2\epsilon}\left(m_u\tilde{a}_{uG}^\dagger + \tilde{a}_{uG}m_u^\dagger\right)\,, \end{aligned} \tag{4.5.70}$$

$$\begin{aligned} Z_{u_R} = 1 &- \frac{1}{3\pi\epsilon}\left[\frac{1}{3}\alpha + \alpha_s\right] - \frac{1}{32\pi^2\epsilon}\left(\tilde{c}_u^\dagger\tilde{c}_u\right) \\ &+ \frac{2\tilde{e}}{16\pi^2\epsilon}\left(\tilde{a}_{uA}^\dagger m_u + m_u^\dagger\tilde{a}_{uA}\right) + \frac{\tilde{g}_3}{4\pi^2\epsilon}\left(\tilde{a}_{uG}^\dagger m_u + m_u^\dagger\tilde{a}_{uG}\right)\,, \end{aligned} \tag{4.5.71}$$

$$\begin{aligned} Z_A = 1 &- \frac{\alpha}{3\pi\epsilon}\left[n_\ell + \frac{1}{3}n_d + \frac{4}{3}n_u\right] \\ &+ \frac{\tilde{e}}{2\pi^2\epsilon}\mathrm{Tr}\left[(\tilde{a}_{eA}^\dagger m_e + m_e^\dagger\tilde{a}_{eA}) - 2(\tilde{a}_{uA}^\dagger m_u + m_u^\dagger\tilde{a}_{uA}) + (\tilde{a}_{dA}^\dagger m_d + m_d^\dagger\tilde{a}_{dA})\right]\,, \end{aligned} \tag{4.5.72}$$

$$Z_G = 1 + \frac{\alpha_s}{4\pi\epsilon}\left[11 - \frac{2}{3}(n_u + n_d)\right] - \frac{\tilde{g}_3}{4\pi^2\epsilon}\mathrm{Tr}\left[\tilde{a}^\dagger_{dG} m_d + m^\dagger_d \tilde{a}_{dG} + \tilde{a}^\dagger_{uG} m_u + m^\dagger_u \tilde{a}_{uG}\right], \tag{4.5.73}$$

$$Z_s = 1 - \frac{1}{8\pi^2\epsilon}\mathrm{Tr}\left[\tilde{c}_e\tilde{c}^\dagger_e + 3\left(\tilde{c}_d\tilde{c}^\dagger_d + \tilde{c}_u\tilde{c}^\dagger_u\right)\right]. \tag{4.5.74}$$

The WCs shifts originating from reducing the redundant operators of Eq. (4.5.57) are given by:

$$\tilde{c}_\psi \to \tilde{c}_\psi + \frac{\tilde{m}_\psi \tilde{r}^\dagger_{\psi\Box}\tilde{c}_\psi + \tilde{c}_\psi \tilde{r}^\dagger_{\psi\Box}\tilde{m}_\psi}{2} + \tilde{r}_{s\psi_L}\tilde{m}_\psi - \tilde{m}_\psi \tilde{r}^\dagger_{s\psi_R}, \tag{4.5.75}$$

$$\tilde{a}_\psi \to \tilde{a}_\psi + \tilde{c}_\psi \tilde{r}^\dagger_{\psi\Box}\tilde{c}_\psi + \tilde{r}_{s\psi_L}\tilde{c}_\psi - \tilde{c}_\psi \tilde{r}^\dagger_{s\psi_R}, \tag{4.5.76}$$

$$\tilde{a}_{\psi A} \to \tilde{a}_{\psi A} + \frac{\tilde{e}Q_\psi \tilde{r}_{\psi\Box}}{2}, \tag{4.5.77}$$

$$\tilde{a}_{\psi G} \to \tilde{a}_{\psi G} + \frac{\tilde{g}_3 \tilde{r}_{\psi\Box}}{2}, \tag{4.5.78}$$

Finally, the couplings in the ALP LEFT evolve following:

$$\begin{aligned}\beta_{\tilde{e}} = &\frac{4}{3}\left[n_\ell + \frac{1}{3}n_d + \frac{4}{3}n_u\right]\tilde{e}^3 \\ &+ 8\tilde{e}^2\mathrm{Tr}\Big[-(\tilde{a}^\dagger_{eA}\tilde{m}_e + \tilde{m}^\dagger_e\tilde{a}_{eA}) + 2(\tilde{a}^\dagger_{uA}\tilde{m}_u + \tilde{m}^\dagger_u\tilde{a}_{uA}) - (\tilde{a}^\dagger_{dA}\tilde{m}_d + \tilde{m}^\dagger_d\tilde{a}_{dA})\Big],\end{aligned} \tag{4.5.79}$$

$$\beta_{\tilde{g}_3} = [-11 + \frac{2}{3}(n_u + n_d)]\tilde{g}_3^3 + 4\tilde{g}_3^2\mathrm{Tr}\left[\tilde{a}^\dagger_{dG}\tilde{m}_d + \tilde{m}^\dagger_d\tilde{a}_{dG} + \tilde{a}^\dagger_{uG}\tilde{m}_u + \tilde{m}^\dagger_u\tilde{a}_{uG}\right], \tag{4.5.80}$$

$$\begin{aligned}\beta_{\tilde{m}_e} = &-6\tilde{e}^2\tilde{m}_e + \frac{1}{2}(\tilde{m}_e\tilde{c}^\dagger_e\tilde{c}_e + \tilde{c}_e\tilde{c}^\dagger_e\tilde{m}_e + 4\tilde{c}_e\tilde{m}^\dagger_e\tilde{c}_e) \\ &+ \mathrm{Tr}(\tilde{c}_e\tilde{m}^\dagger_e + \tilde{c}^\dagger_e\tilde{m}_e + 3\tilde{c}_u\tilde{m}^\dagger_u + 3\tilde{c}^\dagger_u\tilde{m}_u + 3\tilde{m}_d\tilde{c}^\dagger_d + 3\tilde{m}^\dagger_d\tilde{c}_d)\tilde{c}_e \\ &+ 12\tilde{e}\left(\tilde{m}_e\tilde{m}^\dagger_e\tilde{a}_{eA} + \tilde{a}_{eA}\tilde{m}^\dagger_e\tilde{m}_e\right) - 2\tilde{m}^2\tilde{a}_e,\end{aligned} \tag{4.5.81}$$

$$\begin{aligned}\beta_{\tilde{m}_u} = &-8\tilde{g}_3^2\tilde{m}_u - \frac{8}{3}\tilde{e}^2\tilde{m}_u + \frac{1}{2}(\tilde{m}_u\tilde{c}^\dagger_u\tilde{c}_u + \tilde{c}_u\tilde{c}^\dagger_u\tilde{m}_u + 4\tilde{c}_u\tilde{m}^\dagger_u\tilde{c}_u) \\ &+ \mathrm{Tr}(\tilde{c}_e\tilde{m}^\dagger_e + \tilde{c}^\dagger_e\tilde{m}_e + 3\tilde{c}_u\tilde{m}^\dagger_u + 3\tilde{c}^\dagger_u\tilde{m}_u + 3\tilde{m}_d\tilde{c}^\dagger_d + 3\tilde{m}^\dagger_d\tilde{c}_d)\tilde{c}_u \\ &- 8\tilde{e}\left(\tilde{m}_u\tilde{m}^\dagger_u\tilde{a}_{uA} + \tilde{a}_{uA}\tilde{m}^\dagger_u\tilde{m}_u\right) - 16\tilde{g}_3\left(\tilde{m}_u\tilde{m}^\dagger_u\tilde{a}_{uG} + \tilde{a}_{uG}\tilde{m}^\dagger_u\tilde{m}_u\right) - 2\tilde{m}^2\tilde{a}_u,\end{aligned} \tag{4.5.82}$$

$$\beta_{\tilde{m}_d} = -8\tilde{g}_3^2\tilde{m}_d - \frac{2}{3}\tilde{e}^2\tilde{m}_d + \frac{1}{2}(\tilde{m}_d\tilde{c}^\dagger_d\tilde{c}_d + \tilde{c}_d\tilde{c}^\dagger_d\tilde{m}_d + 4\tilde{c}_d\tilde{m}^\dagger_d\tilde{c}_d)$$

$$+\,\mathrm{Tr}(\tilde{c}_e\tilde{m}_e^\dagger+\tilde{c}_e^\dagger\tilde{m}_e+3\tilde{c}_u\tilde{m}_u^\dagger+3\tilde{c}_u^\dagger\tilde{m}_u+3\tilde{m}_d\tilde{c}_d^\dagger+3\tilde{m}_d^\dagger\tilde{c}_d)\tilde{c}_u$$
$$4\tilde{e}\left(\tilde{m}_d\tilde{m}_d^\dagger\tilde{a}_{dA}+\tilde{a}_{dA}\tilde{m}_d^\dagger\tilde{m}_d\right)-16\tilde{g}_3\left(\tilde{m}_d\tilde{m}_d^\dagger\tilde{a}_{dG}+\tilde{a}_{dG}\tilde{m}_d^\dagger\tilde{m}_d\right)-2\tilde{m}^2\tilde{a}_d\,, \tag{4.5.83}$$

$$\begin{aligned}\beta_{\tilde{m}^2}=&\,\tilde{\lambda}_s\tilde{m}^2+4\tilde{m}^2\mathrm{Tr}(\tilde{c}_e\tilde{c}_e^\dagger)+12\tilde{m}^2\mathrm{Tr}(\tilde{c}_d\tilde{c}_d^\dagger)+12\tilde{m}^2\mathrm{Tr}(\tilde{c}_u\tilde{c}_u^\dagger)\\&-24\mathrm{Tr}(\tilde{c}_u\tilde{c}_u^\dagger\tilde{m}_u\tilde{m}_u^\dagger+\tilde{c}_d\tilde{c}_d^\dagger\tilde{m}_d\tilde{m}_d^\dagger)-18\mathrm{Tr}(\tilde{c}_u^\dagger\tilde{c}_u\tilde{m}_u^\dagger\tilde{m}_u+\tilde{c}_d^\dagger\tilde{c}_d\tilde{m}_d^\dagger\tilde{m}_d)\\&-12\mathrm{Tr}(\tilde{c}_u\tilde{m}_u^\dagger\tilde{c}_u\tilde{m}_u^\dagger+\tilde{c}_u^\dagger\tilde{m}_u\tilde{c}_u^\dagger\tilde{m}_u+\tilde{c}_d\tilde{m}_d^\dagger\tilde{c}_d\tilde{m}_d^\dagger+\tilde{c}_d^\dagger\tilde{m}_d\tilde{c}_d^\dagger\tilde{m}_d)\\&-6\mathrm{Tr}(\tilde{c}_u\tilde{m}_u^\dagger\tilde{m}_u\tilde{c}_u^\dagger+\tilde{m}_d\tilde{c}_d^\dagger\tilde{c}_d\tilde{m}_d^\dagger+\tilde{c}_e^\dagger\tilde{c}_e\tilde{m}_e^\dagger\tilde{m}_e)\\&-2\mathrm{Tr}(4\tilde{c}_e\tilde{c}_e^\dagger\tilde{m}_e\tilde{m}_e^\dagger+2\tilde{c}_e\tilde{m}_e^\dagger\tilde{c}_e\tilde{m}_e^\dagger+2\tilde{c}_e^\dagger\tilde{m}_e\tilde{c}_e^\dagger\tilde{m}_e+\tilde{c}_e\tilde{m}_e^\dagger\tilde{m}_e\tilde{c}_e^\dagger)\\&+8\Big[3\mathrm{Tr}\left(\tilde{m}_d^\dagger\tilde{a}_d\tilde{m}_d^\dagger\tilde{m}_d+\tilde{m}_d^\dagger\tilde{m}_d\tilde{a}_d^\dagger\tilde{m}_d\right)+3\mathrm{Tr}\left(\tilde{m}_u^\dagger\tilde{a}_u\tilde{m}_u^\dagger\tilde{m}_u+\tilde{m}_u^\dagger\tilde{m}_u\tilde{a}_u^\dagger\tilde{m}_u\right)\\&+\mathrm{Tr}\left(\tilde{m}_e^\dagger\tilde{a}_e\tilde{m}_e^\dagger\tilde{m}_e+\tilde{m}_e^\dagger\tilde{m}_e\tilde{a}_e^\dagger m_e\right)\Big]\,,\end{aligned} \tag{4.5.84}$$

$$\begin{aligned}\beta_{\tilde{\lambda}_s}=&\,3\tilde{\lambda}_s^2-144\mathrm{Tr}(\tilde{c}_d\tilde{c}_d^\dagger\tilde{c}_d\tilde{c}_d^\dagger)-144\mathrm{Tr}(\tilde{c}_u\tilde{c}_u^\dagger\tilde{c}_u\tilde{c}_u^\dagger)-48\mathrm{Tr}(\tilde{c}_e\tilde{c}_e^\dagger\tilde{c}_e\tilde{c}_e^\dagger)\\&+24\tilde{\lambda}_s\mathrm{Tr}(\tilde{c}_d\tilde{c}_d^\dagger)+24\tilde{\lambda}_s\mathrm{Tr}(\tilde{c}_u\tilde{c}_u^\dagger)+8\tilde{\lambda}_s\mathrm{Tr}(\tilde{c}_e\tilde{c}_e^\dagger)+96\left[\mathrm{Tr}_e^{\tilde{\lambda}}+3\left(\mathrm{Tr}_u^{\tilde{\lambda}}+\mathrm{Tr}_d^{\tilde{\lambda}}\right)\right]\,,\end{aligned} \tag{4.5.85}$$

$$\begin{aligned}\beta_{\tilde{c}_u}=&-\frac{24}{9}(\tilde{e}^2+3\tilde{g}_3^2)\tilde{c}_u+3\tilde{c}_u\tilde{c}_u^\dagger\tilde{c}_u+2\Big[\mathrm{Tr}(\tilde{c}_e\tilde{c}_e^\dagger)+3\mathrm{Tr}(\tilde{c}_d\tilde{c}_d^\dagger)+3\mathrm{Tr}(\tilde{c}_u\tilde{c}_u^\dagger)\Big]\tilde{c}_u+\\&-32\left[\frac{1}{3}\tilde{e}^2\tilde{a}_{s\tilde{A}}+\tilde{g}_3^2\tilde{a}_{s\tilde{G}}\right]\tilde{m}_u+2\left[\tilde{a}_u\left(\tilde{c}_u^\dagger\tilde{m}_u-2\tilde{m}_u^\dagger\tilde{c}_u\right)+\left(\tilde{m}_u\tilde{c}_u^\dagger-2\tilde{c}_u\tilde{m}_u^\dagger\right)\tilde{a}_u\right]\\&+8\tilde{e}\left[\tilde{m}_u\tilde{c}_u^\dagger\tilde{a}_{uA}+\tilde{a}_{uA}\tilde{c}_u^\dagger\tilde{m}_u-\tilde{c}_u\tilde{m}_u^\dagger\tilde{a}_{uA}-\tilde{a}_{uA}\tilde{m}_u^\dagger\tilde{c}_u\right]\\&+16\tilde{g}_3\left[\tilde{m}_u\tilde{c}_u^\dagger\tilde{a}_{uG}+\tilde{a}_{uG}\tilde{c}_u^\dagger\tilde{m}_u-\tilde{c}_u\tilde{m}_u^\dagger\tilde{a}_{uG}-\tilde{a}_{uG}\tilde{m}_u^\dagger\tilde{c}_u\right]\,,\end{aligned} \tag{4.5.86}$$

$$\begin{aligned}\beta_{\tilde{c}_d}=&-\frac{2}{3}(\tilde{e}^2+12\tilde{g}_3^2)\tilde{c}_d+3\tilde{c}_d\tilde{c}_d^\dagger\tilde{c}_d+2\Big[\mathrm{Tr}(\tilde{c}_e\tilde{c}_e^\dagger)+3\mathrm{Tr}(\tilde{c}_d\tilde{c}_d^\dagger)+3\mathrm{Tr}(\tilde{c}_u\tilde{c}_u^\dagger)\Big]\tilde{c}_d\\&-8\left[\frac{1}{3}\tilde{e}^2\tilde{a}_{s\tilde{A}}+4\tilde{g}_3^2\tilde{a}_{s\tilde{G}}\right]\tilde{m}_d+2\left[\tilde{a}_d\left(\tilde{c}_d^\dagger\tilde{m}_d-2\tilde{m}_d^\dagger\tilde{c}_d\right)+\left(\tilde{m}_d\tilde{c}_d^\dagger-2\tilde{c}_d\tilde{m}_d^\dagger\right)\tilde{a}_d\right]\\&-4\tilde{e}\left[\tilde{m}_d\tilde{c}_d^\dagger\tilde{a}_{dA}+\tilde{a}_{dA}\tilde{c}_d^\dagger\tilde{m}_d-\tilde{c}_d\tilde{m}_d^\dagger\tilde{a}_{dA}-\tilde{a}_{dA}\tilde{m}_d^\dagger\tilde{c}_d\right]\\&+16\tilde{g}_3\left[\tilde{m}_d\tilde{c}_d^\dagger\tilde{a}_{dG}+\tilde{a}_{dG}\tilde{c}_d^\dagger\tilde{m}_d-\tilde{c}_d\tilde{m}_d^\dagger\tilde{a}_{dG}-\tilde{a}_{dG}\tilde{m}_d^\dagger\tilde{c}_d\right]\,,\end{aligned} \tag{4.5.87}$$

$$\begin{aligned}\beta_{\tilde{c}_e} &= -6\tilde{e}^2\tilde{c}_e + 3\tilde{c}_e\tilde{c}_e^\dagger\tilde{c}_e + 2\left[\mathrm{Tr}(\tilde{c}_e\tilde{c}_e^\dagger) + 6\mathrm{Tr}(\tilde{c}_d\tilde{c}_d^\dagger) + 6\mathrm{Tr}(\tilde{c}_u\tilde{c}_u^\dagger)\right]\tilde{c}_e \\ &\quad - 8\left[3\tilde{e}^2\tilde{a}_{s\tilde{A}}\right]\tilde{m}_e + 2\left[\tilde{a}_e\left(\tilde{c}_e^\dagger\tilde{m}_e - 2\tilde{m}_e^\dagger\tilde{c}_e\right) + \left(\tilde{m}_e\tilde{c}_e^\dagger - 2\tilde{c}_e\tilde{m}_e^\dagger\right)\tilde{a}_e\right] \\ &\quad - 12\tilde{e}\left[\tilde{m}_e\tilde{c}_e^\dagger\tilde{a}_{eA} + \tilde{a}_{eA}\tilde{c}_e^\dagger\tilde{m}_e - \tilde{c}_e\tilde{m}_e^\dagger\tilde{a}_{eA} - \tilde{a}_{eA}\tilde{m}_e^\dagger\tilde{c}_e\right]; \end{aligned} \tag{4.5.88}$$

for the renormalisable couplings, and we have used `Pyr@te` [261] with manual cross-checks to compute the parts of the beta functions that depend only on renormalisable couplings.

For the non-renormalisable Wilson coefficients, the beta functions read:

$$\begin{aligned}\beta_{\tilde{a}_u} &= \left[-\frac{8}{3}\tilde{e}^2 - 8\tilde{g}_3^2 + \tilde{\lambda}\right]\tilde{a}_u - 32\left[\frac{1}{3}\tilde{e}^2\tilde{a}_{s\tilde{A}} + \tilde{g}_3^2\tilde{a}_{s\tilde{G}}\right]\tilde{c}_u \\ &\quad + 2\left[-\tilde{c}_u\tilde{a}_u^\dagger\tilde{c}_u + \frac{13}{4}\tilde{a}_u\tilde{c}_u^\dagger\tilde{c}_u + \frac{13}{4}\tilde{c}_u\tilde{c}_u^\dagger\tilde{a}_u\right] + 4\mathrm{Tr}\left[\tilde{c}_e\tilde{c}_e^\dagger + 3\left(\tilde{c}_d\tilde{c}_d^\dagger + \tilde{c}_u\tilde{c}_u^\dagger\right)\right]\tilde{a}_u \\ &\quad + 8\tilde{e}\left[\tilde{c}_u\tilde{c}_u^\dagger\tilde{a}_{qA} + \tilde{a}_{uA}\tilde{c}_u^\dagger\tilde{c}_u\right] + 16\tilde{g}_3\left[\tilde{c}_u\tilde{c}_u^\dagger\tilde{a}_{uG} + \tilde{a}_{uG}\tilde{c}_u^\dagger\tilde{c}_u\right], \end{aligned} \tag{4.5.89}$$

$$\begin{aligned}\beta_{\tilde{a}_d} &= \left[-\frac{2}{3}\tilde{e}^2 - 8\tilde{g}_3^2 + \tilde{\lambda}\right]\tilde{a}_d - 32\left[\frac{1}{12}\tilde{e}^2\tilde{a}_{s\tilde{A}} + \tilde{g}_3^2\tilde{a}_{s\tilde{G}}\right]\tilde{c}_d \\ &\quad + 2\left[-\tilde{c}_d\tilde{a}_d^\dagger\tilde{c}_d + \frac{13}{4}\tilde{a}_d\tilde{c}_d^\dagger\tilde{c}_d + \frac{13}{4}\tilde{c}_d\tilde{c}_d^\dagger\tilde{a}_d\right] + 4\mathrm{Tr}\left[\tilde{c}_e\tilde{c}_e^\dagger + 3\left(\tilde{c}_d\tilde{c}_d^\dagger + \tilde{c}_u\tilde{c}_u^\dagger\right)\right]\tilde{a}_d \\ &\quad - 4\tilde{e}\left[\tilde{c}_d\tilde{c}_d^\dagger\tilde{a}_{dA} + \tilde{a}_{dA}\tilde{c}_d^\dagger\tilde{c}_d\right] + 16\tilde{g}_3\left[\tilde{c}_d\tilde{c}_d^\dagger\tilde{a}_{dG} + \tilde{a}_{dG}\tilde{c}_d^\dagger\tilde{c}_d\right], \end{aligned} \tag{4.5.90}$$

$$\begin{aligned}\beta_{\tilde{a}_e} &= \left[-6\tilde{e}^2 + \tilde{\lambda}\right]\tilde{a}_e - 24\tilde{e}^2\tilde{a}_{s\tilde{A}}\tilde{c}_e - 12\tilde{e}\left[\tilde{c}_e\tilde{c}_e^\dagger\tilde{a}_{eA} + \tilde{a}_{eA}\tilde{c}_e^\dagger\tilde{c}_e\right] \\ &\quad + 2\left[-\tilde{c}_e\tilde{a}_e^\dagger\tilde{c}_e + \frac{13}{4}\tilde{a}_e\tilde{c}_e^\dagger\tilde{c}_e + \frac{13}{4}\tilde{c}_e\tilde{c}_e^\dagger\tilde{a}_e\right] + 4\mathrm{Tr}\left[\tilde{c}_e\tilde{c}_e^\dagger + 3\left(\tilde{c}_d\tilde{c}_d^\dagger + \tilde{c}_u\tilde{c}_u^\dagger\right)\right]\tilde{a}_e, \end{aligned} \tag{4.5.91}$$

$$\begin{aligned}\beta_{\tilde{a}_{s\tilde{A}}} &= 4\tilde{e}\mathrm{Tr}\left[\left(\tilde{c}_e\tilde{a}_{eA}^\dagger + \tilde{c}_e^\dagger\tilde{a}_{eA}\right) + \left(\tilde{c}_d\tilde{a}_{dA}^\dagger + \tilde{c}_d^\dagger\tilde{a}_{dA}\right) - 2\left(\tilde{c}_u\tilde{a}_{uA}^\dagger + \tilde{c}_u^\dagger\tilde{a}_{uA}\right)\right] \\ &\quad + 2\mathrm{Tr}\left[\tilde{c}_e\tilde{c}_e^\dagger + 3\left(\tilde{c}_d\tilde{c}_d^\dagger + \tilde{c}_u\tilde{c}_u^\dagger\right)\right]\tilde{a}_{s\tilde{A}} + \frac{8}{3}\tilde{e}^2\left[n_\ell + \frac{1}{3}n_d + \frac{4}{3}n_u\right]\tilde{a}_{s\tilde{A}}, \end{aligned} \tag{4.5.92}$$

$$\begin{aligned}\beta_{\tilde{a}_{s\tilde{G}}} &= -2\tilde{g}_3\mathrm{Tr}\left[\tilde{c}_d\tilde{a}_{dG}^\dagger + \tilde{c}_d^\dagger\tilde{a}_{dG} + \tilde{c}_u\tilde{a}_{uG}^\dagger + \tilde{c}_u^\dagger\tilde{a}_{uG}\right] + 2\mathrm{Tr}\left[\tilde{c}_e\tilde{c}_e^\dagger + 3\left(\tilde{c}_d\tilde{c}_d^\dagger + \tilde{c}_u\tilde{c}_u^\dagger\right)\right]\tilde{a}_{s\tilde{G}} \\ &\quad + 2\tilde{g}_3^2\left[\frac{2}{3}(n_u + n_d) - 11\right]\tilde{a}_{s\tilde{G}}, \end{aligned} \tag{4.5.93}$$

$$\beta_{\tilde{a}_{eA}} = 10\tilde{e}^2\tilde{a}_{eA} + 4\tilde{e}\tilde{c}_e\tilde{a}_{s\tilde{A}} + \frac{1}{2}\left(\tilde{c}_e\tilde{c}_e^\dagger\tilde{a}_{eA} + \tilde{a}_{eA}\tilde{c}_e^\dagger\tilde{c}_e\right)$$

$$+\frac{4}{3}\tilde{e}^2\left[n_\ell+\frac{1}{3}n_d+\frac{4}{3}n_u\right]\tilde{a}_{eA}\,, \tag{4.5.94}$$

$$\beta_{\tilde{a}_{uA}}=\frac{40}{9}\tilde{e}^2\tilde{a}_{uA}-\frac{8}{3}\tilde{e}\tilde{c}_u\tilde{a}_{s\tilde{A}}+\frac{64}{9}\tilde{e}\tilde{g}_3\tilde{a}_{uG}+\frac{8}{3}\tilde{g}_3^2\tilde{a}_{uA}+\frac{1}{2}\left(\tilde{c}_u\tilde{c}_u^\dagger\tilde{a}_{uA}+\tilde{a}_{uA}\tilde{c}_u^\dagger\tilde{c}_u\right)$$
$$+\frac{4}{3}\tilde{e}^2\left[n_\ell+\frac{1}{3}n_d+\frac{4}{3}n_u\right]\tilde{a}_{uA}\,, \tag{4.5.95}$$

$$\beta_{\tilde{a}_{dA}}=\frac{10}{9}\tilde{e}^2\tilde{a}_{dA}+\frac{4}{3}\tilde{e}\tilde{c}_d\tilde{a}_{s\tilde{A}}-\frac{32\tilde{e}}{9}\tilde{g}_3\tilde{a}_{dG}+\frac{8}{3}\tilde{g}_3^2\tilde{a}_{dA}+\frac{1}{2}\left(\tilde{c}_d\tilde{c}_d^\dagger\tilde{a}_{dA}+\tilde{a}_{dA}\tilde{c}_d^\dagger\tilde{c}_d\right)$$
$$+\frac{4}{3}\tilde{e}^2\left[n_\ell+\frac{1}{3}n_d+\frac{4}{3}n_u\right]\tilde{a}_{dA}\,, \tag{4.5.96}$$

$$\beta_{\tilde{a}_{uG}}=\frac{16}{3}\tilde{g}_3\tilde{e}\tilde{a}_{uA}-4\tilde{g}_3\tilde{c}_u\tilde{a}_{s\tilde{G}}+\frac{8}{9}\tilde{e}^2\tilde{a}_{uG}+\frac{1}{2}\left(\tilde{c}_u\tilde{c}_u^\dagger\tilde{a}_{uG}+\tilde{a}_{uG}\tilde{c}_u^\dagger\tilde{c}_q\right)$$
$$+\frac{1}{3}\left[2\left(n_u+n_d\right)-29\right]\tilde{g}_3^2\tilde{a}_{uG}\,, \tag{4.5.97}$$

$$\beta_{\tilde{a}_{dG}}=-\frac{8}{3}\tilde{g}_3\tilde{e}\tilde{a}_{dA}-4\tilde{g}_3\tilde{c}_d^1\tilde{a}_{s\tilde{G}}+\frac{2}{9}\tilde{e}^2\tilde{a}_{dG}+\frac{1}{2}\left(\tilde{c}_d\tilde{c}_d^\dagger\tilde{a}_{dG}+\tilde{a}_{dG}\tilde{c}_d^\dagger\tilde{c}_d\right)$$
$$+\frac{1}{3}\left[2\left(n_u+n_d\right)-29\right]\tilde{g}_3^2\tilde{a}_{dG}\,; \tag{4.5.98}$$

where n_u, n_d and n_e are the number of dynamical up-type quarks, down-type quarks and charged leptons, respectively, for the EFT we are considering.

Once again note that the equations above are fully generic, that is, they are valid regardless if the theory in the UV is the one we have assumed in Section 4.5.2 that leads to the matching conditions in Eqs. (4.5.60)–(4.5.64), or any other theory containing different degrees of freedom.

4.5.4 Some phenomenological applications

Mixing among different effective operators can have important phenomenological effects, in particular for theories in which a WC is not generated at the matching scale but can originate from the running of other WCs. As an example of such a case, let us look at the case of a photophobic ALP [262], whose Lagrangian at $\Lambda = 10\,\text{TeV}$ is given by :

$$\mathcal{L}=\mathcal{L}_{\text{SM}}+\frac{1}{2}\partial_\mu s\partial^\mu s+\frac{1}{2}\tilde{m}^2s^2+\frac{a_{s\widetilde{Z}}}{c_\omega^2-s_\omega^2}s\left(c_\omega^2W_{\mu\nu}\widetilde{W}^{\mu\nu}-s_\omega^2B_{\mu\nu}\widetilde{B}^{\mu\nu}\right)\,, \tag{4.5.99}$$

where $\mathcal{L}_{\text{SM}}$ is the SM Lagrangian. From Eq. (4.5.99), the ALP couples to pairs of Z bosons but not to pairs of photons. This theory is motivated by CHMs based with the symmetry breaking pattern $SO(6)/SO(5)$ [263]. The photophobic condition is stable, that is, $a_{s\tilde{A}}$ remains vanishing at all scales.

Taking the the physical ALP mass to be $\mathcal{O}(\text{keV})$, $a_{s\widetilde{Z}}$ can be directly bounded at colliders. From $pp \to Zs$ searches with LHC Run II data values of $a_{s\widetilde{Z}}$ larger than $0.2\,\text{TeV}^{-1}$ [264] can be excluded, whereas for the High-Luminosity phase of the LHC $a_{s\widetilde{Z}}$ could be constrained to be less than $0.04\,\text{TeV}^{-1}$ [264] .

However, the running of $a_{s\widetilde{Z}}$ generates other WCs, which can also be constrained. In particular, $a_{s\widetilde{Z}}$ generates $a_{se\phi}$ – which can be seen from Eq. (4.5.33) – which is tightly bounded experimentally. For ALPs with a mass $\sim$ keV the strongest constraint is the anomalous cooling of Red Giants from ALP radiation. This observable constrains the ALP coupling to electrons (the coupling in the LEFT + ALP) to be $\tilde{c}_e \lesssim 3 \times 10^{-13}$, for a typical core temperature of $T \approx 10^8$ K [258].

Considering that above the EW scale only the ALP exists besides the SM, $\tilde{c}_e$ runs proportionally to itself. Resumming Eqs. (4.5.80) and (4.5.88), at the EW scale, the bounded coupling reads:

$$\tilde{c}_e(v) \lesssim 2.8 \times 10^{-13}, \tag{4.5.100}$$

which translates into

$$a_{se\phi}(v) \lesssim 1.6 \times 10^{-12}\ \text{TeV}^{-1}\,, \tag{4.5.101}$$

from the matching conditions in Eq. (4.5.64).

Solving numerically Eqs. (4.5.31)-(4.5.36), (4.5.41)-(4.5.43) and (4.5.49)-(4.5.51) for $\lambda_{s\phi} = 0$, we can obtain a bound on $a_{s\widetilde{Z}}(10\,\text{TeV})$ of:

$$a_{s\widetilde{Z}}(10\,\text{TeV}) \lesssim 4.8 \times 10^{-6}\ \text{TeV}^{-1}\,. \tag{4.5.102}$$

This result is four orders of magnitude more constraining than prospects from direct searches.

Another example is the case of a top-philic ALP at $\Lambda = 10$ TeV, with a Lagrangian

$$\mathcal{L} = \mathcal{L}_{\text{SM}} + \frac{1}{2}\partial_\mu s \partial^\mu s + \frac{1}{2}\tilde{m}^2 s^2 + a_t s[i\bar{q}_L \tilde{\phi} t_R + \text{h.c.}]\,, \tag{4.5.103}$$

where q_L stands for the third generation quark doublet and $a_t = (a_{su\phi})^{33}$. Once again, a_t generates through mixing a non-vanishing coupling with electrons. Following the same procedure as above, we obtain $a_t(10\,\text{TeV}) \lesssim 4.3 \times 10^{-6}\ \text{TeV}^{-1}$ from the bound $\tilde{c}_e(\mu \sim \text{KeV}) \lesssim 3 \times 10^{-13}$.

Direct bounds on the coupling with a top quark could in principle be obtained from $pp \to t\bar{t}s$, but they are likely to be very weak due to the difficulty in discriminating this signal from the overwhelming $t\bar{t}$ background. Other indirect constraints on a_t have been studied in Ref. [265] but they are much less constraining than the one obtained above.

5

Connecting theory with experiment through the SMEFT

In this section we follow the top-down approach within the SMEFT at dimension-6, in a sense combining both approaches studied so far, as we will be looking at particular UV completions which can explain the SMEFT results. The measurement of an anomalous magnetic moment of the muon can be parametrized by a non-zero WC of the dipole operators in the SMEFT, in a model-independent way. Our goal in this section is to study the matching conditions of this operator at one-loop, allowing us to study the specific BSM scenarios (up to 3-field extensions) which can accomodate the observed anomaly. In section 5.2, we will also perform a full one-loop phenomenological study of one of these 3-field extensions which can also account for other flavour anomalies. The work presented in this chapter is based on Ref. [8].

5.1 Bridges – UV completions to explain the a_μ anomaly

The anomalous magnetic moment of the muon which we introduced in section 2.3.3, has received a lot of attention, with a significant amount of work done to map the possible BSM scenarios which could account for Δa_μ, given in Eq. (2.26). From an EFT prespective, the contribution to a_μ can be parametrized in the Low-Energy Effective Field Theory (LEFT)[1] of the SM, which is obtained after integrating out the top, the W and Z bosons and the Higgs (similarly to what was done in the LEFT+ALP theory of section 4.5.3). In the LEFT, at tree level, the contribution to a_μ is given by

$$\Delta a_\mu = a_\mu^{\text{NP}} - a_\mu^{\text{SM}} = \frac{4 m_\mu v}{\sqrt{2} e} \text{Re}[\alpha_{eγ}^{2,2}] \,, \tag{5.1.1}$$

[1] The RGEs of the LEFT have been calculated in Ref. [266] and the matching conditions of the SMEFT onto the LEFT have been given in Ref. [267, 268].

where m_μ is the mass of the muon and $\alpha_{e\gamma}^{i,j} v/\sqrt{2}$ is the WC of the photon dipole operator defined as [267]

$$\mathcal{L}_{e\gamma}^{i,j} = (\bar{l}^i \sigma^{\mu\nu} e^j) F_{\mu\nu} + \text{h.c.}\,, \tag{5.1.2}$$

where i and j correspond to flavour indices.

The matching conditions, at tree-level, for the photon dipole operator at the EW scale with the SMEFT result in:

$$\alpha_{e\gamma}^{i,j} = \frac{v}{\sqrt{2}} \left(\alpha_{eB}^{i,j} c_\omega - \alpha_{eW}^{i,j} s_\omega \right) \tag{5.1.3}$$

where the SMEFT dipole operators are defined in table 7. The SMEFT dipole operators can only be generated by weakly-coupled UV completions at loop-level [161, 210, 269]. As such, a complete one-loop study of the contributions to a_μ should involve several other components:

- Tree-level generated operators which renormalise the dipole operators;
- One-loop matching conditions from the SMEFT to LEFT of the photon dipole;
- One-loop contributions to the observable a_μ from tree-level generated operators.

Ref. [270] took into consideration all of these contributions and, in Eq. (5.2) of that reference, it is shown that, for an EFT with a cut-off $\Lambda = 10\ \text{TeV}$, the only relevant SMEFT operators besides the dipoles was $\mathcal{O}_{\ell equ}^{(3)}$. The contribution from this 4-fermion operator is already a one-loop effect and therefore, for a coherent one-loop analysis, we only need to consider the tree-level generation of $\mathcal{O}_{\ell equ}^{(3)}$; according to Ref. [161], only the leptoquarks $S_1 \sim (\mathbf{3}, \mathbf{1}, -1/3)$ and $S_2 \sim (\mathbf{3}, \mathbf{2}, -7/6)$ – where the number in parenthesis are the representations under $(SU(3)_C, SU(2)_L, U(1)_Y)$ – generate this operator at tree-level. Given that this result is known in the literature, for the remainder of the chapter we will not mention it and focus solely on possible UV extensions which generate the dipole operators at one-loop. Note however, that when extensions with S_1 and S_2 are mentioned, one should also add the contribution from $\mathcal{O}_{\ell equ}^{(3)}$.

A wide array of SM extensions (with different number of new fields) have been suggested to generate the dipole operators – Ref. [271] (and references therein) offers a very comprehensive review on these models and their status according to current experimental data. Given the large contribution needed to explain the observed a_μ, any contribution to the dipole operators which is suppressed by a muon Yukawa requires that the heavy particles running in the loop have a mass at most of $\mathcal{O}(100)\ \text{GeV}$. In our SMEFT analysis we are concerned with heavier particles with a clear decoupling between the scale of new physics and the electroweak scale. Therefore, we will focus on chirally enhanced solutions, that is, UV extensions

in which the NP contribution to a_μ is not suppressed by the muon Yukawa coupling. Refs. [117, 272–276] have studied chirally enhanced solutions for several 3-field extensions of the SM.

This work will focus on the (chirally enhanced) contribution to a_μ generated through the diagram of figure 30, which we will refer to as *bridge* hereafter. We will classify all SM extensions which can generate such a topology. Regardless of the matching being performed (on-shell or off-shell matching), the particle which connects the loop and 2 external states (the bridge) must be heavy, otherwise it would give rise to a Yukawa coupling. Furthermore, one or both particles in the loop must be heavy, meaning that either 2- or 3-field extensions can generate this diagram.

This bridge diagram has been considered in particular 2-field extensions with VLLs [277, 278]. However, we perform a complete classification of all 2- and 3-fields extensions of the SM responsible for generating this topology. These extensions can sometimes also generate a box diagram[2] which must also be calculated when computing the full contribution of a particular model to a_μ.

Our approach in the SMEFT allows us to consider several 2-field extensions which have so far been overlooked in the literature, where only the lepton Yukawa-suppressed contributions to a_μ from these models were considered. This ended up excluding these models as viable explanations of the anomaly (either because particles had to be very light or because the contribution had a fixed negative sign). By also taking into account the bridge contribution from these 2-field extensions, we have restored as possible solutions to the observed anomaly in a_μ.

The 3-field UV completions (which produced chirally enhanced contributions to a_μ) considered in Refs. [117, 272–276] generated the dipole operators through a box diagram, shown in figure 33. The heavy fields which could generate such a topology are not the same as those which would generate a bridge diagram. As such, we present a completely new class of 3-field extensions which can account for Δa_μ.

5.1.1 Computation of a_μ

We will consider fermion and scalar[3] extensions of the SM (with 2 or 3 fields) which can generate the bridge diagram of figure 30 where the W or B gauge bosons can couple to any of the internal propagators. In practice, the calculation could be done directly with a photon insertion if the appropriate electric charge is considered; however, in order to maintain our language within the SMEFT consistent, we always refer to diagrams with the gauge bosons in the unbroken phase of the SM. Throughout all computations,

[2] In the LEFT, given that the Higgs takes a vev, this corresponds to the triangle diagram, which is what is usually mentioned in the literature.

[3] Heavy vectors can also take the place of scalars with the same quantum numbers. However, we only show the explicit results for scalars.

contributions suppressed by lepton Yukawas will be neglected, as well as terms proportional to the Higgs mass, of the form (m_ϕ/M).

To compute the one-loop matching conditions for the dipole operators, the 4-point amplitude between $\bar{\ell}_L$, e_R, ϕ, and B/W is calculated, considering all momenta incoming. For simplicity, the momentum of the Higgs, p_ϕ, is taken to zero. We equate the process in both the full theory (the SM extension) and the SMEFT and focus on the kinematic structure $\not{q}\not{\epsilon}$, where q is the momentum of the gauge boson and ϵ its polarization vector, since this is the structure which fixes the dipole operators WC. The following on-shell relation is useful in the calculations:

$$\overline{v_\ell}\,\not{q}\not{\epsilon}\,u_e = -\overline{v_\ell}\,(\not{p}_\ell + \not{p}_e)\not{\epsilon}\,u_e = -2\epsilon\cdot p_e\,\overline{v_\ell}\,u_e\,, \tag{5.1.4}$$

where $p_{e(\ell)}$ is the momentum of the right-handed (left-handed) lepton, and v_ℓ, u_e are the corresponding external spinors. In order to apply the second equality we took the on-shell conditions $\overline{v_\ell}\,\not{p}_\ell = 0$ and $\not{p}_e\,u_e = 0$ valid for massless fermions. This results in $\epsilon\cdot p_e$ being the only relevant kinematic structure that must be calculated to arrive at the matching condiitions.

This matching calculation to the dipole operators is particularly efficient in the on-shell approach unlike what has been done throughout this thesis. That is because, disregarding lepton Yukawa insertions, no other connected diagram can arise. One could wonder whether attaching the gauge boson to the external legs would give a contribution; however, this contribution is either proportional to $\not{p}_\ell\not{\epsilon}$ or $\not{\epsilon}\not{p}_e$, or, if the gauge boson couples to the Higgs, proportional to $q\cdot\epsilon = 0$ or $p_\phi\cdot\epsilon = 0$.

We also do not need to consider the cases in which the gauge boson is attached to the fermionic bridge since all contributions are proportional either to $\not{p}_\ell\not{\epsilon}$ or $\not{\epsilon}\not{p}_e$, which are zero in light of the previous arguments. Therefore, only contributions where the gauge boson is coupling with the particles in the loop must be taken into account.

Results presented in the following sections have been cross-checked with `matchmakereft` [217] [4]. As mentioned previously, this tool calculates the one-loop matching conditions for generic UV extensions of the SM following the diagrammatic approach off-shell. In this case, as explored in section 4.1.2, results are given in terms of operators in a Green's basis, which should then be translated to the Warsaw basis. When using `matchmakereft` the following relations can be used to move to the Warsaw basis:

$$\alpha_{eB} = \alpha^G_{eB} - \frac{g_1}{8}\beta^G_{eHD2} + \frac{g_1}{8}\beta^G_{eHD4} - \frac{g_1}{2}\beta^G_{eHD3}\,, \tag{5.1.5}$$

$$\alpha_{eW} = \alpha^G_{eW} - \frac{g_2}{8}\beta^G_{eHD2} + \frac{g_2}{8}\beta^G_{eHD4}\,, \tag{5.1.6}$$

[4] When results were available in the literature we also cross-checked against those in them.

written in `matchmakereft`'s convention, where the superscript G denotes WC of operators defined in the Green's basis. Yukawa-suppressed contributions and the evanescent operators were neglected.

5.1.2 General results

Before delving into the results for the bridge diagram, let us mention that some of the considered extensions can also contribute to a_μ through the usual box diagrams shown in figures 32 and 33. For completeness, we present in Appendix E the contribution to a_μ for generic heavy fields. With those results and the general results from the bridge topology contribution presented in this section, the full contribution to a_μ can be calculated for arbitrary UV extensions of the SM.

The bridge topologies can be classified depending on the particle that connects the loop with the 2 external particles, that is, the particle in the bridge. This can never be a SM field as it would result in a Yukawa-suppressed contribution. The possible representations for the heavy particles in the bridge are fixed according to the SM particle with which it couples:

1. **Scalar in the bridge**

   The heavy scalar in the bridge must couple to the left- and right-handed muon fixing its quantum numbers to be those of the SM Higgs. However, all contributions to a_μ with a scalar bridge are zero since they are always proportional to $\epsilon \cdot q$.

2. **Fermion in the bridge coupled to right-handed muon**

   The heavy fermion must have the same quantum numbers as the SM left-handed lepton, $\Delta \sim (1, 2, -1/2)$. These three numbers in parenthesis correspond to the representations of the heavy fields under ($SU(3)_c$, $SU(2)_L$ and $U(1)_Y$).

3. **Fermion in the bridge coupled to left-handed muon**

   The heavy fermion must either have the quantum numbers of a SM right-handed lepton, $E \sim (1, 1, -1)$, or $\Sigma \sim (1, 3, -1)$.

For the case of a heavy fermion in the bridge, there are 3 possible combinations for the particles within the loop: 1 extra heavy fermion, Ψ, and the SM Higgs, figure 29a; 1 heavy fermion and 1 heavy scalar, Φ, figure 30; 1 heavy scalar and a SM fermion, figure 29b. The latter case of figure 29b does not contribute to a_μ. This is so because a mass insertion in the bridge propagator is needed in order to provide a non-zero result for the dipole operators which in turn, requires an extra mass insertion from the

fermion in the loop to result in the correct chirality of the external fermions. Therefore, a heavy fermion inside the loop is needed.

Once the particle in the bridge is fixed, we present the results of the contribution to a_μ for generic representations of the remaining heavy fields in the next subsections.

For concreteness, we fix a particular orientation for the internal propagators shown in the diagrams which avoids the presence of fermion-number violating terms. For some representations of the heavy fields, one might need to consider the diagram with a flipped propagator; in this case adding a minus sign in the contribution coming from the gauge boson insertion in the flipped propagator is enough.

5.1.2.1 VLL doublet bridge

Let us write a general Lagrangian which extends the SM with the VLL doublet, Δ, and extra fields such that it can generate the bridge contribution. The relevant terms read:

$$\begin{aligned}\mathcal{L} \supset\ & g Y_\Psi \overline{\Psi} \gamma_\mu \Psi B^\mu + g_W T^{W,\Psi}_{IKI'} \overline{\Psi_I} \gamma_\mu \Psi_{I'} W^\mu_K \\ & - i g Y_\Phi B^\mu (\partial_\mu \Phi^\dagger \Phi - \Phi^\dagger \partial_\mu \Phi) - i g_W T^{W,\Phi}_{JKJ'} W^\mu_K (\partial_\mu \Phi^\dagger_J \Phi_{J'} - \Phi^\dagger_J \partial_\mu \Phi_{J'}) \\ & + y_M \overline{\Delta}\, e_R\, \phi + T_{IKJ} \left(y^R_b\, \overline{\Psi}_I\, P_R\, \Delta_K \Phi_J + y^L_b\, \overline{\Psi}_I\, P_L\, \Delta_K \Phi_J \right) + y_F\, T'_{KIJ}\, \overline{\ell_{L,K}} \Psi_I \Phi^\dagger_J + \text{h.c.}\,,\end{aligned} \tag{5.1.7}$$

where Φ can stand generically for a heavy scalar or the SM Higgs (ϕ always stands for the SM Higgs), Ψ is an extra heavy fermion (besides Δ) and ℓ_L is the left-handed SM lepton. No family indices are considered in the couplings with the SM leptons as we only need the couplings to the second generation. The indices $I^{(\prime)}$, $J^{(\prime)}$, $K^{(\prime)}$ correspond to the SU(2) components of the fields, $Y_{\Psi(\Phi)}$ is the hypercharge of $\Psi(\Phi)$, and T^W, T and T' are the Clebsch-Gordan coefficients of the corresponding interaction term, determined by the representations of the fields comprising that term.

Following this notation and defining $T^{\gamma,\psi}_{ij} \equiv Y_\psi \delta_{ij} + T^{W,\psi}_{i3j}$[5], where ψ correpsonds to any particle, we can now write the result for $\alpha_{e\gamma}$ from the bridge topology generated by generic fields as:

$$\alpha^{2,2}_{e\gamma} = \frac{iNe}{4} y_M y_F y^R_b \sum_{IJ} T_{I2J} \left[\gamma_\Psi T^{\gamma,\Psi}_{I'I} T'_{2JI'} + \gamma_\Phi T^{\gamma,\Phi}_{JJ'} T'_{2IJ'} \right], \tag{5.1.8}$$

with $\gamma_{\Psi,\Phi}$ being kinematic factors which will be defined below. Each γ term corresponds to insertions of the gauge boson in the fermion and scalar propagators within the loop. N is the dimension of the $SU(3)$ representation of the particles within the loop.

[5] $T^{\gamma,\psi}$ would be diagonal and proportional to the electric charge if the charge eigenstate basis is chosen for the ψ multiplet, i.e., $T^{W,\psi}$ is diagonal.

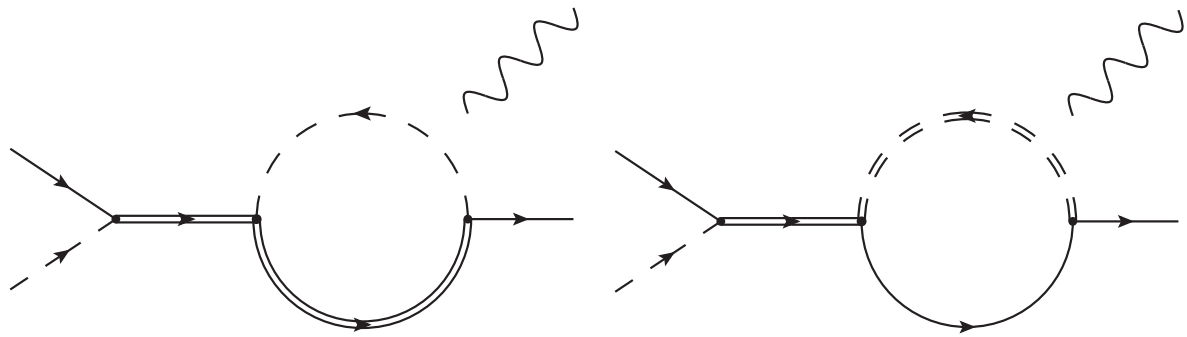

(a) (b)

Figure 29: *Left:* Bridge diagram for a fermion in the bridge with a heavy fermion and the SM Higgs in the loop. *Right:* Bridge diagram for a fermion in the bridge with a heavy scalar and a SM fermion in the loop. In both diagrams, doubled (single) lines correspond to heavy (SM) particles. The B or W bosons can be attached to any of the internal lines.

The kinematic factors $\gamma_{\Psi,\Phi}$ are always expressed through two functions of the masses of the involved particles:

$$f(M_A, M_B, M_C) \equiv -\frac{iM_B}{(4\pi)^2 M_A} \frac{M_B^4 - 4M_B^2 M_C^2 + 3M_C^4 + 2M_C^4 \mathrm{Log}[M_B^2/M_C^2]}{(M_B^2 - M_C^2)^3}, \tag{5.1.9}$$

$$h(M_A, M_B, M_C) \equiv -\frac{iM_B}{(4\pi)^2 M_A} \frac{M_B^4 - M_C^4 - 2M_B^2 M_C^2 \mathrm{Log}[M_B^2/M_C^2]}{(M_B^2 - M_C^2)^3}. \tag{5.1.10}$$

When inside the loop there is a heavy fermion, Ψ and the SM Higgs, figure 29a, the kinematic factors in Eq. (5.1.8) are given by:

$$\gamma_\Psi = \gamma_\Phi = \lim_{M_\Phi \to 0} f(M_\Delta, M_\Psi, M_\Phi) = \frac{-i}{(4\pi)^2 M_\Delta M_\Psi}. \tag{5.1.11}$$

If the bridge diagram composed of three heavy propagators is generated, figure 30, the contribution to $\alpha_{e\gamma}$ is given with:

$$\gamma_\Psi = f(M_\Delta, M_\Psi, M_\Phi), \tag{5.1.12}$$

$$\gamma_\Phi = h(M_\Delta, M_\Psi, M_\Phi). \tag{5.1.13}$$

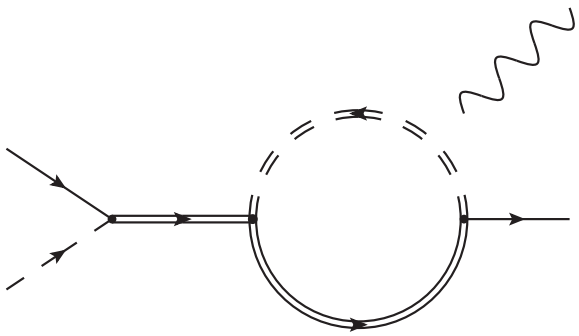

Figure 30: Bridge diagram with a fermion in the bridge and only heavy particles in the loop. Doubled (single) lines correspond to heavy (SM) particles. The B or W bosons can be attached to any of the internal lines.

5.1.2.2 VLL singlet (triplet) bridge

The relevant Lagrangian extending the SM with a VLL triplet, Σ, that can be responsible for generating the bridge contribution can be written as:

$$\mathcal{L} \supset y_M \bar{\ell}_L \sigma^I \phi P_R \Sigma_I + y_F \overline{\Psi}_I \Phi_I e_R + T_{KIJ} \left(y_b^R \overline{\Sigma}_K P_R \Psi_I \Phi_J^\dagger + y_b^L \overline{\Sigma}_K P_L \Psi_I \Phi_J^\dagger \right) + \text{h.c.}, \tag{5.1.14}$$

where σ^I denotes the Pauli matrices and we use the same gauge conventions and general notation as introduced previously in Eqs. (5.1.7) and (5.1.8).

The general result for the bridge contribution to $\alpha_{e\gamma}$ is given by:

$$\alpha_{e\gamma}^{2,2} = \frac{-iNe}{4} y_M y_F y_b^R \sum_{IJ} T_{3IJ} \left[\gamma_\Psi T_{IJ}^{\gamma,\Psi} + \gamma_\Phi T_{IJ}^{\gamma,\Phi} \right] . \tag{5.1.15}$$

The relevant Lagrangian for extending the SM with a singlet VLL which can generate the bridge diagram is the following:

$$\mathcal{L} \supset y_M \bar{\ell}_L \phi P_R E + y_F \overline{\Psi}_I \Phi_I e_R + y_b^R \overline{E} P_R \Psi_I \Phi_I^\dagger + y_b^L \overline{E} P_L \Psi_I \Phi_I^\dagger + \text{h.c.}\,, \tag{5.1.16}$$

where, once again, the same conventions as in Eqs. (5.1.7),(5.1.8) are used. Contributions to $\alpha_{e\gamma}$ are given by:

$$\alpha_{e\gamma}^{2,2} = \frac{iNe}{4} y_M y_F y_b^R \left(\text{Tr}[T^{\gamma,\Psi}] \gamma_\Psi + \text{Tr}[T^{\gamma,\Phi}] \gamma_\Phi \right) . \tag{5.1.17}$$

Table 15: SM extensions with 2 heavy fields which can generate the bridge topology, with two heavy propagators. The presented a_μ result for these completions include all contributions (not only the one generated through the bridge diagram).

Bridge	Other Fermion	a_μ result
$E \sim (1,1,-1)$	$\Delta \sim (1,2,-1/2)$	Eq. (5.1.21)
	$\Delta_3 \sim (1,2,-3/2)$	Eq. (5.1.22)
$\Delta \sim (1,2,-1/2)$	$E \sim (1,1,-1)$	Eq. (5.1.21)
	$\Sigma \sim (1,3,-1)$	Eq. (5.1.23)
	$N \sim (1,1,0)$	Eq. (5.1.24)
	$\Sigma_0 \sim (1,3,0)$	Eq. (5.1.25)
$\Sigma \sim (1,3,-1)$	$\Delta \sim (1,2,-1/2)$	Eq. (5.1.23)
	$\Delta_3 \sim (1,2,-3/2)$	Eq. (5.1.26)

The kinematic factors are the same on both Eqs. (5.1.17) and (5.1.15) and, for the case of a heavy fermion and the SM Higgs in the loop, are given by:

$$\gamma_\Psi = \gamma_\Phi = \lim_{M_\Phi \to 0} f(M_{E(\Sigma)}, M_\Psi, M_\Phi)\,, \tag{5.1.18}$$

whereas for a heavy fermion and a heavy scalar in the loop are given by:

$$\gamma_\psi = f(M_{E(\Sigma)}, M_\Psi, M_\Phi)\,, \tag{5.1.19}$$

$$\gamma_\Phi = h(M_{E(\Sigma)}, M_\Psi, M_\Phi)\,. \tag{5.1.20}$$

5.1.3 Two-field extensions

Since the number of 2-field extensions which generate the bridge diagram is finite, we will calculate the full contribution to $\alpha_{e\gamma}$ for all these models. Such models are presented in table 15 for the case in which the bridge diagram is generated with only one extra heavy propagator besides the bridge, figure 29a. In this case, once the particle in the bridge is chosen, the quantum numbers of the extra heavy field are fixed.

The contributions to $\alpha_{e\gamma}$ are given below:

1. $E \sim (1,1,-1)$ and $\Delta \sim (1,2,-1/2)$

Two different diagrams must be taken into account for this completion: one with the VLL singlet on the bridge and the VLL doublet in the loop, and vice-versa.

$$\alpha_{e\gamma}^{2,2} = -\frac{1}{16\pi^2}\frac{e\, y_M y_F y_b^R}{4M_E M_\Delta}\,. \tag{5.1.21}$$

The couplings above can be equivalently interpreted from the Lagrangian in Eq. (5.1.7) or Eq. (5.1.16).

2. $E \sim (1,1,-1)$ and $\Delta_3 \sim (1,2,-3/2)$

$$\alpha_{e\gamma}^{2,2} = -\frac{1}{16\pi^2}\frac{5e\, y_M y_F y_b^R}{4M_E M_{\Delta_3}}\,; \tag{5.1.22}$$

3. $\Delta \sim (1,2,-1/2)$ and $\Sigma \sim (1,3,-1)$

Two different diagrams must be taken into account for this completion: one with the doublet on the bridge and the triplet in the loop, and vice-versa.

$$\alpha_{e\gamma}^{2,2} = -\frac{1}{16\pi^2}\frac{3e\, y_M y_F y_b^R}{4M_\Delta M_\Sigma}\,. \tag{5.1.23}$$

Both (5.1.7) and (5.1.14) can be used to interpret this result.

4. $\Delta \sim (1,2,-1/2)$ and $N \sim (1,1,0)$

$$\alpha_{e\gamma}^{2,2} = 0\,. \tag{5.1.24}$$

This null result has been discussed in the literature in Refs. [277, 278].

5. $\Delta \sim (1,2,-1/2)$ and $\Sigma_0 \sim (1,3,0)$

$$\alpha_{e\gamma}^{2,2} = -\frac{1}{16\pi^2}\frac{e\, y_M y_F y_b^R}{2M_\Delta M_{\Sigma_0}}\,; \tag{5.1.25}$$

6. $\Sigma \sim (1,3,-1)$ and $\Delta_3 \sim (1,2,-3/2)$

$$\alpha_{e\gamma}^{2,2} = -\frac{1}{16\pi^2}\frac{5e\, y_M y_F y_b^R}{4M_\Sigma M_{\Delta_3}}\,. \tag{5.1.26}$$

A 2-field extension can be responsible for a bridge diagram with 3 heavy propagators if the bridge fermion can also be the heavy fermion inside the loop, resulting in the diagram of figure 30. The representations of heavy fields for which this can happen are listed in table 16 and their contributions to $\alpha_{e\gamma}$ are given by:

1. $E \sim (1,1,-1)$ and $\mathcal{S}_0 \sim (1,1,0)$

$$\alpha_{e\gamma}^{2,2} = -\frac{1}{16\pi^2} e y_b^R y_M y_F \frac{M_E^4 - 4M_E^2 M_{\mathcal{S}_0}^2 + 3M_{\mathcal{S}_0}^4 + 2M_{\mathcal{S}_0}^4 \mathrm{Log}[M_E^2/M_{\mathcal{S}_0}^2]}{4(M_E^2 - M_{\mathcal{S}_0}^2)^3}\,; \tag{5.1.27}$$

2. $E \sim (1,1,-1)$ and $\mathcal{S}_2 \sim (1,1,-2)$

$$\alpha_{e\gamma}^{2,2} = \frac{1}{16\pi^2} e y_b^R y_M y_F \frac{3M_E^4 - 4M_E^2 M_{\mathcal{S}_2}^2 + M_{\mathcal{S}_2}^4 + (2M_{\mathcal{S}_2}^4 - 4M_E^2 M_{\mathcal{S}_2}^2)\mathrm{Log}[M_E^2/M_{\mathcal{S}_2}^2]}{2(M_E^2 - M_{\mathcal{S}_2}^2)^3}\,; \tag{5.1.28}$$

3. $\Delta \sim (1,2,-1/2)$ and $\mathcal{S}_0 \sim (1,1,0)$

$$\alpha_{e\gamma}^{2,2} = -\frac{1}{16\pi^2} e y_b^R y_M y_F \frac{M_\Delta^4 - 4M_\Delta^2 M_{\mathcal{S}_0}^2 + 3M_{\mathcal{S}_0}^4 + 2M_{\mathcal{S}_0}^4 \mathrm{Log}[M_\Delta^2/M_{\mathcal{S}_0}^2]}{4(M_\Delta^2 - M_{\mathcal{S}_0}^2)^3}\,; \tag{5.1.29}$$

4. $\Delta \sim (1,2,-1/2)$ and $\mathcal{S}_1 \sim (1,1,-1)$

$$\alpha_{e\gamma}^{2,2} = 0\,; \tag{5.1.30}$$

5. $\Delta \sim (1,2,-1/2)$ and $\Xi_0 \sim (1,3,0)$

$$\alpha_{e\gamma}^{2,2} = \frac{1}{16\pi^2} e y_b^R y_M y_F \frac{M_\Delta^4 + 4M_\Delta^2 M_{\Xi_0}^2 - 5M_{\Xi_0}^4 - (4M_{\Xi_0}^2 M_\Delta^2 + 2M_{\Xi_0}^4)\mathrm{Log}[M_\Delta^2/M_{\Xi_0}^2]}{4(M_\Delta^2 - M_{\Xi_0}^2)^3}\,; \tag{5.1.31}$$

6. $\Delta \sim (1,2,-1/2)$ and $\Xi_1 \sim (1,3,-1)$

$$\alpha_{e\gamma}^{2,2} = -\frac{1}{16\pi^2} e y_b^R y_M y_F \frac{7M_\Delta^4 - 8M_\Delta^2 M_{\Xi_1}^2 + M_{\Xi_1}^4 + (-10M_{\Xi_1}^2 M_\Delta^2 + 4M_{\Xi_1}^4)\mathrm{Log}[M_\Delta^2/M_{\Xi_1}^2]}{2(M_\Delta^2 - M_{\Xi_1}^2)^3}\,; \tag{5.1.32}$$

7. $\Sigma \sim (1,3,-1)$ and $\Xi_0 \sim (1,3,0)$

$$\alpha_{e\gamma}^{2,2} = -\frac{1}{16\pi^2} e y_b^R y_M y_F \frac{M_\Sigma^2 - M_{\Xi_0}^2 + M_{\Xi_0}^2 \mathrm{Log}[M_{\Xi_0}^2/M_\Sigma^2]}{(M_\Sigma^2 - M_{\Xi_0}^2)^2}\,; \tag{5.1.33}$$

8. $\Sigma \sim (1,3,-1)$ and $\Xi_2 \sim (1,3,-2)$

$$\alpha_{e\gamma}^{2,2} = 0\,. \tag{5.1.34}$$

The zero obtained for completions (5.1.30) and (5.1.34) can be explained from the fact that the bridge coupling y_b involves two equal fields whereas the gauge symmetry of that interaction is antisymmetric (this would not be true if we were dealing with more than 1 generation for the heavy fields). Furthermore, note that for models (5.1.27), (5.1.29),(5.1.31) and (5.1.33), the operators associated with the couplings y_b^R and y_b^L are related by hermitian conjugation leading us to redefine $y_b^R \equiv y_b^R + y_b^{L\,*}$ as the right-handed coupling.

The contribution from these models to Δa_μ had already been considered in the literature [114, 272, 279] (apart from the ones that involve fermion number violating (FNV) vertices). However, only the Yukawa-proportional contribution had been calculated, which excluded these models as solutions to the anomaly since the new particles had to be lighter than what is allowed by collider experiments. However, by doing our computations in the unbroken phase of the SM (in the SMEFT) it becomes simpler to verify the existence of the chirally enhanced contribution arising from the bridge diagram; this allows the BSM particles to be heavier than before, restoring this class of models as viable explanations of the Δa_μ anomaly.

From these models, an interesting example is the $\Delta \sim (1,2,-1/2) + \Xi_0 \sim (1,3,0)$ extension whose contribution was calculated to be always negative in the literature and would therefore be incapable of accounting for the observed anomaly. However the contribution from the bridge diagram was neglected and we see, from Eq. (5.1.31), this contribution from the bridge topology is proportional to 3 distinct couplings, resulting in a contribution which does not have a fixed sign.

5.1.4 Three-field extensions

Due to the presence of a loop with heavy particles, the possible representations of three-field extensions which can generate the bridge diagram of figure 30 are infinite. As such, we will present the conditions on the gauge representation on the new fields such that the bridge diagram can be generated. All conditions are shown by considering no FNV vertices; if a model has those interactions, the conditions should be applied to the conjugate versions of the fields.

The extra heavy scalar, Φ, and heavy fermion, Ψ, must respect:

1. VLL singlet

$$Y_\Psi - Y_\Phi = -1\,, \tag{5.1.35}$$

Table 16: SM extensions with 2 heavy fields (a fermion and a scalar) which generate the bridge topology with 3 heavy propagators. The grey color corresponds to models with fermion number violating interactions.

Fermion	Scalar	Result
$E \sim (1,1,-1)$	$\mathcal{S}_0 \sim (1,1,0)$	Eq. (5.1.27)
	$\mathcal{S}_2 \sim (1,1,-2)$	Eq. (5.1.28)
$\Delta \sim (1,2,-1/2)$	$\mathcal{S}_0 \sim (1,1,0)$	Eq. (5.1.29)
	$\mathcal{S}_1 \sim (1,1,-1)$	Eq. (5.1.30)
	$\Xi_0 \sim (1,3,0)$	Eq. (5.1.31)
	$\Xi_1 \sim (1,3,-1)$	Eq. (5.1.32)
$\Sigma \sim (1,3,-1)$	$\Xi_0 \sim (1,3,0)$	Eq. (5.1.33)
	$\Xi_2 \sim (1,3,-2)$	Eq. (5.1.34)

$$SU(2)_\Phi \otimes SU(2)_\Psi = 1\,; \tag{5.1.36}$$

2. VLL doublet

$$Y_\Psi - Y_\Phi = -1/2\,, \tag{5.1.37}$$
$$SU(2)_\Phi \otimes SU(2)_\Psi = 2\,; \tag{5.1.38}$$

3. VLL triplet

$$Y_\Psi - Y_\Phi = -1\,, \tag{5.1.39}$$
$$SU(2)_\Phi \otimes SU(2)_\Psi = 3\,, \tag{5.1.40}$$
$$SU(2)_\Phi \otimes SU(2)_\Psi = 1\,, \tag{5.1.41}$$

where Eq. (5.1.40) refers to the coupling with the bridge triplet and Eq. (5.1.41) to the coupling with the SM right-handed muon.

The color charge of the heavy fields within the loop must always form a singlet. Larger color representations result in an enhancement factor to the diagram, as mentioned in [275] for the case of box diagrams.

Table 17: SM extensions with 3 heavy fields which generate the bridge topology. We limited ourselves to considering only singlet, doublet and triplet $SU(2)$ representations. Only the $SU(2)$ representation of the 2 extra fields, Φ and Ψ, is shown since color representation must be the conjugate of each other and hypercharge is constrained from the conditions specified in the text. Exchanging the assigned $SU(2)$ representations between Φ and Ψ gives also a valid extension.

Bridge	$(SU(2)_\Psi, SU(2)_\Phi)$	Result
$E \sim (1,1,-1)$	(1,1)	Eq. (5.1.42)
	(2,2)	Eq. (5.1.43)
	(3,3)	Eq. (5.1.44)
$\Delta \sim (1,2,-1/2)$	(2,1)	Eqs. (5.1.45), (5.1.46)
	(2,3)	Eqs. (5.1.47), (5.1.48)
$\Sigma \sim (1,3,-1)$	(2,2)	Eq. (5.1.49)
	(3,3)	Eq. (5.1.50)

Limiting the analysis to singlets, doublets and triplets of $SU(2)$, the UV completions which can be responsible for the bridge topology are listed in table 17.

None of these extensions is among the ones studied in Refs. [117, 272–276] and are therefore novel extensions of the SM which can serve as an explanation to the a_μ anomaly. The contribution to $\alpha_{e\gamma}$ from these models is shown following the the notation introduced in Eqs. (5.1.7),(5.1.14) and (5.1.16). Results are presented in terms of a generic hypercharge for Ψ, Y_Ψ, and we use the notation $(\Psi,\Phi) \sim (SU(2)_\Psi, SU(2)_\Phi)$ to denote the $SU(2)$ representations of the fields, as listed in table 17.

1. $E \sim (1,1,-1) + (\Psi,\Phi) \sim (1,1)$

$$\alpha_{e\gamma}^{2,2} = \frac{1}{16\pi^2}\frac{eNM_\Psi y_M y_F y_b^R}{4M_E(M_\Psi^2 - M_\Phi^2)^3}\Big\{(M_\Psi^2 - M_\Phi^2)(M_\Phi^2(1-2Y_\Psi) + M_\Psi^2(1+2Y_\Psi)) \\ - 2(-M_\Phi^4 Y_\Psi + M_\Psi^2 M_\Phi^2(1+Y_\Psi))\mathrm{Log}[M_\Psi^2/M_\Phi^2]\Big\}; \tag{5.1.42}$$

2. $E \sim (1,1,-1) + (\Psi,\Phi) \sim (2,2)$

$$\alpha_{e\gamma}^{2,2} = \frac{1}{16\pi^2}\frac{eNM_\Psi y_M y_F y_b^R}{2M_E(M_\Psi^2 - M_\Phi^2)^3}\Big\{(M_\Psi^2 - M_\Phi^2)(M_\Phi^2(1-2Y_\Psi) + M_\Psi^2(1+2Y_\Psi)) \\ -2(-M_\Phi^4 Y_\Psi + M_\Psi^2 M_\Phi^2(1+Y_\Psi))\mathrm{Log}[M_\Psi^2/M_\Phi^2]\Big\}; \tag{5.1.43}$$

3. $E \sim (1,1,-1) + (\Psi,\Phi) \sim (3,3)$

$$\alpha_{e\gamma}^{2,2} = \frac{1}{16\pi^2}\frac{3eNM_\Psi y_M y_F y_b^R}{4M_E(M_\Psi^2 - M_\Phi^2)^3}\Big\{(M_\Psi^2 - M_\Phi^2)(M_\Phi^2(1-2Y_\Psi) + M_\Psi^2(1+2Y_\Psi)) \\ -2(-M_\Phi^4 Y_\Psi + M_\Psi^2 M_\Phi^2(1+Y_\Psi))\mathrm{Log}[M_\Psi^2/M_\Phi^2]\Big\}; \tag{5.1.44}$$

4. $\Delta \sim (1,2,-1/2) + (\Psi,\Phi) \sim (2,1)$

$$\alpha_{e\gamma}^{2,2} = \frac{1}{16\pi^2}\frac{eNM_\Psi y_M y_F y_b^R}{4M_\Delta(M_\Psi^2 - M_\Phi^2)^3}\Big\{2(M_\Psi^2 - M_\Phi^2)(M_\Phi^2(1-Y_\Psi) + M_\Psi^2 Y_\Psi) \\ -(M_\Phi^4(1-2Y_\Psi) + M_\Psi^2 M_\Phi^2(1+2Y_\Psi))\mathrm{Log}[M_\Psi^2/M_\Phi^2]\Big\}; \tag{5.1.45}$$

5. $\Delta \sim (1,2,-1/2) + (\Psi,\Phi) \sim (1,2)$

$$\alpha_{e\gamma}^{2,2} = \frac{1}{16\pi^2}\frac{eNM_\Psi y_M y_F y_b^R}{4M_\Delta(M_\Psi^2 - M_\Phi^2)^3}\Big\{(M_\Psi^2 - M_\Phi^2)(M_\Phi^2(1-2Y_\Psi) + M_\Psi^2(1+2Y_\Psi)) \\ -2(-M_\Phi^4 Y_\Psi + M_\Psi^2 M_\Phi^2(1+Y_\Psi))\mathrm{Log}[M_\Psi^2/M_\Phi^2]\Big\}; \tag{5.1.46}$$

6. $\Delta \sim (1,2,-1/2) + (\Psi,\Phi) \sim (2,3)$

$$\alpha_{e\gamma}^{2,2} = \frac{1}{16\pi^2}\frac{eNM_\Psi y_M y_F y_b^R}{4M_\Delta(M_\Psi^2 - M_\Phi^2)^3}\Big\{2(M_\Psi^2 - M_\Phi^2)(M_\Phi^2(1-3Y_\Psi) + M_\Psi^2(2+3Y_\Psi)) \\ +(M_\Phi^4(1+6Y_\Psi) - M_\Psi^2 M_\Phi^2(7+6Y_\Psi))\mathrm{Log}[M_\Psi^2/M_\Phi^2]\Big\}; \tag{5.1.47}$$

7. $\Delta \sim (1,2,-1/2) + (\Psi,\Phi) \sim (3,2)$

$$\alpha_{e\gamma}^{2,2} = \frac{1}{16\pi^2} - \frac{eNM_\Psi y_M y_F y_b^R}{4M_\Delta(M_\Psi^2 - M_\Phi^2)^3}\Big\{(M_\Psi^2 - M_\Phi^2)(M_\Phi^2(7-6Y_\Psi) + M_\Psi^2(-1+6Y_\Psi)) \\ -2(M_\Phi^4(2-3Y_\Psi) + M_\Psi^2 M_\Phi^2(1+3Y_\Psi))\mathrm{Log}[M_\Psi^2/M_\Phi^2]\Big\}; \tag{5.1.48}$$

8. $\Sigma \sim (1,3,-1) + (\Psi,\Phi) \sim (2,2)$

$$\alpha_{e\gamma}^{2,2} = \frac{1}{16\pi^2} - \frac{eNM_\Psi y_M y_F y_b^R}{2M_\Sigma (M_\Psi^2 - M_\Phi^2)^2}\left\{M_\Psi^2 - M_\Phi^2 - M_\Phi^2 \mathrm{Log}[M_\Psi^2/M_\Phi^2]\right\}; \tag{5.1.49}$$

9. $\Sigma \sim (1,3,-1) + (\Psi,\Phi) \sim (3,3)$

$$\alpha_{e\gamma}^{2,2} = \frac{1}{16\pi^2} - \frac{eNM_\Psi y_M y_F y_b^R}{M_\Sigma (M_\Psi^2 - M_\Phi^2)^2}\left\{M_\Psi^2 - M_\Phi^2 - M_\Phi^2 \mathrm{Log}[M_\Psi^2/M_\Phi^2]\right\}. \tag{5.1.50}$$

5.1.5 General phenomenological considerations

The VLL in the bridge is the most general feature of all the models presented thus far. Also since it mix with the SM muon, it is bounded by electroweak precision observables (EWPO) [120, 121]:

$$\frac{v}{M_E} y_M \lesssim 0.03\,(0.04)\,, \tag{5.1.51}$$

$$\frac{v}{M_\Delta} y_M \lesssim 0.065\,(0.075)\,, \tag{5.1.52}$$

$$\frac{v}{M_\Sigma} y_M \lesssim 0.1\,(0.11)\,, \tag{5.1.53}$$

for the singlet, doublet and triplet of $SU(2)$ respectively at 1 (2) σ confidence levels.

Collider searches for these VLLs can set lower limits on their masses. Indeed we have seen that in section 3.2 and for a VLL decaying to SM final state we estimated that the HL phase of the LHC could exclude masses lighter than $800\ \mathrm{GeV}$ for an $SU(2)$ singlet. The doublet case has been more recently searched by CMS [125], where masses below $\sim 800\,\mathrm{GeV}$ were excluded; these are conservative results since only tau decays were considered. For the triplet case, Ref. [280] estimates the discovery reach of the LHC at $3\,\mathrm{ab}^{-1}$ at $5\,\sigma$ to be of approximately $1.4\ \mathrm{TeV}$.

Further direct bounds can be obtained from the heavy particles running in the loop, through EW or QCD (when possible) pair production. However, this and other probes are very dependent on the particular choice of model, and it is beyond the scope of this thesis to go over the particular implications of every model.

A common issue which most chirally enhanced solutions to a_μ face is the generation of a large contribution to the muon Yukawa coupling. This happens through the same diagrams which accounts for a_μ but without the gauge boson. Note that this is actually not a problem for the bridge solution when there is a VLL triplet in the bridge; this is because in order to have a non-zero contribution, a W-boson insertion is needed in this case. For the singlet and doublet VLL bridges, indeed a sizable contribution to the muon

Yukawa should be expected which can result in a fine-tuning problem to explain the observed coupling. Several UV scenarios have been explored in which the dipole operators and the Yukawa couplings have the same origin [281–283].

5.2 The triple triplet model

The previous section introduced several new models and their contributions towards a_μ. However, given the new degrees of freedom introduced by considering multi-field extensions, there is enough room to accommodate other anomalous observations. This section shows how the bridge topology can connect explanations of different anomalies.

Let us focus on $R_K^{(*)}$ and the CAA, introduced in section 2.3.3. In [284], it is shown that the CAA can be directly related to a correction in the muonic vertex with the W boson, which we denote by $\epsilon_{\mu\mu}$.

To explain these two anomalies, we consider one specific realization of the last class of models in table 17, in which the SM is extended with the VLL triplet, Σ, a triplet scalar leptoquark with hypercharge $-1/3$, S_3, and a triplet vector-like quark, Ψ_Q, with hypercharge $-4/3$.

The triplet leptoquark is a well-known solution to the neutral flavour anomalies at tree-level [285–288] and the VLL triplet can account for the CAA, in spite of creating some tension with EWPO [121, 284][6]. Using the bridge to to explain a_μ including these two fields, fixes the quantum numbers of Ψ_Q.

The Lagrangian of this model is the following:

$$\begin{aligned}\mathcal{L} \supset\ & y_T^i \bar{\ell}_{Li}\phi\sigma^I\Sigma_R^I + y_Q^i \overline{\Psi}_{QL}^I S_3^I\, e_{Ri} + i y_b^L \epsilon^{IJK}\overline{\Sigma}_R^I \Psi_{Q,L}^J S_3^{K\dagger} + i y_b^R \epsilon^{IJK}\overline{\Sigma}_L^I \Psi_{Q,R}^J S_3^{K\dagger} \\ & + \lambda_S^{ij}\overline{q}_{Li}^c i\sigma^2\sigma^I \ell_{Lj} S_3^{I\dagger} + \lambda_U^i \overline{u_R}_i\, \Sigma^{c,I} S_3^I + \text{h.c.},\end{aligned} \tag{5.2.1}$$

with $q^c \equiv C\overline{q}^T$ and C the charge conjugation matrix. The SM $SU(2)$ doublets q_L and ℓ_L are in the down-quark and charged lepton diagonal basis, respectively.

We will consider the minimal set of couplings which explain the observed discrepancies in B-meson decays, V_{CKM} unitarity and the anomalous magnetic moment of the muon, without mention of a possible UV origin. Therefore, we assume that new physics only couples to the second generation of leptons. This allows the evasion of constraints from the Lepton Flavour Violating (LFV) decay $\mu \to e\gamma$. As for quarks, we will only consider couplings with the second and third generations in λ_S^{ij}, namely $\lambda_S^{s\mu}$ and $\lambda_S^{b\mu}$.

[6] The latest CDF II measurement of the W-boson mass [289] has increased this tension between explaining CAA and EWPO (see [290] for a recent analysis).

The anomalies are explained in this model by the generation of $\mathcal{O}_{\ell q}^{(1),(3)}$ at tree-level by S_3 exchange, $\mathcal{O}_{H\ell}^{(3)}$ also at tree-level by integrating Σ and a bridge-like one-loop contribution to Δa_μ. The matching expressions for the relevant Wilson coefficients are:

$$[\alpha_{\ell q}^{(1)}]_{i,j,k,l} = \frac{3\lambda_S^{*ki}\lambda_S^{lj}}{4M_{S_3}^2} + \mathcal{O}(\frac{1}{16\pi^2}), \tag{5.2.2}$$

$$[\alpha_{\ell q}^{(3)}]_{i,j,k,l} = \frac{\lambda_S^{*ki}\lambda_S^{lj}}{4M_{S_3}^2} + \mathcal{O}(\frac{1}{16\pi^2}), \tag{5.2.3}$$

$$[\alpha_{H\ell}^{(3)}]_{i,j} = \frac{y_T^i y_T^{*j}}{4M_\Sigma^2} + \mathcal{O}(\frac{1}{16\pi^2}), \tag{5.2.4}$$

$$[\alpha_{eB}]_{i,j} \simeq 0, \tag{5.2.5}$$

$$[\alpha_{eW}]_{i,j} \simeq \frac{3g_W y_b^R\, y_T^i y_Q^j}{16\pi^2}\frac{M_{\Psi_Q}}{M_\Sigma}\left(\frac{M_{\Psi_Q}^2 - M_{S_3}^2 + M_{S_3}^2\,\mathrm{Log}\left[\frac{M_{S_3}^2}{M_{\Psi_Q}^2}\right]}{(M_{\Psi_Q}^2 - M_{S_3}^2)^2}\right), \tag{5.2.6}$$

where the $\simeq$ means that we are neglecting Yukawa-suppressed contributions.

Explaining $R_K^{(*)}$ and CAA fixes the ratios $x_S \equiv \lambda_S^{*s\mu}\lambda_S^{b\mu}/M_S^2$ and $x_T \equiv y_T^\mu/M_\Sigma$, up to one-loop corrections that break this scale invariance in couplings over masses. However, the loop factor suppression makes it so that observables are relatively flat on the values of the masses (in a certain range). The x_T ratio also enters in the expression for Δa_μ, but the couplings y_b^R and $x_F \equiv y_Q^\mu/M_F$ give us enough freedom to fix both observables to the measured values. Since they couple only two and three heavy fields, both y_b and x_F always generate coefficients at one-loop order, so one can expect a wider parameter space in comparison with other couplings.

To explore the one-loop low-energy phenomenology of this model, we computed the complete one-loop matching with `matchmakereft` [217] – which was provided as an auxiliary notebook in Ref. [8]– and used `smelli` [175, 291] to construct the χ^2 function from the observables at low energy in terms of the WCs matched at a high scale. Then, we performed a fit, using the `iminuit` [292] python package, to the mentioned anomalies, EWPO and quark-related observables like $B - \overline{B}$ mixing.

We considered couplings smaller than 1, and fixed the masses to $M_\Sigma = 3.4$ TeV, $M_{S_3} = 2$ TeV and $M_{\Psi_Q} = 4.6$ TeV. The observables were relatively insensitive to the masses between 1-5 TeV, so we chose this hierarchy as a benchmark. Other hierarchies and values between 1-5 TeV would yield similar results.

Table 18: Pulls from the SM and from the experimental value for the most relevant observables as given by `smelli`.

Observable	Pull experiment (σ)	Pull SM (σ)
a_μ	0.82	-4.16
$\langle R_{\mu e}\rangle(B^\pm \to K^\pm \ell^+\ell^-)^{[1.0,6.0]}$	1.41	-2.89
$\langle R_{\mu e}\rangle(B^0 \to K^{*0} \ell^+\ell^-)^{[0.045,1.1]}$	1.98	-1.32
$\langle R_{\mu e}\rangle(B^0 \to K^{*0} \ell^+\ell^-)^{[1.1,6.0]}$	1.04	-2.33
$\epsilon_{\mu\mu}$	1.20	-3.87
ΔM_s	1.08	0.06
ΔM_d	1.25	0.002
M_W	2.28	1.50
A_e	2.77	1.66

The best-fit point in this setup is:

$$\begin{aligned} x_F &= 0.2\ \text{TeV}^{-1}, & x_S &= 0.00078\ \text{TeV}^{-2}, \\ x_T &= 0.17\ \text{TeV}^{-1}, & \lambda_S^{b\mu} &= 0.07, \\ y_b^L &= 0.10, & y_b^R &= 0.13, \end{aligned} \tag{5.2.7}$$

which corresponds to a global pull from the SM of 6.2 σ. For the calculation of this pull we took the observables that were fitted, i.e., the ones available in `smelli` in the classes EWPO, leptonic observables, lepton flavour universality for neutral currents and quark flavour observables. In table 18, we present some pulls for individual observables.

Finally, in figure 31 we show the 1- and 2-σ regions from the best-fit point for the model parameters x_S and x_T obtained using the global likelihood provided by `smelli`. For each point, we minimize χ^2 by varying the other parameters. The results for the rest of the variables are very similar to what one would expect from only taking the tree level solutions, showing that the one loop effects give us enough freedom to explain Δa_μ, without entering in tension with the tree-level solutions to the other anomalies.

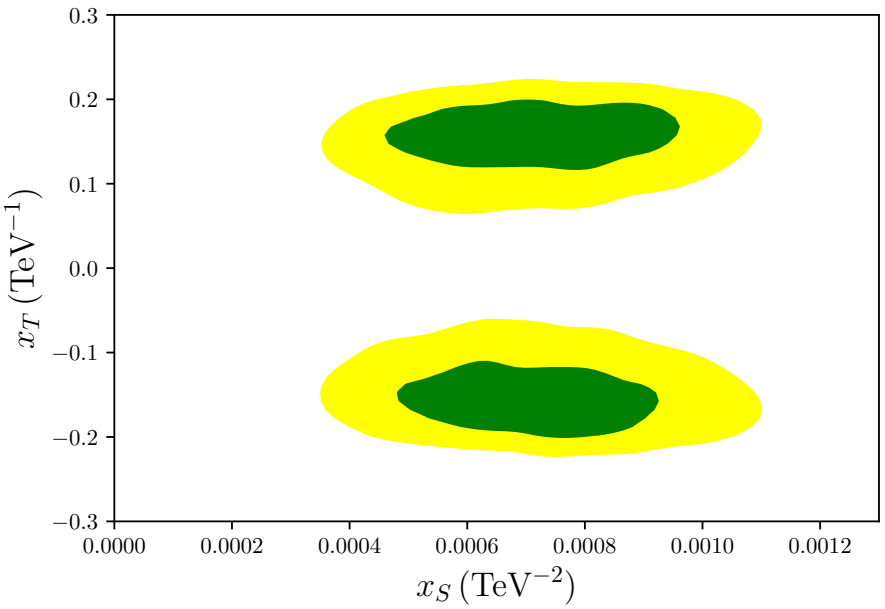

Figure 31: The 1 and 2-σ regions in green and yellow, respectively, around the obtained best-fit point. For each point in the grid, the other couplings were marginalized in order to minimize the χ^2 function. As mentioned in the text, the observables included in the fit were the ones available in `smelli` in the classes EWPO, leptonic observables, lepton flavour universality for neutral currents and quark flavour observables, and $\epsilon_{\mu\mu}$.

6

Summary and Conclusions

There is plenty of motivation to search for BSM physics, both from direct experimental evidence which the SM cannot explain and also from theoretical questions to which the SM cannot answer. With the vast amount of models for new physics being proposed in the literature to face these challenges, from the phenomenological point of view, we are confronted with the difficult task of developing strategies to search for BSM physics in a way that encompasses the largest possible number of models.

Our attempt at following a global approach for the search of BSM physics led us to two complementarity directions: a model-driven approach, focusing on signatures motivated by specific models; or a model-independent approach, following the SMEFT paradigm, in which heavy new physics effects are parametrized in terms of higher dimensional operators constructed from the degrees of freedom of the SM.

In principle, following a model-independent approach seems preferable given its wider applicability; however it is not always the case that the effective description of new physics is available. This is because EFTs suppose a decoupling between the UV scale and the scale at which the experiment takes place. As such, theories which predict light new physics cannot be described by the SMEFT. Furthermore, from the collider perspective, the SMEFT also cannot account for processes in which the final state contains a heavy (stable) particle since it can only contain operators with the SM fields. Therefore, choosing a particular signature can be the best way to follow, particularly when the BSM resonances can be produced at current experimental setups. Moreover, the EFT parametrization can only point to a direction of new physics, but *a priori* it does not explain the structures that appear, which can only be predicted by specific models. For example, if a particular WC with a specific flavour structure is preferred by data to be non-zero (for example, the second diagonal entry in the WC of $\mathcal{O}_{eB,W}$ to explain a_μ), it is relevant to explain why this is the flavour structure that arises (why the off-diagonal terms are suppressed to avoid $\mu \to e\gamma$ constraints)

from a full UV model which, in turn, can point to new particles with a particular phenomenology that could potentially be seen at future experiments. The highlights of each approach followed in this thesis are presented below.

The model-driven approach

To follow the model-driven direction, we focused on CHMs, which explain the HP by considering the Higgs as a pNGB arising from the SSB of a strongly interacting sector. The choice of CHMs as our object of study boils down to the fact that a solution to the fine-tuning problem should lie at the TeV scale, predicting resonances which could lie within the reach of current – or expected – collider experiments. Furthermore, CHMs predict several new BSM fields which can also serve as solutions to other SM shortcomings. We concretized the compositeness framework in the LHT, a model based on the collective symmetry breaking mechanism which alleviates the contributions of heavy physics to the Higgs mass. Moreover, since this model possesses a discrete symmetry under which most new fields are odd, the lightest odd field is a suitable DM candidate.

We explored the signatures of VLLs not only because they are a generic prediction of composite scenarios, but also because when included in complete models they can have a drastically different phenomenology than what is covered by current searches, which focus on the VLL decaying to SM final states. Indeed, due to T-parity in the LHT, VLLs cannot decay solely to SM particles, decaying instead to a heavy neutral vector and a SM lepton. Therefore, we proposed dedicated analyses to test VLLs with arbitrary BRs to the common SM decay channels and an exotic channel of a heavy vector (stable, resulting in a MET signature) and a SM lepton. Given that the results were presented for arbitrary BRs, the analysis can be easily interpreted in the limiting cases of a SM only decaying VLL, a VLL within the LHT which decays solely through the exotic channel or any other model which can have the 4 channels available, e.g. DM models where the relic density is set through freeze-in, by the decay of a VLL.

We showed that current LHC data can probe $M_E \lesssim 405\,\mathrm{GeV}$ for a singlet VLL decaying to SM final states whereas a VLL decaying solely through the exotic channel can be excluded up to $M_E \lesssim 895\,\mathrm{GeV}$. We also studied the prospects for the high-luminosity phase of the LHC and for possible future proton-proton colliders, running at a center of mass energy $\sqrt{s} = 27$ and $100\,\mathrm{TeV}$.

Furthermore, we explored the case in which the heavy vector is not only stable at detector scales, but also at cosmological scales, constituting a viable dark matter candidate. After showing that the standard freeze-out scenario for generating the appropriate relic density presents tension with limits from direct detection, resulting in only a small region of viable parameter space, we considered the possibility that the VLL and the heavy vector have very similar masses. This leads to a successful generation of dark

matter via co-annihilation, compatible with all current experimental limits. If the exotic vector is very light and feebly interacting, it can generate the observed relic density through the freeze-in mechanism. We have shown that in this case collider searches looking for displaced vertices can be very useful in probing a large part of the parameter space.

The model-independent approach

For the model-independent approach we aimed to expand the current description of the SMEFT. The first direction in the effort of improving the predictions of the SMEFT was to consider dimension-8 effects. The study of the SMEFT at this order is not only relevant from the experimental point of view, as certain observables receive their leading contribution from dimension-8 operators, but it is also interesting since the parameter space for some WCs of dimension-8 operators is bounded solely from principles of unitarity and analyticity, limiting the space of EFTs which can be UV completed.

While a physical basis of the SMEFT at dimension-8 had already been constructed in the literature, performing calculations off-shell is sometimes preferable as they scale slower as the number of external legs grows when compared with on-shell computations. The main bottleneck in the off-shell computation is the knowledge of the extended Green's basis and its reduction to the physical operators. As such, we started our work by building the Green's basis of the bosonic sector at dimension-8, extending the on-shell bosonic sector with 86 new interactions. Their off-shell independence was verified in momentum space.

Knowing the Green's basis of bosonic operators, we proceeded with the computation of the RGEs of the WCs at dimension-8. The RGEs at this order have co-leading contributions from two insertions of dimension-6 terms and one insertion of dimension-8 interactions. There were no renormalisation theorems for the former contribution which made their explicit computation especially important. We verified that no combination of tree-level generated dimension-6 operators renormalises dimension-8 operators induced at loop-level. This results, for instance, in the conclusion that tree-level generated dimension-6 operators cannot contribute to the S and U parameters (to one-loop accuracy) up to $\mathcal{O}(v^4/\Lambda^4)$. Furthermore, we also observed several numerical factors which deviated significantly from naive power counting which can result in non-negligible results when the RGE contribution is included; we showed this explicitly by considering the SMEFT parameter space compatible with a strong first order EWPT.

As for the RGE component arising from a single insertion of dimension-8 operators, we verified that one-loop generated operators can in general be renormalised by tree-level induced ones. Therefore, this running effect can in principle be non-negligible when compared with the one-loop matching contribution from a UV model. Once again, we also found large coefficient in the RGEs of some WCs which compensated in part the one-loop suppression, possibly resulting in significant effects.

We also explored the stability of the positivity bounds obtained in the literature under one-loop running. For the dimension-8 4-Higgs WCs, we concluded that the contribution with two insertions of dimension-6 operators respects the positivity bounds obtained at tree-level, while the contribution from one insertion of dimension-8 operators does not need to respect the positivity condition in general. We also applied the positivity condition to operators in the $X^2\phi^2D^2$ class concluding that the RGE resulting from an insertion of a dimension-8 operator respects the positivity conditions derived when considering only tree-level effects, and therefore, these conditions hold at all scales at one-loop accuracy. This bolsters the idea that these positivity restrictions can be used as priors in experimental fits looking to probe the WC of quartic-gauge operators.

As mentioned before, light new physics cannot be described within the SMEFT. Therefore our second step in extending the SMEFT was to include an extra light degree of freedom, a light pseudo-scalar, resulting in the SMEFT+ALP theory. This scenario is motivated by the axion, a solution to the strong-CP problem, but also by CHMs where, besides the Higgs, other pNGBs can arise with a naturally light mass. Given that the experimental effort to look for these particles spans several orders of magnitude in energy scale, we computed the RGEs of this theory to improve the interpretation of the obtained experimental bounds. We applied the RGEs to specific cases, namely that of a photophobic ALP, obtaining an indirect bound on the UV couplings of the ALP to Z bosons roughly 4 orders of magnitude stronger than direct bounds from searches at colliders.

Finally, we studied the connection between experiment and UV extensions of the SM through the SMEFT. We focused on the recent measurement of the anomalous magnetic moment of the muon which seems to deviate significantly from the SM prediction, possibly pointing to a new physics contribution. In the SMEFT, this observable is parametrized by the dipole operators involving muons and the B and W bosons, which can only be generated at one-loop by weakly-coupled renormalisable UV theories. Given that Yukawa-suppressed contributions to a_μ demand light new physics, we instead studied chirally enhanced contributions which could be generated through a particular Feynman diagram, the bridge. We classified all possible representations of 2- and 3-field extensions which could generate the bridge diagram and provided general results for their contribution to a_μ in terms of their representations under the SM gauge groups. Through our approach within the SMEFT we proposed a class of 2-field UV extensions capable of explaining the a_μ measurement, which had been neglected so far in the literature. Furthermore, we presented a novel class of 3-field extensions which can also account for the observed anomaly. This study shows the importance of systematically considering the one-loop matching contributions to the SMEFT in order to accurately classify UV explanations of anomalies.

As theoretical predictions and experimental measurements abound, we showed the importance of

extending the current efforts for searching for new physics beyond minimality, by exploring signatures motivated in complete and non-oversimplified scenarios and by improving the accuracy of our model-independent predictions, to ensure no stone is left unturned in our quest for physics BSM.

Bibliography

[1] ATLAS collaboration. “Observation of a new particle in the search for the Standard Model Higgs boson with the ATLAS detector at the LHC”. In: *Phys. Lett. B* 716 (2012), pp. 1–29. doi: 10.1016/j.physletb.2012.08.020. arXiv: 1207.7214 [hep-ex] (cit. on p. 1).

[2] CMS collaboration. “Observation of a New Boson at a Mass of 125 GeV with the CMS Experiment at the LHC”. In: *Phys. Lett. B* 716 (2012), pp. 30–61. doi: 10.1016/j.physletb.2012.08.021. arXiv: 1207.7235 [hep-ex] (cit. on p. 1).

[3] G. Guedes and J. Santiago. “New leptons with exotic decays: collider limits and dark matter complementarity”. In: *JHEP* 01 (2022), p. 111. doi: 10.1007/JHEP01(2022)111. arXiv: 2107.03429 [hep-ph] (cit. on pp. 3, 18).

[4] M. Chala, Á. Dı̄az-Carmona, and G. Guedes. “A Green’s basis for the bosonic SMEFT to dimension 8”. In: (2021-12). arXiv: 2112.12724 [hep-ph] (cit. on pp. 3, 62).

[5] M. Chala et al. “Towards the renormalisation of the Standard Model effective field theory to dimension eight: Bosonic interactions I”. In: *SciPost Phys.* 11 (2021), p. 065. doi: 10.21468/SciPostPhys.11.3.065. arXiv: 2106.05291 [hep-ph] (cit. on pp. 3, 79).

[6] S. Das Bakshi et al. “Towards the renormalisation of the Standard Model effective field theory to dimension eight: Bosonic interactions II”. In: (2022-05). arXiv: 2205.03301 [hep-ph] (cit. on pp. 3, 79).

[7] M. Chala et al. “Running in the ALPs”. In: *Eur. Phys. J. C* 81.2 (2021), p. 181. doi: 10.1140/epjc/s10052-021-08968-2. arXiv: 2012.09017 [hep-ph] (cit. on pp. 3, 96).

[8] G. Guedes and P. Olgoso. “A bridge to new physics: proposing new – and reviving old – explanations of a_μ”. In: (2022-05). arXiv: 2205.04480 [hep-ph] (cit. on pp. 3, 111, 128).

[9] M. D. Schwartz. *Quantum Field Theory and the Standard Model*. Cambridge University Press, 2014-03. isbn: 978-1-107-03473-0, 978-1-107-03473-0 (cit. on pp. 6, 19, 46, 52).

[10] P. Fileviez Perez and H. H. Patel. "The Electroweak Vacuum Angle". In: *Phys. Lett. B* 732 (2014), pp. 241–243. doi: 10.1016/j.physletb.2014.03.064. arXiv: 1402.6340 [hep-ph] (cit. on p. 6).

[11] P. W. Anderson. "Plasmons, Gauge Invariance, and Mass". In: *Phys. Rev.* 130 (1 1963-04), pp. 439–442. doi: 10.1103/PhysRev.130.439. url: https://link.aps.org/doi/10.1103/PhysRev.130.439 (cit. on p. 6).

[12] F. Englert and R. Brout. "Broken Symmetry and the Mass of Gauge Vector Mesons". In: *Phys. Rev. Lett.* 13 (9 1964-08), pp. 321–323. doi: 10.1103/PhysRevLett.13.321. url: https://link.aps.org/doi/10.1103/PhysRevLett.13.321 (cit. on p. 6).

[13] P. W. Higgs. "Broken Symmetries and the Masses of Gauge Bosons". In: *Phys. Rev. Lett.* 13 (16 1964-10), pp. 508–509. doi: 10.1103/PhysRevLett.13.508. url: https://link.aps.org/doi/10.1103/PhysRevLett.13.508 (cit. on p. 6).

[14] P. A. Zyla et al. "Review of Particle Physics". In: *PTEP* 2020.8 (2020), p. 083C01. doi: 10.1093/ptep/ptaa104 (cit. on pp. 7, 11).

[15] K. Abe et al. "Observation of Electron Neutrino Appearance in a Muon Neutrino Beam". In: *Phys. Rev. Lett.* 112 (2014), p. 061802. doi: 10.1103/PhysRevLett.112.061802. arXiv: 1311.4750 [hep-ex] (cit. on p. 8).

[16] J. K. Ahn et al. "Observation of Reactor Electron Antineutrino Disappearance in the RENO Experiment". In: *Phys. Rev. Lett.* 108 (2012), p. 191802. doi: 10.1103/PhysRevLett.108.191802. arXiv: 1204.0626 [hep-ex] (cit. on p. 8).

[17] Y. Abe et al. "Reactor electron antineutrino disappearance in the Double Chooz experiment". In: *Phys. Rev. D* 86 (2012), p. 052008. doi: 10.1103/PhysRevD.86.052008. arXiv: 1207.6632 [hep-ex] (cit. on p. 8).

[18] F. P. An et al. "Observation of electron-antineutrino disappearance at Daya Bay". In: *Phys. Rev. Lett.* 108 (2012), p. 171803. doi: 10.1103/PhysRevLett.108.171803. arXiv: 1203.1669 [hep-ex] (cit. on p. 8).

[19] T. Araki et al. "Measurement of neutrino oscillation with KamLAND: Evidence of spectral distortion". In: *Phys. Rev. Lett.* 94 (2005), p. 081801. doi: 10.1103/PhysRevLett.94.081801. arXiv: hep-ex/0406035 (cit. on p. 8).

[20] P. Adamson et al. “Measurement of Neutrino Oscillations with the MINOS Detectors in the NuMI Beam”. In: *Phys. Rev. Lett.* 101 (2008), p. 131802. doi: 10.1103/PhysRevLett.101.131802. arXiv: 0806.2237 [hep-ex] (cit. on p. 8).

[21] Y. Fukuda et al. “Evidence for oscillation of atmospheric neutrinos”. In: *Phys. Rev. Lett.* 81 (1998), pp. 1562–1567. doi: 10.1103/PhysRevLett.81.1562. arXiv: hep-ex/9807003 (cit. on p. 8).

[22] Q. R. Ahmad et al. “Direct evidence for neutrino flavor transformation from neutral current interactions in the Sudbury Neutrino Observatory”. In: *Phys. Rev. Lett.* 89 (2002), p. 011301. doi: 10.1103/PhysRevLett.89.011301. arXiv: nucl-ex/0204008 (cit. on p. 8).

[23] N. Aghanim et al. “Planck 2018 results. VI. Cosmological parameters”. In: *Astron. Astrophys.* 641 (2020). [Erratum: Astron.Astrophys. 652, C4 (2021)], A6. doi: 10.1051/0004-6361/201833910. arXiv: 1807.06209 [astro-ph.CO] (cit. on pp. 8, 9, 11).

[24] K. G. Begeman, A. H. Broeils, and R. H. Sanders. “Extended rotation curves of spiral galaxies : dark haloes and modified dynamics.” In: 249 (1991-04), p. 523. doi: 10.1093/mnras/249.3.523 (cit. on p. 9).

[25] R. Gavazzi et al. “A weak lensing study of the Coma cluster”. In: 498.2 (2009-05), pp. L33–L36. doi: 10.1051/0004-6361/200911841. arXiv: 0904.0220 [astro-ph.CO] (cit. on p. 9).

[26] D. Clowe et al. “A direct empirical proof of the existence of dark matter”. In: *Astrophys. J. Lett.* 648 (2006), pp. L109–L113. doi: 10.1086/508162. arXiv: astro-ph/0608407 (cit. on p. 9).

[27] G. Bertone, D. Hooper, and J. Silk. “Particle dark matter: Evidence, candidates and constraints”. In: *Phys. Rept.* 405 (2005), pp. 279–390. doi: 10.1016/j.physrep.2004.08.031. arXiv: hep-ph/0404175 (cit. on p. 9).

[28] G. Bertone and D. Hooper. “History of dark matter”. In: *Rev. Mod. Phys.* 90.4 (2018), p. 045002. doi: 10.1103/RevModPhys.90.045002. arXiv: 1605.04909 [astro-ph.CO] (cit. on p. 9).

[29] L. Canetti, M. Drewes, and M. Shaposhnikov. “Matter and Antimatter in the Universe”. In: *New J. Phys.* 14 (2012), p. 095012. doi: 10.1088/1367-2630/14/9/095012. arXiv: 1204.4186 [hep-ph] (cit. on p. 9).

[30] A. D. Sakharov. "Violation of CP Invariance, C asymmetry, and baryon asymmetry of the universe". In: *Pisma Zh. Eksp. Teor. Fiz.* 5 (1967), pp. 32–35. doi: 10.1070/PU1991v034n05ABEH002497 (cit. on p. 9).

[31] M. B. Gavela et al. "Standard model CP violation and baryon asymmetry". In: *Mod. Phys. Lett. A* 9 (1994), pp. 795–810. doi: 10.1142/S0217732394000629. arXiv: hep-ph/9312215 (cit. on p. 9).

[32] C. A. Baker et al. "An Improved experimental limit on the electric dipole moment of the neutron". In: *Phys. Rev. Lett.* 97 (2006), p. 131801. doi: 10.1103/PhysRevLett.97.131801. arXiv: hep-ex/0602020 (cit. on p. 9).

[33] J. E. Kim and G. Carosi. "Axions and the Strong CP Problem". In: *Rev. Mod. Phys.* 82 (2010). [Erratum: Rev.Mod.Phys. 91, 049902 (2019)], pp. 557–602. doi: 10.1103/RevModPhys.82.557. arXiv: 0807.3125 [hep-ph] (cit. on p. 9).

[34] C. Abel et al. "Measurement of the Permanent Electric Dipole Moment of the Neutron". In: *Phys. Rev. Lett.* 124.8 (2020), p. 081803. doi: 10.1103/PhysRevLett.124.081803. arXiv: 2001.11966 [hep-ex] (cit. on p. 9).

[35] M. S. Turner. "Λ CDM: Much More Than We Expected, but Now Less Than What We Want". In: *Found. Phys.* 48.10 (2018), pp. 1261–1278. doi: 10.1007/s10701-018-0178-8. arXiv: 2109.01760 [astro-ph.CO] (cit. on p. 9).

[36] B. Abi et al. "Measurement of the Positive Muon Anomalous Magnetic Moment to 0.46 ppm". In: *Phys. Rev. Lett.* 126.14 (2021), p. 141801. doi: 10.1103/PhysRevLett.126.141801. arXiv: 2104.03281 [hep-ex] (cit. on pp. 10, 12, 40).

[37] G. W. Bennett et al. "Final Report of the Muon E821 Anomalous Magnetic Moment Measurement at BNL". In: *Phys. Rev. D* 73 (2006), p. 072003. doi: 10.1103/PhysRevD.73.072003. arXiv: hep-ex/0602035 (cit. on pp. 10, 12).

[38] T. Aoyama et al. "The anomalous magnetic moment of the muon in the Standard Model". In: *Phys. Rept.* 887 (2020), pp. 1–166. doi: 10.1016/j.physrep.2020.07.006. arXiv: 2006.04822 [hep-ph] (cit. on pp. 10, 13).

[39] G. 't Hooft. "Naturalness, chiral symmetry, and spontaneous chiral symmetry breaking". In: *NATO Sci. Ser. B* 59 (1980). Ed. by G. 't Hooft et al., pp. 135–157. doi: 10.1007/978-1-4684-7571-5_9 (cit. on p. 10).

[40] M. K. Gaillard and B. W. Lee. "Rare decay modes of the K mesons in gauge theories". In: *Phys. Rev. D* 10 (3 1974-08), pp. 897–916. doi: 10.1103/PhysRevD.10.897. url: https://link.aps.org/doi/10.1103/PhysRevD.10.897 (cit. on p. 11).

[41] M. Bauer and T. Plehn. *Yet Another Introduction to Dark Matter: The Particle Physics Approach*. Vol. 959. Lecture Notes in Physics. Springer, 2019. doi: 10.1007/978-3-030-16234-4. arXiv: 1705.01987 [hep-ph] (cit. on pp. 11, 12).

[42] T. R. Slatyer. "Indirect Detection of Dark Matter". In: *Theoretical Advanced Study Institute in Elementary Particle Physics: Anticipating the Next Discoveries in Particle Physics*. 2018, pp. 297–353. doi: 10.1142/9789813233348_0005. arXiv: 1710.05137 [hep-ph] (cit. on pp. 11, 12).

[43] M. J. Baker et al. "The Coannihilation Codex". In: *JHEP* 12 (2015), p. 120. doi: 10.1007/JHEP12(2015)120. arXiv: 1510.03434 [hep-ph] (cit. on pp. 12, 42).

[44] K. Griest and D. Seckel. "Three exceptions in the calculation of relic abundances". In: *Phys. Rev. D* 43 (1991), pp. 3191–3203. doi: 10.1103/PhysRevD.43.3191 (cit. on p. 12).

[45] N. F. Bell, Y. Cai, and A. D. Medina. "Co-annihilating Dark Matter: Effective Operator Analysis and Collider Phenomenology". In: *Phys. Rev. D* 89.11 (2014), p. 115001. doi: 10.1103/PhysRevD.89.115001. arXiv: 1311.6169 [hep-ph] (cit. on p. 12).

[46] J. P. Lees et al. "Evidence for an excess of $\bar{B} \to D^{(*)}\tau^-\bar{\nu}_\tau$ decays". In: *Phys. Rev. Lett.* 109 (2012), p. 101802. doi: 10.1103/PhysRevLett.109.101802. arXiv: 1205.5442 [hep-ex] (cit. on p. 12).

[47] J. P. Lees et al. "Measurement of an Excess of $\bar{B} \to D^{(*)}\tau^-\bar{\nu}_\tau$ Decays and Implications for Charged Higgs Bosons". In: *Phys. Rev. D* 88.7 (2013), p. 072012. doi: 10.1103/PhysRevD.88.072012. arXiv: 1303.0571 [hep-ex] (cit. on p. 12).

[48] M. Huschle et al. "Measurement of the branching ratio of $\bar{B} \to D^{(*)}\tau^-\bar{\nu}_\tau$ relative to $\bar{B} \to D^{(*)}\ell^-\bar{\nu}_\ell$ decays with hadronic tagging at Belle". In: *Phys. Rev. D* 92.7 (2015), p. 072014. doi: 10.1103/PhysRevD.92.072014. arXiv: 1507.03233 [hep-ex] (cit. on p. 12).

[49] R. Aaij et al. "Measurement of the ratio of branching fractions $\mathcal{B}(\bar{B}^0 \to D^{*+}\tau^-\bar{\nu}_\tau)/\mathcal{B}(\bar{B}^0 \to D^{*+}\mu^-\bar{\nu}_\mu)$". In: *Phys. Rev. Lett.* 115.11 (2015). [Erratum: Phys.Rev.Lett. 115, 159901 (2015)], p. 111803. doi: 10.1103/PhysRevLett.115.111803. arXiv: 1506.08614 [hep-ex] (cit. on p. 12).

[50] S. Hirose et al. "Measurement of the τ lepton polarization and $R(D^*)$ in the decay $\bar{B} \to D^* \tau^- \bar{\nu}_\tau$". In: *Phys. Rev. Lett.* 118.21 (2017), p. 211801. doi: 10.1103/PhysRevLett.118.211801. arXiv: 1612.00529 [hep-ex] (cit. on p. 12).

[51] S. Hirose et al. "Measurement of the τ lepton polarization and $R(D^*)$ in the decay $\bar{B} \to D^* \tau^- \bar{\nu}_\tau$ with one-prong hadronic τ decays at Belle". In: *Phys. Rev. D* 97.1 (2018), p. 012004. doi: 10.1103/PhysRevD.97.012004. arXiv: 1709.00129 [hep-ex] (cit. on p. 12).

[52] R. Aaij et al. "Measurement of the ratio of the $B^0 \to D^{*-} \tau^+ \nu_\tau$ and $B^0 \to D^{*-} \mu^+ \nu_\mu$ branching fractions using three-prong τ-lepton decays". In: *Phys. Rev. Lett.* 120.17 (2018), p. 171802. doi: 10.1103/PhysRevLett.120.171802. arXiv: 1708.08856 [hep-ex] (cit. on p. 12).

[53] R. Aaij et al. "Test of Lepton Flavor Universality by the measurement of the $B^0 \to D^{*-} \tau^+ \nu_\tau$ branching fraction using three-prong τ decays". In: *Phys. Rev. D* 97.7 (2018), p. 072013. doi: 10.1103/PhysRevD.97.072013. arXiv: 1711.02505 [hep-ex] (cit. on p. 12).

[54] A. Abdesselam et al. "Measurement of $\mathcal{R}(D)$ and $\mathcal{R}(D^*)$ with a semileptonic tagging method". In: (2019-04). arXiv: 1904.08794 [hep-ex] (cit. on p. 12).

[55] Y. Amhis et al. "Averages of b-hadron, c-hadron, and τ-lepton properties as of summer 2016". In: *Eur. Phys. J. C* 77.12 (2017), p. 895. doi: 10.1140/epjc/s10052-017-5058-4. arXiv: 1612.07233 [hep-ex] (cit. on p. 12).

[56] R. Aaij et al. "Test of lepton universality in beauty-quark decays". In: *Nature Phys.* 18.3 (2022), pp. 277–282. doi: 10.1038/s41567-021-01478-8. arXiv: 2103.11769 [hep-ex] (cit. on p. 12).

[57] R. Aaij et al. "Test of lepton universality with $B^0 \to K^{*0} \ell^+ \ell^-$ decays". In: *JHEP* 08 (2017), p. 055. doi: 10.1007/JHEP08(2017)055. arXiv: 1705.05802 [hep-ex] (cit. on p. 12).

[58] B. Belfatto, R. Beradze, and Z. Berezhiani. "The CKM unitarity problem: A trace of new physics at the TeV scale?" In: *Eur. Phys. J. C* 80.2 (2020), p. 149. doi: 10.1140/epjc/s10052-020-7691-6. arXiv: 1906.02714 [hep-ph] (cit. on p. 12).

[59] Y. Grossman, E. Passemar, and S. Schacht. "On the Statistical Treatment of the Cabibbo Angle Anomaly". In: *JHEP* 07 (2020), p. 068. doi: 10.1007/JHEP07(2020)068. arXiv: 1911.07821 [hep-ph] (cit. on p. 12).

[60] S. Borsanyi et al. "Leading hadronic contribution to the muon magnetic moment from lattice QCD". In: *Nature* 593.7857 (2021), pp. 51–55. doi: 10.1038/s41586-021-03418-1. arXiv: 2002.12347 [hep-lat] (cit. on p. 13).

[61] A. Keshavarzi et al. “Muon $g-2$ and $\Delta\alpha$ connection”. In: *Phys. Rev. D* 102.3 (2020), p. 033002. doi: 10.1103/PhysRevD.102.033002. arXiv: 2006.12666 [hep-ph] (cit. on p. 13).

[62] A. Crivellin et al. “Hadronic Vacuum Polarization: $(g-2)_\mu$ versus Global Electroweak Fits”. In: *Phys. Rev. Lett.* 125.9 (2020), p. 091801. doi: 10.1103/PhysRevLett.125.091801. arXiv: 2003.04886 [hep-ph] (cit. on p. 13).

[63] B. Malaescu and M. Schott. “Impact of correlations between a_μ and α_{QED} on the EW fit”. In: *Eur. Phys. J. C* 81.1 (2021), p. 46. doi: 10.1140/epjc/s10052-021-08848-9. arXiv: 2008.08107 [hep-ph] (cit. on p. 13).

[64] G. Colangelo, M. Hoferichter, and P. Stoffer. “Constraints on the two-pion contribution to hadronic vacuum polarization”. In: *Phys. Lett. B* 814 (2021), p. 136073. doi: 10.1016/j.physletb.2021.136073. arXiv: 2010.07943 [hep-ph] (cit. on p. 13).

[65] L. Evans. “The Large Hadron Collider”. In: *New Journal of Physics* 9.9 (2007-09), pp. 335–335. doi: 10.1088/1367-2630/9/9/335. url: https://doi.org/10.1088/1367-2630/9/9/335 (cit. on p. 13).

[66] A. Airapetian et al. “ATLAS: Detector and physics performance technical design report. Volume 1”. In: (1999-05) (cit. on p. 13).

[67] A. Airapetian et al. “ATLAS: Detector and physics performance technical design report. Volume 2”. In: (1999-05) (cit. on p. 13).

[68] G. L. Bayatian et al. “CMS Physics: Technical Design Report Volume 1: Detector Performance and Software”. In: (2006) (cit. on p. 13).

[69] G. L. Bayatian et al. “CMS technical design report, volume II: Physics performance”. In: *J. Phys. G* 34.6 (2007), pp. 995–1579. doi: 10.1088/0954-3899/34/6/S01 (cit. on p. 13).

[70] S. Amato et al. “LHCb technical proposal: A Large Hadron Collider Beauty Experiment for Precision Measurements of CP Violation and Rare Decays”. In: (1998-02) (cit. on p. 13).

[71] A. A. Alves Jr. et al. “The LHCb Detector at the LHC”. In: *JINST* 3 (2008), S08005. doi: 10.1088/1748-0221/3/08/S08005 (cit. on p. 13).

[72] “ALICE: Technical proposal for a large ion collider experiment at the CERN LHC”. In: (1995-12) (cit. on p. 13).

[73] M. D. Schwartz. "TASI Lectures on Collider Physics". In: *Proceedings, Theoretical Advanced Study Institute in Elementary Particle Physics : Anticipating the Next Discoveries in Particle Physics (TASI 2016): Boulder, CO, USA, June 6-July 1, 2016*. Ed. by R. Essig and I. Low. 2018, pp. 65–100. doi: 10.1142/9789813233348_0002. arXiv: 1709.04533 [hep-ph] (cit. on pp. 14, 15).

[74] G. P. Salam. "Towards Jetography". In: *Eur. Phys. J. C* 67 (2010), pp. 637–686. doi: 10.1140/epjc/s10052-010-1314-6. arXiv: 0906.1833 [hep-ph] (cit. on p. 15).

[75] M. Cacciari, G. P. Salam, and G. Soyez. "The anti-k_t jet clustering algorithm". In: *JHEP* 04 (2008), p. 063. doi: 10.1088/1126-6708/2008/04/063. arXiv: 0802.1189 [hep-ph] (cit. on p. 15).

[76] A. Alloul et al. "FeynRules 2.0 - A complete toolbox for tree-level phenomenology". In: *Comput. Phys. Commun.* 185 (2014), pp. 2250–2300. doi: 10.1016/j.cpc.2014.04.012. arXiv: 1310.1921 [hep-ph] (cit. on pp. 15, 27, 78).

[77] C. Degrande et al. "UFO - The Universal FeynRules Output". In: *Comput. Phys. Commun.* 183 (2012), pp. 1201–1214. doi: 10.1016/j.cpc.2012.01.022. arXiv: 1108.2040 [hep-ph] (cit. on p. 15).

[78] J. Alwall et al. "The automated computation of tree-level and next-to-leading order differential cross sections, and their matching to parton shower simulations". In: *JHEP* 07 (2014), p. 079. doi: 10.1007/JHEP07(2014)079. arXiv: 1405.0301 [hep-ph] (cit. on pp. 15, 17, 27).

[79] T. Sjöstrand et al. "An introduction to PYTHIA 8.2". In: *Comput. Phys. Commun.* 191 (2015), pp. 159–177. doi: 10.1016/j.cpc.2015.01.024. arXiv: 1410.3012 [hep-ph] (cit. on pp. 15, 27).

[80] J. de Favereau et al. "DELPHES 3, A modular framework for fast simulation of a generic collider experiment". In: *JHEP* 02 (2014), p. 057. doi: 10.1007/JHEP02(2014)057. arXiv: 1307.6346 [hep-ex] (cit. on pp. 15, 27).

[81] A. L. Read. "Presentation of search results: The CL(s) technique". In: *J. Phys. G* 28 (2002). Ed. by M. Whalley and L. Lyons, pp. 2693–2704. doi: 10.1088/0954-3899/28/10/313 (cit. on pp. 16, 27).

[82] E. Busato, D. Calvet, and T. Theveneaux-Pelzer. "OpTHyLiC: an Optimised Tool for Hybrid Limits Computation". In: *Comput. Phys. Commun.* 226 (2018), pp. 136–150. doi: 10.1016/j.cpc.2018.01.009. arXiv: 1502.02610 [hep-ex] (cit. on pp. 17, 27).

[83] L. Heinrich et al. “pyhf: pure-Python implementation of HistFactory statistical models”. In: *Journal of Open Source Software* 6.58 (2021), p. 2823. doi: 10.21105/joss.02823. url: https://doi.org/10.21105/joss.02823 (cit. on p. 17).

[84] D. B. Kaplan and H. Georgi. “SU(2) × U(1) breaking by vacuum misalignment”. In: *Physics Letters B* 136.3 (1984), pp. 183–186. issn: 0370-2693. doi: https://doi.org/10.1016/0370-2693(84)91177-8. url: https://www.sciencedirect.com/science/article/pii/0370269384911778 (cit. on p. 18).

[85] D. B. Kaplan, H. Georgi, and S. Dimopoulos. “Composite Higgs Scalars”. In: *Phys. Lett. B* 136 (1984), pp. 187–190. doi: 10.1016/0370-2693(84)91178-X (cit. on p. 18).

[86] K. Agashe, R. Contino, and A. Pomarol. “The Minimal composite Higgs model”. In: *Nucl. Phys. B* 719 (2005), pp. 165–187. doi: 10.1016/j.nuclphysb.2005.04.035. arXiv: hep-ph/0412089 (cit. on p. 18).

[87] R. Contino, L. Da Rold, and A. Pomarol. “Light custodians in natural composite Higgs models”. In: *Phys. Rev. D* 75 (2007), p. 055014. doi: 10.1103/PhysRevD.75.055014. arXiv: hep-ph/0612048 (cit. on p. 18).

[88] C. Anastasiou, E. Furlan, and J. Santiago. “Realistic Composite Higgs Models”. In: *Phys. Rev. D* 79 (2009), p. 075003. doi: 10.1103/PhysRevD.79.075003. arXiv: 0901.2117 [hep-ph] (cit. on p. 18).

[89] J. Goldstone. “Field Theories with Superconductor Solutions”. In: *Nuovo Cim.* 19 (1961), pp. 154–164. doi: 10.1007/BF02812722 (cit. on p. 19).

[90] S. Coleman, J. Wess, and B. Zumino. “Structure of Phenomenological Lagrangians. I”. In: *Phys. Rev.* 177 (5 1969-01), pp. 2239–2247. doi: 10.1103/PhysRev.177.2239. url: https://link.aps.org/doi/10.1103/PhysRev.177.2239 (cit. on p. 19).

[91] C. G. Callan et al. “Structure of Phenomenological Lagrangians. II”. In: *Phys. Rev.* 177 (5 1969-01), pp. 2247–2250. doi: 10.1103/PhysRev.177.2247. url: https://link.aps.org/doi/10.1103/PhysRev.177.2247 (cit. on p. 19).

[92] M. Schmaltz and D. Tucker-Smith. “Little Higgs review”. In: *Ann. Rev. Nucl. Part. Sci.* 55 (2005), pp. 229–270. doi: 10.1146/annurev.nucl.55.090704.151502. arXiv: hep-ph/0502182 (cit. on p. 19).

[93] N. Arkani-Hamed, A. G. Cohen, and H. Georgi. "Electroweak symmetry breaking from dimensional deconstruction". In: *Phys. Lett. B* 513 (2001), pp. 232–240. doi: 10.1016/S0370-2693(01)00741-9. arXiv: hep-ph/0105239 (cit. on p. 19).

[94] N. Arkani-Hamed et al. "Phenomenology of electroweak symmetry breaking from theory space". In: *JHEP* 08 (2002), p. 020. doi: 10.1088/1126-6708/2002/08/020. arXiv: hep-ph/0202089 (cit. on p. 19).

[95] C. Csáki, S. Lombardo, and O. Telem. "TASI Lectures on Non-supersymmetric BSM Models". In: *Proceedings, Theoretical Advanced Study Institute in Elementary Particle Physics : Anticipating the Next Discoveries in Particle Physics (TASI 2016): Boulder, CO, USA, June 6-July 1, 2016*. Ed. by R. Essig and I. Low. WSP, 2018, pp. 501–570. doi: 10.1142/9789813233348_0007. arXiv: 1811.04279 [hep-ph] (cit. on pp. 19, 20).

[96] N. Arkani-Hamed et al. "The Littlest Higgs". In: *JHEP* 07 (2002), p. 034. doi: 10.1088/1126-6708/2002/07/034. arXiv: hep-ph/0206021 (cit. on p. 21).

[97] J. L. Hewett, F. J. Petriello, and T. G. Rizzo. "Constraining the littlest Higgs". In: *JHEP* 10 (2003), p. 062. doi: 10.1088/1126-6708/2003/10/062. arXiv: hep-ph/0211218 (cit. on pp. 21, 23).

[98] C. Csaki et al. "Big corrections from a little Higgs". In: *Phys. Rev. D* 67 (2003), p. 115002. doi: 10.1103/PhysRevD.67.115002. arXiv: hep-ph/0211124 (cit. on pp. 21, 23).

[99] T. Han et al. "Phenomenology of the little Higgs model". In: *Phys. Rev. D* 67 (2003), p. 095004. doi: 10.1103/PhysRevD.67.095004. arXiv: hep-ph/0301040 (cit. on p. 23).

[100] H.-C. Cheng and I. Low. "TeV symmetry and the little hierarchy problem". In: *JHEP* 09 (2003), p. 051. doi: 10.1088/1126-6708/2003/09/051. arXiv: hep-ph/0308199 (cit. on p. 23).

[101] H.-C. Cheng and I. Low. "Little hierarchy, little Higgses, and a little symmetry". In: *JHEP* 08 (2004), p. 061. doi: 10.1088/1126-6708/2004/08/061. arXiv: hep-ph/0405243 (cit. on p. 23).

[102] I. Low. "T parity and the littlest Higgs". In: *JHEP* 10 (2004), p. 067. doi: 10.1088/1126-6708/2004/10/067. arXiv: hep-ph/0409025 (cit. on p. 23).

[103] J. Hubisz and P. Meade. "Phenomenology of the littlest Higgs with T-parity". In: *Phys. Rev. D* 71 (2005), p. 035016. doi: 10.1103/PhysRevD.71.035016. arXiv: hep-ph/0411264 (cit. on pp. 24, 45).

[104] F. del Aguila et al. “Lepton Flavor Changing Higgs decays in the Littlest Higgs Model with T-parity”. In: *JHEP* 08 (2017). [Erratum: JHEP 02, 047 (2019)], p. 028. doi: 10.1007/JHEP08(2017)028. arXiv: 1705.08827 [hep-ph] (cit. on pp. 24, 25).

[105] A. Birkedal et al. “Little Higgs dark matter”. In: *Phys. Rev. D* 74 (2006), p. 035002. doi: 10.1103/PhysRevD.74.035002. arXiv: hep-ph/0603077 (cit. on pp. 24, 39).

[106] R. Balkin, G. Perez, and A. Weiler. “Little composite dark matter”. In: *Eur. Phys. J. C* 78.2 (2018), p. 104. doi: 10.1140/epjc/s10052-018-5552-3. arXiv: 1707.09980 [hep-ph] (cit. on p. 24).

[107] D. Pappadopulo and A. Vichi. “T-parity, its problems and their solution”. In: *JHEP* 03 (2011), p. 072. doi: 10.1007/JHEP03(2011)072. arXiv: 1007.4807 [hep-ph] (cit. on p. 25).

[108] D. Dercks et al. “The fate of the Littlest Higgs Model with T-parity under 13 TeV LHC Data”. In: *JHEP* 05 (2018), p. 049. doi: 10.1007/JHEP05(2018)049. arXiv: 1801.06499 [hep-ph] (cit. on pp. 25, 26).

[109] J. I. Illana and J. M. Pérez-Poyatos. “A new and gauge-invariant littlest Higgs model with T-parity”. In: *Eur. Phys. J. Plus* 137.1 (2022), p. 42. doi: 10.1140/epjp/s13360-021-02222-0. arXiv: 2103.17078 [hep-ph] (cit. on p. 25).

[110] G. Panico and A. Wulzer. *The Composite Nambu-Goldstone Higgs*. Vol. 913. Springer, 2016. doi: 10.1007/978-3-319-22617-0. arXiv: 1506.01961 [hep-ph] (cit. on p. 26).

[111] C. Arina, R. N. Mohapatra, and N. Sahu. “Co-genesis of Matter and Dark Matter with Vector-like Fourth Generation Leptons”. In: *Phys. Lett. B* 720 (2013), pp. 130–136. doi: 10.1016/j.physletb.2013.01.059. arXiv: 1211.0435 [hep-ph] (cit. on p. 26).

[112] C. Delaunay, T. Ma, and Y. Soreq. “Stealth decaying spin-1 dark matter”. In: *JHEP* 02 (2021), p. 010. doi: 10.1007/JHEP02(2021)010. arXiv: 2009.03060 [hep-ph] (cit. on pp. 26, 33, 43, 165).

[113] K. Kannike et al. “Anthropic solution to the magnetic muon anomaly: the charged see-saw”. In: *JHEP* 02 (2012). [Erratum: JHEP 10, 136 (2012)], p. 106. doi: 10.1007/JHEP02(2012)106. arXiv: 1111.2551 [hep-ph] (cit. on p. 26).

[114] A. Freitas et al. “Testing the Muon g-2 Anomaly at the LHC”. In: *JHEP* 05 (2014). [Erratum: JHEP 09, 155 (2014)], p. 145. doi: 10.1007/JHEP09(2014)155. arXiv: 1402.7065 [hep-ph] (cit. on pp. 26, 122).

[115] F.-Z. Xu et al. "Search for the vectorlike leptons in the U(1)$_X$ model inspired by the B-meson decay anomalies". In: *Phys. Rev. D* 98.11 (2018), p. 115033. doi: 10.1103/PhysRevD.98.115033. arXiv: 1809.01472 [hep-ph] (cit. on p. 26).

[116] J. Kawamura, S. Raby, and A. Trautner. "Complete vectorlike fourth family with U(1)' : A global analysis". In: *Phys. Rev. D* 101.3 (2020), p. 035026. doi: 10.1103/PhysRevD.101.035026. arXiv: 1911.11075 [hep-ph] (cit. on p. 26).

[117] P. Arnan et al. "Generic Loop Effects of New Scalars and Fermions in $b \to s\ell^+\ell^-$, $(g-2)_\mu$ and a Vector-like 4^{th} Generation". In: *JHEP* 06 (2019), p. 118. doi: 10.1007/JHEP06(2019)118. arXiv: 1904.05890 [hep-ph] (cit. on pp. 26, 113, 124).

[118] P. Escribano, J. Terol-Calvo, and A. Vicente. "$\boldsymbol{g-2}_{e,\mu}$ in an extended inverse type-III seesaw model". In: *Phys. Rev. D* 103.11 (2021), p. 115018. doi: 10.1103/PhysRevD.103.115018. arXiv: 2104.03705 [hep-ph] (cit. on p. 26).

[119] C. Bonilla et al. "Collider signatures of vector-like fermions from a flavor symmetric model". In: *JHEP* 01 (2022), p. 154. doi: 10.1007/JHEP01(2022)154. arXiv: 2107.14165 [hep-ph] (cit. on p. 26).

[120] J. de Blas. "Electroweak limits on physics beyond the Standard Model". In: *EPJ Web Conf.* 60 (2013). Ed. by M. Bosman et al., p. 19008. doi: 10.1051/epjconf/20136019008. arXiv: 1307.6173 [hep-ph] (cit. on pp. 26, 126, 168).

[121] A. Crivellin et al. "Global Electroweak Fit and Vector-Like Leptons in Light of the Cabibbo Angle Anomaly". In: *JHEP* 12 (2020), p. 166. doi: 10.1007/JHEP12(2020)166. arXiv: 2008.01113 [hep-ph] (cit. on pp. 26, 126, 127, 168).

[122] A. Falkowski, D. M. Straub, and A. Vicente. "Vector-like leptons: Higgs decays and collider phenomenology". In: *JHEP* 05 (2014), p. 092. doi: 10.1007/JHEP05(2014)092. arXiv: 1312.5329 [hep-ph] (cit. on p. 26).

[123] R. Dermisek et al. "Limits on Vectorlike Leptons from Searches for Anomalous Production of Multi-Lepton Events". In: *JHEP* 12 (2014), p. 013. doi: 10.1007/JHEP12(2014)013. arXiv: 1408.3123 [hep-ph] (cit. on p. 26).

[124] G. Aad et al. "Search for heavy lepton resonances decaying to a Z boson and a lepton in pp collisions at $\sqrt{s} = 8$ TeV with the ATLAS detector". In: *JHEP* 09 (2015), p. 108. doi: 10.1007/JHEP09(2015)108. arXiv: 1506.01291 [hep-ex] (cit. on pp. 26, 27).

[125] A. M. Sirunyan et al. “Search for vector-like leptons in multilepton final states in proton-proton collisions at $\sqrt{s}$ = 13 TeV”. In: *Phys. Rev. D* 100.5 (2019), p. 052003. doi: 10.1103/PhysRevD.100.052003. arXiv: 1905.10853 [hep-ex] (cit. on pp. 26, 126).

[126] ATLAS collaboration. “Search for type-III seesaw heavy leptons in dilepton final states in pp collisions at $\sqrt{s}$ = 13 TeV with the ATLAS detector”. In: *Eur. Phys. J. C* 81.3 (2021), p. 218. doi: 10.1140/epjc/s10052-021-08929-9. arXiv: 2008.07949 [hep-ex] (cit. on p. 26).

[127] ATLAS collaboration. “Search for electroweak production of supersymmetric particles in final states with two or three leptons at $\sqrt{s} = 13$ TeV with the ATLAS detector”. In: *Eur. Phys. J. C* 78.12 (2018), p. 995. doi: 10.1140/epjc/s10052-018-6423-7. arXiv: 1803.02762 [hep-ex] (cit. on pp. 26, 27).

[128] C. T. Hill and R. J. Hill. “T^- Parity Violation by Anomalies”. In: *Phys. Rev. D* 76 (2007), p. 115014. doi: 10.1103/PhysRevD.76.115014. arXiv: 0705.0697 [hep-ph] (cit. on p. 26).

[129] A. Freitas, P. Schwaller, and D. Wyler. “Consequences of T-parity breaking in the Littlest Higgs model”. In: *JHEP* 09 (2008), p. 013. doi: 10.1088/1126-6708/2008/09/013. arXiv: 0806.3674 [hep-ph] (cit. on p. 26).

[130] F. del Aguila, A. Carmona, and J. Santiago. “Tau Custodian searches at the LHC”. In: *Phys. Lett. B* 695 (2011), pp. 449–453. doi: 10.1016/j.physletb.2010.11.054. arXiv: 1007.4206 [hep-ph] (cit. on p. 27).

[131] N. Kumar and S. P. Martin. “Vectorlike Leptons at the Large Hadron Collider”. In: *Phys. Rev. D* 92.11 (2015), p. 115018. doi: 10.1103/PhysRevD.92.115018. arXiv: 1510.03456 [hep-ph] (cit. on p. 27).

[132] P. N. Bhattiprolu and S. P. Martin. “Prospects for vectorlike leptons at future proton-proton colliders”. In: *Phys. Rev. D* 100.1 (2019), p. 015033. doi: 10.1103/PhysRevD.100.015033. arXiv: 1905.00498 [hep-ph] (cit. on p. 27).

[133] M. Chala and J. Santiago. “Hbb production in composite Higgs models”. In: *Phys. Rev. D* 88.3 (2013), p. 035010. doi: 10.1103/PhysRevD.88.035010. arXiv: 1305.1940 [hep-ph] (cit. on p. 27).

[134] R. D. Ball et al. “Parton distributions with LHC data”. In: *Nucl. Phys. B* 867 (2013), pp. 244–289. doi: 10.1016/j.nuclphysb.2012.10.003. arXiv: 1207.1303 [hep-ph] (cit. on p. 27).

[135] G. Aad et al. "Search for heavy lepton resonances decaying to a Z boson and a lepton in pp collisions at $\sqrt{s} = 8$ TeV with the ATLAS detector". In: *JHEP* 09 (2015), p. 108. doi: 10.1007/JHEP09(2015)108. arXiv: 1506.01291 [hep-ex] (cit. on p. 27).

[136] A. M. Sirunyan et al. "Search for vector-like leptons in multilepton final states in proton-proton collisions at $\sqrt{s} = 13$ TeV". In: *Phys. Rev. D* 100.5 (2019), p. 052003. doi: 10.1103/PhysRevD.100.052003. arXiv: 1905.10853 [hep-ex] (cit. on p. 31).

[137] M. Aaboud et al. "Search for electroweak production of supersymmetric particles in final states with two or three leptons at $\sqrt{s} = 13$ TeV with the ATLAS detector". In: *Eur. Phys. J. C* 78.12 (2018), p. 995. doi: 10.1140/epjc/s10052-018-6423-7. arXiv: 1803.02762 [hep-ex] (cit. on pp. 31–33).

[138] A. Barr, C. Lester, and P. Stephens. "m(T2): The Truth behind the glamour". In: *J. Phys. G* 29 (2003), pp. 2343–2363. doi: 10.1088/0954-3899/29/10/304. arXiv: hep-ph/0304226 (cit. on p. 31).

[139] C. Lester and D. Summers. "Measuring masses of semiinvisibly decaying particles pair produced at hadron colliders". In: *Phys. Lett. B* 463 (1999), pp. 99–103. doi: 10.1016/S0370-2693(99)00945-4. arXiv: hep-ph/9906349 (cit. on p. 31).

[140] G. Salam and A. Weiler. *Collider Reach*. http://collider-reach.web.cern.ch/ (cit. on pp. 36, 38).

[141] F. del Aguila, J. I. Illana, and M. D. Jenkins. "Precise limits from lepton flavour violating processes on the Littlest Higgs model with T-parity". In: *JHEP* 01 (2009), p. 080. doi: 10.1088/1126-6708/2009/01/080. arXiv: 0811.2891 [hep-ph] (cit. on p. 39).

[142] N. Aghanim et al. "Planck 2018 results. VI. Cosmological parameters". In: (2018-07). arXiv: 1807.06209 [astro-ph.CO] (cit. on p. 39).

[143] F. Ambrogi et al. "MadDM v.3.0: a Comprehensive Tool for Dark Matter Studies". In: *Phys. Dark Univ.* 24 (2019), p. 100249. doi: 10.1016/j.dark.2018.11.009. arXiv: 1804.00044 [hep-ph] (cit. on p. 39).

[144] E. Aprile et al. "Dark Matter Search Results from a One Ton-Year Exposure of XENON1T". In: *Phys. Rev. Lett.* 121.11 (2018), p. 111302. doi: 10.1103/PhysRevLett.121.111302. arXiv: 1805.12562 [astro-ph.CO] (cit. on p. 40).

[145] P. Agrawal, Z. Chacko, and C. B. Verhaaren. "Leptophilic Dark Matter and the Anomalous Magnetic Moment of the Muon". In: *JHEP* 08 (2014), p. 147. doi: 10.1007/JHEP08(2014)147. arXiv: 1402.7369 [hep-ph] (cit. on pp. 40, 41).

[146] T. Aoyama et al. "Tenth-Order QED Contribution to the Electron g-2 and an Improved Value of the Fine Structure Constant". In: *Phys. Rev. Lett.* 109 (2012), p. 111807. doi: 10.1103/PhysRevLett.109.111807. arXiv: 1205.5368 [hep-ph] (cit. on p. 40).

[147] G. Aad et al. "Searches for electroweak production of supersymmetric particles with compressed mass spectra in $\sqrt{s} = 13$ TeV pp collisions with the ATLAS detector". In: *Phys. Rev. D* 101.5 (2020), p. 052005. doi: 10.1103/PhysRevD.101.052005. arXiv: 1911.12606 [hep-ex] (cit. on p. 43).

[148] L. J. Hall et al. "Freeze-In Production of FIMP Dark Matter". In: *JHEP* 03 (2010), p. 080. doi: 10.1007/JHEP03(2010)080. arXiv: 0911.1120 [hep-ph] (cit. on p. 43).

[149] J. A. Aguilar-Saavedra et al. "Handbook of vectorlike quarks: Mixing and single production". In: *Phys. Rev. D* 88.9 (2013), p. 094010. doi: 10.1103/PhysRevD.88.094010. arXiv: 1306.0572 [hep-ph] (cit. on p. 45).

[150] A. Roy et al. "Novel interpretation strategy for searches of singly produced vectorlike quarks at the LHC". In: *Phys. Rev. D* 101.11 (2020), p. 115027. doi: 10.1103/PhysRevD.101.115027. arXiv: 2003.00640 [hep-ph] (cit. on p. 45).

[151] B. Yang et al. "Single production of vectorlike T quark decaying into Wb at the LHC and the future pp colliders". In: *Phys. Rev. D* 103.3 (2021), p. 036006. doi: 10.1103/PhysRevD.103.036006 (cit. on p. 45).

[152] A. Deandrea et al. "Single production of vector-like quarks: the effects of large width, interference and NLO corrections". In: *JHEP* 08 (2021), p. 107. doi: 10.1007/JHEP08(2021)107. arXiv: 2105.08745 [hep-ph] (cit. on p. 45).

[153] ATLAS collaboration. "Search for large missing transverse momentum in association with one top-quark in proton-proton collisions at $\sqrt{s}$ = 13 TeV with the ATLAS detector". In: *JHEP* 05 (2019), p. 041. doi: 10.1007/JHEP05(2019)041. arXiv: 1812.09743 [hep-ex] (cit. on p. 45).

[154] T. Appelquist and J. Carazzone. "Infrared Singularities and Massive Fields". In: *Phys. Rev. D* 11 (1975), p. 2856. doi: 10.1103/PhysRevD.11.2856 (cit. on p. 46).

[155] I. Brivio and M. Trott. "The Standard Model as an Effective Field Theory". In: *Phys. Rept.* 793 (2019), pp. 1–98. doi: 10.1016/j.physrep.2018.11.002. arXiv: 1706.08945 [hep-ph] (cit. on pp. 47, 48).

[156] S. Weinberg. "Baryon- and Lepton-Nonconserving Processes". In: *Phys. Rev. Lett.* 43 (21 1979-11), pp. 1566–1570. doi: 10.1103/PhysRevLett.43.1566. url: https://link.aps.org/doi/10.1103/PhysRevLett.43.1566 (cit. on p. 48).

[157] B. Grzadkowski et al. "Dimension-Six Terms in the Standard Model Lagrangian". In: *JHEP* 10 (2010), p. 085. doi: 10.1007/JHEP10(2010)085. arXiv: 1008.4884 [hep-ph] (cit. on p. 48).

[158] G. F. Giudice et al. "The Strongly-Interacting Light Higgs". In: *JHEP* 06 (2007), p. 045. doi: 10.1088/1126-6708/2007/06/045. arXiv: hep-ph/0703164 (cit. on p. 48).

[159] R. Contino et al. "Effective Lagrangian for a light Higgs-like scalar". In: *JHEP* 07 (2013), p. 035. doi: 10.1007/JHEP07(2013)035. arXiv: 1303.3876 [hep-ph] (cit. on p. 48).

[160] J. Elias-Miró et al. "Scaling and tuning of EW and Higgs observables". In: *JHEP* 05 (2014), p. 019. doi: 10.1007/JHEP05(2014)019. arXiv: 1312.2928 [hep-ph] (cit. on p. 48).

[161] J. de Blas et al. "Effective description of general extensions of the Standard Model: the complete tree-level dictionary". In: *JHEP* 03 (2018), p. 109. doi: 10.1007/JHEP03(2018)109. arXiv: 1711.10391 [hep-ph] (cit. on pp. 48–50, 112).

[162] C. Grojean et al. "Renormalization Group Scaling of Higgs Operators and $\Gamma(h \to \gamma\gamma)$". In: *JHEP* 04 (2013), p. 016. doi: 10.1007/JHEP04(2013)016. arXiv: 1301.2588 [hep-ph] (cit. on p. 51).

[163] J. Elias-Miro et al. "Renormalization of dimension-six operators relevant for the Higgs decays $h \to \gamma\gamma, \gamma Z$". In: *JHEP* 08 (2013), p. 033. doi: 10.1007/JHEP08(2013)033. arXiv: 1302.5661 [hep-ph] (cit. on p. 51).

[164] J. Elias-Miro et al. "Higgs windows to new physics through d=6 operators: constraints and one-loop anomalous dimensions". In: *JHEP* 11 (2013), p. 066. doi: 10.1007/JHEP11(2013)066. arXiv: 1308.1879 [hep-ph] (cit. on p. 51).

[165] E. E. Jenkins, A. V. Manohar, and M. Trott. "Renormalization Group Evolution of the Standard Model Dimension Six Operators I: Formalism and lambda Dependence". In: *JHEP* 10 (2013), p. 087. doi: 10.1007/JHEP10(2013)087. arXiv: 1308.2627 [hep-ph] (cit. on p. 51).

[166] E. E. Jenkins, A. V. Manohar, and M. Trott. "Renormalization Group Evolution of the Standard Model Dimension Six Operators II: Yukawa Dependence". In: *JHEP* 01 (2014), p. 035. doi: 10.1007/JHEP01(2014)035. arXiv: 1310.4838 [hep-ph] (cit. on pp. 51, 85).

[167] R. Alonso et al. "Renormalization Group Evolution of the Standard Model Dimension Six Operators III: Gauge Coupling Dependence and Phenomenology". In: *JHEP* 04 (2014), p. 159. doi: 10.1007/JHEP04(2014)159. arXiv: 1312.2014 [hep-ph] (cit. on pp. 51, 85).

[168] I. V. Tyutin. "Once again on the equivalence theorem". In: *Phys. Atom. Nucl.* 65 (2002), pp. 194–202. doi: 10.1134/1.1446571. arXiv: hep-th/0001050 (cit. on p. 52).

[169] A. V. Manohar. "Introduction to Effective Field Theories". In: (2018-04). Ed. by S. Davidson et al. doi: 10.1093/oso/9780198855743.003.0002. arXiv: 1804.05863 [hep-ph] (cit. on p. 52).

[170] J. C. Criado and M. Pérez-Victoria. "Field redefinitions in effective theories at higher orders". In: *JHEP* 03 (2019), p. 038. doi: 10.1007/JHEP03(2019)038. arXiv: 1811.09413 [hep-ph] (cit. on pp. 53, 54).

[171] J. Ellis et al. "Top, Higgs, Diboson and Electroweak Fit to the Standard Model Effective Field Theory". In: *JHEP* 04 (2021), p. 279. doi: 10.1007/JHEP04(2021)279. arXiv: 2012.02779 [hep-ph] (cit. on pp. 57, 58).

[172] I. Brivio, Y. Jiang, and M. Trott. "The SMEFTsim package, theory and tools". In: *JHEP* 12 (2017), p. 070. doi: 10.1007/JHEP12(2017)070. arXiv: 1709.06492 [hep-ph] (cit. on p. 58).

[173] C. Degrande et al. "Automated one-loop computations in the standard model effective field theory". In: *Phys. Rev. D* 103.9 (2021), p. 096024. doi: 10.1103/PhysRevD.103.096024. arXiv: 2008.11743 [hep-ph] (cit. on p. 58).

[174] J. Aebischer et al. "A Global Likelihood for Precision Constraints and Flavour Anomalies". In: *Eur. Phys. J. C* 79.6 (2019), p. 509. doi: 10.1140/epjc/s10052-019-6977-z. arXiv: 1810.07698 [hep-ph] (cit. on p. 58).

[175] P. Stangl. "smelli – the SMEFT Likelihood". In: *PoS* TOOLS2020 (2021), p. 035. doi: 10.22323/1.392.0035. arXiv: 2012.12211 [hep-ph] (cit. on pp. 58, 128).

[176] D. M. Straub. "flavio: a Python package for flavour and precision phenomenology in the Standard Model and beyond". In: (2018-10). arXiv: 1810.08132 [hep-ph] (cit. on p. 58).

[177] Anisha et al. “Connecting electroweak-scale observables to BSM physics through EFT and Bayesian statistics”. In: *Phys. Rev. D* 103.7 (2021), p. 076007. doi: 10.1103/PhysRevD.103.076007. arXiv: 2010.04088 [hep-ph] (cit. on p. 58).

[178] A. Adams et al. “Causality, analyticity and an IR obstruction to UV completion”. In: *JHEP* 10 (2006), p. 014. doi: 10.1088/1126-6708/2006/10/014. arXiv: hep-th/0602178 (cit. on pp. 58, 61, 92).

[179] G. N. Remmen and N. L. Rodd. “Consistency of the Standard Model Effective Field Theory”. In: *JHEP* 12 (2019), p. 032. doi: 10.1007/JHEP12(2019)032. arXiv: 1908.09845 [hep-ph] (cit. on pp. 58–60, 76, 78, 179, 180).

[180] C. Zhang and S.-Y. Zhou. “Positivity bounds on vector boson scattering at the LHC”. In: *Phys. Rev. D* 100.9 (2019), p. 095003. doi: 10.1103/PhysRevD.100.095003. arXiv: 1808.00010 [hep-ph] (cit. on pp. 58, 78).

[181] Q. Bi, C. Zhang, and S.-Y. Zhou. “Positivity constraints on aQGC: carving out the physical parameter space”. In: *JHEP* 06 (2019), p. 137. doi: 10.1007/JHEP06(2019)137. arXiv: 1902.08977 [hep-ph] (cit. on pp. 58, 59, 78, 94).

[182] J. Gu, L.-T. Wang, and C. Zhang. “An unambiguous test of positivity at lepton colliders”. In: (2020-11). arXiv: 2011.03055 [hep-ph] (cit. on p. 58).

[183] Q. Bonnefoy, E. Gendy, and C. Grojean. “Positivity bounds on Minimal Flavor Violation”. In: *JHEP* 04 (2021), p. 115. doi: 10.1007/JHEP04(2021)115. arXiv: 2011.12855 [hep-ph] (cit. on pp. 58, 78).

[184] G. N. Remmen and N. L. Rodd. “Flavor Constraints from Unitarity and Analyticity”. In: *Phys. Rev. Lett.* 125.8 (2020), p. 081601. doi: 10.1103/PhysRevLett.125.081601. arXiv: 2004.02885 [hep-ph] (cit. on pp. 58, 78).

[185] C. Zhang and S.-Y. Zhou. “Convex Geometry Perspective on the (Standard Model) Effective Field Theory Space”. In: *Phys. Rev. Lett.* 125.20 (2020), p. 201601. doi: 10.1103/PhysRevLett.125.201601. arXiv: 2005.03047 [hep-ph] (cit. on p. 58).

[186] J. Gu and L.-T. Wang. “Sum Rules in the Standard Model Effective Field Theory from Helicity Amplitudes”. In: *JHEP* 03 (2021), p. 149. doi: 10.1007/JHEP03(2021)149. arXiv: 2008.07551 [hep-ph] (cit. on p. 58).

[187] B. Fuks et al. “Positivity in electron-positron scattering: testing the axiomatic quantum field theory principles and probing the existence of UV states”. In: *Chin. Phys. C* 45.2 (2021), p. 023108. doi: 10.1088/1674-1137/abcd8c. arXiv: 2009.02212 [hep-ph] (cit. on p. 58).

[188] K. Yamashita, C. Zhang, and S.-Y. Zhou. “Elastic positivity vs extremal positivity bounds in SMEFT: a case study in transversal electroweak gauge-boson scatterings”. In: *JHEP* 01 (2021), p. 095. doi: 10.1007/JHEP01(2021)095. arXiv: 2009.04490 [hep-ph] (cit. on p. 58).

[189] M. Froissart. “Asymptotic behavior and subtractions in the Mandelstam representation”. In: *Phys. Rev.* 123 (1961), pp. 1053–1057. doi: 10.1103/PhysRev.123.1053 (cit. on p. 58).

[190] X. Li and S. Zhou. “Origin of Neutrino Masses on the Convex Cone of Positivity Bounds”. In: (2022-02). arXiv: 2202.12907 [hep-ph] (cit. on pp. 59, 95).

[191] C. W. Murphy. “Dimension-8 operators in the Standard Model Eective Field Theory”. In: *JHEP* 10 (2020), p. 174. doi: 10.1007/JHEP10(2020)174. arXiv: 2005.00059 [hep-ph] (cit. on pp. 60, 61, 66, 76, 85).

[192] ATLAS collaboration. “Observation of light-by-light scattering in ultraperipheral Pb+Pb collisions with the ATLAS detector”. In: *Phys. Rev. Lett.* 123.5 (2019), p. 052001. doi: 10.1103/PhysRevLett.123.052001. arXiv: 1904.03536 [hep-ex] (cit. on p. 60).

[193] O. J. P. Eboli, M. C. Gonzalez-Garcia, and J. K. Mizukoshi. “p p –> j j e+- mu+- nu nu and j j e+- mu-+ nu nu at O(alpha(em)**6) and O(alpha(em)**4 alpha(s)**2) for the study of the quartic electroweak gauge boson vertex at CERN LHC”. In: *Phys. Rev. D* 74 (2006), p. 073005. doi: 10.1103/PhysRevD.74.073005. arXiv: hep-ph/0606118 (cit. on p. 60).

[194] G. Perez, M. Sekulla, and D. Zeppenfeld. “Anomalous quartic gauge couplings and unitarization for the vector boson scattering process $pp \to W^+W^+jjX \to \ell^+\nu_\ell\ell^+\nu_\ell jjX$”. In: *Eur. Phys. J. C* 78.9 (2018), p. 759. doi: 10.1140/epjc/s10052-018-6230-1. arXiv: 1807.02707 [hep-ph] (cit. on p. 60).

[195] J. Kalinowski et al. “Same-sign WW scattering at the LHC: can we discover BSM effects before discovering new states?” In: *Eur. Phys. J. C* 78.5 (2018), p. 403. doi: 10.1140/epjc/s10052-018-5885-y. arXiv: 1802.02366 [hep-ph] (cit. on p. 60).

[196] S. Brass et al. “Transversal Modes and Higgs Bosons in Electroweak Vector-Boson Scattering at the LHC”. In: *Eur. Phys. J. C* 78.11 (2018), p. 931. doi: 10.1140/epjc/s10052-018-6398-4. arXiv: 1807.02512 [hep-ph] (cit. on p. 60).

[197] Y.-C. Guo, Y.-Y. Wang, and J.-C. Yang. "Constraints on anomalous quartic gauge couplings by W+W− scattering". In: *Nuclear Physics B* 961 (2020), p. 115222. issn: 0550-3213. doi: https://doi.org/10.1016/j.nuclphysb.2020.115222. url: https://www.sciencedirect.com/science/article/pii/S0550321320303072 (cit. on p. 60).

[198] C. Degrande. "A basis of dimension-eight operators for anomalous neutral triple gauge boson interactions". In: *JHEP* 02 (2014), p. 101. doi: 10.1007/JHEP02(2014)101. arXiv: 1308.6323 [hep-ph] (cit. on p. 60).

[199] J. Ellis et al. "Probing the scale of new physics in the $ZZ\gamma$ coupling at e^+e^- colliders". In: *Chin. Phys. C* 44.6 (2020), p. 063106. doi: 10.1088/1674-1137/44/6/063106. arXiv: 1902.06631 [hep-ph] (cit. on p. 60).

[200] J. Ellis, H.-J. He, and R.-Q. Xiao. "Probing new physics in dimension-8 neutral gauge couplings at e^+e^- colliders". In: *Sci. China Phys. Mech. Astron.* 64.2 (2021), p. 221062. doi: 10.1007/s11433-020-1617-3. arXiv: 2008.04298 [hep-ph] (cit. on p. 60).

[201] G. Panico, A. Pomarol, and M. Riembau. "EFT approach to the electron Electric Dipole Moment at the two-loop level". In: *JHEP* 04 (2019), p. 090. doi: 10.1007/JHEP04(2019)090. arXiv: 1810.09413 [hep-ph] (cit. on p. 60).

[202] M. Ardu and S. Davidson. "What is Leading Order for LFV in SMEFT?" In: (2021-03). arXiv: 2103.07212 [hep-ph] (cit. on p. 60).

[203] T. Corbett et al. "EWPD in the SMEFT to dimension eight". In: (2021-02). arXiv: 2102.02819 [hep-ph] (cit. on p. 60).

[204] S. Alioli et al. "Theoretical developments in the SMEFT at dimension-8 and beyond". In: *2022 Snowmass Summer Study*. 2022-03. arXiv: 2203.06771 [hep-ph] (cit. on p. 60).

[205] C. Hays et al. "On the impact of dimension-eight SMEFT operators on Higgs measurements". In: *JHEP* 02 (2019), p. 123. doi: 10.1007/JHEP02(2019)123. arXiv: 1808.00442 [hep-ph] (cit. on p. 61).

[206] C. Hays et al. "Exact SMEFT formulation and expansion to $\mathcal{O}(v^4/\Lambda^4)$". In: *JHEP* 11 (2020), p. 087. doi: 10.1007/JHEP11(2020)087. arXiv: 2007.00565 [hep-ph] (cit. on pp. 61, 85).

[207] S. Dawson, S. Homiller, and M. Sullivan. "Impact of dimension-eight SMEFT contributions: A case study". In: *Phys. Rev. D* 104.11 (2021), p. 115013. doi: 10.1103/PhysRevD.104.115013. arXiv: 2110.06929 [hep-ph] (cit. on p. 61).

[208] S. Dawson et al. “Beyond 6: the role of dimension-8 operators in an EFT for the 2HDM”. In: (2022-05). arXiv: 2205.01561 [hep-ph] (cit. on p. 61).

[209] H.-L. Li et al. “Complete Set of Dimension-8 Operators in the Standard Model Effective Field Theory”. In: (2020-04). arXiv: 2005.00008 [hep-ph] (cit. on p. 61).

[210] N. Craig et al. “Loops and Trees in Generic EFTs”. In: *JHEP* 08 (2020), p. 086. doi: 10.1007/JHEP08(2020)086. arXiv: 2001.00017 [hep-ph] (cit. on pp. 61, 78, 85–87, 89, 112).

[211] J. C. Criado. “BasisGen: automatic generation of operator bases”. In: *Eur. Phys. J. C* 79.3 (2019), p. 256. doi: 10.1140/epjc/s10052-019-6769-5. arXiv: 1901.03501 [hep-ph] (cit. on p. 61).

[212] R. M. Fonseca. “Enumerating the operators of an effective field theory”. In: (2019). arXiv: 1907.12584 [hep-ph] (cit. on p. 61).

[213] H.-L. Li et al. “Operators for generic effective field theory at any dimension: on-shell amplitude basis construction”. In: *JHEP* 04 (2022), p. 140. doi: 10.1007/JHEP04(2022)140. arXiv: 2201.04639 [hep-ph] (cit. on p. 61).

[214] S. Das Bakshi, J. Chakrabortty, and S. K. Patra. “CoDEx: Wilson coefficient calculator connecting SMEFT to UV theory”. In: *Eur. Phys. J. C* 79.1 (2019), p. 21. doi: 10.1140/epjc/s10052-018-6444-2. arXiv: 1808.04403 [hep-ph] (cit. on pp. 75, 76).

[215] T. Cohen, X. Lu, and Z. Zhang. “STrEAMlining EFT Matching”. In: *SciPost Phys.* 10.5 (2021), p. 098. doi: 10.21468/SciPostPhys.10.5.098. arXiv: 2012.07851 [hep-ph] (cit. on pp. 75, 76).

[216] J. Fuentes-Martin et al. “SuperTracer: A Calculator of Functional Supertraces for One-Loop EFT Matching”. In: *JHEP* 04 (2021), p. 281. doi: 10.1007/JHEP04(2021)281. arXiv: 2012.08506 [hep-ph] (cit. on pp. 75, 76).

[217] A. Carmona et al. “Matchmakereft: automated tree-level and one-loop matching”. In: (2021-12). arXiv: 2112.10787 [hep-ph] (cit. on pp. 75, 78, 114, 128).

[218] J. Quevillon, C. Smith, and S. Touati. “Effective action for gauge bosons”. In: *Phys. Rev. D* 99.1 (2019), p. 013003. doi: 10.1103/PhysRevD.99.013003. arXiv: 1810.06994 [hep-ph] (cit. on p. 76).

[219] M. K. Gaillard. “The Effective One Loop Lagrangian With Derivative Couplings”. In: *Nucl. Phys. B* 268 (1986), pp. 669–692. doi: 10.1016/0550-3213(86)90264-6 (cit. on p. 76).

[220] O. Cheyette. "Effective Action for the Standard Model With Large Higgs Mass". In: *Nucl. Phys. B* 297 (1988), pp. 183–204. doi: 10.1016/0550-3213(88)90205-2 (cit. on p. 76).

[221] B. Henning, X. Lu, and H. Murayama. "How to use the Standard Model effective field theory". In: *JHEP* 01 (2016), p. 023. doi: 10.1007/JHEP01(2016)023. arXiv: 1412.1837 [hep-ph] (cit. on p. 76).

[222] J. C. Criado. "MatchingTools: a Python library for symbolic effective field theory calculations". In: *Comput. Phys. Commun.* 227 (2018), pp. 42–50. doi: 10.1016/j.cpc.2018.02.016. arXiv: 1710.06445 [hep-ph] (cit. on pp. 77, 179).

[223] T. Hahn. "Feynman Diagram Calculations with FeynArts, FormCalc, and LoopTools". In: *PoS* ACAT2010 (2010). Ed. by T. Speer et al., p. 078. doi: 10.22323/1.093.0078. arXiv: 1006.2231 [hep-ph] (cit. on p. 77).

[224] G. N. Remmen and N. L. Rodd. "Signs, Spin, SMEFT: Positivity at Dimension Six". In: (2020-10). arXiv: 2010.04723 [hep-ph] (cit. on p. 78).

[225] B. Bellazzini et al. "Positive Moments for Scattering Amplitudes". In: (2020-10). arXiv: 2011.00037 [hep-th] (cit. on p. 78).

[226] T. Hahn. "Generating Feynman diagrams and amplitudes with FeynArts 3". In: *Comput. Phys. Commun.* 140 (2001), pp. 418–431. doi: 10.1016/S0010-4655(01)00290-9. arXiv: hep-ph/0012260 (cit. on p. 78).

[227] T. Hahn and M. Perez-Victoria. "Automatized one loop calculations in four-dimensions and D-dimensions". In: *Comput. Phys. Commun.* 118 (1999), pp. 153–165. doi: 10.1016/S0010-4655(98)00173-8. arXiv: hep-ph/9807565 (cit. on p. 78).

[228] A. Barzinji, M. Trott, and A. Vasudevan. "Equations of Motion for the Standard Model Effective Field Theory: Theory and Applications". In: *Phys. Rev. D* 98.11 (2018), p. 116005. doi: 10.1103/PhysRevD.98.116005. arXiv: 1806.06354 [hep-ph] (cit. on pp. 79, 80).

[229] V. Gherardi, D. Marzocca, and E. Venturini. "Matching scalar leptoquarks to the SMEFT at one loop". In: (2020-03). arXiv: 2003.12525 [hep-ph] (cit. on p. 81).

[230] C. Cheung and C.-H. Shen. "Nonrenormalization Theorems without Supersymmetry". In: *Phys. Rev. Lett.* 115.7 (2015), p. 071601. doi: 10.1103/PhysRevLett.115.071601. arXiv: 1505.01844 [hep-ph] (cit. on p. 85).

[231] J. Elias Miró, J. Ingoldby, and M. Riembau. "EFT anomalous dimensions from the S-matrix". In: *JHEP* 09 (2020), p. 163. doi: 10.1007/JHEP09(2020)163. arXiv: 2005.06983 [hep-ph] (cit. on p. 85).

[232] P. Baratella, C. Fernandez, and A. Pomarol. "Renormalization of Higher-Dimensional Operators from On-shell Amplitudes". In: *Nucl. Phys. B* 959 (2020), p. 115155. doi: 10.1016/j.nuclphysb.2020.115155. arXiv: 2005.07129 [hep-ph] (cit. on p. 85).

[233] M. E. Peskin and T. Takeuchi. "A New constraint on a strongly interacting Higgs sector". In: *Phys. Rev. Lett.* 65 (1990), pp. 964–967. doi: 10.1103/PhysRevLett.65.964 (cit. on p. 85).

[234] J. de Blas et al. "Electroweak precision constraints at present and future colliders". In: *PoS* ICHEP2016 (2017), p. 690. doi: 10.22323/1.282.0690. arXiv: 1611.05354 [hep-ph] (cit. on p. 86).

[235] F. Maltoni, L. Mantani, and K. Mimasu. "Top-quark electroweak interactions at high energy". In: *JHEP* 10 (2019), p. 004. doi: 10.1007/JHEP10(2019)004. arXiv: 1904.05637 [hep-ph] (cit. on p. 86).

[236] X.-m. Zhang. "Operators analysis for Higgs potential and cosmological bound on Higgs mass". In: *Phys. Rev. D* 47 (1993), pp. 3065–3067. doi: 10.1103/PhysRevD.47.3065. arXiv: hep-ph/9301277 (cit. on p. 86).

[237] C. Grojean, G. Servant, and J. D. Wells. "First-order electroweak phase transition in the standard model with a low cutoff". In: *Phys. Rev. D* 71 (2005), p. 036001. doi: 10.1103/PhysRevD.71.036001. arXiv: hep-ph/0407019 (cit. on p. 86).

[238] D. Bodeker et al. "The Baryon asymmetry in the standard model with a low cut-off". In: *JHEP* 02 (2005), p. 026. doi: 10.1088/1126-6708/2005/02/026. arXiv: hep-ph/0412366 (cit. on p. 86).

[239] C. Delaunay, C. Grojean, and J. D. Wells. "Dynamics of Non-renormalizable Electroweak Symmetry Breaking". In: *JHEP* 04 (2008), p. 029. doi: 10.1088/1126-6708/2008/04/029. arXiv: 0711.2511 [hep-ph] (cit. on p. 86).

[240] J. de Vries et al. "Electroweak Baryogenesis and the Standard Model Effective Field Theory". In: *JHEP* 01 (2018), p. 089. doi: 10.1007/JHEP01(2018)089. arXiv: 1710.04061 [hep-ph] (cit. on p. 86).

[241] M. Chala, C. Krause, and G. Nardini. “Signals of the electroweak phase transition at colliders and gravitational wave observatories”. In: *JHEP* 07 (2018), p. 062. doi: 10.1007/JHEP07(2018)062. arXiv: 1802.02168 [hep-ph] (cit. on p. 86).

[242] V. A. Kuzmin, V. A. Rubakov, and M. E. Shaposhnikov. “On the Anomalous Electroweak Baryon Number Nonconservation in the Early Universe”. In: *Phys. Lett. B* 155 (1985), p. 36. doi: 10.1016/0370-2693(85)91028-7 (cit. on p. 86).

[243] C. Caprini et al. “Detecting gravitational waves from cosmological phase transitions with LISA: an update”. In: *JCAP* 03 (2020), p. 024. doi: 10.1088/1475-7516/2020/03/024. arXiv: 1910.13125 [astro-ph.CO] (cit. on p. 86).

[244] M. Accettulli Huber and S. De Angelis. “Standard Model EFTs via on-shell methods”. In: *JHEP* 11 (2021), p. 221. doi: 10.1007/JHEP11(2021)221. arXiv: 2108.03669 [hep-th] (cit. on pp. 86, 89, 177, 178).

[245] M. Chala and J. Santiago. “Positivity bounds in the Standard Model effective field theory beyond tree level”. In: (2021-10). arXiv: 2110.01624 [hep-ph] (cit. on pp. 90–94).

[246] B. Bellazzini. “Softness and amplitudes’ positivity for spinning particles”. In: *JHEP* 02 (2017), p. 034. doi: 10.1007/JHEP02(2017)034. arXiv: 1605.06111 [hep-th] (cit. on p. 95).

[247] R. D. Peccei and H. R. Quinn. “CP Conservation in the Presence of Pseudoparticles”. In: *Phys. Rev. Lett.* 38 (25 1977-06), pp. 1440–1443. doi: 10.1103/PhysRevLett.38.1440. url: https://link.aps.org/doi/10.1103/PhysRevLett.38.1440 (cit. on p. 95).

[248] J. E. Kim. “Weak-Interaction Singlet and Strong CP Invariance”. In: *Phys. Rev. Lett.* 43 (2 1979-07), pp. 103–107. doi: 10.1103/PhysRevLett.43.103. url: https://link.aps.org/doi/10.1103/PhysRevLett.43.103 (cit. on p. 95).

[249] M. Dine, W. Fischler, and M. Srednicki. “A simple solution to the strong CP problem with a harmless axion”. In: *Physics Letters B* 104.3 (1981), pp. 199–202. issn: 0370-2693. doi: https://doi.org/10.1016/0370-2693(81)90590-6. url: https://www.sciencedirect.com/science/article/pii/0370269381905906 (cit. on p. 95).

[250] B. Gripaios et al. “Beyond the Minimal Composite Higgs Model”. In: *JHEP* 04 (2009), p. 070. doi: 10.1088/1126-6708/2009/04/070. arXiv: 0902.1483 [hep-ph] (cit. on p. 95).

[251] J. Preskill, M. B. Wise, and F. Wilczek. "Cosmology of the invisible axion". In: *Physics Letters B* 120.1 (1983), pp. 127–132. issn: 0370-2693. doi: https://doi.org/10.1016/0370-2693(83)90637-8. url: https://www.sciencedirect.com/science/article/pii/0370269383906378 (cit. on p. 95).

[252] L. Abbott and P. Sikivie. "A cosmological bound on the invisible axion". In: *Physics Letters B* 120.1 (1983), pp. 133–136. issn: 0370-2693. doi: https://doi.org/10.1016/0370-2693(83)90638-X. url: https://www.sciencedirect.com/science/article/pii/037026938390638X (cit. on p. 95).

[253] Y. Ema et al. "Flaxion: a minimal extension to solve puzzles in the standard model". In: *JHEP* 01 (2017), p. 096. doi: 10.1007/JHEP01(2017)096. arXiv: 1612.05492 [hep-ph] (cit. on p. 95).

[254] L. Calibbi et al. "Minimal axion model from flavor". In: *Phys. Rev. D* 95.9 (2017), p. 095009. doi: 10.1103/PhysRevD.95.095009. arXiv: 1612.08040 [hep-ph] (cit. on p. 95).

[255] M. A. Buen-Abad et al. "Challenges for an axion explanation of the muon $g-2$ measurement". In: *JHEP* 09 (2021), p. 101. doi: 10.1007/JHEP09(2021)101. arXiv: 2104.03267 [hep-ph] (cit. on p. 96).

[256] K. Mimasu and V. Sanz. "ALPs at Colliders". In: *JHEP* 06 (2015), p. 173. doi: 10.1007/JHEP06(2015)173. arXiv: 1409.4792 [hep-ph] (cit. on p. 96).

[257] J. Jaeckel and M. Spannowsky. "Probing MeV to 90 GeV axion-like particles with LEP and LHC". In: *Phys. Lett. B* 753 (2016), pp. 482–487. doi: 10.1016/j.physletb.2015.12.037. arXiv: 1509.00476 [hep-ph] (cit. on p. 96).

[258] G. G. Raffelt. "Astrophysical axion bounds". In: *Lect. Notes Phys.* 741 (2008). Ed. by M. Kuster, G. Raffelt, and B. Beltran, pp. 51–71. doi: 10.1007/978-3-540-73518-2_3. arXiv: hep-ph/0611350 (cit. on pp. 96, 110).

[259] M. Bauer, M. Neubert, and A. Thamm. "Collider Probes of Axion-Like Particles". In: *JHEP* 12 (2017), p. 044. doi: 10.1007/JHEP12(2017)044. arXiv: 1708.00443 [hep-ph] (cit. on p. 97).

[260] Q. Bonnefoy, C. Grojean, and J. Kley. "The shift-invariant orders of an ALP". In: (2022-06). arXiv: 2206.04182 [hep-ph] (cit. on p. 97).

[261] F. Lyonnet and I. Schienbein. "PyR@TE 2: A Python tool for computing RGEs at two-loop". In: *Comput. Phys. Commun.* 213 (2017), pp. 181–196. doi: 10.1016/j.cpc.2016.12.003. arXiv: 1608.07274 [hep-ph] (cit. on pp. 102, 108).

[262] N. Craig, A. Hook, and S. Kasko. "The Photophobic ALP". In: *JHEP* 09 (2018), p. 028. doi: 10.1007/JHEP09(2018)028. arXiv: 1805.06538 [hep-ph] (cit. on p. 109).

[263] B. Gripaios, M. Nardecchia, and T. You. "On the Structure of Anomalous Composite Higgs Models". In: *Eur. Phys. J. C* 77.1 (2017), p. 28. doi: 10.1140/epjc/s10052-017-4603-5. arXiv: 1605.09647 [hep-ph] (cit. on p. 109).

[264] I. Brivio et al. "ALPs Effective Field Theory and Collider Signatures". In: *Eur. Phys. J. C* 77.8 (2017), p. 572. doi: 10.1140/epjc/s10052-017-5111-3. arXiv: 1701.05379 [hep-ph] (cit. on p. 110).

[265] J. Ebadi, S. Khatibi, and M. Mohammadi Najafabadi. "New probes for axionlike particles at hadron colliders". In: *Phys. Rev. D* 100.1 (2019), p. 015016. doi: 10.1103/PhysRevD.100.015016. arXiv: 1901.03061 [hep-ph] (cit. on p. 110).

[266] E. E. Jenkins, A. V. Manohar, and P. Stoffer. "Low-Energy Effective Field Theory below the Electroweak Scale: Anomalous Dimensions". In: *JHEP* 01 (2018), p. 084. doi: 10.1007/JHEP01(2018)084. arXiv: 1711.05270 [hep-ph] (cit. on p. 111).

[267] E. E. Jenkins, A. V. Manohar, and P. Stoffer. "Low-Energy Effective Field Theory below the Electroweak Scale: Operators and Matching". In: *JHEP* 03 (2018), p. 016. doi: 10.1007/JHEP03(2018)016. arXiv: 1709.04486 [hep-ph] (cit. on pp. 111, 112).

[268] W. Dekens and P. Stoffer. "Low-energy effective field theory below the electroweak scale: matching at one loop". In: *JHEP* 10 (2019), p. 197. doi: 10.1007/JHEP10(2019)197. arXiv: 1908.05295 [hep-ph] (cit. on p. 111).

[269] C. Arzt, M. B. Einhorn, and J. Wudka. "Patterns of deviation from the standard model". In: *Nucl. Phys. B* 433 (1995), pp. 41–66. doi: 10.1016/0550-3213(94)00336-D. arXiv: hep-ph/9405214 (cit. on p. 112).

[270] J. Aebischer et al. "Effective field theory interpretation of lepton magnetic and electric dipole moments". In: *JHEP* 07 (2021), p. 107. doi: 10.1007/JHEP07(2021)107. arXiv: 2102.08954 [hep-ph] (cit. on p. 112).

[271] P. Athron et al. “New physics explanations of a_μ in light of the FNAL muon g − 2 measurement”. In: *JHEP* 09 (2021), p. 080. doi: 10.1007/JHEP09(2021)080. arXiv: 2104.03691 [hep-ph] (cit. on p. 112).

[272] L. Calibbi, R. Ziegler, and J. Zupan. “Minimal models for dark matter and the muon g−2 anomaly”. In: *JHEP* 07 (2018), p. 046. doi: 10.1007/JHEP07(2018)046. arXiv: 1804.00009 [hep-ph] (cit. on pp. 113, 122, 124).

[273] L. Calibbi et al. “Simple model for large CP violation in charm decays, B-physics anomalies, muon g-2 and dark matter”. In: *JHEP* 10 (2020), p. 070. doi: 10.1007/JHEP10(2020)070. arXiv: 1912.02676 [hep-ph] (cit. on pp. 113, 124).

[274] A. Crivellin and M. Hoferichter. “Consequences of chirally enhanced explanations of $(g-2)_\mu$ for $h \to \mu\mu$ and $Z \to \mu\mu$”. In: *JHEP* 07 (2021), p. 135. doi: 10.1007/JHEP07(2021)135. arXiv: 2104.03202 [hep-ph] (cit. on pp. 113, 124).

[275] L. Allwicher et al. “What is the scale of new physics behind the muon g-2?” In: *Phys. Rev. D* 104.5 (2021), p. 055035. doi: 10.1103/PhysRevD.104.055035. arXiv: 2105.13981 [hep-ph] (cit. on pp. 113, 123, 124, 186).

[276] G. Arcadi et al. “Muon $g-2$ and B-anomalies from Dark Matter”. In: *Phys. Rev. Lett.* 127.6 (2021), p. 061802. doi: 10.1103/PhysRevLett.127.061802. arXiv: 2104.03228 [hep-ph] (cit. on pp. 113, 124).

[277] N. Arkani-Hamed and K. Harigaya. “Naturalness and the muon magnetic moment”. In: *JHEP* 09 (2021), p. 025. doi: 10.1007/JHEP09(2021)025. arXiv: 2106.01373 [hep-ph] (cit. on pp. 113, 120).

[278] L. D. Rose, B. von Harling, and A. Pomarol. “Wilson Coefficients and Natural Zeros from the On-Shell Viewpoint”. In: (2022-01). arXiv: 2201.10572 [hep-ph] (cit. on pp. 113, 120).

[279] K. Kowalska and E. M. Sessolo. “Expectations for the muon g-2 in simplified models with dark matter”. In: *JHEP* 09 (2017), p. 112. doi: 10.1007/JHEP09(2017)112. arXiv: 1707.00753 [hep-ph] (cit. on p. 122).

[280] S. Ashanujjaman, D. Choudhury, and K. Ghosh. “Search for exotic leptons in final states with two or three leptons and fat-jets at 13 TeV LHC”. In: (2022-01). arXiv: 2201.09645 [hep-ph] (cit. on p. 126).

[281] M. J. Baker, P. Cox, and R. R. Volkas. "Radiative muon mass models and $(g-2)_\mu$". In: *JHEP* 05 (2021), p. 174. doi: 10.1007/JHEP05(2021)174. arXiv: 2103.13401 [hep-ph] (cit. on p. 127).

[282] A. Greljo et al. "Muonic force behind flavor anomalies". In: *JHEP* 04 (2022), p. 151. doi: 10.1007/JHEP04(2022)151. arXiv: 2107.07518 [hep-ph] (cit. on p. 127).

[283] W. Yin. "Radiative lepton mass and muon g – 2 with suppressed lepton flavor and CP violations". In: *JHEP* 08 (2021), p. 043. doi: 10.1007/JHEP08(2021)043. arXiv: 2103.14234 [hep-ph] (cit. on p. 127).

[284] M. Kirk. "Cabibbo anomaly versus electroweak precision tests: An exploration of extensions of the Standard Model". In: *Phys. Rev. D* 103.3 (2021), p. 035004. doi: 10.1103/PhysRevD.103.035004. arXiv: 2008.03261 [hep-ph] (cit. on p. 127).

[285] V. Gherardi, D. Marzocca, and E. Venturini. "Low-energy phenomenology of scalar leptoquarks at one-loop accuracy". In: *JHEP* 01 (2021), p. 138. doi: 10.1007/JHEP01(2021)138. arXiv: 2008.09548 [hep-ph] (cit. on p. 127).

[286] A. Angelescu et al. "Single leptoquark solutions to the B-physics anomalies". In: *Phys. Rev. D* 104.5 (2021), p. 055017. doi: 10.1103/PhysRevD.104.055017. arXiv: 2103.12504 [hep-ph] (cit. on p. 127).

[287] J. Kumar, D. London, and R. Watanabe. "Combined Explanations of the $b \to s\mu^+\mu^-$ and $b \to c\tau^-\bar{\nu}$ Anomalies: a General Model Analysis". In: *Phys. Rev. D* 99.1 (2019), p. 015007. doi: 10.1103/PhysRevD.99.015007. arXiv: 1806.07403 [hep-ph] (cit. on p. 127).

[288] A. Crivellin, D. Müller, and L. Schnell. "Combined constraints on first generation leptoquarks". In: *Physical Review D* 103.11 (2021-06). doi: 10.1103/physrevd.103.115023. url: https://doi.org/10.1103%2Fphysrevd.103.115023 (cit. on p. 127).

[289] C. collaboration et al. "High-precision measurement of the W boson mass with the CDF II detector". In: *Science* 376.6589 (2022), pp. 170–176. doi: 10.1126/science.abk1781. eprint: https://www.science.org/doi/pdf/10.1126/science.abk1781. url: https://www.science.org/doi/abs/10.1126/science.abk1781 (cit. on p. 127).

[290] M. Blennow et al. "Right-handed neutrinos and the CDF II anomaly". In: (2022-04). arXiv: 2204.04559 [hep-ph] (cit. on p. 127).

[291] J. Aebischer et al. “A global likelihood for precision constraints and flavour anomalies”. In: *The European Physical Journal C* 79.6 (2019-06). doi: 10.1140/epjc/s10052-019-6977-z. url: https://doi.org/10.1140%2Fepjc%2Fs10052-019-6977-z (cit. on p. 128).

[292] H. Dembinski and P. O. et al. “scikit-hep/iminuit”. In: (2020-12). doi: 10.5281/zenodo.3949207. url: https://doi.org/10.5281/zenodo.3949207 (cit. on p. 128).

[293] B. Holdom. “Two U(1)’s and Epsilon Charge Shifts”. In: *Phys. Lett. B* 166 (1986), pp. 196–198. doi: 10.1016/0370-2693(86)91377-8 (cit. on p. 165).

[294] E. J. Chun, J.-C. Park, and S. Scopel. “Dark matter and a new gauge boson through kinetic mixing”. In: *JHEP* 02 (2011), p. 100. doi: 10.1007/JHEP02(2011)100. arXiv: 1011.3300 [hep-ph] (cit. on p. 165).

[295] F. del Aguila and M. J. Bowick. “The Possibility of New Fermions With Δ I = 0 Mass”. In: *Nucl. Phys. B* 224 (1983), p. 107. doi: 10.1016/0550-3213(83)90316-4 (cit. on p. 166).

[296] J. de Blas et al. “Observable Effects of General New Scalar Particles”. In: *JHEP* 04 (2015), p. 078. doi: 10.1007/JHEP04(2015)078. arXiv: 1412.8480 [hep-ph] (cit. on p. 179).

A

An explicit realization of a vector-like lepton with arbitrary branching ratios

The goal of this appendix is to demonstrate a minimal setup with a VLL with arbitrary BRs through the SM decay channels and an extra channel $A_H\ell$ which motivates the dedicated analysis presented in 3.2. The explicit realization described here follows from the FIMP DM candidate introduced in [112] [1]. Let us consider a model with the $SU(3)_C \times SU(2)_L \times U(1)_Y \times U(1)_H$ gauge symmetry. The matter content is given by the SM particles, neutral under $U(1)_H$, a VLL with the following quantum numbers (with the notation $(SU(3)_C, SU(2)_L)_{U(1)_Y, U(1)_H}$),

$$E^{(0)}_{L,R} \sim (1,1)_{-1,1}, \tag{A.0.1}$$

and a complex scalar

$$\Phi \sim (1,1)_{0,1}. \tag{A.0.2}$$

The renormalisable Lagrangian for this model reads

$$\mathcal{L} = \mathcal{L}_{\rm SM} - \frac{1}{4} F^{\mu\nu}_H F_{H\,\mu\nu} + |D_\mu \Phi|^2 - V(\Phi) + \bar{E}^{(0)}(\mathrm{i}\not{D} - M_0)E^{(0)} - \Lambda_1(\bar{E}^{(0)}_L \Phi e^{(0)}_R + \mathrm{h.c.}) + \ldots, \tag{A.0.3}$$

where $V(\Phi)$ is a potential that triggers the spontaneous breaking of $U(1)_H$ and that makes the physical Higgs scalar of such breaking much heavier than all other fields so that it can be safely neglected. For simplicity we assume negligible kinetic mixing between the abelian group [2] and that the VLL only couples to the right-handed electron (every conclusion could also be extrapolated for a coupling with a muon or tau).

[1] Indeed this model can be translated to the one in [112] with the replacements: $M_0 \to M_E, \Lambda_1 \to x_E, V \to \omega/\sqrt{2}, s \to \theta_R$.

[2] The expected order of magnitude for kinetic mixing [293] is small enough in the parameter space we will consider [294].

The relevant part of the covariant derivative for the new fields reads

$$D_\mu = \partial_\mu - \mathrm{i} g_H A_{H\,\mu}, \tag{A.0.4}$$

where we considered $Q_H = 1$.

After the spontaneous breaking of $U(1)_H$ the corresponding gauge boson, A_H, gains a mass term

$$M_{A_H} = \sqrt{2} g_H V, \tag{A.0.5}$$

where $V \equiv \langle \Phi \rangle$ is the vev of Φ, and $e_R^{(0)}$ and $E_R^{(0)}$ mix through

$$\mathcal{L} = -\bar{E}_L^{(0)} (\Lambda_1 V e_R^{(0)} + M_0 E_R^{(0)}) + \text{h.c.} + \dots \ . \tag{A.0.6}$$

To define the SM RH lepton we can rotate this mixing through

$$\begin{pmatrix} e_R^{(0)} \\ E_R^{(0)} \end{pmatrix} = \begin{pmatrix} c & s \\ -s & c \end{pmatrix} \begin{pmatrix} e_R \\ E_R \end{pmatrix}, \tag{A.0.7}$$

where

$$s \equiv \frac{\Lambda_1 V}{M}, \quad c \equiv \frac{M_0}{M}, \quad M \equiv \sqrt{M_0^2 + \Lambda_1^2 V^2}. \tag{A.0.8}$$

Denoting $E_R^{(0)} \equiv E_L$ we have extended the SM with a VLL singlet, resulting in the following mass matrix for the charged leptons

$$\mathcal{L} = \begin{pmatrix} \bar{e}_L & \bar{E}_L \end{pmatrix} \begin{pmatrix} m & m' \\ 0 & M \end{pmatrix} \begin{pmatrix} e_R \\ E_R \end{pmatrix} + \dots, \tag{A.0.9}$$

where m and m' arise after EWSB:

$$\frac{m'}{m} = \frac{s}{c}. \tag{A.0.10}$$

The couplings of A_H are given by

$$\mathcal{L} = g_H A_H^\mu \begin{pmatrix} \bar{e} & \bar{E} \end{pmatrix} \gamma_\mu \left[\begin{pmatrix} 0 & 0 \\ 0 & 1 \end{pmatrix} P_L + \begin{pmatrix} s^2 & -sc \\ -sc & c^2 \end{pmatrix} P_R \right] \begin{pmatrix} e \\ E \end{pmatrix} + \dots \ . \tag{A.0.11}$$

The mixing effect of a VLL with a SM lepton is well known in the literature known [295]. Diagonalizing the mass matrix in (A.0.9) gives rise to

$$\begin{aligned} \mathcal{L}^Z &= \frac{g}{2c_W} Z_\mu \bar{\psi}_Q^i \gamma^\mu [X_{ij}^{QL} P_L + X_{ij}^{QR} P_R - 2 s_W^2 Q \delta_{ij}] \psi_Q^j, \\ \mathcal{L}^W &= \frac{g}{\sqrt{2}} W_\mu^+ \bar{\psi}_Q^i \gamma^\mu [V_{ij}^{QL} P_L + V_{ij}^{QR} P_R] \psi_{Q-1}^j + \text{h.c.}, \end{aligned}$$

$$\mathcal{L}^H = -\frac{H}{\sqrt{2}}\bar{\psi}_Q^i Y_{ij}^Q P_R \psi_Q^j + \text{h.c.},$$
$$\mathcal{L}^{A_H} = g_H A_{H\,\mu}\bar{\psi}_Q^i \gamma^\mu [Z_{ij}^{QL} P_L + Z_{ij}^{QR} P_R]\psi_Q^j, \tag{A.0.12}$$

where ψ_Q^i is a fermion of electric charge Q and i, j are flavor indices. The couplings are given by

$$X_L^{-1} \approx \begin{pmatrix} -1 & -\frac{m'}{M} \\ -\frac{m'}{M} & -\frac{m'^2}{M^2} \end{pmatrix}, \quad X_R^{-1} = (0),$$
$$W_L^0 \approx \begin{pmatrix} U_{i1} & U_{i,1}\frac{m'}{M} \end{pmatrix}, \quad W_R^0 \approx (0),$$
$$vY^{-1} \approx \begin{pmatrix} m & m' \\ m\frac{m'}{M} & \frac{m'^2}{M^2} \end{pmatrix},$$
$$Z_L^{-1} \approx \begin{pmatrix} \frac{m'^2}{M^2} & -\frac{m'}{M} \\ -\frac{m'}{M} & 1 \end{pmatrix}, \quad Z_R^{-1} \approx \begin{pmatrix} s^2 + 2sc\frac{mm'}{M^2} & -sc + (s^2 - c^2)\frac{mm'}{M^2} \\ -sc + (s^2 - c^2)\frac{mm'}{M^2} & c^2 - 2sc\frac{mm'}{M^2} \end{pmatrix}, \tag{A.0.13}$$

where $v \approx 174\,\text{GeV}$ is the Higgs vev, i denotes the neutrino flavor. Note that these are only to leading order in the m'/M expansion.

Our intended scenario needs $M_{A_H} < M_E$ so that the VLL can decay to Ze, He, Wv and $A_H e$. The corresponding decay widths are given by

$$\sum_{i=1}^{3}\Gamma(E \to W\nu_i) \approx \sum_i \frac{g^2}{64\pi}\left[(V_L^0)_{iE}^2 + (V_R^0)_{iE}^2\right]\frac{M_E^3}{m_W^2} \approx \frac{g^2 s^2}{64\pi c^2}\frac{m_e^2 M_E}{m_W^2}, \tag{A.0.14}$$
$$\Gamma(E \to Ze) \approx \frac{g^2}{128\pi c_W^2}\left[(X_L^{-1})_{eE}^2 + (X_R^{-1})_{eE}^2\right]\frac{M_E^3}{m_Z^2} \approx \frac{g^2 s^2}{128\pi c_W^2 c^2}\frac{m_e^2 M_E}{m_Z^2}, \tag{A.0.15}$$
$$\Gamma(E \to He) \approx \frac{1}{64\pi}\left[|(Y^{-1})_{eE}|^2 + |(Y^{-1})_{Ee}|^2\right]M_E\left(1 - 2\frac{m_H^2}{M_E^2}\right)$$
$$\approx \frac{s^2}{64\pi c^2}\frac{m_e^2 M_E}{v^2}\left(1 - 2\frac{m_H^2}{M_E^2}\right), \tag{A.0.16}$$
$$\Gamma(E \to A_H e) \approx \frac{g_H^2}{32\pi}\left[(Z_L^{-1})_{eE}^2 + (Z_R^{-1})_{eE}^2\right]\frac{M_E^3}{M_{A_H}^2}$$
$$\approx \frac{g_H^2}{32\pi}\left[\frac{m'^2}{M_E^2} + \left(-sc + (s^2 - c^2)\frac{m_e m'}{M_E^2}\right)^2\right]\frac{M_E^3}{M_{A_H}^2} \approx \frac{g_H^2 s^2 c^2}{32\pi}\frac{M_E^3}{M_{A_H}^2}, \tag{A.0.17}$$

where we considered only the leading terms in the x/M_E, with $x = m_e, m_Z, m_W, m_H$, except for the case

of m_H, for which the subleading term is relevant for low M_E. Considering

$$m_W = \frac{gv}{\sqrt{2}} = c_W m_Z, \tag{A.0.18}$$

we recover the standard $2:1:1$ decay pattern into W, Z and H for large masses of the VLL.

If $M_{AH} \gg 2m_e$ then the gauge boson can decay to $\bar{e}e$ with the decay width

$$\begin{aligned}\Gamma(A_H \to e^+e^-) \approx& \frac{g_H^2}{24\pi}\left[(Z_L^{-1})_{ee}^2 + (Z_R^{-1})_{ee}^2\right] M_{A_H} \\ \approx& \frac{g_H^2}{24\pi}\left[\left(\frac{m'^2}{M_E^2}\right)^2 + \left(s^2 + 2sc\frac{m_e m'}{M_E^2}\right)^2\right] M_{A_H} \approx \frac{g_H^2 s^4}{24\pi} M_{A_H}.\end{aligned} \tag{A.0.19}$$

A_H needs to be stable at detector scales, E should decay promptly and the branching ratios of E should be of similar order. Considering a decay length larger than ~ 10 m for A_H (for it not to decay in the detector) and smaller than 10^{-2} m for E (in order to be prompt), these conditions translate into

$$\Gamma(A_H \to e^+e^-) \lesssim 2\times 10^{-17}\ \text{GeV}, \quad \text{(Invisible } A_H\text{)}, \tag{A.0.20}$$

$$\Gamma(E \to Ze, A_H e) \gtrsim 2\times 10^{-14}\ \text{GeV}, \quad \text{(Prompt } E \text{ decays)}. \tag{A.0.21}$$

Knowing the decay widths, we can find for each value of M_E and M_{A_H}, the allowed values of g_H and s. Requiring prompt $E \to Ze$ decays results in

$$\frac{s}{c} \gtrsim \left[\frac{128\pi c_W^2}{g^2}\frac{m_Z^2}{m_e^2 M_E} 2\times 10^{-14}\ \text{GeV}\right]^{\frac{1}{2}} = \begin{cases} 3.1\times 10^{-2}\sqrt{\frac{500\ \text{GeV}}{M_E}}, & \text{electron,} \\ 1.5\times 10^{-4}\sqrt{\frac{500\ \text{GeV}}{M_E}}, & \text{muon.}\end{cases} \tag{A.0.22}$$

In the electron case this is close to the bounds obtained by electroweak precision data [120, 121]; for the muon there is still room.

Requiring that A_H does not decay within the detector and that the decay $E \to A_H e$ is prompt provides an upper limit on s

$$\frac{\Gamma(A_H \to e^+e^-)}{\Gamma(E \to A_H e)} \leq 10^{-3} \Rightarrow \frac{s}{c} \lesssim 2.7\times 10^{-2}\left(\frac{M_E}{M_{A_H}}\right)^{\frac{3}{2}}. \tag{A.0.23}$$

Note that for the values of M_E we are interested, unless M_{A_H} is very close to M_E, the obtained two limits are always compatible. Provided s is fixed in the allowed range, requiring $E \to A_H e$ to be prompt can fix a minimum value for g_H such that

$$g_H \gtrsim \left[\frac{32\pi}{s^2c^2}\frac{M_{A_H}^2}{M_E^3} 2\times 10^{-14}\text{GeV}\right]^{\frac{1}{2}} \approx \frac{1.3\times 10^{-8}}{sc}\frac{M_{A_H}}{100\ \text{GeV}}\left[\frac{500\ \text{GeV}}{M_E}\right]^{\frac{3}{2}}. \tag{A.0.24}$$

Requiring A_H to be stable at detector scales results in an upper bound given by

$$g_H \lesssim \left[\frac{24\pi}{s^4}\frac{2\times 10^{-17}}{M_{A_H}}\right]^{\frac{1}{2}} \approx \frac{4\times 10^{-9}}{s^2}\left[\frac{100\text{ GeV}}{M_{A_H}}\right]^{\frac{1}{2}}. \tag{A.0.25}$$

The relative decay of E into A_H and Z is also fixed, once g_H and s are chosen, up to the dependence on the masses involved. For the muon case we get

$$\mathcal{R} \equiv \frac{\Gamma(E\to Z\mu)}{\Gamma(E\to A_H\mu)} \approx \frac{g^2}{4c_W^2c^4g_H^2}\frac{M_{A_H}^2}{m_Z^2}\frac{m_\mu^2}{M_E^2} \approx \frac{7.3\times 10^{-9}}{g_H^2c^4}\left(\frac{M_{A_H}}{100\text{ GeV}}\right)^2\left(\frac{500\text{ GeV}}{M_E}\right)^2. \tag{A.0.26}$$

Taking the minimum and maximum values of g_H we arrive at

$$4.5\times 10^8\frac{s^4}{c^4}\left(\frac{M_{A_H}}{100\text{ GeV}}\right)^3\left(\frac{500\text{GeV}}{M_E}\right)^2 \lesssim \mathcal{R} \lesssim 4.3\times 10^7\frac{s^2}{c^2}\left(\frac{M_E}{500\text{ GeV}}\right). \tag{A.0.27}$$

As an example, let us take $M_E = 500$GeV and $M_{A_H} = 100$ GeV resulting in

$$1.5\times 10^{-4} \lesssim \frac{s}{c} \lesssim 0.3. \tag{A.0.28}$$

Choosing for instance $s = 10^{-3}$ results in

$$1.3\times 10^{-5} \lesssim g_H \lesssim 4.4\times 10^{-3}, \tag{A.0.29}$$

and

$$4.5\times 10^{-4} \lesssim \mathcal{R} \lesssim 43. \tag{A.0.30}$$

Had we considered an electron instead of a muon mixing would decrease $\mathcal{R}$ by a factor $(m_e/m_\mu)^2 \approx 2.3\times 10^{-5}$ and increases the lower limit of s/c by a factor $m_\mu/m_e \approx 210$.

B

Dimension-8 Operators

$\boldsymbol{\phi^8}$	
O_{ϕ^8}	$(\phi^\dagger\phi)^4$

$\boldsymbol{\phi^6 D^2}$	
$O^{(1)}_{\phi^6}$	$(\phi^\dagger\phi)^2(D_\mu\phi^\dagger D^\mu\phi)$
$O^{(2)}_{\phi^6}$	$(\phi^\dagger\phi)(\phi^\dagger\tau^I\phi)(D_\mu\phi^\dagger\tau^I D^\mu\phi)$

$\boldsymbol{\phi^4 D^4}$	
$O^{(1)}_{\phi^4}$	$(D_\mu\phi^\dagger D_\nu\phi)(D^\nu\phi^\dagger D^\mu\phi)$
$O^{(2)}_{\phi^4}$	$(D_\mu\phi^\dagger D_\nu\phi)(D^\mu\phi^\dagger D^\nu\phi)$
$O^{(3)}_{\phi^4}$	$(D^\mu\phi^\dagger D_\mu\phi)(D^\nu\phi^\dagger D_\nu\phi)$

$\boldsymbol{X^3\phi^2}$	
$O^{(1)}_{G^3\phi^2}$	$f^{ABC}(\phi^\dagger\phi)G^{A\nu}_\mu G^{B\rho}_\nu G^{C\mu}_\rho$
$O^{(2)}_{G^3\phi^2}$	$f^{ABC}(\phi^\dagger\phi)G^{A\nu}_\mu G^{B\rho}_\nu \widetilde{G}^{C\mu}_\rho$
$O^{(1)}_{W^3\phi^2}$	$\epsilon^{IJK}(\phi^\dagger\phi)W^{I\nu}_\mu W^{J\rho}_\nu W^{K\mu}_\rho$
$O^{(2)}_{W^3\phi^2}$	$\epsilon^{IJK}(\phi^\dagger\phi)W^{I\nu}_\mu W^{J\rho}_\nu \widetilde{W}^{K\mu}_\rho$
$O^{(1)}_{W^2B\phi^2}$	$\epsilon^{IJK}(\phi^\dagger\tau^I\phi)B^{\ \nu}_\mu W^{J\rho}_\nu W^{K\mu}_\rho$
$O^{(2)}_{W^2B\phi^2}$	$\epsilon^{IJK}(\phi^\dagger\tau^I\phi)(\widetilde{B}^{\mu\nu}W^J_{\nu\rho}W^{K\rho}_\mu + B^{\mu\nu}W^J_{\nu\rho}\widetilde{W}^{K\rho}_\mu)$

$\boldsymbol{X^2\phi^4}$	
$O^{(1)}_{G^2\phi^4}$	$(\phi^\dagger\phi)^2 G^A_{\mu\nu}G^{A\mu\nu}$
$O^{(2)}_{G^2\phi^4}$	$(\phi^\dagger\phi)^2 \widetilde{G}^A_{\mu\nu}G^{A\mu\nu}$
$O^{(1)}_{W^2\phi^4}$	$(\phi^\dagger\phi)^2 W^I_{\mu\nu}W^{I\mu\nu}$
$O^{(2)}_{W^2\phi^4}$	$(\phi^\dagger\phi)^2 \widetilde{W}^I_{\mu\nu}W^{I\mu\nu}$
$O^{(3)}_{W^2\phi^4}$	$(\phi^\dagger\tau^I\phi)(\phi^\dagger\tau^J\phi)W^I_{\mu\nu}W^{J\mu\nu}$
$O^{(4)}_{W^2\phi^4}$	$(\phi^\dagger\tau^I\phi)(\phi^\dagger\tau^J\phi)\widetilde{W}^I_{\mu\nu}W^{J\mu\nu}$
$O^{(1)}_{WB\phi^4}$	$(\phi^\dagger\phi)(\phi^\dagger\tau^I\phi)W^I_{\mu\nu}B^{\mu\nu}$
$O^{(2)}_{WB\phi^4}$	$(\phi^\dagger\phi)(\phi^\dagger\tau^I\phi)\widetilde{W}^I_{\mu\nu}B^{\mu\nu}$
$O^{(1)}_{B^2\phi^4}$	$(\phi^\dagger\phi)^2 B_{\mu\nu}B^{\mu\nu}$
$O^{(2)}_{B^2\phi^4}$	$(\phi^\dagger\phi)^2 \widetilde{B}_{\mu\nu}B^{\mu\nu}$

Table 19: Table with the dimension-8 operators of the classes ϕ^8, ϕ^6D^2, ϕ^4D^4, $X^3\phi^2$ and $X^2\phi^4$.

$X^2\phi^2D^2$	
$O^{(1)}_{G^2\phi^2D^2}$	$(D^\mu\phi^\dagger D^\nu\phi)G^A_{\mu\rho}G^{A\rho}_\nu$
$O^{(2)}_{G^2\phi^2D^2}$	$(D^\mu\phi^\dagger D_\mu\phi)G^A_{\nu\rho}G^{A\nu\rho}$
$O^{(3)}_{G^2\phi^2D^2}$	$(D^\mu\phi^\dagger D_\mu\phi)G^A_{\nu\rho}\widetilde{G}^{A\nu\rho}$
$O^{(1)}_{W^2\phi^2D^2}$	$(D^\mu\phi^\dagger D^\nu\phi)W^I_{\mu\rho}W^{I\rho}_\nu$
$O^{(2)}_{W^2\phi^2D^2}$	$(D^\mu\phi^\dagger D_\mu\phi)W^I_{\nu\rho}W^{I\nu\rho}$
$O^{(3)}_{W^2\phi^2D^2}$	$(D^\mu\phi^\dagger D_\mu\phi)W^I_{\nu\rho}\widetilde{W}^{I\nu\rho}$
$O^{(4)}_{W^2\phi^2D^2}$	$i\epsilon^{IJK}(D^\mu\phi^\dagger\tau^I D^\nu\phi)W^J_{\mu\rho}W^{K\rho}_\nu$
$O^{(5)}_{W^2\phi^2D^2}$	$\epsilon^{IJK}(D^\mu\phi^\dagger\tau^I D^\nu\phi)(W^J_{\mu\rho}\widetilde{W}^{K\rho}_\nu - \widetilde{W}^J_{\mu\rho}W^{K\rho}_\nu)$
$O^{(6)}_{W^2\phi^2D^2}$	$i\epsilon^{IJK}(D^\mu\phi^\dagger\tau^I D^\nu\phi)(W^J_{\mu\rho}\widetilde{W}^{K\rho}_\nu + \widetilde{W}^J_{\mu\rho}W^{K\rho}_\nu)$
$O^{(1)}_{WB\phi^2D^2}$	$(D^\mu\phi^\dagger\tau^I D_\mu\phi)B_{\nu\rho}W^{I\nu\rho}$
$O^{(2)}_{WB\phi^2D^2}$	$(D^\mu\phi^\dagger\tau^I D_\mu\phi)B_{\nu\rho}\widetilde{W}^{I\nu\rho}$
$O^{(3)}_{WB\phi^2D^2}$	$i(D^\mu\phi^\dagger\tau^I D^\nu\phi)(B_{\mu\rho}W^{I\rho}_\nu - B_{\nu\rho}W^{I\rho}_\mu)$
$O^{(4)}_{WB\phi^2D^2}$	$(D^\mu\phi^\dagger\tau^I D^\nu\phi)(B_{\mu\rho}W^{I\rho}_\nu + B_{\nu\rho}W^{I\rho}_\mu)$
$O^{(5)}_{WB\phi^2D^2}$	$i(D^\mu\phi^\dagger\tau^I D^\nu\phi)(B_{\mu\rho}\widetilde{W}^{I\rho}_\nu - B_{\nu\rho}\widetilde{W}^{I\rho}_\mu)$
$O^{(6)}_{WB\phi^2D^2}$	$(D^\mu\phi^\dagger\tau^I D^\nu\phi)(B_{\mu\rho}\widetilde{W}^{I\rho}_\nu + B_{\nu\rho}\widetilde{W}^{I\rho}_\mu)$
$O^{(1)}_{B^2\phi^2D^2}$	$(D^\mu\phi^\dagger D^\nu\phi)B_{\mu\rho}B_\nu{}^\rho$
$O^{(2)}_{B^2\phi^2D^2}$	$(D^\mu\phi^\dagger D_\mu\phi)B_{\nu\rho}B^{\nu\rho}$
$O^{(3)}_{B^2\phi^2D^2}$	$(D^\mu\phi^\dagger D_\mu\phi)B_{\nu\rho}\widetilde{B}^{\nu\rho}$

$X\phi^4D^2$	
$O^{(1)}_{W\phi^4D^2}$	$(\phi^\dagger\phi)(D^\mu\phi^\dagger\tau^I D^\nu\phi)W^I_{\mu\nu}$
$O^{(2)}_{W\phi^4D^2}$	$(\phi^\dagger\phi)(D^\mu\phi^\dagger\tau^I D^\nu\phi)\widetilde{W}^I_{\mu\nu}$
$O^{(3)}_{W\phi^4D^2}$	$\epsilon^{IJK}(\phi^\dagger\tau^I\phi)(D^\mu\phi^\dagger\tau^J D^\nu\phi)W^K_{\mu\nu}$
$O^{(4)}_{W\phi^4D^2}$	$\epsilon^{IJK}(\phi^\dagger\tau^I\phi)(D^\mu\phi^\dagger\tau^J D^\nu\phi)\widetilde{W}^K_{\mu\nu}$
$O^{(1)}_{B\phi^4D^2}$	$(\phi^\dagger\phi)(D^\mu\phi^\dagger D^\nu\phi)B_{\mu\nu}$
$O^{(2)}_{B\phi^4D^2}$	$(\phi^\dagger\phi)(D^\mu\phi^\dagger D^\nu\phi)\widetilde{B}_{\mu\nu}$

Table 20: Table with the dimension-8 operators of the classes $X^2\phi^2D^2$ and $X\phi^4D^2$.

$\psi^2 X\phi^3 + \text{h.c.}$	
$O^{(1)}_{leW\phi^3}$	$(\bar{l}_p\sigma^{\mu\nu}e_r)\tau^I\phi(\phi^\dagger\phi)W^I_{\mu\nu}$
$O^{(2)}_{leW\phi^3}$	$(\bar{l}_p\sigma^{\mu\nu}e_r)\phi(\phi^\dagger\tau^I\phi)W^I_{\mu\nu}$
$O_{leB\phi^3}$	$(\bar{l}_p\sigma^{\mu\nu}e_r)\phi(\phi^\dagger\phi)B_{\mu\nu}$
$O_{quG\phi^3}$	$(\bar{q}_p\sigma^{\mu\nu}T^Au_r)\widetilde{\phi}(\phi^\dagger\phi)G^A_{\mu\nu}$
$O^{(1)}_{quW\phi^3}$	$(\bar{q}_p\sigma^{\mu\nu}u_r)\tau^I\widetilde{\phi}(\phi^\dagger\phi)W^I_{\mu\nu}$
$O^{(2)}_{quW\phi^3}$	$(\bar{q}_p\sigma^{\mu\nu}u_r)\widetilde{\phi}(\phi^\dagger\tau^I\phi)W^I_{\mu\nu}$
$O_{quB\phi^3}$	$(\bar{q}_p\sigma^{\mu\nu}u_r)\widetilde{\phi}(\phi^\dagger\phi)B_{\mu\nu}$
$O_{qdG\phi^3}$	$(\bar{q}_p\sigma^{\mu\nu}T^Ad_r)\phi(\phi^\dagger\phi)G^A_{\mu\nu}$
$O^{(1)}_{qdW\phi^3}$	$(\bar{q}_p\sigma^{\mu\nu}d_r)\tau^I\phi(\phi^\dagger\phi)W^I_{\mu\nu}$
$O^{(2)}_{qdW\phi^3}$	$(\bar{q}_p\sigma^{\mu\nu}d_r)\phi(\phi^\dagger\tau^I\phi)W^I_{\mu\nu}$
$O_{qdB\phi^3}$	$(\bar{q}_p\sigma^{\mu\nu}d_r)\phi(\phi^\dagger\phi)B_{\mu\nu}$

$\psi^2\phi^2D^3$	
$O^{(1)}_{l^2\phi^2D^3}$	$i(\bar{l}_p\gamma^\mu D^\nu l_r)(D_{(\mu}D_{\nu)}\phi^\dagger\phi)$
$O^{(2)}_{l^2\phi^2D^3}$	$i(\bar{l}_p\gamma^\mu D^\nu l_r)(\phi^\dagger D_{(\mu}D_{\nu)}\phi)$
$O^{(3)}_{l^2\phi^2D^3}$	$i(\bar{l}_p\gamma^\mu\tau^I D^\nu l_r)(D_{(\mu}D_{\nu)}\phi^\dagger\tau^I\phi)$
$O^{(4)}_{l^2\phi^2D^3}$	$i(\bar{l}_p\gamma^\mu\tau^I D^\nu l_r)(\phi^\dagger\tau^I D_{(\mu}D_{\nu)}\phi)$
$O^{(1)}_{e^2\phi^2D^3}$	$i(\bar{e}_p\gamma^\mu D^\nu e_r)(D_{(\mu}D_{\nu)}\phi^\dagger\phi)$
$O^{(2)}_{e^2\phi^2D^3}$	$i(\bar{e}_p\gamma^\mu D^\nu e_r)(\phi^\dagger D_{(\mu}D_{\nu)}\phi)$
$O^{(1)}_{q^2\phi^2D^3}$	$i(\bar{q}_p\gamma^\mu D^\nu q_r)(D_{(\mu}D_{\nu)}\phi^\dagger\phi)$
$O^{(2)}_{q^2\phi^2D^3}$	$i(\bar{q}_p\gamma^\mu D^\nu q_r)(\phi^\dagger D_{(\mu}D_{\nu)}\phi)$
$O^{(3)}_{q^2\phi^2D^3}$	$i(\bar{q}_p\gamma^\mu\tau^I D^\nu q_r)(D_{(\mu}D_{\nu)}\phi^\dagger\tau^I\phi)$
$O^{(4)}_{q^2\phi^2D^2}$	$i(\bar{q}_p\gamma^\mu\tau^I D^\nu q_r)(\phi^\dagger\tau^I D_{(\mu}D_{\nu)}\phi)$
$O^{(1)}_{u^2\phi^2D^3}$	$i(\bar{u}_p\gamma^\mu D^\nu u_r)(D_{(\mu}D_{\nu)}\phi^\dagger\phi)$
$O^{(2)}_{u^2\phi^2D^3}$	$i(\bar{u}_p\gamma^\mu D^\nu u_r)(\phi^\dagger D_{(\mu}D_{\nu)}\phi)$
$O^{(1)}_{d^2\phi^2D^3}$	$i(\bar{d}_p\gamma^\mu D^\nu d_r)(D_{(\mu}D_{\nu)}\phi^\dagger\phi)$
$O^{(2)}_{d^2\phi^2D^3}$	$i(\bar{d}_p\gamma^\mu D^\nu d_r)(\phi^\dagger D_{(\mu}D_{\nu)}\phi)$
$O_{ud\phi^2D^3} + \text{h.c.}$	$i(\bar{u}_p\gamma^\mu D^\nu d_r)(\widetilde{\phi}^\dagger D_{(\mu}D_{\nu)}\phi)$

Table 21: Table with the dimension-8 operators of the classes $\psi^2X\phi^3$ and $\psi^2\phi^2D^3$.

$(\overline{\psi}_R\psi_R)X\phi^2D$	
$O^{(1)}_{e^2W\phi^2D}$	$(\bar{e}_p\gamma^\nu e_r)D^\mu(\phi^\dagger\tau^I\phi)W^I_{\mu\nu}$
$O^{(2)}_{e^2W\phi^2D}$	$(\bar{e}_p\gamma^\nu e_r)D^\mu(\phi^\dagger\tau^I\phi)\widetilde{W}^I_{\mu\nu}$
$O^{(3)}_{e^2W\phi^2D}$	$(\bar{e}_p\gamma^\nu e_r)(\phi^\dagger\overleftrightarrow{D}^{I\mu}\phi)W^I_{\mu\nu}$
$O^{(4)}_{e^2W\phi^2D}$	$(\bar{e}_p\gamma^\nu e_r)(\phi^\dagger\overleftrightarrow{D}^{I\mu}\phi)\widetilde{W}^I_{\mu\nu}$
$O^{(1)}_{e^2B\phi^2D}$	$(\bar{e}_p\gamma^\nu e_r)D^\mu(\phi^\dagger\phi)B_{\mu\nu}$
$O^{(2)}_{e^2B\phi^2D}$	$(\bar{e}_p\gamma^\nu e_r)D^\mu(\phi^\dagger\phi)\widetilde{B}_{\mu\nu}$
$O^{(3)}_{e^2B\phi^2D}$	$(\bar{e}_p\gamma^\nu e_r)(\phi^\dagger\overleftrightarrow{D}^{\mu}\phi)B_{\mu\nu}$
$O^{(4)}_{e^2B\phi^2D}$	$(\bar{e}_p\gamma^\nu e_r)(\phi^\dagger\overleftrightarrow{D}^{\mu}\phi)\widetilde{B}_{\mu\nu}$
$O^{(1)}_{u^2G\phi^2D}$	$(\bar{u}_p\gamma^\nu T^A u_r)D^\mu(\phi^\dagger\phi)G^A_{\mu\nu}$
$O^{(2)}_{u^2G\phi^2D}$	$(\bar{u}_p\gamma^\nu T^A u_r)D^\mu(\phi^\dagger\phi)\widetilde{G}^A_{\mu\nu}$
$O^{(3)}_{u^2G\phi^2D}$	$(\bar{u}_p\gamma^\nu T^A u_r)(\phi^\dagger\overleftrightarrow{D}^{\mu}\phi)G^A_{\mu\nu}$
$O^{(4)}_{u^2G\phi^2D}$	$(\bar{u}_p\gamma^\nu T^A u_r)(\phi^\dagger\overleftrightarrow{D}^{\mu}\phi)\widetilde{G}^A_{\mu\nu}$
$O^{(1)}_{u^2W\phi^2D}$	$(\bar{u}_p\gamma^\nu u_r)D^\mu(\phi^\dagger\tau^I\phi)W^I_{\mu\nu}$
$O^{(2)}_{u^2W\phi^2D}$	$(\bar{u}_p\gamma^\nu u_r)D^\mu(\phi^\dagger\tau^I\phi)\widetilde{W}^I_{\mu\nu}$
$O^{(3)}_{u^2W\phi^2D}$	$(\bar{u}_p\gamma^\nu u_r)(\phi^\dagger\overleftrightarrow{D}^{I\mu}\phi)W^I_{\mu\nu}$
$O^{(4)}_{u^2W\phi^2D}$	$(\bar{u}_p\gamma^\nu u_r)(\phi^\dagger\overleftrightarrow{D}^{I\mu}\phi)\widetilde{W}^I_{\mu\nu}$
$O^{(1)}_{u^2B\phi^2D}$	$(\bar{u}_p\gamma^\nu u_r)D^\mu(\phi^\dagger\phi)B_{\mu\nu}$
$O^{(2)}_{u^2B\phi^2D}$	$(\bar{u}_p\gamma^\nu u_r)D^\mu(\phi^\dagger\phi)\widetilde{B}_{\mu\nu}$
$O^{(3)}_{u^2B\phi^2D}$	$(\bar{u}_p\gamma^\nu u_r)(\phi^\dagger\overleftrightarrow{D}^{\mu}\phi)B_{\mu\nu}$
$O^{(4)}_{u^2B\phi^2D}$	$(\bar{u}_p\gamma^\nu u_r)(\phi^\dagger\overleftrightarrow{D}^{\mu}\phi)\widetilde{B}_{\mu\nu}$

$(\overline{\psi}_R\psi_R)X\phi^2D$	
$O^{(1)}_{d^2G\phi^2D}$	$(\bar{d}_p\gamma^\nu T^A d_r)D^\mu(\phi^\dagger\phi)G^A_{\mu\nu}$
$O^{(2)}_{d^2G\phi^2D}$	$(\bar{d}_p\gamma^\nu T^A d_r)D^\mu(\phi^\dagger\phi)\widetilde{G}^A_{\mu\nu}$
$O^{(3)}_{d^2G\phi^2D}$	$(\bar{d}_p\gamma^\nu T^A d_r)(\phi^\dagger\overleftrightarrow{D}^{\mu}\phi)G^A_{\mu\nu}$
$O^{(4)}_{d^2G\phi^2D}$	$(\bar{d}_p\gamma^\nu T^A d_r)(\phi^\dagger\overleftrightarrow{D}^{\mu}\phi)\widetilde{G}^A_{\mu\nu}$
$O^{(1)}_{d^2W\phi^2D}$	$(\bar{d}_p\gamma^\nu d_r)D^\mu(\phi^\dagger\tau^I\phi)W^I_{\mu\nu}$
$O^{(2)}_{d^2W\phi^2D}$	$(\bar{d}_p\gamma^\nu d_r)D^\mu(\phi^\dagger\tau^I\phi)\widetilde{W}^I_{\mu\nu}$
$O^{(3)}_{d^2W\phi^2D}$	$(\bar{d}_p\gamma^\nu d_r)(\phi^\dagger\overleftrightarrow{D}^{I\mu}\phi)W^I_{\mu\nu}$
$O^{(4)}_{d^2W\phi^2D}$	$(\bar{d}_p\gamma^\nu d_r)(\phi^\dagger\overleftrightarrow{D}^{I\mu}\phi)\widetilde{W}^I_{\mu\nu}$
$O^{(1)}_{d^2B\phi^2D}$	$(\bar{d}_p\gamma^\nu d_r)D^\mu(\phi^\dagger\phi)B_{\mu\nu}$
$O^{(2)}_{d^2B\phi^2D}$	$(\bar{d}_p\gamma^\nu d_r)D^\mu(\phi^\dagger\phi)\widetilde{B}_{\mu\nu}$
$O^{(3)}_{d^2B\phi^2D}$	$(\bar{d}_p\gamma^\nu d_r)(\phi^\dagger\overleftrightarrow{D}^{\mu}\phi)B_{\mu\nu}$
$O^{(4)}_{d^2B\phi^2D}$	$(\bar{d}_p\gamma^\nu d_r)(\phi^\dagger\overleftrightarrow{D}^{\mu}\phi)\widetilde{B}_{\mu\nu}$
$O^{(1)}_{udG\phi^2}+\text{h.c.}$	$(\bar{u}_p\gamma^\nu T^A d_r)(\widetilde{\phi}^\dagger\overleftrightarrow{D}^{\mu}\phi)G^A_{\mu\nu}$
$O^{(2)}_{udG\phi^2}+\text{h.c.}$	$(\bar{u}_p\gamma^\nu T^A d_r)(\widetilde{\phi}^\dagger\overleftrightarrow{D}^{\mu}\phi)\widetilde{G}^A_{\mu\nu}$
$O^{(1)}_{udW\phi^2}+\text{h.c.}$	$(\bar{u}_p\gamma^\nu d_r)(\widetilde{\phi}^\dagger\overleftrightarrow{D}^{I\mu}\phi)W^I_{\mu\nu}$
$O^{(2)}_{udW\phi^2}+\text{h.c.}$	$(\bar{u}_p\gamma^\nu d_r)(\widetilde{\phi}^\dagger\overleftrightarrow{D}^{I\mu}\phi)\widetilde{W}^I_{\mu\nu}$
$O^{(1)}_{udB\phi^2}+\text{h.c.}$	$(\bar{u}_p\gamma^\nu d_r)(\widetilde{\phi}^\dagger\overleftrightarrow{D}^{\mu}\phi)B_{\mu\nu}$
$O^{(2)}_{udB\phi^2}+\text{h.c.}$	$(\bar{u}_p\gamma^\nu d_r)(\widetilde{\phi}^\dagger\overleftrightarrow{D}^{\mu}\phi)\widetilde{B}_{\mu\nu}$

Table 22: Table with the dimension-8 operators of the class $(\overline{\psi}_R\psi_R)X\phi^2D$.

$(\overline{\psi}_L\psi_L)X\phi^2D$	
$O^{(1)}_{l^2W\phi^2D}$	$(\bar{l}_p\gamma^\nu l_r)D^\mu(\phi^\dagger\tau^I\phi)W^I_{\mu\nu}$
$O^{(2)}_{l^2W\phi^2D}$	$(\bar{l}_p\gamma^\nu l_r)D^\mu(\phi^\dagger\tau^I\phi)\widetilde{W}^I_{\mu\nu}$
$O^{(3)}_{l^2W\phi^2D}$	$(\bar{l}_p\gamma^\nu l_r)(\phi^\dagger\overleftrightarrow{D}^{I\mu}\phi)W^I_{\mu\nu}$
$O^{(4)}_{l^2W\phi^2D}$	$(\bar{l}_p\gamma^\nu l_r)(\phi^\dagger\overleftrightarrow{D}^{I\mu}\phi)\widetilde{W}^I_{\mu\nu}$
$O^{(5)}_{l^2W\phi^2D}$	$(\bar{l}_p\gamma^\nu\tau^I l_r)D^\mu(\phi^\dagger\phi)W^I_{\mu\nu}$
$O^{(6)}_{l^2W\phi^2D}$	$(\bar{l}_p\gamma^\nu\tau^I l_r)D^\mu(\phi^\dagger\phi)\widetilde{W}^I_{\mu\nu}$
$O^{(7)}_{l^2W\phi^2D}$	$(\bar{l}_p\gamma^\nu\tau^I l_r)(\phi^\dagger\overleftrightarrow{D}^{\mu}\phi)W^I_{\mu\nu}$
$O^{(8)}_{l^2W\phi^2D}$	$(\bar{l}_p\gamma^\nu\tau^I l_r)(\phi^\dagger\overleftrightarrow{D}^{\mu}\phi)\widetilde{W}^I_{\mu\nu}$
$O^{(9)}_{l^2W\phi^2D}$	$\epsilon^{IJK}(\bar{l}_p\gamma^\nu\tau^I l_r)D^\mu(\phi^\dagger\tau^J\phi)W^K_{\mu\nu}$
$O^{(10)}_{l^2W\phi^2D}$	$\epsilon^{IJK}(\bar{l}_p\gamma^\nu\tau^I l_r)D^\mu(\phi^\dagger\tau^J\phi)\widetilde{W}^K_{\mu\nu}$
$O^{(11)}_{l^2W\phi^2D}$	$\epsilon^{IJK}(\bar{l}_p\gamma^\nu\tau^I l_r)(\phi^\dagger\overleftrightarrow{D}^{J\mu}\phi)W^K_{\mu\nu}$
$O^{(12)}_{l^2W\phi^2D}$	$\epsilon^{IJK}(\bar{l}_p\gamma^\nu\tau^I l_r)(\phi^\dagger\overleftrightarrow{D}^{J\mu}\phi)\widetilde{W}^K_{\mu\nu}$
$O^{(1)}_{l^2B\phi^2D}$	$(\bar{l}_p\gamma^\nu\tau^I l_r)D^\mu(\phi^\dagger\tau^I\phi)B_{\mu\nu}$
$O^{(2)}_{l^2B\phi^2D}$	$(\bar{l}_p\gamma^\nu\tau^I l_r)D^\mu(\phi^\dagger\tau^I\phi)\widetilde{B}_{\mu\nu}$
$O^{(3)}_{l^2B\phi^2D}$	$(\bar{l}_p\gamma^\nu\tau^I l_r)(\phi^\dagger\overleftrightarrow{D}^{I\mu}\phi)B_{\mu\nu}$
$O^{(4)}_{l^2B\phi^2D}$	$(\bar{l}_p\gamma^\nu\tau^I l_r)(\phi^\dagger\overleftrightarrow{D}^{I\mu}\phi)\widetilde{B}_{\mu\nu}$
$O^{(5)}_{l^2B\phi^2D}$	$(\bar{l}_p\gamma^\nu l_r)D^\mu(\phi^\dagger\phi)B_{\mu\nu}$
$O^{(6)}_{l^2B\phi^2D}$	$(\bar{l}_p\gamma^\nu l_r)D^\mu(\phi^\dagger\phi)\widetilde{B}_{\mu\nu}$
$O^{(7)}_{l^2B\phi^2D}$	$(\bar{l}_p\gamma^\nu l_r)(\phi^\dagger\overleftrightarrow{D}^{\mu}\phi)B_{\mu\nu}$
$O^{(8)}_{l^2B\phi^2D}$	$(\bar{l}_p\gamma^\nu l_r)(\phi^\dagger\overleftrightarrow{D}^{\mu}\phi)\widetilde{B}_{\mu\nu}$
$O^{(4)}_{q^2B\phi^2D}$	$(\bar{q}_p\gamma^\nu\tau^I q_r)(\phi^\dagger\overleftrightarrow{D}^{I\mu}\phi)\widetilde{B}_{\mu\nu}$
$O^{(5)}_{q^2B\phi^2D}$	$(\bar{q}_p\gamma^\nu q_r)D^\mu(\phi^\dagger\phi)B_{\mu\nu}$
$O^{(6)}_{q^2B\phi^2D}$	$(\bar{q}_p\gamma^\nu q_r)D^\mu(\phi^\dagger\phi)\widetilde{B}_{\mu\nu}$
$O^{(7)}_{q^2B\phi^2D}$	$(\bar{q}_p\gamma^\nu q_r)(\phi^\dagger\overleftrightarrow{D}^{\mu}\phi)B_{\mu\nu}$
$O^{(8)}_{q^2B\phi^2D}$	$(\bar{q}_p\gamma^\nu q_r)(\phi^\dagger\overleftrightarrow{D}^{\mu}\phi)\widetilde{B}_{\mu\nu}$

$(\overline{\psi}_L\psi_L)X\phi^2D$	
$O^{(1)}_{q^2G\phi^2D}$	$(\bar{q}_p\gamma^\nu T^A\tau^I q_r)D^\mu(\phi^\dagger\tau^I\phi)G^A_{\mu\nu}$
$O^{(2)}_{q^2G\phi^2D}$	$(\bar{q}_p\gamma^\nu T^A\tau^I q_r)D^\mu(\phi^\dagger\tau^I\phi)\widetilde{G}^A_{\mu\nu}$
$O^{(3)}_{q^2G\phi^2D}$	$(\bar{q}_p\gamma^\nu T^A\tau^I q_r)(\phi^\dagger\overleftrightarrow{D}^{I\mu}\phi)G^A_{\mu\nu}$
$O^{(4)}_{q^2G\phi^2D}$	$(\bar{q}_p\gamma^\nu T^A\tau^I q_r)(\phi^\dagger\overleftrightarrow{D}^{I\mu}\phi)\widetilde{G}^A_{\mu\nu}$
$O^{(5)}_{q^2G\phi^2D}$	$(\bar{q}_p\gamma^\nu T^A q_r)D^\mu(\phi^\dagger\phi)G^A_{\mu\nu}$
$O^{(6)}_{q^2G\phi^2D}$	$(\bar{q}_p\gamma^\nu T^A q_r)D^\mu(\phi^\dagger\phi)\widetilde{G}^A_{\mu\nu}$
$O^{(7)}_{q^2G\phi^2D}$	$(\bar{q}_p\gamma^\nu T^A q_r)(\phi^\dagger\overleftrightarrow{D}^{\mu}\phi)G^A_{\mu\nu}$
$O^{(8)}_{q^2G\phi^2D}$	$(\bar{q}_p\gamma^\nu T^A q_r)(\phi^\dagger\overleftrightarrow{D}^{\mu}\phi)\widetilde{G}^A_{\mu\nu}$
$O^{(1)}_{q^2W\phi^2D}$	$(\bar{q}_p\gamma^\nu q_r)D^\mu(\phi^\dagger\tau^I\phi)W^I_{\mu\nu}$
$O^{(2)}_{q^2W\phi^2D}$	$(\bar{q}_p\gamma^\nu q_r)D^\mu(\phi^\dagger\tau^I\phi)\widetilde{W}^I_{\mu\nu}$
$O^{(3)}_{q^2W\phi^2D}$	$(\bar{q}_p\gamma^\nu q_r)(\phi^\dagger\overleftrightarrow{D}^{I\mu}\phi)W^I_{\mu\nu}$
$O^{(4)}_{q^2W\phi^2D}$	$(\bar{q}_p\gamma^\nu q_r)(\phi^\dagger\overleftrightarrow{D}^{I\mu}\phi)\widetilde{W}^I_{\mu\nu}$
$O^{(5)}_{q^2W\phi^2D}$	$(\bar{q}_p\gamma^\nu\tau^I q_r)D^\mu(\phi^\dagger\phi)W^I_{\mu\nu}$
$O^{(6)}_{q^2W\phi^2D}$	$(\bar{q}_p\gamma^\nu\tau^I q_r)D^\mu(\phi^\dagger\phi)\widetilde{W}^I_{\mu\nu}$
$O^{(7)}_{q^2W\phi^2D}$	$(\bar{q}_p\gamma^\nu\tau^I q_r)(\phi^\dagger\overleftrightarrow{D}^{\mu}\phi)W^I_{\mu\nu}$
$O^{(8)}_{q^2W\phi^2D}$	$(\bar{q}_p\gamma^\nu\tau^I q_r)(\phi^\dagger\overleftrightarrow{D}^{\mu}\phi)\widetilde{W}^I_{\mu\nu}$
$O^{(9)}_{q^2W\phi^2D}$	$\epsilon^{IJK}(\bar{q}_p\gamma^\nu\tau^I q_r)D^\mu(\phi^\dagger\tau^J\phi)W^K_{\mu\nu}$
$O^{(10)}_{q^2W\phi^2D}$	$\epsilon^{IJK}(\bar{q}_p\gamma^\nu\tau^I q_r)D^\mu(\phi^\dagger\tau^J\phi)\widetilde{W}^K_{\mu\nu}$
$O^{(11)}_{q^2W\phi^2D}$	$\epsilon^{IJK}(\bar{q}_p\gamma^\nu\tau^I q_r)(\phi^\dagger\overleftrightarrow{D}^{J\mu}\phi)W^K_{\mu\nu}$
$O^{(12)}_{q^2W\phi^2D}$	$\epsilon^{IJK}(\bar{q}_p\gamma^\nu\tau^I q_r)(\phi^\dagger\overleftrightarrow{D}^{J\mu}\phi)\widetilde{W}^K_{\mu\nu}$

Table 23: Table with the dimension-8 operators of the class $(\overline{\psi}_L\psi_L)X\phi^2D$.

$(\overline{\psi}_L\psi_L)X\phi^2D$	
$O^{(1)}_{q^2B\phi^2D}$	$(\bar{q}_p\gamma^\nu\tau^I q_r)D^\mu(\phi^\dagger\tau^I\phi)B_{\mu\nu}$
$O^{(2)}_{q^2B\phi^2D}$	$(\bar{q}_p\gamma^\nu\tau^I q_r)D^\mu(\phi^\dagger\tau^I\phi)\widetilde{B}_{\mu\nu}$
$O^{(3)}_{q^2B\phi^2D}$	$(\bar{q}_p\gamma^\nu\tau^I q_r)(\phi^\dagger\overleftrightarrow{D}^{I\mu}\phi)B_{\mu\nu}$
$O^{(4)}_{q^2B\phi^2D}$	$(\bar{q}_p\gamma^\nu\tau^I q_r)(\phi^\dagger\overleftrightarrow{D}^{I\mu}\phi)\widetilde{B}_{\mu\nu}$
$O^{(5)}_{q^2B\phi^2D}$	$(\bar{q}_p\gamma^\nu q_r)D^\mu(\phi^\dagger\phi)B_{\mu\nu}$
$O^{(6)}_{q^2B\phi^2D}$	$(\bar{q}_p\gamma^\nu q_r)D^\mu(\phi^\dagger\phi)\widetilde{B}_{\mu\nu}$
$O^{(7)}_{q^2B\phi^2D}$	$(\bar{q}_p\gamma^\nu q_r)(\phi^\dagger\overleftrightarrow{D}^{\mu}\phi)B_{\mu\nu}$
$O^{(8)}_{q^2B\phi^2D}$	$(\bar{q}_p\gamma^\nu q_r)(\phi^\dagger\overleftrightarrow{D}^{\mu}\phi)\widetilde{B}_{\mu\nu}$

$\psi^2\phi^3D^2+\text{h.c.}$	
$O^{(1)}_{le\phi^3D^2}$	$(D_\mu\phi^\dagger D^\mu\phi)(\bar{l}_p e_r\phi)$
$O^{(2)}_{le\phi^3D^2}$	$(D_\mu\phi^\dagger\tau^I D^\mu\phi)(\bar{l}_p e_r\tau^I\phi)$
$O^{(3)}_{le\phi^3D^2}$	$(D_\mu\phi^\dagger D_\nu\phi)(\bar{l}_p\sigma^{\mu\nu}e_r\phi)$
$O^{(4)}_{le\phi^3D^2}$	$(D_\mu\phi^\dagger\tau^I D_\nu\phi)(\bar{l}_p\sigma^{\mu\nu}e_r\tau^I\phi)$
$O^{(5)}_{le\phi^3D^2}$	$(\phi^\dagger D_\mu\phi)(\bar{l}_p e_r D^\mu\phi)$
$O^{(6)}_{le\phi^3D^2}$	$(\phi^\dagger D_\mu\phi)(\bar{l}_p\sigma^{\mu\nu}e_r D_\nu\phi)$
$O^{(1)}_{qu\phi^3D^2}$	$(D_\mu\phi^\dagger D^\mu\phi)(\bar{q}_p u_r\widetilde{\phi})$
$O^{(2)}_{qu\phi^3D^2}$	$(D_\mu\phi^\dagger\tau^I D^\mu\phi)(\bar{q}_p u_r\tau^I\widetilde{\phi})$
$O^{(3)}_{qu\phi^3D^2}$	$(D_\mu\phi^\dagger D_\nu\phi)(\bar{q}_p\sigma^{\mu\nu}u_r\widetilde{\phi})$
$O^{(4)}_{qu\phi^3D^2}$	$(D_\mu\phi^\dagger\tau^I D_\nu\phi)(\bar{q}_p\sigma^{\mu\nu}u_r\tau^I\widetilde{\phi})$
$O^{(5)}_{qu\phi^3D^2}$	$(D_\mu\phi^\dagger\phi)(\bar{q}_p u_r D^\mu\widetilde{\phi})$
$O^{(6)}_{qu\phi^3D^2}$	$(D_\mu\phi^\dagger\phi)(\bar{q}_p\sigma^{\mu\nu}u_r D_\nu\widetilde{\phi})$
$O^{(1)}_{qd\phi^3D^2}$	$(D_\mu\phi^\dagger D^\mu\phi)(\bar{q}_p d_r\phi)$
$O^{(2)}_{qd\phi^3D^2}$	$(D_\mu\phi^\dagger\tau^I D^\mu\phi)(\bar{q}_p d_r\tau^I\phi)$
$O^{(3)}_{qd\phi^3D^2}$	$(D_\mu\phi^\dagger D_\nu\phi)(\bar{q}_p\sigma^{\mu\nu}d_r\phi)$
$O^{(4)}_{qd\phi^3D^2}$	$(D_\mu\phi^\dagger\tau^I D_\nu\phi)(\bar{q}_p\sigma^{\mu\nu}d_r\tau^I\phi)$
$O^{(5)}_{qd\phi^3D^2}$	$(\phi^\dagger D_\mu\phi)(\bar{q}_p d_r D^\mu\phi)$
$O^{(6)}_{qd\phi^3D^2}$	$(\phi^\dagger D_\mu\phi)(\bar{q}_p\sigma^{\mu\nu}d_r D_\nu\phi)$

Table 24: Table with the dimension-8 operators of the classes $(\overline{\psi}_L\psi_L)X\phi^2D$ and $\psi^2\phi^3D^2$.

$\psi^2\phi^4 D$		$\psi^2\phi^5 + \text{h.c.}$	
$O^{(1)}_{l^2\phi^4 D}$	$i(l_p\gamma^\mu l_r)(\phi^\dagger \overleftrightarrow{D}_\mu \phi)(\phi^\dagger\phi)$	$O_{le\phi^5}$	$(\phi^\dagger\phi)^2(\bar{l}_p e_r \phi)$
$O^{(2)}_{l^2\phi^4 D}$	$i(l_p\gamma^\mu \tau^I l_r)[(\phi^\dagger \overleftrightarrow{D}^I_\mu \phi)(\phi^\dagger\phi) + (\phi^\dagger \overleftrightarrow{D}_\mu \phi)(\phi^\dagger\tau^I\phi)]$	$O_{qu\phi^5}$	$(\phi^\dagger\phi)^2(\bar{q}_p u_r \widetilde{\phi})$
$O^{(3)}_{l^2\phi^4 D}$	$i\epsilon^{IJK}(l_p\gamma^\mu \tau^I l_r)(\phi^\dagger \overleftrightarrow{D}^J_\mu \phi)(\phi^\dagger\tau^K\phi)$	$O_{qd\phi^5}$	$(\phi^\dagger\phi)^2(\bar{q}_p d_r \phi)$
$O^{(4)}_{l^2\phi^4 D}$	$\epsilon^{IJK}(l_p\gamma^\mu \tau^I l_r)(\phi^\dagger\tau^J\phi)D_\mu(\phi^\dagger\tau^K\phi)$		
$O_{e^2\phi^4 D}$	$i(e_p\gamma^\mu e_r)(\phi^\dagger \overleftrightarrow{D}_\mu \phi)(\phi^\dagger\phi)$		
$O^{(1)}_{q^2\phi^4 D}$	$i(q_p\gamma^\mu q_r)(\phi^\dagger \overleftrightarrow{D}_\mu \phi)(\phi^\dagger\phi)$		
$O^{(2)}_{q^2\phi^4 D}$	$i(q_p\gamma^\mu \tau^I q_r)[(\phi^\dagger \overleftrightarrow{D}^I_\mu \phi)(\phi^\dagger\phi) + (\phi^\dagger \overleftrightarrow{D}_\mu \phi)(\phi^\dagger\tau^I\phi)]$		
$O^{(3)}_{q^2\phi^4 D}$	$i\epsilon^{IJK}(q_p\gamma^\mu \tau^I q_r)(\phi^\dagger \overleftrightarrow{D}^J_\mu \phi)(\phi^\dagger\tau^K\phi)$		
$O^{(4)}_{q^2\phi^4 D}$	$\epsilon^{IJK}(q_p\gamma^\mu \tau^I q_r)(\phi^\dagger\tau^J\phi)D_\mu(\phi^\dagger\tau^K\phi)$		
$O_{u^2\phi^4 D}$	$i(u_p\gamma^\mu u_r)(\phi^\dagger \overleftrightarrow{D}_\mu \phi)(\phi^\dagger\phi)$		
$O_{d^2\phi^4 D}$	$i(d_p\gamma^\mu d_r)(\phi^\dagger \overleftrightarrow{D}_\mu \phi)(\phi^\dagger\phi)$		
$O_{ud\phi^4 D} + \text{h.c.}$	$i(u_p\gamma^\mu d_r)(\widetilde{\phi}^\dagger \overleftrightarrow{D}_\mu \phi)(\phi^\dagger\phi)$		

Table 25: Table with the dimension-8 operators of the classes $\psi^2\phi^4 D$ and $\psi^2\phi^5$.

C

Comparison with the dimension-8 basis of Ref. [244]

The $\mathcal{O}(g^2, \lambda)$ contributions to the RGEs of the dimension-8 WCs were calculated in Ref. [244], using a completely distinct approach than the one we present in 4.4.2. Here we check the consistency between both results.

Let us show the method considering only the sub-matrix of the RGEs defined by the operators ϕ^8, $\phi^6 D^2$, $\phi^4 D^4$, $X^2\phi^4$, $X\phi^4 D^2$. In Ref. [244], these operators correspond to the minimal amplitudes $\mathcal{A}_i$, $i = 1, 19, 18, 44, 45, 46, 11, 10, 8, 6, 9, 7, 5, 4, 3, 2, 43, 41, 42, 40, 25, 24$. The rotation matrix that moves the corresponding WCs in our work to the WCs considered in Ref. [244] reads:

$$\mathcal{P} = \begin{pmatrix} 1 & & & & \\ & P_{\phi^6 D^2} & & & \\ & & P_{\phi^4 D^4} & & \\ & & & P_{X^2\phi^4} & \\ & & & & P_{X\phi^4 D^2} \end{pmatrix}, \tag{C.0.1}$$

with

$$P_{\phi^6 D^2} = \begin{pmatrix} -1 & 2 \\ -1 & 1 \end{pmatrix}, \quad P_{\phi^4 D^2} = \begin{pmatrix} 1 & 1 & 0 \\ 1 & 0 & 1 \\ 2 & 0 & 0 \end{pmatrix}, \tag{C.0.2}$$

$$P_{X^2\phi^4} = \begin{pmatrix} Q & & & & \\ & Q & Q & & \\ & & 4Q & & \\ & & & Q & \\ & & & & Q \end{pmatrix}, \quad P_{X\phi^4D^2} = \frac{1}{2}\begin{pmatrix} Q & Q & \\ -Q & Q & \\ & & 2Q \end{pmatrix}, \tag{C.0.3}$$

whereas

$$Q = \begin{pmatrix} 1 & -i \\ 1 & i \end{pmatrix}. \tag{C.0.4}$$

Only if our results agree with those in Ref. [244], can our RGE matrix γ truncated to order $\mathcal{O}(g^2, \lambda)$ be related to theirs, $\tilde{\gamma}$, through:

$$P^{-1}\tilde{\gamma}P = \gamma\,. \tag{C.0.5}$$

We have checked that Eq. (C.0.5) holds.

D

A completion of the Standard Model

This appendix serves the purpose of proving the existence of a UV completion of the SM that generates arbitrary values of c_ϕ, $c_{\phi D}$ and $c_{\phi\Box}$. Let us extend the SM with three uncolored scalars: $\mathcal{S} \sim (1,1)_0$, $\Xi_0 \sim (1,3)_0$ and $\Xi_1 \sim (1,3)_1$. The numbers in parenthesis and the subscript indicate the representations of $SU(3)_c$, $SU(2)_L$ and $U(1)_Y$, respectively.

Let us assume that these fields all have the same mass M much larger than the EW scale, and that the full theory Lagrangian is:

$$\mathcal{L}_{\text{NP}} = \kappa_{\mathcal{S}}\mathcal{S}\phi^\dagger\phi + \lambda_{\mathcal{S}}\mathcal{S}^2\phi^\dagger\phi + \kappa_{\Xi_0}\phi^\dagger\Xi_0^a\sigma_a\phi + \left(\kappa_{\Xi_1}\Xi_1^{a\dagger}\tilde{\phi}^\dagger\sigma_a\phi + \text{h.c.}\right) . \tag{D.0.1}$$

(We ignored other terms for simplicity.) Integrating out the heavy fields at tree level at the scale M, we obtain [296]:

$$\begin{aligned}
\frac{c_\phi}{\Lambda^2} &= -\lambda_{\mathcal{S}}\frac{\kappa_{\mathcal{S}}^2}{M^4}\,, \\
\frac{c_{\phi D}}{\Lambda^2} &= \frac{2}{M^4}(2\kappa_{\Xi_1}^2 - \kappa_{\Xi_0}^2)\,, \\
\frac{c_{\phi\Box}}{\Lambda^2} &= \frac{1}{2M^4}(4\kappa_{\Xi_1}^2 + \kappa_{\Xi_0}^2 - \kappa_{\mathcal{S}}^2)\,.
\end{aligned} \tag{D.0.2}$$

The signs of the three tree-level generated dimension-6 WCs can be seen to be arbitrary and uncorrelated.

Note that dimension-eight operators arise too. Using `MatchingTools` [222], we find that (see also Ref. [179]):

$$\frac{c_{\phi^4}^{(1)}}{\Lambda^4} = 4\frac{\kappa_{\Xi_0}^2}{M^6}\,, \qquad \frac{c_{\phi^4}^{(2)}}{\Lambda^4} = 8\frac{\kappa_{\Xi_1}^2}{M^6}\,, \qquad \frac{c_{\phi^4}^{(3)}}{\Lambda^4} = \frac{2}{M^6}(\kappa_{\mathcal{S}}^2 - \kappa_{\Xi_0}^2)\,. \tag{D.0.3}$$

These couplings fullfill the positivity bounds $c_{\phi^4}^{(2)} \geq 0$, $c_{\phi^4}^{(1)} + c_{\phi^4}^{(2)} \geq 0$ and $c_{\phi^4}^{(1)} + c_{\phi^4}^{(2)} + c_{\phi^4}^{(3)} \geq 0$ obtained in Ref. [179] for arbitrary values of the κs. Note also that dimension-8 couplings can be zero, for instance $c_{\phi^4}^{(2)}$, with non-zero dimension-6 WCs.

E

Results for the box diagram

In this appendix we present the contribution to a_μ from box diagrams. These contributions are the ones commonly considered in the literature.

For the box diagram with two heavy fermion propagators, figure 32a, the relevant (schematic) Lagrangian reads

$$\begin{aligned}\mathcal{L} \supset\ & y_R T_{IJ} \overline{\Psi_{1I}} \phi_J e_R + y_L T_{IJK} \overline{\ell_{L,I}} \phi_J^\dagger \Psi_{2K} + y_H^R T_{IJK}^H \overline{\Psi_{2I}} \phi_J P_R \Psi_{1K} \\ & + T_{IJK}^H y_H^L \overline{\Psi_{2I}} \phi_J P_L \Psi_{1K} + \text{h.c.}\,,\end{aligned} \tag{E.0.1}$$

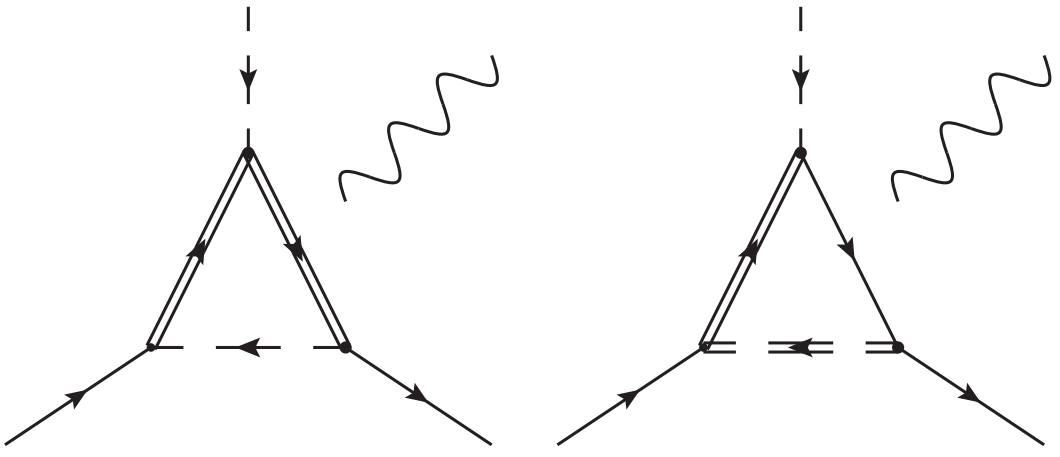

(a) (b)

Figure 32: *Left:* Box diagram which can contribute to $\alpha_{e\gamma}$ with 2 heavy fermions. *Right:* Box diagram which can contribute to $\alpha_{e\gamma}$ with 1 heavy fermion and 1 heavy scalar. Doubled (single) lines correspond to heavy (SM) particles. The B or W bosons can be attached to any of the internal lines.

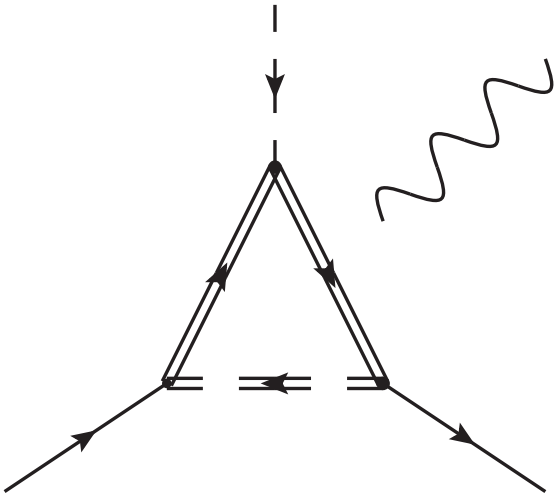

Figure 33: Box diagram which can contribute to $\alpha_{e\gamma}$ with all heavy internal propagators. Doubled (single) lines correspond to heavy (SM) particles. The B or W bosons can be attached to any of the internal lines.

where we kept the same conventions for the gauge interactions of Ψ and Φ as in Eq. (5.1.7).

The contribution to $\alpha_{e\gamma}$ is given by:

$$\alpha_{e\gamma}^{2,2} = \left(\frac{i}{4}\right) e y_R y_L \sum_{\chi=R,L} y_H^{\chi} \Big[T_{IJ} T_{2JK} T^{\gamma}_{I'I} T^{H}_{K2I'} \gamma^{\chi}_{\Psi_1} + T_{IJ} T_{2JK} T^{H}_{K'2I} T^{\gamma}_{KK'} \gamma^{\chi}_{\Psi_2} + T_{IJ} T_{2J'K} T^{H}_{K2I} T^{\gamma}_{J'J} \gamma^{\chi}_{\phi} \Big], \tag{E.0.2}$$

where χ sums over the RH and LH chiralities and the kinematic factors read:

$$\gamma^{L}_{\Psi_1} = 0\,,$$

$$\gamma^{R}_{\Psi_1} = -\frac{i}{16\pi^2} \frac{M_{\Psi_2}\left(M^2_{\Psi_1} \mathrm{Log}\left(\frac{M^2_{\Psi_1}}{M^2_{\Psi_2}}\right) - M^2_{\Psi_1} + M^2_{\Psi_2}\right)}{M_{\Psi_1}\left(M^2_{\Psi_1} - M^2_{\Psi_2}\right)^2},$$

$$\gamma^{L}_{\Psi_2} = 0\,,$$

$$\gamma^{R}_{\Psi_2} = -\frac{i}{16\pi^2} \frac{M_{\Psi_1}\left(-M^2_{\Psi_2} \mathrm{Log}\left(\frac{M^2_{\Psi_1}}{M^2_{\Psi_2}}\right) + M^2_{\Psi_1} - M^2_{\Psi_2}\right)}{M_{\Psi_2}\left(M^2_{\Psi_1} - M^2_{\Psi_2}\right)^2},$$

$$\gamma^{L}_{\Phi} = 0\,,$$

$$\gamma_\Phi^R = \frac{-i}{16\pi^2 M_{\Psi_1} M_{\Psi_2}}\,. \tag{E.0.3}$$

For the box diagram with a light fermion and in which the heavy fermion couples to the RH muon, the relevant Lagrangian reads:

$$\mathcal{L} \supset y_R T^e_{IJ} \overline{\Psi_{1I}} \Phi_J e_R + y_L T^1_{IJ} \overline{\psi} \phi_J P_L \Psi_{1I} + y_\Phi T^\Phi_{IJ} \overline{\ell_{LI}} \Phi^\dagger_J P_R \psi + \text{h.c.}\,, \tag{E.0.4}$$

where ψ is any light SM fermion which fits with the heavy field representations. The resulting contribution to $\alpha_{e\gamma}$ is:

$$\begin{aligned}\alpha^{22}_{e\gamma} = \left(\frac{i}{4}\right) e N y_R y_L y_\Phi \Big[& T^e_{IJ} T^\gamma_{I'I} T^1_{I'2} T^\Phi_{2J} \gamma_\Psi \\ & + T^e_{IJ} T^1_{I2} Y_\psi T^\Phi_{2J} \gamma_\psi + T^e_{IJ} T^1_{I2} T^\gamma_{JJ'} T^\Phi_{2J'} \gamma_\Phi \Big]\,,\end{aligned} \tag{E.0.5}$$

with the following kinematic factors:

$$\begin{aligned}\gamma_\Psi &= -\frac{M^2_\Phi \left(\left(M^2_\Psi + M^2_\Phi\right) \text{Log}\left(\frac{M^2_\Psi}{M^2_\Phi}\right) - 2M^2_\Psi + 2M^2_\Phi \right)}{\left(M^2_\Phi - M^2_\Psi\right)^3}\,, \\ \gamma_\psi &= \frac{-M^2_\Phi \text{Log}\left(\frac{M^2_\Psi}{M^2_\Phi}\right) + M^2_\Psi - M^2_\Phi}{\left(M^2_\Psi - M^2_\Phi\right)^2}\,, \\ \gamma_\Phi &= \frac{M^4_\Psi - 2M^2_\Psi M^2_\Phi \text{Log}\left(\frac{M^2_\Psi}{M^2_\Phi}\right) - M^4_\Phi}{\left(M^2_\Psi - M^2_\Phi\right)^3}\,.\end{aligned} \tag{E.0.6}$$

In the case the heavy fermion couples with the LH muon, the Lagrangian can be written as:

$$\mathcal{L} \supset y_R T^\ell_{IJK} \overline{\ell_{LI}} \Phi^\dagger_J \Psi_{1K} + y_L T^2_{IJK} \overline{\Psi}_I \phi_J P_L \psi_K + y_\Phi T^\Phi_{IJ} \overline{\psi}_I \Phi_J e_R + \text{h.c.}\,, \tag{E.0.7}$$

resulting in the following contribution to $\alpha_{e\gamma}$:

$$\begin{aligned}\alpha^{22}_{e\gamma} = \left(\frac{i}{4}\right) e N y_R y_L y_\Phi \Big[& T^\ell_{2JI} T^\gamma_{II'} T^2_{I'2K} T^\Phi_{KJ} \gamma_\Psi \\ & + T^\ell_{2JI} T^2_{I2K} T^\gamma_{KK'} T^\Phi_{K'J} \gamma_\psi + T^\ell_{2JI} T^2_{I2K} T^\Phi_{KJ'} T^\gamma_{J'J} \gamma_\Phi \Big]\,,\end{aligned} \tag{E.0.8}$$

where

$$\gamma_\Psi = \frac{M^2_\Phi \left(\left(M^2_{\Psi_1} + M^2_\Phi\right) \text{Log}\left(\frac{M^2_{\Psi_1}}{M^2_\Phi}\right) - 2M^2_{\Psi_1} + 2M^2_\Phi \right)}{\left(M^2_{\Psi_1} - M^2_\Phi\right)^3}\,,$$

$$\gamma_\psi = -\frac{\left(M_{\Psi_1}^2 \text{Log}\left(\frac{M_{\Psi_1}^2}{M_\Phi^2}\right) - M_{\Psi_1}^2 + M_\Phi^2\right)}{\left(M_{\Psi_1}^2 - M_\Phi^2\right)^2},$$
$$\gamma_\Phi = \frac{M_\Psi^4 - 2M_\Psi^2 M_\Phi^2 \text{Log}\left(\frac{M_\Psi^2}{M_\Phi^2}\right) - M_\Phi^4}{\left(M_\Psi^2 - M_\Phi^2\right)^3}. \tag{E.0.9}$$

When there are 3 heavy propagators in the box diagram, as shown in figure 33, the Lagrangian reads:

$$\mathcal{L} \supset y_R T^1_{IJ} \overline{\Psi_{1I}} \Phi_J e_R + y_L T^2_{IJ} \overline{\ell_L} \Psi_{2I} \Phi^\dagger_J + y^R_H T_{IJK} \overline{\Psi_{2I}} \phi_J P_R \Psi_{1K}$$
$$+ y^L_H T_{IJK} \overline{\Psi_{2I}} \phi_J P_L \Psi_{1K} + \text{h.c.}, \tag{E.0.10}$$

and the resulting $\alpha_{e\gamma}$ is given by:

$$\alpha^{22}_{e\gamma} = \left(\frac{i}{4}\right) y_R y_L \sum_{\chi=R,L} y^\chi_H \left[T^2_{IJ} T^H_{I2K} T^\gamma_{KK'} T^1_{K'J} \gamma^\chi_{\Psi_1}\right.$$
$$\left. + T^2_{IJ} T^\gamma_{II'} T_{I'2K} T^1_{KJ} \gamma^\chi_{\Psi_2} + T^2_{IJ} T_{I2K} T_{KJ'2} T^\gamma_{JJ'} \gamma^\chi_\Phi\right], \tag{E.0.11}$$

where

$$\gamma^L_{\Psi_1} = \frac{i}{16\pi^2} M_\Phi^2 \left[\left((M_{\Psi_2} - M_{\Psi_1})(M_{\Psi_1} + M_{\Psi_2})\left(M_\Phi^2 (M_{\Psi_2} - M_{\Psi_1})(M_{\Psi_1} + M_{\Psi_2})\left(M_{\Psi_1}^2\left(M_\Phi^2 - 2M_{\Psi_2}^2\right)\right.\right.\right.\right.$$
$$\left. + M_\Phi^4\right) \text{Log}\left(\frac{M_{\Psi_1}^2}{M_\Phi^2}\right) - (M_\Phi - M_{\Psi_1})(M_{\Psi_1} + M_\Phi)(M_{\Psi_2} - M_\Phi)(M_{\Psi_2} + M_\Phi)\left(M_{\Psi_1}^2\left(M_{\Psi_2}^2 - 2M_\Phi^2\right)\right.$$
$$\left.\left.\left. + M_{\Psi_2}^2 M_\Phi^2\right)\right) + M_{\Psi_2}^4 \left(M_{\Psi_1}^2 - M_\Phi^2\right)^3 \text{Log}\left(\frac{M_{\Psi_1}^2}{M_{\Psi_2}^2}\right)\right] \times$$
$$\frac{1}{(M_{\Psi_1} - M_{\Psi_2})^2 (M_{\Psi_1} + M_{\Psi_2})^2 \left(M_\Phi^2 - M_{\Psi_1}^2\right)^3 (M_{\Psi_2} - M_\Phi)^2 (M_{\Psi_2} + M_\Phi)^2}, \tag{E.0.12}$$

$$\gamma^R_{\Psi_1} = \frac{i}{16\pi^2} M_{\Psi_1} \left(M_{\Psi_2}(M_{\Psi_2} - M_{\Psi_1})(M_{\Psi_1} + M_{\Psi_2})\left((M_{\Psi_1} - M_\Phi)(M_{\Psi_1} + M_\Phi)\right.\right.$$
$$(M_{\Psi_2} - M_\Phi)(M_{\Psi_2} + M_\Phi)\left(M_{\Psi_1}^2 M_{\Psi_2}^2 - 3M_{\Psi_2}^2 M_\Phi^2 + 2M_\Phi^4\right) + M_\Phi^4 (M_{\Psi_2} - M_{\Psi_1})(M_{\Psi_1} + M_{\Psi_2})$$
$$\left.\left(M_{\Psi_1}^2 + 2M_{\Psi_2}^2 - 3M_\Phi^2\right) \text{Log}\left(\frac{M_{\Psi_1}^2}{M_\Phi^2}\right)\right) + M_{\Psi_2}^3 \left(M_{\Psi_1}^2 - M_\Phi^2\right)^3 \left(M_{\Psi_2}^2 - 2M_\Phi^2\right) \text{Log}\left(\frac{M_{\Psi_1}^2}{M_{\Psi_2}^2}\right)\Bigg) \times$$

$$\frac{1}{(M_{\Psi_1}-M_{\Psi_2})^2(M_{\Psi_1}+M_{\Psi_2})^2(M_{\Psi_1}-M_\Phi)^3(M_{\Psi_1}+M_\Phi)^3(M_{\Psi_2}-M_\Phi)^2(M_{\Psi_2}+M_\Phi)^2}\,, \tag{E.0.13}$$

$$\gamma^L_{\Psi_2} = -\frac{i}{16\pi^2}\left[M^6_{\Psi_1}\left(-\left(M^2_{\Psi_2}-M^2_\Phi\right)^3\right)\mathrm{Log}\left(\frac{M^2_{\Psi_1}}{M^2_\Phi}\right)+M^4_{\Psi_1}(M_{\Psi_1}-M_\Phi)(M_{\Psi_1}+M_\Phi)\right.$$
$$(M_{\Psi_2}-M_\Phi)^3(M_{\Psi_2}+M_\Phi)^3\mathrm{Log}\left(\frac{M^2_{\Psi_1}}{M^2_{\Psi_2}}\right)+(M_{\Psi_1}-M_\Phi)(M_{\Psi_1}+M_\Phi)\left(M^2_\Phi(M_{\Psi_1}-M_{\Psi_2})(M_{\Psi_1}+M_{\Psi_2})\right.$$
$$(M_{\Psi_2}-M_\Phi)(M_{\Psi_2}+M_\Phi)\left(M^2_{\Psi_1}\left(M^2_{\Psi_2}+M^2_\Phi\right)-2M^2_{\Psi_2}M^2_\Phi\right)+\left(M^4_{\Psi_1}M^6_{\Psi_2}-M^6_\Phi\left(M^2_{\Psi_1}-M^2_{\Psi_2}\right)^2\right.$$
$$\left.\left.\left.+M^2_{\Psi_1}M^4_{\Psi_2}M^2_\Phi\left(M^2_{\Psi_2}-3M^2_{\Psi_1}\right)+M^2_{\Psi_2}M^4_\Phi\left(M^4_{\Psi_1}+M^2_{\Psi_1}M^2_{\Psi_2}-M^4_{\Psi_2}\right)\right)\mathrm{Log}\left(\frac{M^2_{\Psi_2}}{M^2_\Phi}\right)\right)\right]\times$$
$$\frac{1}{(M_{\Psi_1}-M_{\Psi_2})^2(M_{\Psi_1}+M_{\Psi_2})^2(M_{\Psi_1}-M_\Phi)^2(M_{\Psi_1}+M_\Phi)^2(M_{\Psi_2}-M_\Phi)^3(M_{\Psi_2}+M_\Phi)^3}\,, \tag{E.0.14}$$

$$\gamma^R_{\Psi_2} = \frac{i}{16\pi^2}M_{\Psi_1}M_{\Psi_2}\left(2M^2_{\Psi_1}(M_{\Psi_1}-M_\Phi)(M_{\Psi_1}+M_\Phi)\left(M^2_\Phi-M^2_{\Psi_2}\right)^3\mathrm{Log}\left(\frac{M^2_{\Psi_1}}{M^2_{\Psi_2}}\right)\right.$$
$$+M^4_{\Psi_1}\left(M^2_{\Psi_2}-M^2_\Phi\right)^3\mathrm{Log}\left(\frac{M^2_{\Psi_1}}{M^2_\Phi}\right)+(M_\Phi-M_{\Psi_1})(M_{\Psi_1}+M_\Phi)\left((M_{\Psi_2}-M_{\Psi_1})(M_{\Psi_1}+M_{\Psi_2})\right.$$
$$(M_{\Psi_2}-M_\Phi)(M_{\Psi_2}+M_\Phi)\left(M^2_{\Psi_1}\left(M^2_{\Psi_2}-3M^2_\Phi\right)+2M^4_\Phi\right)+\left(M^2_{\Psi_1}M^6_{\Psi_2}+M^4_{\Psi_2}M^2_\Phi\left(M^2_{\Psi_2}-3M^2_{\Psi_1}\right)\right.$$
$$\left.\left.\left.+M^4_\Phi\left(-2M^4_{\Psi_1}+6M^2_{\Psi_1}M^2_{\Psi_2}-3M^4_{\Psi_2}\right)\right)\mathrm{Log}\left(\frac{M^2_{\Psi_2}}{M^2_\Phi}\right)\right)\right)\times$$
$$\frac{1}{(M_{\Psi_1}-M_{\Psi_2})^2(M_{\Psi_1}+M_{\Psi_2})^2(M_{\Psi_1}-M_\Phi)^2(M_{\Psi_1}+M_\Phi)^2(M_{\Psi_2}-M_\Phi)^3(M_{\Psi_2}+M_\Phi)^3}\,, \tag{E.0.15}$$

$$\gamma^L_\Phi = \frac{iM^2_\Phi}{16\pi^2}\left[\frac{1}{\left(M^2_{\Psi_2}-M^2_\Phi\right)^3}\left(2\left(M^4_{\Psi_1}M^4_{\Psi_2}+M^6_\Phi\left(M^2_{\Psi_1}+M^2_{\Psi_2}\right)-3M^2_{\Psi_1}M^2_{\Psi_2}M^4_\Phi\right)\mathrm{Log}\left(\frac{M^2_{\Psi_2}}{M^2_\Phi}\right)\right.\right.$$
$$-(M_\Phi-M_{\Psi_1})(M_{\Psi_1}+M_\Phi)(M_{\Psi_2}-M_\Phi)(M_{\Psi_2}+M_\Phi)\left(M^2_\Phi\left(M^2_{\Psi_1}+M^2_{\Psi_2}\right)-3M^2_{\Psi_1}M^2_{\Psi_2}+M^4_\Phi\right)$$
$$\left.\left.-\frac{2M^4_{\Psi_1}\mathrm{Log}\left(\frac{M^2_{\Psi_1}}{M^2_{\Psi_2}}\right)}{M^2_{\Psi_1}-M^2_{\Psi_2}}\right)\right]\times\frac{1}{\left(M_{\Psi_1}-M_\Phi\right)^3\left(M_{\Psi_1}+M_\Phi\right)^3}\,, \tag{E.0.16}$$

$$\gamma_{\Phi}^{R} = \frac{i}{16\pi^2} M_{\Psi_1} M_{\Psi_2} \left(2M_{\Psi_1}^2 M_{\Phi}^2 \left(M_{\Psi_2}^2 - M_{\Phi}^2 \right)^3 \mathrm{Log}\left(\frac{M_{\Psi_1}^2}{M_{\Psi_2}^2} \right) + (M_{\Psi_1} - M_{\Psi_2})(M_{\Psi_1} + M_{\Psi_2}) \right.$$
$$\left((M_{\Psi_1} - M_{\Phi})(M_{\Psi_1} + M_{\Phi})(M_{\Psi_2} - M_{\Phi})(M_{\Psi_2} + M_{\Phi}) \left(M_{\Phi}^2 \left(M_{\Psi_1}^2 + M_{\Psi_2}^2 \right) + M_{\Psi_1}^2 M_{\Psi_2}^2 - 3M_{\Phi}^4 \right) \right.$$
$$\left. \left. -2M_{\Phi}^2 \left(M_{\Psi_1}^4 M_{\Psi_2}^2 + M_{\Psi_1}^2 \left(M_{\Psi_2}^4 - 3M_{\Psi_2}^2 M_{\Phi}^2 \right) + M_{\Phi}^6 \right) \mathrm{Log}\left(\frac{M_{\Psi_2}^2}{M_{\Phi}^2} \right) \right) \right) \times$$
$$\frac{1}{(-M_{\Psi_1}^2 + M_{\Psi_2}^2)(M_{\Psi_1}^2 - M_{\Phi}^2)^3 (M_{\Psi_2}^2 - M_{\Phi}^2)^3} \,. \tag{E.0.17}$$

We cross-checked this last result considering a box diagram with only heavy internal propagators with Eq. (4.4) of Ref. [275] and found perfect agreement in the limit of degenerate masses.